Hydrology, temperature, and water source dynamics across river basins of western North America

Lillian McGill

A dissertation

submitted in partial fulfillment of the

requirements for the degree of

Doctor of Philosophy

University of Washington

2022

Reading Committee:

Gordon Holtgrieve, Co-Chair

E. Ashley Steel, Co-Chair

Mark Scheuerell

Program Authorized to Offer Degree:

Quantitative Ecology and Resource Management

University of Washington

Abstract

Hydrology, temperature, and water source dynamics across river basins of western North America

Lillian McGill

Co-Chairs of the Supervisory Committee:

Gordon Holtgrieve
School of Aquatic and Fishery Sciences

E. Ashley Steel
Department of Statistics

Climate change is altering temperature and precipitation regimes across the globe, resulting in often extreme modifications to river dynamics. Such impacts are particularly pronounced in western North America, a region with both water surplus and scarcity and therefore a long history of water resource challenges. To preserve riverine ecosystems, it is essential to improve our understanding of fundamental processes governing river dynamics, how river systems have and continue to change with anthropogenic forcing, and what tools and management actions may best facilitate conservation. Despite the breadth of studies examining western river hydrology and temperature, a persistent need remains for fundamental understanding and predictions on a management-relevant scale and the generation of insights that considers both temporal and spatial

variation simultaneously. My dissertation research answers questions relating to how we describe and model patterns in riverine ecosystems and consists of a portfolio of projects aimed at improving our ability to understand fundamental drivers of, and predict and mitigate anthropogenic induced changes to, river hydrology, temperature, and water source.

TABLE OF CONTENTS

List of Figures vi

List of Tables x

Chapter 1. Introduction 13

Chapter 2. Elevation and spatial structure explain most surface-water isotopic variation across five pacific coast basins 17

2.1 Abstract 17

2.2 Introduction 18

2.3 Methods 22

2.3.1 Study Sites 22

2.3.2 Data collection and processing 24

2.3.3 Data analysis 25

2.4 Results 29

2.4.1 General description and relationship with MWE 29

2.4.2 Landscape covariates 30

2.4.3 Univariate and best fit linear models 31

2.4.4 Semivariograms and spatial stream network models 32

2.5 Discussion 34

2.5.1 MWE gradient 34

2.5.2 Other drivers of observed isotope patterns 36

2.5.3 In-stream and landscape processes shape isotope values 41

2.5.4 Study limitations 43
2.5.5 Management implications 44
2.5.6 Conclusions 46
Chapter 3. Spatiotemporal dynamics of water sources in a mountain river basin inferred through δ2H and δ18O of water 58
3.1 Abstract 58
3.2 Introduction 59
3.3 Methods 62
3.3.1 Study site 62
3.3.2 Data collection 63
3.3.3 Analysis 66
3.4 Results 68
3.4.1 General patterns in isotope ratios 68
3.4.2 Relationship between isotope ratios and MWE 68
3.4.3 Seasonal variance in isotope ratios 70
3.4.4 Relationship between discharge and geology 71
3.5 Discussion 72
3.5.1 Isotope ratios vary strongly with MWE 72
3.5.2 Seasonality in isotope ratios reflects hydrological processes 73
3.5.3 Catchment geology controls summer baseflow 75
3.5.4 Caveats and limitations 79
3.5.5 Climate and management implications 80

Chapter 4. Spatial covariance of hydrologic change among river discharge time series across Western North America 93

4.1 Abstract 93

4.2 Introduction 94

4.3 Methods 98

4.3.1 Watershed selection 98

4.3.2 Hydrograph metrics 99

4.3.3 Climate covariates 99

4.3.4 Directional trend tests 100

4.3.5 Non-monotonic trend dynamics 101

4.4 Results 103

4.4.1 River classification 103

4.4.2 Mann-Kendall trend results 104

4.4.3 Dynamic factor analysis results 105

4.5 Discussion 106

4.5.1 Metrics capture important facets of the hydrologic regime 107

4.5.2 Trends in peak flows are driven by interannual variability in precipitation 108

4.5.3 Trends in recession flow cluster by river type 110

4.5.4 Trends in minimum flows show large, widespread decreases 111

4.5.5 Caveats and limitations 114

4.5.6 Management implications 115

Chapter 5. Empirical stream thermal sensitivities cluster on the landscape according to geology and climate 128

5.1 Abstract 128
5.2 Introduction 129
5.3 Methods 132
5.3.1 Study area 132
5.3.2 Exploration of air-water correlation summary metrics 134
5.3.3 Spatially weighted clustering of thermal sensitivity 134
5.4 Results 139
5.4.1 General patterns in temperature, precipitation, and thermal sensitivity 139
5.4.2 How do water temperature, air temperature, and thermal sensitivity cluster? 141
5.5 Discussion 143
5.5.1 Patterns of thermal sensitivity clustering 143
5.5.2 Importance of underlying geology for thermal sensitivity 145
5.5.3 Climate controls on thermal sensitivity 148
5.5.4 Landscape controls on thermal sensitivity 150
5.5.5 Caveats and limitations 151
5.5.6 Implications for management and future directions 153
Chapter 6. Conclusion 166
6.1 Chapter conclusions 166
6.2 Understanding drivers of river regimes across scales 168
6.3 Modeling spatial data within and across watershed 169
6.4 Modeling temporal data within and across years 171
6.5 Future directions 172

Bibliography 174

Chapter 3 Appendix 218

Chapter 4 Appendix 222

Chapter 5 Appendix 226

LIST OF FIGURES

Figure 2.1. Geographic locations of study basins, the Snoqualmie (A), Green (B), Skagit (C), and Wenatchee (D) Rivers in Washington and Cowee Creek (E) in southwestern Alaska. Between 31-58 water samples were collected within each basin ($n_{Snoqualime}$ = 58, n_{Green} = 31, n_{Skagit} = 38, $n_{Wenatchee}$ = 44, n_{Cowee} = 38) and are shown in yellow. Red points indicate a major dam and blue shading indicates an ice mass. 48

Figure 2.2. Regressions of $\delta^{18}O$ values with mean watershed elevation for samples collected during summer low flow for each basin. Lines represent the least squares relationships. Triangle points are mainstem sites and circle points are tributary sites. Points are colored according to the mean annual precipitation (MAP) within the upstream watershed. 49

Figure 2.3. Correlation matrices for the Snoqualmie, Green, Skagit, and Wenatchee Rivers, and Cowee Creek. Both isotope metrics and landscape covariates are included. Red indicates a negative correlation between two variables, and blue indicates a positive correlation. The darker the color, the stronger the correlation. See Table 2 for a description of covariates. 50

Figure 2.4. Semivariograms for raw δ18O values, residual δ18O values from the best-fit linear models, and residual δ18O values from the best-fit SSNMs for the Snoqualmie and Wenatchee basins. Circles are proportional to the number of sites used to estimate each bin value. 51

Figure 2.5. Isoscapes from the Snoqualmie best-fit linear model (A), Snoqualmie best-fit SSNM (B), Wenatchee best-fit linear model (C), and Wenatchee best-fit SSNM (D). Colors represent predicted δ18O values and the size of each point is inversely proportional to the prediction standard error. 52

Figure 2.6. Variance decomposition into the proportion of variation explained by covariates (blue), tail-up covariance structure (yellow), Euclidean covariance structure (red), and the nugget (gray) for each of the SSNMs (categories on the x-axis) in the Snoqualmie and Wenatchee basins. TU = tail-up; Euc = Euclidean; TU.Euc = tail-up and Euclidean. 53

Figure 3.1. The Snoqualmie River basin and sub-basins, and the Snoqualmie's location in Washington, USA (A), water sample, USGS gage, and SNOTEL site locations (B), elevation of the Snoqualmie basin (C), and generalized geology of the Snoqualmie basin (D). 82
Figure 3.2. Climatic time series over our study period. Mainstem Snoqualmie discharge from USGS station 12149000 (A), total daily incoming precipitation from SNOTEL site 908 (Alpine Meadows) (B), snow-water-equivalent (SWE) from all SNOTEL sites within the basin (C), and mean daily air temperature from SNOTEL site 908 (Alpine Meadows) (D). The ticks on the x-axis are the median date of our whole basin, seasonal sampling events. 83
Figure 3.3. Relationships with elevation for d-excess (A), $\delta^{18}O$ values (B), and $\delta^{2}H$ values, (C) for all seasonal sampling events. Color indicates the month that each water sample was collected. For September and June, there are two sets of sampling events shown (2017 and 2018), with 2017 having a faded color. 84
Figure 3.4. Semivariograms for the residuals from the δ2H-MWE linear regression. Circles are proportional to the number of sites used to estimate each bin value. 85
Figure 3.5. The $\delta^{2}H$ values for all seasonal sites throughout the year. Color indicates the MWE of the basin. 86
Figure 3.6. Black lines are $\delta^{2}H$ values for biweekly samples collected at the mouth of the mainstem Snoqualmie and each major tributary over WY 2018. Dark gray lines along the bottom are daily streamflow hydrographs from nearby USGS gages, normalized by drainage area. Gray bars along the top are weekly averages of precipitation. 87
Figure 3.7. Relationships between water source variability and the baseflow index (A) and water source elevation and average unit discharge at baseflow (B) for all streamflow gages within the basin. Points are colored by year. Point size is related to the log watershed area for each site. 88
Figure 3.8. Relationships between the proportion of glacial deposits within a watershed and the average unit discharge at baseflow (A) and baseflow index (B) for all streamflow gages within the basin. Points are colored by year. Point size is related to the log watershed area

for each site. The inset panel shows the Snoqualmie basin generalized geology (see Figure 1A for legend colors) and streamflow gage locations. 89
Figure 4.1. Locations and upstream watershed area of gages in each of the three seasonal flow regime classes. 119
Figure 4.2. Hydrographs of normalized mean daily streamflow for three seasonal flow regime classes: snow, mixed, and rain, colored by state and ordered by latitude. Normalized mean daily streamflow is shown on a linear scale. The black dotted line shows April 1st, which is commonly considered the date of peak SWE across western North America. 120
Figure 4.3. Median values and standard deviation across each site's period of record for each of the six metrics versus latitude. Points are colored by river basin type. All magnitude metrics are standardized by watershed area to facilitate comparison. 121
Figure 4.4. Mann-kendall trend test tau estimates, representing the monotonic trends through time, for each of our six metrics versus SWE to winter precipitation ratios. Colored by state. Significant results are shown in color. A loess smoothing line using all trend estimates is shown in black. 122
Figure 4.5. Covariate coefficients for all flow magnitude metrics from best fit DFA models. The size of each circle indicates the proportion of variance explained by all covariates within the best-fit model. 123
Figure 4.6. Latent variables (top row) and factor loadings per latent variable for the best-fitting model for peak flow magnitude. Points are colored by their factor loading, where their values indicate strength of latent variable association. 124
Figure 4.7. Latent variables (top row) and factor loadings per latent variable for the best-fitting model for minimum flow magnitude. Points are colored by their factor loading, where their values indicate strength of latent variable association. 125
Figure 4.8. Latent variables (top row) and factor loadings per latent variable for the best-fitting model for recession flow timing. Points are colored by their factor loading, where their values indicate strength of latent variable association. 126
Figure 5.1. A map of the Snoqualmie (A) and Wenatchee (B) basins water and air temperature monitoring sites and the most downstream USGS gage for each basin. Thermal sensitivity,

defined as the change in water temperature with a single degree change in air temperature, versus mean watershed elevation for each site-year combination (C). 155
Figure 5.2. **T**hermal sensitivities for all seasons for sites with consistent data coverage (at least 6 years of data) for all seasons throughout the sampling timeframe. The color of each point corresponds to the mean watershed elevation. 156
Figure 5.3. Spring thermal sensitivity values for all site-year combinations in the Snoqualmie and Wenatchee basins versus total snow water equivalent in spring and summer (A), precipitation (B), and air temperature (C) from gridded DAYMET data for each sampling point. Points are colored by basin. Basins that have no snowmelt in a given year are not shown on graph (A). 157
Figure 5.4. The relationship between landscape variables and thermal sensitivities in summer. See Figure S3 for a detailed description of how river attributes covary with one another. 159
Figure 5.5. Average time series (A) and spatial clustering results (columns/colors indicate unique clusters) for average annual air temperature (B), water temperature (C), and thermal sensitivity (D) in the Snoqualmie basin. The spatial distribution for Colored lines indicates mean average annual values for each cluster, and gray lines denote average annual values for each site within a given cluster. 160
Figure 5.6. Average time series (A) and spatial clustering results (columns/colors indicate unique clusters) for average annual air temperature (B), water temperature (C), and thermal sensitivity (D) in the Wenatchee basin. The spatial distribution for Colored lines indicates mean average annual values for each cluster, and gray lines denote average annual values for each site within a given cluster. 161
Figure 5.7. Relative variable importance for all covariates in the Snoqualmie (A) Wenatchee (B) basins, and the distributions of variables for the four most important variables (C) in the Snoqualmie basin (Mean Slope, Elevation, Soil Depth, and Baseflow Index) and in the Wenatchee basin (Elevation, Baseflow Index, Mean Slope, and Hydraulic Conductivity). Boxes are grouped and colored by cluster membership. See Figure S5 for plots of the remaining relative variable importances. 162

LIST OF TABLES

Table 2.1. Climate and physical characteristics for each basin. 54
Table 2.2. List of covariates considered for inclusion in each model. Here, "watershed" indicates the upstream area draining to a sample. 55
Table 2.3. Best fit linear models from the Snoqualmie, Green, Skagit, Wenatchee, and Cowee basins. The independent effect weight is the percentage of explained variance by each covariate. 56
Table 2.4. Model fit statistics from SSNMs in the Snoqualmie and Wenatchee basins. Variance component values are the percentage of variance explained by fixed effects (covariates) and spatial error. Models in bold were selected as the best fit models. 57
Table 3.5. Watershed characteristics for the Snoqualmie River and each of its major tributaries. The "snow zone" in the Snoqualmie is considered to be areas greater than 900 m (Jefferson 2011). Mean Annual Precipitation was calculated over the period 1980-2010. 90
Table 3.6. Model fit statistics from linear regressions with mean watershed elevation in the Snoqualmie River basin. Units for the coefficients are ‰/m. Numbers in parentheses are the standard error (SE) for model parameters. 91
Table 3.7. Spatial stream network model (SSNM) statistics for each month. All sites were included in these regressions. Units for the coefficients are ‰/m. 92
Table 4.8. Delta AIC values for each of the DFA models run with covariates. The covariates included in each final best-fit model are shown in bold. 127
Table 5.9. Physical environmental data and basin characteristics used to predict air-water clusters. 163
Table 5.10. Air water correlation summary metrics by basin and season. 164
Table 5.11. Metrics averaged for all sites within each thermal sensitivity regime determined with the spatially weighted agglomerative hierarchical clustering. 165

ACKNOWLEDGEMENTS

As I look back on my time as a graduate student at the University of Washington, I am grateful to so many people for offering me support, friendship, and mentorship.

Thank you to my advisors, Gordon Holtgrieve and E. Ashley Steel, both of whom encouraged my individual research interests and supported me in reaching professional and personal goals. Gordon challenged me to always keep the driving questions and big picture in mind, and Ashley ensured that my statistical analyses were robust and the results meaningful. My other committee members - J. Renée Brooks, Aimee Fullerton, Mark Scheuerell, Jessica Lundquist, and Christian Torgersen – have each been invaluable mentors and challenged me to think broadly, communicate clearly, and get excited about the interesting questions in science. I can truly say that my research and time at UW would not have been the same without you all.

I also extend my deepest gratitude to collaborators and volunteers that aided in this research, including the co-authors of the manuscripts that have or will result from this work, members of the Snoqualmie Science Coordination and Advisory Team, Seattle City Light for granting access to the Tolt River, Amy Marsha for temperature data cleaning, and the many volunteers who helped collect water samples and temperature data for the Snoqualmie and Wenatchee Rivers. Thank you to all past and present members of the Holtgrieve lab for offering advice on presentations, publications, half-baked ideas, and everything in between. Getting to know you all and share in both the ups and the downs of graduate school has bene a wonderful

gift. And lastly, I'd like to thank my fellow QERM and SAFS students for your support and friendship through the years.

My research would not have been possible without the support of funding agencies. My dissertation research was funded by several fellowships, including a Department of the Interior Northwest Climate Adaptation Science Center graduate fellowship, a National Science Foundation Graduate Research Fellowship (Grant No. DGE-1762114), a National Science Foundation Graduate Research Internship Program fellowship, and a Quantitative Ecology and Resource Management first year fellowship.

Most importantly, thank you to my family, friends, and wonderful partner Zack! Your unconditional love and support has meant the world to me.

Chapter 1. INTRODUCTION

Flowing waters sustain an immense amount of freshwater, terrestrial, and marine biodiversity (Strayer and Dudgeon 2010, Maasri et al. 2022), make important contributions to global biogeochemical cycles (Maavara et al. 2020), and from the earliest recorded history have formed the backbone of human civilizations (Macklin and Lewin 2019, Paine 2019). Modern civilizations rely on stream and river ecosystems to meet drinking water, irrigation, hydropower, and food needs by storing, moving, and modifying water in complex ways. Due to human dependence on rivers, widespread development and degradation of these systems has occurred. Flowing waters are particularly sensitive to anthropogenic disturbance, as rivers integrate across their catchments, resulting in upstream processes impacting downstream points. These catchment-river linkages can concentrate and compound disturbances that occur throughout a watershed. Threats to aquatic ecosystems include hydrological alteration due to dams, diversion, and abstraction of water, habitat modification due to land-use conversion, and chemical and nutrient pollution (Dudgeon et al. 2006, Holtgrieve et al. 2011, Ruhi et al. 2018b, Grill et al. 2019, Flitcroft et al. 2019). Over the past century, the ubiquitous threat of anthropogenic induced climate change has emerged, adding new stressors and compounding existing ones (Vörösmarty et al. 2010). To preserve riverine ecosystems while supporting societal needs, it is therefore essential to improve our understanding of 1) fundamental processes governing river dynamics, 2) how river systems have and continue to change with anthropogenic forcing, and 3) what tools and management actions may best facilitate conservation.

Anthropogenic climate change is altering temperature and precipitation regimes across the globe, resulting in often extreme modifications to river dynamics (Thompson et al. 2021).

Such impacts are particularly pronounced in western North America, a region with both water surplus and scarcity and therefore a long history of water resource challenges (Dettinger et al. 2015). In western North America, global climate change has resulted in increasing temperatures, decreased mountain snowpack, and sharpened seasonal cycle of precipitation with more intense precipitation over a shorter time period (Whitfield and Cannon 2000, Barnett et al. 2008, Cayan et al. 2008, Mote and Salathé 2010, Hagos et al. 2016, Swain et al. 2018). River hydrology within the region is particularly sensitive to changes in climate due to strong seasonality in precipitation and dependence on mountain snowpack to sustain warm season stream flow (Stewart et al. 2005, Elsner et al. 2010, Safeeq et al. 2016, Dierauer et al. 2018). A changing climate affects the timing and balance of precipitation falling as rain and snow, and therefore the timing, magnitude, source, and temperature of streamflow over the course of the year (Knowles et al. 2006, van Vliet et al. 2013).

Anticipated shifts have implications for ecologically and economically relevant facets of discharge, water temperature, and water source. Shifts in discharge will likely strain human water resource systems, where the seasonal asynchrony between winter precipitation and runoff and summer water demand (i.e., the combination of atmospheric demands, ecological requirements, and consumptive use) already makes water supplies scarce and vulnerable (Barnett et al. 2005, Jaeger et al. 2017). Aquatic and riparian species that are highly adapted to the signals of seasonal flooding and drought disturbances (Gasith and Resh 1999, Bonada et al. 2007) and water temperature regimes (Mantua et al. 2010) may have difficulty adapting to the changes in the timing or intensity of these signals. Thermal and hydrologic conditions outside the tolerance of species, such as warm water temperatures and low summer baseflows, are expect to prove challenging for species such as Pacific salmon (Mantua et al. 2010, Steel et al. 2019). As changes

will not be uniform across rivers, there is an urgent challenge and opportunity to identify how climate and catchment parameters influence individual river response.

To understand biodiversity and sustainability of river ecosystems, it is essential to appreciate the central organizing role of a dynamic physical environment (Poff et al. 1997). Temperature and hydrologic regimes are fundamental properties of rivers that drive both physical and ecological processes. Modifications to these regimes are widespread, threatening ecosystem function and structure. A critical challenge for resource managers seeking to prioritize restoration or research actions is in identifying overall river sensitivity to climate change. To do so, we need to simultaneously consider multiple key physical properties, including hydrology, temperature, and water source regimes. Seasonal flow regimes, or the characteristic pattern of flow variation, support river processes such as disturbance regimes, habitat provisions, and native species life history cues; long-term patterns of flow variability have historically selected for organismal life histories related to growth, reproduction, and dispersal (Ward and Stanford 1979, Beacham & Murray 1990, Poff et al. 1997). Stream temperature regime controls the rates of many biological, chemical, and physical processes in flowing waters and is a key driver of ecological processes controlling population and community structure in aquatic ecosystems. Both temperature and hydrology are profoundly impacted by water source (e.g., surface runoff, groundwater, etc.). Understanding spatial and temporal dynamics of where water originates in a basin informs mechanisms of runoff generation and aids in predictions of where and how streamflow and temperature patterns are likely to shift. Despite the breadth of studies examining wester river hydrology and temperature, a persistent need remains for fundamental understanding and predictions on a management-relevant scale that incorporate both temporal and spatial variation simultaneously. Furthermore, basin morphological characteristics are the local-scale

lens through which climatic changes will be filtered and translated into streamflow. It is therefore essential to improve understanding of how local processes interact with climate to generate streamflow.

My dissertation research answers questions relating to how we describe and model patterns in riverine ecosystems. This research consists of a portfolio of projects aimed at improving our ability to understand fundamental drivers of, and predict and mitigate anthropogenic induced changes to, river hydrology, temperature, and water source. Specifically, I aim to:

1. Compare basin-specific patterns of surface water isotope ratios (2H:1H & 18O:16O) to explore the utility of using stable isotopes for estimating river water source within the Pacific Northwest.
2. Characterize spatial and temporal surface water isotope variation within a Pacific Northwest river basin to understand the vulnerability of river flow to source water dynamics across space and time.
3. Map the magnitude and extent of historical changes to streamflow across western North America and resolve the relative influence of local-scale morphological and regional-scale climactic processes in governing streamflow and patterns of change.
4. Understand patterns and drivers of clustering of annual air-water temperature correlations to articulate when and how this type of monitoring can provide insight on stream sensitivities to climate and other drivers of change.

Chapter 2. ELEVATION AND SPATIAL STRUCTURE EXPLAIN MOST SURFACE-WATER ISOTOPIC VARIATION ACROSS FIVE PACIFIC COAST BASINS

A version of this paper is published as *McGill, L.M., Steel, E.A., Brooks, J.R., Edwards, R.T., Fullerton, A.H. 2020. Elevation and spatial structure explain most surface-water isotopic variation across five Pacific coast basins, Journal of Hydrology. DOI: 10.1016/j.jhydrol.2020.124610*

2.1 ABSTRACT

The stable isotope ratios of stream water can be used to trace water sources within river basins; however, drivers of variation in water isotopic spatial patterns across basins must be understood before ecologically relevant and isotopically distinct water sources can be identified and this tool efficiently applied. We measured the isotope ratios of surface-water samples collected during summer low-flow across five basins in Washington and southeast Alaska (Snoqualmie, Green, Wenatchee, and Skagit Rivers, and Cowee Creek) and compared models (isoscapes) describing the spatial variation in surface-water isotope ratios across a range of hydraulic and climatic conditions. We found strong correlations between mean catchment elevation and surface-water isotopic ratios on the windward west side of the Cascades and in Alaska, explaining 48-90% of variation in δ18O values. Conversely, in the Wenatchee basin, located leeward east of the Cascade Range, mean catchment elevation alone had no predicative power. The elevation relationship, and predictive isoscapes varied between basins, even those adjacent to each other. Applying spatial stream network models (SSNMs) to two of our study basins, the Snoqualmie and Wenatchee Rivers, we found incorporating Euclidean and flow-connected spatial autocovariance improved explanatory power. SSNMs improved the accuracy of river water isoscapes in all cases; however,

their utility was greater for the Wenatchee basin, where covariates explained only a small proportion of total variation. Our study provides insights into why basin-scale surface-water isoscapes may vary even in adjacent basins and the importance of incorporating spatial autocorrelation in isoscapes. For determining source water contributions to downstream waters, our results indicate that surface water isoscapes should be developed for each basin of interest.

2.2 INTRODUCTION

Isoscapes are a framework that describe the spatial patterns in isotopic ratios across a landscape and are useful for addressing a variety of basic and applied research questions (West 2010, Bowen and Good 2015). Stable isotopes of oxygen and hydrogen can be harnessed to determine source-water contributions to streamflow on a range of spatial and temporal scales (Rock and Mayer 2007, Wang et al. 2009, Koeniger et al. 2009, Mountain et al. 2015), estimate mean transit times (McGuire et al. 2005 p. 2, McGuire and McDonnell 2006, Jasechko et al. 2016), delineate animal migration paths (Chamberlain et al. 1997, Hobson and Wassenaar 1997), and understand hydrologic flow paths (Rodgers et al. 2005, Singh et al. 2016, Nickolas et al. 2017). Despite the widespread use of water isotope ratios in research and their potential application for predicting future flows under a changing climate or identifying likely areas of cool water for fisheries management, few studies have compared drivers of variation in isotopic ratios at the basin scale or across basins.

The generation of accurate isoscapes is possible in part because water stable isotope ratios exhibit systematic spatial and temporal variation resulting from the process of isotope fractionation that accompanies water cycle phase changes and diffusion. Isotope fractionation is the primary force acting to produce variations in $\delta^{18}O$ and $\delta^{2}H$ values (both spatially and temporally) in water sources across the globe (Gat 1996, Araguas-Araguas et al. 2000). An

example of this process is the Rayleigh rainout effect, wherein progressive isotopic depletion of a vapor cloud occurs as it moves along its storm trajectory. Rayleigh rainout occurs because heavy isotopes preferentially fall as precipitation (Dansgaard 1964, Clark and Fritz 1997). As a result, both precipitation and surface water isotopic ratios of $\delta^{18}O$ and $\delta^{2}H$ are highly correlated with changes in elevation, latitude, and longitude (Yonge et al. 1989, Ingraham and Taylor 1991, Dutton et al. 2005, Lechler and Niemi 2011), although the strength and presence of these relationships can vary among river basins due to local processes such as evaporation (Bowen and Good 2015).

Although broad-scale patterns in water isotopic ratios are well documented, when generating isoscapes for use in water resource management, basin-scale factors that may affect isotope distributions must be incorporated. Previous studies have shown consistent relationships between elevation and surface water stable isotopes at the basin scale (Biggs et al. 2015, Peng et al. 2015, Vespasiano et al. 2015, Fan et al. 2016). When the elevation-isotope relationship is clear and consistent, water isoscapes can be a valuable tool for assessing the proportion of water that comes from high elevation, climate sensitive snowmelt that is often critical for sustaining summer baseflow in mountainous regions (Barnett et al. 2005, Brooks et al. 2012). However, within certain regions, the elevation-isotope relationship is weak, absent, or inverse (Wassenaar et al. 2009, Lechler and Niemi 2011, Bershaw et al. 2012), suggesting that local atmospheric or hydrologic mechanisms are overriding the elevation effect within these regions. Basins in close geographic proximity can have fundamentally different relationships between surface water isotope ratios and elevation (Brooks et al. 2012, Nickolas et al. 2017). Therefore, cross-basin analyses are needed to describe the variation in the landscape covariates that are highly

correlated with surface water isotope ratios in order to identify where and how isotopic variation can be leveraged to identify distinct water sources within a river basin.

Previous studies have predominately generated water isoscapes in two-dimensional space. Such models may be appropriate for terrestrial, oceanic, or atmospheric systems such as precipitation over the continental United States or the surface of the Atlantic Ocean (Vachon et al. 2010, McMahon et al. 2013). The movement of stream surface water, however, is constrained by the topology of the dendritic stream network, which strongly affects the distribution of surface water stable isotopes that are conserved as water moves downstream(Clark and Fritz 1997). To date, isoscapes of stream networks have largely relied on interpolation using Euclidean distance (the straight-line distance between two sites) and have been restricted to predicting inputs from the local catchment(Brooks et al. 2012, Katsuyama et al. 2015). Although Bowen et al. (2011) modeled continuous river water isotope values by accumulating elevation-explicit, gridded precipitation isotope maps downstream and correcting them with model residuals, no explicit statistical method was used to partition the effects of downstream transport versus landscape predictors such as geology. Given that typical models do not account for the branching structure of stream networks, longitudinal connectivity, or flow direction, they may be inappropriate for use on river networks.

Ver Hoef and Peterson (2010) developed a class of geostatistical models, spatial stream network models (SSNMs), which account for spatial dependencies across stream networks. SSNMs are similar to conventional linear mixed models in that the deterministic mean of the dependent variable is modeled as a linear function of explanatory variables. However, the assumption of independent errors is relaxed and an atuocovariance model is used to account for spatial autocorrelation in the errors (Ver Hoef et al. 2006, Peterson and Ver Hoef 2010, Ver Hoef

and Peterson 2010). The autocovariance model can be specified using any combination of tail-up, tail-down, or Euclidean autocovariance functions. Tail-up and tail-down functions use hydrologic rather than Euclidean distance, and, in the tail-up model, spatial autocorrelation is restricted to flow-connected locations (i.e., water flows from an upstream location to a downstream location). SSNMs have been applied to answer a broad suite of questions, in each case improving model fit by explicitly modeling spatial autocorrelation in the data (Isaak et al. 2014, Brennan et al. 2016, Filipe et al. 2017). Application of these models to water isotopes might provide information on the relative influence of environmental versus spatial processes on isotope distribution, improve estimation of the covariates-isotope relationship absent confounding spatial autocorrelation, and generate more robust predictions of isotope values at unmeasured sites.

In this study, we compare the spatial patterns of surface water isotopes across five basins within Washington and Southeastern Alaska to quantify and compare local controls on isotopic variability of surface water and to explore the utility of applying simple elevation regressions models for estimating water source across river basins. We also compare the performance of models with and without network-based spatial autocorrelation. Specifically, the objectives of our study are (1) to compare the strength with which isotope ratios vary by mean watershed elevation (MWE) across five river basins, (2) to assess and compare whether additional landscape predictors improve models of isotope ratios across basins, and (3) to explore where SNNMs might be used to improve river water isoscape generation.

2.3 METHODS

2.3.1 *Study Sites*

We selected five climatically and geographically distinct watersheds across Washington and Alaska (Figure 2.1). The Washington river basins (Snoqualmie, Skagit, Green, and Wenatchee) are within the Cascade Range with the Wenatchee River draining to the east (leeward), and the other three rivers draining to the west (windward). Western Washington has a Mediterranean climate with dry summers and wet, mild winters influenced by its proximity to the Pacific Ocean. Eastern Washington has a Continental climate with warmer summers, colder winters, and comparatively less precipitation (Mote and Salathé 2010). The Alaska river basin, Cowee Creek, has a Temperate Rain Forest climate characteristic of higher latitudes with cold, wet winters and cool, wet summers. Precipitation in all regions occurs predominately from October to March and falls as snow or rain, depending on latitude, elevation, and proximity to the Pacific Ocean. Precipitation within all basins originates from vapor coming from the Pacific Ocean. Average climate and physical characteristics for each basin are displayed in Table 2.1.

The Snoqualmie River begins as three distinct forks in the Mt. Baker-Snoqualmie National Forest and drains 1,793 km^2 on the west side of the Cascade Range, Washington. The three forks originate in forested public land before converging and flowing through a mix of agricultural, residential, and commercial land use. On one major tributary, the Tolt River, a dam and a large reservoir exist that provide drinking water for the City of Seattle.

The Green River drains a 1,185 km^2 watershed on the west side of the Cascade Range, Washington. During the 19^{th} and 20^{th} centuries there was extensive railroad and logging activity in the upper Green River valley; however, it has now become a gated water supply for the city of

Tacoma via damming of the river at the Howard Hansen Dam. The lower portion of the river flows through downtown Seattle and is heavily modified and urbanized.

The Skagit River drains 8,163 km^2 of the western Cascade Range before emptying into Puget Sound. It originates from headwaters in southwestern British Columbia and flows southwest before meeting up with the Sauk River, which flows northwest and drains the North Cascades. Five major hydropower projects are present on the Upper Skagit its tributaries. The river experiences year-round glacial influence from numerous mountains, including Mount Baker and Glacier Peak, both of which exceed 3,200 m.

The Wenatchee River drains 3,440 km^2 of the eastern Cascades before flowing into the Columbia River. Land use is similar to that of other basins, wherein the headwaters originate in forested public lands before flowing through a mix of agricultural, residential, and commercial land use. As described above, the climate on the east side of the Cascades is drier than that of the west side; however, the prevailing westerly winds, which cross the Cascades, create temperature and precipitation patterns that vary widely across the Wenatchee basin. For example, annual precipitation on the crest of the mountains averages over 2,900 mm, the majority of which falls as snow, while eastward and at only 780 meters, the city of Wenatchee averages less than 235 mm of annual precipitation.

Cowee Creek drains 118 km^2 of the United States Forest Service Héen Latinee Experimental Forest located in the Tongass National Forest, Alaska. The watershed is approximately 15% glaciated and experiences substantial influence from three alpine glaciers (18.2-km^2) and extensive perennial snowfields. The glaciers are rapidly diminishing and loss of the cool summer discharge from glacial melt is a concern in fish habitat management. Cowee Creek is characteristic of the thousands of moderately sized watersheds that drain the Coast Mountains of

Alaska and British Columbia, and encompasses perennial snowfields, alpine meadows, spruce-hemlock forests, and extensive valley-bottom wetlands.

2.3.2 *Data collection and processing*

We collected between 31-58 spatially distributed water samples within each of our five basins in Summer 2017 during baseflow (Figure 2.1). Sampling sites within each basin were selected to include a mix of mainstem and tributary locations and to span the geographic and elevation range found within each basin. Water samples were collected within wading distance from the stream edge, but in flowing current. Samples were collected in 20 ml vials with conical plastic cap inserts to prevent evaporation, and duplicates were collected for every 20th sample.

Watersheds for each sampling point were delineated and landscape variables describing the watersheds were derived from commonly available geostatistical products (Table 2). We chose candidate covariates that were known to influence water isotope fractionation in some basins, e.g., elevation and longitude (Dansgaard 1964, Clark and Fritz 1997), as well as those that had some mechanistic basis for influencing isotopic ratios, e.g., aquifer and soil permeability (Tague and Grant 2009, Nickolas et al. 2017). Covariates examined include catchment area, mean watershed elevation (MWE), latitude, longitude, mean annual precipitation (MAP), mean annual air temperature (MAT), aquifer permeability, and soil permeability (Table 2.2).

Water isotopes were analyzed on a a Laser Absorption Water-Vapor Isotope Spectrometer (Model 908-0004, Los Gatos Research, Mountain View, CA) located at the Integrated Stable Isotope Research Facility at the Western Ecology Division of the Environmental Protection Agency, Corvallis Oregon. Oxygen and Hydrogen isotope ratios were reported as delta (δ) values and presented in parts per thousand (‰) deviation from the adopted standard representing mean isotopic composition of the global ocean (Vienna Standard Mean

Ocean Water). Measurement precision estimates (±1 standard deviation) were determined on repeated measures of both field and lab duplicates and was 0.12‰ for $\delta^{18}O$ and 0.17‰ for $\delta^{2}H$. Deuterium excess (d-excess = $\delta^{2}H - 8\delta^{18}O$; Dansgaard 1964) is a measure of the evaporative influence on water isotopes. The global meteoric water line (GMWL) has a d-excess value of 10‰, but precipitation events vary around this value. Based on d-excess variance in a 14-year record of precipitation isotopes collected in Corvallis OR, we considered samples with d-excess values below 5‰ to have been influenced by evaporation since falling as precipitation and removed those values from our analyses.

2.3.3 *Data analysis*

In all five basins, we first conducted extensive exploratory and mapping analyses to understand and display the spatial distribution of landscape attributes. We examined maps of and correlations between landscape attributes to understand the distribution and structure of predictor variables within and across watersheds. The goal of these exploratory analyses was to understand underlying collinearity between covariates that might hinder our ability to interpret statistical models.

In all five basins, we first conducted exploratory and mapping analyses to understand and display the spatial distribution of landscape covariates (Table 2.2). We examined maps of and correlations between landscape covariates to understand the distribution of and relationships between predictor variables within and across watersheds. The goal of these exploratory analyses was to understand underlying collinearity between covariates that might hinder our ability to interpret statistical models.

We then examined relationships between landscape covariates and isotope values using exploratory single variable analyses and explanatory multiple regression models. As $\delta^{18}O$ and $\delta^{2}H$ values are highly correlated (Clark and Fritz 1997), all regression analyses considered only $\delta^{18}O$ values. We used ordinary least squares regression to fit a linear model to each basin independently; the model explained variation in isotope ratios as a function of a single landscape characteristic (for the exploratory analyses) or suites of landscape characteristics (for the explanatory models). For each univariate model, we conducted a t-test to test whether or not the regression coefficient was statistically different from zero. An alpha level of 0.001 was chosen to indicate a significant relationship. A conservative cutoff was chosen because of the large quantity of statistical tests necessary to explore all potential predictors.

To identify the suite of landscape characteristics most closely associated with $\delta^{18}O$ values, we constructed a best fit multiple regression model for each basin. We selected variables in our final best-fit models using a modified forward stepwise regression where we always included MWE, if significant in the univariate model, as the first term in the models. Only predictors significant at the univariate level were additionally considered for inclusion. We did not include landscape predictors highly correlated with predictors already in the model (pairwise correlation > 0.8). To constrain the number of statistical tests, total size of each model was limited to four covariates and only main effects were examined. Covariates were individually added to the model if they reduced the RMSE more than other potential covariates, were significant at the univariate level, and increased the overall coefficient of determination (R^2). For each best-fit model, we calculated the squared Pearson correlation coefficient (R^2) and the root mean squared prediction error (RMSPE) using leave one out cross validation (LOOCV). To quantify variable importance in models with more than one covariate, we calculated the

independent effect of each covariate by comparing the fit of all models containing a particular covariate to the fit of all nested models lacking that covariate, through the process of hierarchical partitioning (Murray and Conner 2009, Walsh and Mac Nally 2013). The resulting independent effect weights represent the average contribution of each covariate to the variance in $\delta^{18}O$ values over all possible models and are an estimate of the proportion of variance in $\delta^{18}O$ values explained by each covariate.

In the Snoqualmie and Wenatchee basins, we further modeled the spatial relationship of $\delta^{18}O$ values using semivariograms and SSNMs. We chose to test the use of spatial tools in the Snoqualmie and Wenatchee as these basins are similar in size and network configuration, but differ in the amount of isotopic variation explained by covariates. Semivariograms depict how the semivariance, or average variation between measurement values separated by some distance, changes in relation to the distance separating them. Semivariograms are useful for visualizing patterns of spatial autocorrelation in the measured data and model residuals. Low semivariance values indicate that sample pairs within some distance are similar, whereas high values indicate dissimilar sample pairs. If positive autocorrelation occurs within a data set, the semivariance values are smallest at short distance lags and increase with distance. We displayed and compared two measures of distance between points: flow-connected distance (a network-based measure) and Euclidean distance (a straight-line measure). Semivariograms of the network-based distance consider only the topological distance between sites and illustrate how relationships between sites change when flow-connectedness is taken into account. Semivariograms of Euclidean distance reveal interactions or lateral connectivity between the stream network and the landscape. Semivariance was calculated using the robust estimator (Cressie 1993). We estimated the semivariogram at lag distances whose bins contained >10 site-pairs and that were less than

half the maximum flow-connected distance between sites (Zimmerman and Ver Hoef 2017). We examined semivariograms to visualize dependencies in both raw $\delta^{18}O$ values and residuals from the best-fit linear models and SSNMs. Semivariograms were compared to one another to identify scales of spatial autocorrelation (McGuire et al. 2014, Brennan et al. 2016).

The SSNMs described in Ver Hoef and Peterson (2010) extend the standard linear model as:

$$Y = X\beta + z_{TD} + z_{TU} + z_{EUC} + \epsilon \quad (2.1)$$

where Y is a vector of the response (i.e. isotope ratios), X is a matrix of predictors (i.e. covariates from Table 2.2), β is a vector of estimated coefficients, z_{TD}, z_{TU}, and z_{EUC} are the tail-down, tail-up, and Euclidean autocovariance models, and ε is a vector of independent normally distributed random errors. We followed a two-step procedure in fitting the SSNMs (Peterson and Ver Hoef 2010). First, we selected fixed effects while maintaining a constant spatial component consisting of exponential tail-up and exponential Euclidean spatial autocovariance functions. Fixed effects in our final SSNMs were selected independently of the linear model approach, but were selected according to the same process described above for best-fit linear models. Second, we used Akaike Information Criterion (AIC) to select a covariance structure while maintaining the fixed effect(s) selected in the first step. We considered models having four possible spatial components: an exponential tail-up and Euclidean covariance structure, an exponential covariance structure alone, an exponential tail-up covariance structure alone, and a nugget-only model (i.e. assuming no spatial autocorrelation). We examined the predictive accuracy using LOOCV, and calculated the R^2, AIC, and RMSPE. We also decomposed the variation explained in each model into the proportion explained by the predictors and by the covariance structure in order to examine how each component contributed to model fit. Although the SSNM framework

can include a mixture of autocovariance models based on tail-up, tail-down (i.e., based on network distance of flow-unconnected sites), and Euclidean distance, we chose to consider only tail-up and Euclidean (Steel et al. 2016, 2019). We elected to do this as isotopes move in a downstream direction and we had no reason to believe that any explanatory power achieved by using a tail-down covariance structure would reflect the underlying mechanism. All data analyses were conducted in R (http://cran.r-project.org) using the Spatial Stream Network (SSN) package (Ver Hoef et al. 2014) and Spatial Tools for the Analysis of River Systems (STARS) toolbox in ArcGIS 10.6 (Peterson and Ver Hoef 2014).

2.4 RESULTS

2.4.1 *General description and relationship with MWE*

The measured $\delta^{18}O$ and $\delta^{2}H$ values in stream water samples ranged from -16.50 ‰ to -9.37 ‰ (mean = -12.85 ‰) and from -119.93 ‰ to -66.33 ‰ (mean = -92.42 ‰) respectively. In general, the highest values were found in the Snoqualmie and Green Rivers and the lowest values in the Wenatchee River. Only three samples in our analysis had d-excess values less than 5‰. All of these samples were collected in the Snoqualmie basin from streams that drained small, stagnant ponds and were removed from further analyses. After their removal, the measured d-excess values in stream water samples ranged from 5.01 ‰ to 15.43 ‰ (mean = 10.28 ‰).

The regression models between MWE and isotopic signature displayed an inverse relationship for all basins except the Wenatchee River, which displayed no relationship (Figure 2.2). The $\delta^{18}O$-MWE slopes for the regression models using both mainstem and tributary sites were -2.5 ± 0.13 ‰ km^{-1} (R^2 =0.90) for the Snoqualmie River, -2.2 ± 0.20 ‰ km^{-1} (R^2 =0.82) for the Green River, -4.4 ± 0.66 ‰ km^{-1} (R^2 =0.49) for the Skagit River, and -1.7 ± 0.28 ‰ km^{-1} (R^2

=0.48) for Cowee Creek. For the Wenatchee River, the R^2 value was 0.05 and the $\delta^{18}O$-MWE slope was -0.4 ± 0.41 ‰ km^{-1}. In four basins, tributaries and mainstem samples fall together on the same regression, but in the Skagit River, mainstem samples have lower isotopic values for a given MWE than smaller tributaries.

2.4.2 *Landscape covariates*

The structure of landscape covariates differed dramatically across basins and impacted our ability to model $\delta^{18}O$ values as a function of landscape covariates (Figure 2.3). In the Snoqualmie and the Green basins, most landscape predictors were highly correlated with one another. For example, in the Snoqualmie basin, MWE had a correlation coefficient greater than or equal to 0.75 with all landscape predictors except area and latitude. Similarly, in the Green basin MWE had a correlation coefficient greater or equal to 0.69 with all landscape predictors except area. In the Skagit, Wenatchee and Cowee basins, correlation among landscape predictors existed, but was less extreme. In the Skagit basin, no correlation among predictors exceeded 0.75, with the exception of MAT and MWE, which were almost perfectly correlated (-0.98). Additionally, the Skagit is the only basin in which MAP and MWE were negatively correlated (Figure 2.3). The Wenatchee basin displayed the lowest average correlation among landscape predictors. Only longitude was moderately correlated (greater than 0.40) with all landscape covariates except soil and aquifer permeability. In Cowee basin, there was a tight coupling among MWE, MAP, and MAT where all correlations exceeded 0.92; however, beyond these relationships no correlation exceeded 0.55.

2.4.3 *Univariate and best fit linear models*

The direction and magnitude of relationships between $\delta^{18}O$ and $\delta^{2}H$ values and landscape covariates varied across basins (Figure 2.3). For example, in the Snoqualmie and Green basins, $\delta^{18}O$ and $\delta^{2}H$ values were highly negatively correlated with mean annual precipitation (MAP) (-0.85, -0.69 for $\delta^{18}O$ and -0.80, -0.72 for $\delta^{2}H$), while in the Skagit, Wenatchee and Cowee basins this relationship was reversed (0.86, 0.44, 0.76 for $\delta^{18}O$ and 0.87, 0.67, 0.66 for $\delta^{2}H$). We note again that the high collinearly of landscape predictors within basins made it difficult to parse apart some effects.

Best-fit models for all basins included MWE but displayed clear differences in both level of complexity and predictive accuracy. In the Snoqualmie, Green and Cowee basins, best-fit models included only MWE (Table 2.3). Calculated R^2 values were 0.90 for the Snoqualmie, 0.82 for the Green, and 0.48 for Cowee. The RMSPE for these models was 0.26, 0.36 and 0.42 ‰, respectively. In the Skagit and Wenatchee basins, on the other hand, incorporating additional predictors beyond MWE increased the amount of variance explained in our isotope data. Additional covariates included in the Skagit model were MAP, area, and aquifer permeability, while the only additional covariate included in the Wenatchee model was longitude (Table 2.3). The Skagit River, similar to other west side basins, displayed high predicative accuracy (R^2 =0.87; RMSPE=0.41 ‰) whereas the Wenatchee River displayed low predictive accuracy (R^2=0.47; RMSPE=0.42 ‰). Independent effect weights for the Skagit model shows a relatively even partitioning of variance among all predictors (I_{elev} = 21 %, I_{precip} = 33 %, I_{area}= 26 %, I_{perm}= 20 %), whereas in the Wenatchee model the majority of variation in $\delta^{18}O$ values is explained by longitude (I_{lon} = 70 %, I_{elev}= 30 %).

2.4.4 *Semivariograms and spatial stream network models*

The Snoqualmie and Wenatchee basins showed spatial dependencies for raw $\delta^{18}O$ values (Figure 2.4). For the Snoqualmie basin raw $\delta^{18}O$ values, semivariance for Euclidean distance (i.e. the straight line distance between all sites) increased rapidly and linearly before leveling off around 35 km. This change in semivariance suggests that sites beyond 35 km apart were uncorrelated, while sites closer together were more highly correlated with one another. Semivariance for flow-connected sites (i.e. the network distance between sites that share flow) for raw $\delta^{18}O$ values was generally much smaller and increased slowly with distance. Furthermore, semivariance of raw $\delta^{18}O$ values between flow-connected sites never leveled off, suggesting the presence of an unmodeled trend such as MWE. Similar patterns of semivariance were apparent in the Wenatchee basin raw $\delta^{18}O$ values, although overall values and the difference between the magnitude of Euclidean and flow-connected semivariance were both smaller. In addition, the semivariance for the Euclidean distance leveled off at around 25 km in the Wenatchee basin.

We compared model fit and variance decomposition for SSNMs with four distinct autocovariance models (Table 2.4; Figure 2.5; Figure 2.6). For the Snoqualmie basin, similar to the best-fit linear model, only MWE was selected as a fixed effect, capturing between 81-90 % of the variance in $\delta^{18}O$ values (Table 2.4; Figure 2.6). When spatial autocorrelation was explicitly accounted for by including a covariance structure in the model, the total variance explained was greater than the non-spatial model; however, between 3-9 % of the variance previously explained by the covariates was shifted onto the covariance structure (Table 2.4; Figure 2.6). The SSNM with a tail-up covariance structure outperformed all others and had the lowest AIC, RMSPE and R^2. RMSPE decreased from 0.26 ‰ in the linear model to 0.16 ‰,

similar to analytical precision (0.12 ‰), and R^2 increased from 0.90 in the linear model to 0.96 (Table 2.4). Adding a Euclidean covariance structure did not improve prediction accuracy as much as the tail-up model.

For the Wenatchee basin, longitude and MWE were again selected as fixed effects, explaining 45-47 % of the variation in $\delta^{18}O$ values, significantly less variation than in the Snoqualmie models. Spatial autocorrelation explained an additional 14-26 % of the variance not explained by covariates. Contrary to the Snoqualmie basin, models that included a Euclidean covariance structure outperformed all others and had the lowest AIC, RMSPE, and R^2, suggesting that network structure was less important in this basin (Table 2.4; Figure 2.6). Including both tail-up and Euclidean covariance structures improved the R^2 and RMSPE over the simple Euclidean model (0.71 vs 0.67 and 0.31 ‰ vs 0.33 ‰, respectively), but resulted in a nearly identical AIC value (51.67 vs. 51.24, respectively). Although the models are comparable, we selected the model with both a tail-up and Euclidean covariance structure to move forward with further analyses.

Semivariograms of spatial and linear model residuals displayed a reduction in semivariance as compared to the raw data for both basins and distance measures (Figure 2.4). This reduction suggests that by accounting for spatially structured covariates such as MWE and longitude, regression models remove some spatial autocorrelation. The decrease in semivariance between raw data and linear residuals was more pronounced for the Snoqualmie basin, whereas the decrease in semivariance between linear and spatial residuals was more pronounced for the Wenatchee basin. For both the Snoqualmie and Wenatchee basins, semivariance of spatial model residuals is relatively flat. This pattern suggests that accounting for spatial structure through SSNMs removes the majority of spatial autocorrelation in the $\delta^{18}O$ values.

2.5 DISCUSSION

2.5.1 *MWE gradient*

Although we expected MWE to be the main determinant of isotopic variation in surface water, our analysis revealed differences in surface water MWE-$\delta^{18}O$ slopes between basins based on basin size, shape and location on the windward and leeward sides of mountains. The strong elevation gradient observed in western Washington basins and Cowee Creek, all of which drain windward mountainsides, can be attributed to the rainout effect, or Rayleigh distillation (Dansgaard 1964, Clark and Fritz 1997). Storms bringing precipitation to western Washington and coastal Alaskan basins originate from the Pacific Ocean and move eastward. Continued rainout produces isotopically depleted precipitation at higher elevations, with the most depleted precipitation found at the crest. Close proximity to the Pacific Ocean exacerbates the rainout process. As the warm, wet air mass travels up the Cascade and Alaskan Coast Mountains, it experiences orographic lifting and adiabatic cooling, resulting in increased precipitation and the observed elevation trends. Similar to most other studies globally, our observed $\delta^{18}O$-MWE relationship is close to linear over the sampled elevation range for windward basins (Poage and Chamberlain 2002). The combination of processes dominantly responsible for isotopic distillation during rainout behaves linearly over much of the world; however, basin specific processes such as mixing of baseflow sources from differential geologies may contribute to differences in $\delta^{18}O$-MWE slopes and proportion of isotopic variation explained by MWE across basins.

Several studies have found global average isotopic-elevation relationships, or lapse rates for precipitation, snow, and river water between -2.1 ‰ km^{-1} and 2.9 ‰ km^{-1}, except at latitudes greater than 70° where isotopic lapse rates are higher (Bowen and Wilkinson 2002, Poage and

Chamberlain 2002, Dutton et al. 2005). In our study the Snoqualmie and Green basin δ^{18}O-MWE slopes fall within this range (-2.5 ± 0.13 ‰ km^{-1} and -2.2 ± 0.20 ‰ km^{-1}, respectively). The similar δ^{18}O-MWE slopes of the Green and Snoqualmie Rivers are likely due to the close geographic proximity of the basins and similar orientation with respect to incoming coastal weather. Additionally, MWE explains most of the variation in isotope ratios for the Snoqualmie and Green Rivers, indicating that elevation-induced rainout is the greatest control on δ^{18}O values. The higher δ^{18}O-MWE slope of the Skagit River is surprising, given its close proximity to the Green and Snoqualmie basins, but this basin has unique attributes discussed in the next section. Our observed δ^{18}O-MWE slope for Cowee Creek was lower (-1.7 ± 0.28 ‰ km^{-1}) than windward Washington basins even though MWE was the only significant driver. However, Cowee basin is small and glaciated and samples were collected over several months. This is further discussed in the next section. Even though MWE was a strong driver of isotopic variance, each windward basin responded uniquely, reiterating the importance of basin specific isoscapes.

We did not observe a large δ^{18}O-MWE slope in the Wenatchee basin, which is located on the leeward side of the Cascade Range. For leeward basins, if precipitation results from continued rainout of air masses as they traverse topographic barriers, then continued Rayleigh distillation on the leeward slope should produce an inverse relationship with altitude. Although less prevalent in the literature than windward, orographically induced rainout (Poage and Chamberlain 2001), inverse or ambiguous δ^{18}O-elevation relationships have been reported from leeward slopes in the Sierra Nevadas (Friedman and Smith 1970) and the Canadian Rockies (Grasby and Lepitzki 2002, Moran et al. 2007) for precipitation isotopes, and from the Oregon Coast Range for stream water isotopes (Brooks et al. 2012; Nikolas et al. 2017). Potential reasons for the ambiguous δ^{18}O-MWE relationship in the Wenatchee basin are threefold. First,

the amount of precipitation falling in the Wenatchee basin is lower than in west side basins (e.g. Snoqualmie MAP is 2,435 mm/year and Wenatchee MAP is 1,210 mm/year). Within this drier climate, local evaporation of surface water could add to the atmospheric vapor or subcloud evaporation could be influential, which would negate isotope depletion from the rainout effect. Previous studies have documented this dampened rainout effect (Ingraham and Taylor 1991, Guan et al. 2009, Wassenaar et al. 2009, Bershaw et al. 2012). However, we did not see the changes in d-excess expected if subcloud evaporation were significant in the Wenatchee basin. Second, although the Wenatchee samples show no systematic relationship with MWE alone, when longitude, which is a proxy for distance inland, and MWE are included together in the best-fit model, a δ^{18}O-MWE slope similar to windward basins emerges, although longitude was still the most important variable within the model. The Wenatchee basin is oriented north to south and shares a long border with the Cascade crest (Figure 2.1). Consequently, the heaviest precipitation occurs near the crest. As a vapor cloud moves eastward along the typical storm trajectory, precipitation becomes more depleted as a result of rainout. Rainout with increasing distance from the Pacific coast may counteract the less pronounced elevation gradient. Lastly, turbulent atmospheric mixing of air masses as they are forced up and over the Cascade crest may contribute to the lack of an observable δ^{18}O-MWE slope (Moran et al. 2007). More research is needed into leeward basins to distinguish among these three potential factors.

2.5.2 *Other drivers of observed isotope patterns*

The Skagit basin was unique among the windward basins in that the best-fit model included MAP, watershed area, and aquifer permeability as covariates in addition to MWE. Orientation with respect to storm path alignment and topographic features of each basin likely drive differences in the strength and slope of river ^{18}O-MWE slopes observed in windward

basins and resulted in the inclusion of MAP in the Skagit best-fit model (Scheihing et al. 2017). The Green and Snoqualmie Rivers flow northwest. The Skagit River generally flows west; however, the largest tributary to the Skagit, the Sauk, flows northwest (Figure 2.1). Due to the rain-shadowing effects of Mt. Rainier and the Olympic mountains, southwestern Puget Sound watersheds like the Green and Snoqualmie tend to receive maximum precipitation during westerly air flow, while watersheds in the northwest Puget Sound like the Skagit tend to receive maximum precipitation during west-southwesterly air flow (Neiman et al. 2011, Siler et al. 2013). As a result, precipitation and elevation gradients largely align in the Green and Snoqualmie basins, with the greatest amount of precipitation occurring at high elevations leading to strong covariation (Figure 2.3). In contrast, the greatest amount of precipitation in the Skagit basin occurs at mid elevations on the western side of the basin, including in headwaters of the Sauk and Baker Rivers. East of the mainstem Skagit dams, at some of the highest elevations in the basin, precipitation amount declines substantially due to a rain shadow effect produced by the high peaks of the Skagit Crest within the basin. Storms approaching the Skagit basin on a west-southwesterly track reach the Sauk basin first as they move inland. As they progress along their trajectory, continued rainout results in progressively more isotopically depleted precipitation. The influence of complex precipitation patterns in the Skagit basin was reflected in our data. Samples collected from the Sauk basin were systematically more isotopically enriched than samples collected from the upper Skagit basin, even at identical elevations. Additionally, in our best-fit model, MAP was positively related to $\delta^{18}O$ values, indicating that in areas of high MAP isotope ratios were more enriched. High MAP at mid elevations likely contributes to the high $\delta^{18}O$-MWE slope observed in the Skagit basin.

Basin attributes not examined within our modeling framework may influence isotope ratios. Within the Skagit River, mainstem samples displayed the lowest isotope ratios, likely indicating that the mainstem of the Skagit is fed by higher elevation source water than small tributaries (Figure 2.2). The negative relationship between watershed area and $\delta^{18}O$ values in the Skagit best-fit model reflects this, indicating that in large watersheds isotope ratios were more depleted. Glaciation in the Skagit River points to the importance of high elevation glacial and snowpack melt as a significant source of summer baseflow. Riedel and Larrabee (2016) found that surface melt from glaciers contributes 6-12% of the Skagit River's total summer runoff, and roughly twice that fraction in August and September. This same study also noted that glacial meltwater is concentrated in the tributaries Thunder Creek, White Chuck River, Suiattle River, Baker River, and Cascade River. Our Skagit River water samples showed $\delta^{18}O$ values below the average $\delta^{18}O$-MWE regression line for the outlets of the White Chuck and Suiattle Rivers and isotope ratios above the average $\delta^{18}O$-MWE regression line for the Baker and Cascade River outlets. We would expect samples to fall below the line if a greater proportion of flow originated from high-elevation glacial meltwater. The presence of glacial meltwater and snowmelt may have skewed the high elevation watersheds to lower isotopic ratios and may have contributed to the high $\delta^{18}O$-MWE slope observed in the Skagit basin.

Although the Cowee Creek basin was heavily glaciated, we did not observe the same pattern of highly depleted mainstem isotope ratios present in the Skagit basin and watershed area was not included in our best-fit model. This was surprising, as previous studies have found seasonal patterns in $\delta^{18}O$ at the outflow of Cowee Creek that are consistent with an increase in the proportion of streamflow derived from $\delta^{18}O$-depleted snow and glacial melt in higher elevation watersheds from late May into August (Fellman et al. 2014, 2015). Fellman et al.

(2015) found an average $\delta^{18}O$ ratio of -14.5‰ at the outflow of Cowee Creek across summer months (May – August) and $\delta^{18}O$ ratios below -15.0‰ through most of August, reflecting the contribution of glacial meltwater (average $\delta^{18}O$ = -16.4‰), as the winter snowpack is typically ablated by early summer. At the lowest site on Cowee Creek in our study, samples collected in late May already had values (-15.5 ‰) that were as low as those measured in late August during Fellman et al. (2015) study. The weak $\delta^{18}O$-MWE relationship in Cowee Creek could be because high elevation, glacial sources of water dominated the flow in most tributaries sampled during our study. Higher resolution temporal sampling of the area is necessary to parse these mechanisms.

Within the Snoqualmie and Green basins, all water isotopes samples fell upon a similar MWE gradient, regardless if it was a small tributary, or mainstem samples that aggregate the entire basin (Figure 2.2). The isotopic composition of river water samples is determined by water isotopes in precipitation infiltrating into mountain blocks. The subsequent stream water is a mixture of groundwater baseflows with different transit times. The tight $\delta^{18}O$-MWE coupling suggests summer baseflow derives from inputs more evenly dispersed throughout the basin, potentially because of shallow groundwater influx (i.e., as opposed to deep groundwater flowpaths or snowmelt sources). The isotopic composition of shallow groundwater does not deviate significantly from the mean weighted annual composition of precipitation in temperate climates in areas without seasonal or spatial bias in recharge (Clark and Fritz 1997, Bowen et al. 2011). In the Snoqualmie and Green basins, nearly all precipitation falls within the winter months, and previous studies have not found significant seasonal differences in precipitation isotopes ratios in the Pacific Northwestern USA (Brooks et al. 2012). Several studies find similar patterns for summer baseflow (Yeh et al. 2014, Rautio and Korkka-Niemi 2015, Singh et al.

2016). In contrast, Brooks et al (2012) found that the mainstem Willamette River, and outlets of other large rivers feeding the Willamette had isotopic values that were lower than the predicted elevation gradient relationship estimated from small watersheds, which we also found in the Skagit River. They interpreted this difference as a bias towards high elevation water sources dominating the flow within the river, likely due to deep groundwater flowpaths within the Oregon High Cascades. This suggests that the Green and Snoqualmie Rivers are much less dependent on high elevation snowmelt for summer baseflow as compared to the Cascade rivers in Oregon, and the Skagit River. Future studies should more explicitly consider the geologic context of each basin in order to understand the interaction between potentially complex ground and surface water flowpaths.

Dams, reservoirs, and lakes are pervasive across our study basins and have the potential to alter water storage and transport, thus impacting our interpretation of isotope values below these structures. In our data, we found small differences when examining isotope ratios above and below the Howard Hansen Reservoir and Lake Wenatchee. The Howard Hansen Reservoir on the Green River and the Tolt Reservoir, a similar hydropower structure in the Snoqualmie River, are operated for flood control in the winter, flow augmentation in the summer, and provide drinking water year-round. The reservoirs fill in the late winter and spring, potentially holding back winter precipitation and high elevation snowmelt and releasing it during summer low flow. However, in our data isotope ratios of water sampled above the Howard Hansen Reservoir ($\delta^{18}O$ = -11.92‰ and d-excess = 10.33) were only slightly more depleted than those sampled at the outflow ($\delta^{18}O$ = -11.03‰ and d-excess = 7.24). Conversely, isotope ratios of water sampled at the Lake Wenatchee outflow ($\delta^{18}O$ = -15.32‰ and d-excess = 11.29) were more depleted than ratios from both the inflowing Little Wenatchee ($\delta^{18}O$ = -14.09‰ and d-

excess = 11.47) and White Rivers ($\delta^{18}O$ = -14.94‰ and d-excess = 10.16), which join together to form Lake Wenatchee. The isotopic signature of the Lake Wenatchee likely reflects the long-term average of river water input which may be more depleted than isotope ratios of September river flows due to a large influx high-elevation snowmelt in Spring. Previous studies have found muted temporal isotopic variation below artificial impoundments and natural lakes, reflecting extended retention times and elevated river water mixing (Kendall and Coplen 2001, Wassenaar et al. 2011, Trinh et al. 2017). Although the retention time of water within impoundments is an important consideration when interpreting downstream isotope ratios, our results illustrate that despite the presence of extensive hydrologic modification within our basins, isotopes can preserve signals of mainstem source water dynamics.

2.5.3 *In-stream and landscape processes shape isotope values*

Ours is one of the first studies to use a class of geostatistical models, Spatial Stream Network Models (SSNM), to model stream water isotope ratios (but see Segura et al. 2019). The SSNM approach also allowed us to model spatial correlation explicitly, taking advantage of the unique topology of stream networks. Similar to studies of other ecological phenomena (Isaak et al. 2014, Brennan et al. 2016, Filipe et al. 2017), water isotopic ratios on stream networks showed substantial autocorrelation and predictive accuracy was improved by spatial models compared to non-spatial models (Bowen et al. 2011; Table 2.4; Figure 2.5). Inherent covariation in river basins can hinder statistical efforts to identify mechanistic links between landscape gradients and features of aquatic ecosystems and result in negative consequences such as inflated goodness-of-fit metrics and inflated error terms on key coefficients that may undermine model building (Lucero et al. 2011). Linear regression assumes that each measurement is independent from others and contains non-redundant information. Therefore, if measurements are spatially

autocorrelated, standard error estimates will be artificially small, tests of statistical significance will be too liberal, and estimates of R^2 will be too large (Dale and Fortin 2009, Isaak et al. 2014). SSNMs explicitly model spatial autocorrelation and therefore provide better estimates of the effect of landscape covariates on isotope ratios.

For the Snoqualmie River, incorporating an autocovariance function accounting for the branching river network structure resulted in modest improvements to model performance. Most variation in $\delta^{18}O$ values was already explained by MWE, which is spatially-structured, resulting in little residual variation or autocorrelation (Table 2.4; Figure 2.5). However, the best-fit model did include a tail-up component, illustrating the importance of passive longitudinal transport of water isotopes along stream networks. The dominance of MWE in the model likely occurs in part due to the structure of landscape covariates in the Snoqualmie River. Most landscape predictors known to drive isotope ratios were highly correlated with one another, and the influence on isotope ratios aligned in the same direction (e.g. MWE and longitude were positively correlated). In basins such as the Snoqualmie, where covariates covary strongly and the subsequent relationship between water isotopes and covariates is simple, spatial models only slightly improve our understanding of river water isoscapes.

In the Wenatchee River, on the other hand, incorporating spatial structure in Euclidean space dramatically improved model performance. The role of covariates in the Wenatchee models were limited, with fixed-effects explaining only 47% of variation in non-spatial models and 45-49% of the variation in spatial models. Approximately two-thirds of the variance in the best-fit SSNM could be attributed to fixed effects and one-third to spatial structure in the Wenatchee model residuals (Table 2.4). The strong Euclidean component in the Wenatchee best-fit model, illustrated by the large proportion of variation explained in Figure 2.6, suggests that

linear relationships with longitude and MWE were insufficient to describe landscape processes influencing stream water isotope values (McGuire et al. 2014, Zimmerman and Ver Hoef 2017). Landscape features affecting isotope ratios could include local geological features associated with groundwater upwelling, beyond the general descriptor of aquifer permeability. Previous studies have shown that geologic features, such as porous lava flows, sandstone, and earthflows, and hillslope characteristics (e.g. slope and roughness) can influence baseflow isotopic composition (Nicolas et al. 2017, Singh et al. 2016; Segura et al. 2019). Furthermore, in the Wenatchee basin landscape covariates display little correlation with one another and often align in opposing directions (e.g. MWE and longitude were negatively correlated). These competing forces likely work against each other to create a complex isotopic landscape that is difficult to model using standard linear models. In basins such as the Wenatchee, where the influence of covariates on isotope signature is weak and covariates display little correlation with one another, including spatial structure provided insight about the presence of key structuring processes that were unaccounted for in our covariate selection.

2.5.4 *Study limitations*

As in any study, our ability to generalize results and make inferences about other watersheds is limited by our sampling design, dataset, and the models considered. In this study, water sample collection locations were limited to areas easily accessed by roads, and collection of samples across a large portion of the Upper Skagit basin into Canada did not occur. Increased spatial coverage would improve predictions of drivers of isotope ratios and allow us to consider a greater number of predictors in our analyses. Additionally, although we considered five basins across a single sampling season (summer low flow, 2017), only one basin was located on the leeward side of mountains.

Although our snapshot in time provides a picture of drivers of the isotope ratios during baseflow, it does not give insight into temporal variation in drivers of isotope signature. Several studies have found differences in drivers of isotope patterns across time (Liu et al. 2004, Payn et al. 2012), and therefore our results should not be generalized to other seasons. It should also be noted that while sampling of the Washington basins took place over no more than two weeks, Cowee Creek was sampled over the course of three months due to logistical challenges in accessing its remote sites by aircraft. Lastly, it is important to recognize that SSNMs are an extension of linear regression and both methods predict at unsampled locations using smoothed averages. Therefore, when we generated isoscapes, features not included in our sampling design (e.g. local point sources of groundwater) were not included.

2.5.5 *Management implications*

Our study summarizes current knowledge of basin factors driving variability in surface-water isotope ratios and provides a foundation for future monitoring work as well as for leveraging the isotopic signature of surface water in river basins and fisheries management. We observed a strong MWE gradient across all rivers draining windward basins. Furthermore, in the Snoqualmie and Green basins MWE was highly correlated with other parameters known to drive isotopic ratios. In these basins, these simple MWE-based relationships permit easy interpretation of isotope data. Future work could harness the information they contain for river basin management, such as predicting the contribution of climate sensitive, high-elevation snowmelt to summer baseflow. Changes to climate and hydrology are expected across the Pacific Northwest. Climate models predict substantial winter warming, leading to increased precipitation falling as rain and decreased snowpack, translating to increased winter river runoff and reduced summer

baseflow discharge (Elsner et al. 2010). Measuring water stable isotopes would be a simple method for monitoring these changes over time.

Impacts of global change will be heterogeneous both within river basins and across the region, and understanding how high elevation water contributes to stream discharge across basins will be a valuable tool (Steel et al. 2019). For example, all basins in this study host populations of ESA-listed salmonids, which are limited by high summer temperatures and low flows. Resource managers could easily access and plot covariate data such as MWE, longitude, and MAP to determine in which basins these covariates are correlated, suggesting an easy to interpret isotope-MWE relationship. The same simple isotope-MWE relationship could also be applied to other midlatitude mountain ranges with prevailing westerly winds and a north-south orientation, such as the Sierra Nevada, the southern Alps, and the southern Andes (Siler et al. 2013).

For Cowee Creek and the Skagit River, interpretation of water isotope monitoring within the basins becomes more challenging. In the Cowee basin the $\delta^{18}O$-MWE slope was much lower than expected. Temporal isotopic variance at the outlet may indicate the dominance of glacial sources over time, and we sampled over a period of high glacial output. However, additional sampling over a more condensed time period would be necessary for accurate interpretation. In the Skagit Basin interpretation of isotopic variation is difficult, as the orographic rainout process becomes complicated by the complex topography and sampling in the upper basin was limited. In basins with similar accessibility issues, accurate isoscapes could help in monitoring the proportion of streamflow derived from glacial and snowmelt and relieve some of the burden of expensive field campaigns.

Our results provide guidance for future monitoring or research on stable isotopes in surface waters. In the basins described above, with expected simple and strong relationships between MWE and isotope values, fewer samples may be necessary to create customized and effective models or management tools. In larger basins or in areas where complex local atmospheric or hydrologic processes occur, greater temporal and spatial sampling may be necessary in order to partition water sources in ways that are both isotopically distinct and environmentally relevant.

Our study also provides guidance for understanding the types, advantages, and disadvantages of methods for stream isoscape generation. We found that in basins where correlation between covariates and isotope ratios is weak, spatial models can improve predictions and demonstrate evidence of landscape level patterns not captured by non-spatial models. We also found that in basins where covariates known to influence isotope signature correlate strongly with one another and are themselves highly spatially structured, spatial models do little to improve predictions. The choice to use spatial or non-spatial models should be determined by data availability and the relevant questions. Our results provide insight as to where the additional effort to build these models may be a particularly good investment.

2.5.6 *Conclusions*

In this study we demonstrated that elevation was the dominant predictor of isotope ratios across five Pacific Northwest basins, but the importance of elevation varied between basins and depended on geographic location, landscape attribute configuration, and basin size. Elevation explained a range of the isotopic variation in surface water across the five basins, but the nature of this relationship (δ^{18}O-MWE slope, other covariates) was different even between adjacent basins. Incorporating spatial structure though the SSNM framework captured aspects of water

isotopic variation even in basins where variance explained by covariates was high. Spatial structure was particularly important to consider in the Wenatchee, our leeward side basin, where covariates explained the least of the isotopic variation. Our results illustrate that basin-specific models that include spatial structure improve accuracy of surface-water isoscapes for understanding hydrologic function, interpreting source contributions downstream, or assisting in basin management.

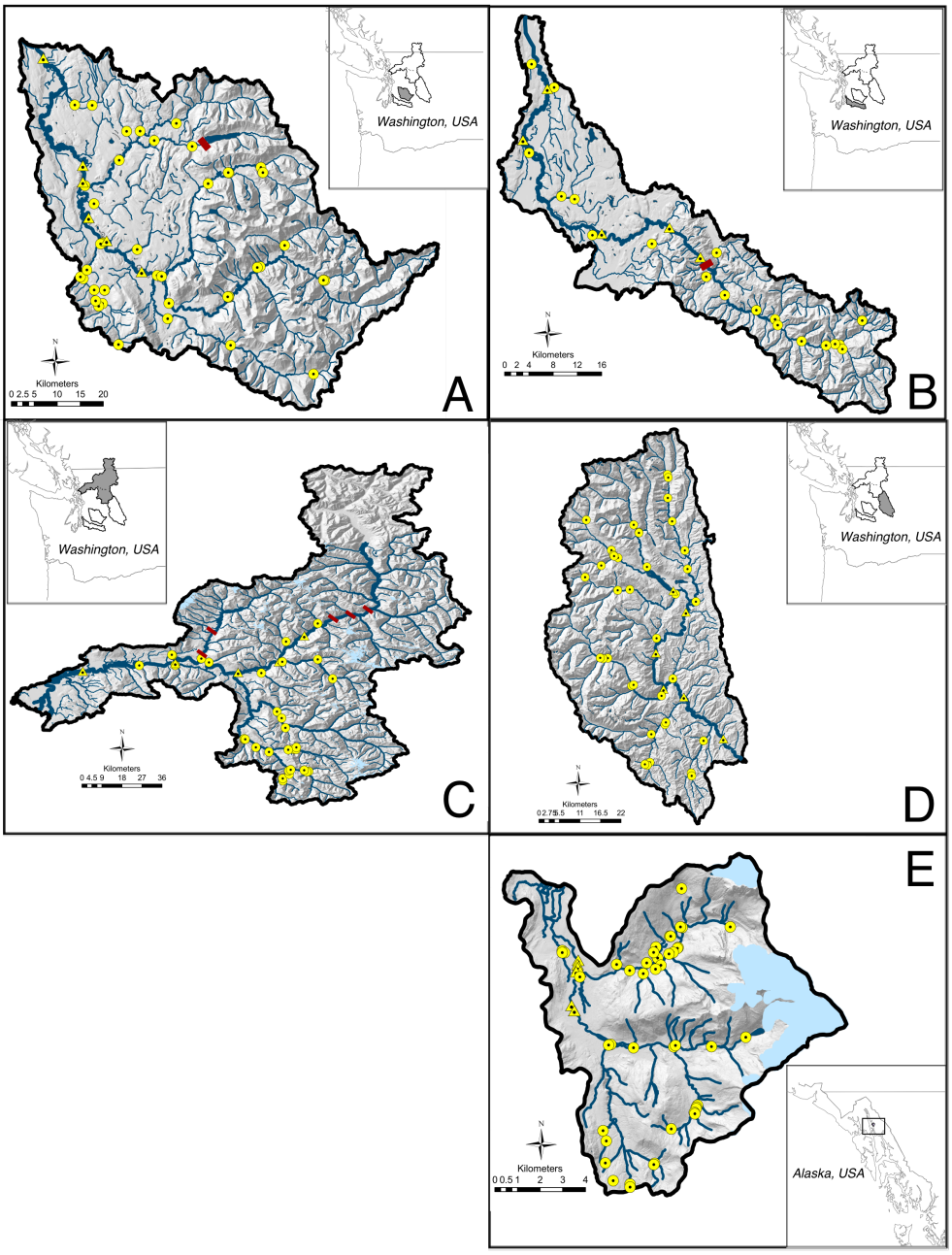

Figure 2.1. Geographic locations of study basins, the Snoqualmie (A), Green (B), Skagit (C), and Wenatchee (D) Rivers in Washington and Cowee Creek (E) in southwestern Alaska. Between 31-58 water samples were collected within each basin ($n_{Snoqualime}$ = 58, n_{Green} = 31, n_{Skagit} = 38, $n_{Wenatchee}$ = 44, n_{Cowee} = 38) and are shown in yellow. Red points indicate a major dam and blue shading indicates an ice mass.

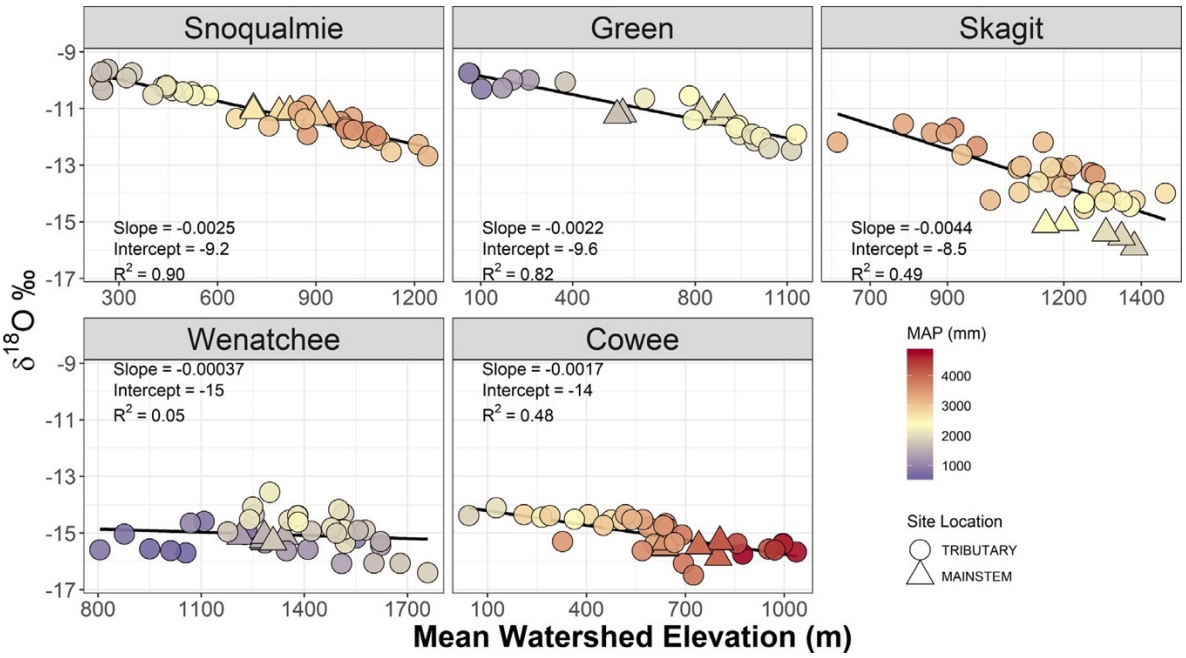

Figure 2.2. Regressions of $\delta^{18}O$ values with mean watershed elevation for samples collected during summer low flow for each basin. Lines represent the least squares relationships. Triangle points are mainstem sites and circle points are tributary sites. Points are colored according to the mean annual precipitation (MAP) within the upstream watershed.

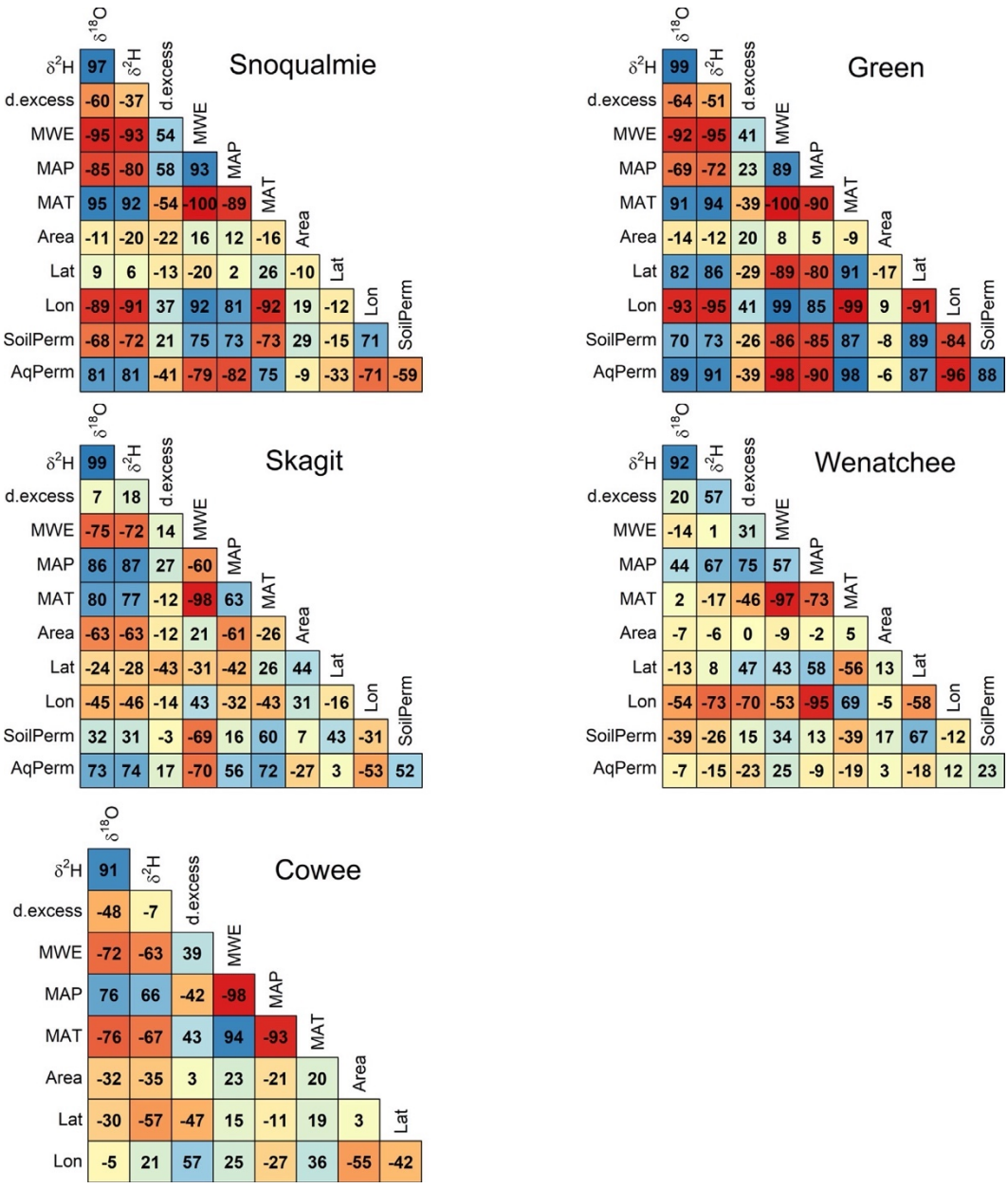

Figure 2.3. Correlation matrices for the Snoqualmie, Green, Skagit, and Wenatchee Rivers, and Cowee Creek. Both isotope metrics and landscape covariates are included. Red indicates a negative correlation between two variables, and blue indicates a positive correlation. The darker the color, the stronger the correlation. See Table 2 for a description of covariates.

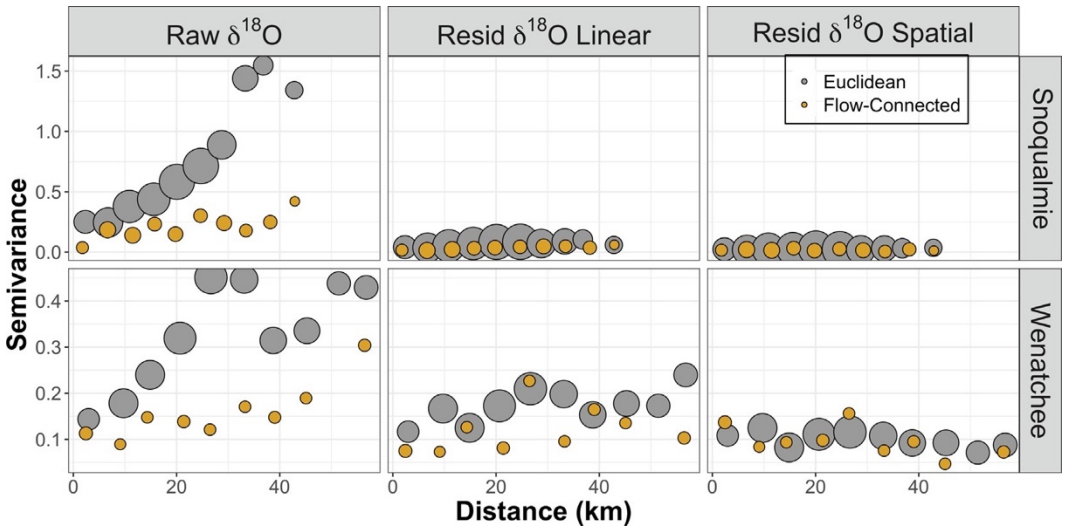

Figure 2.4. Semivariograms for raw δ18O values, residual δ18O values from the best-fit linear models, and residual δ18O values from the best-fit SSNMs for the Snoqualmie and Wenatchee basins. Circles are proportional to the number of sites used to estimate each bin value.

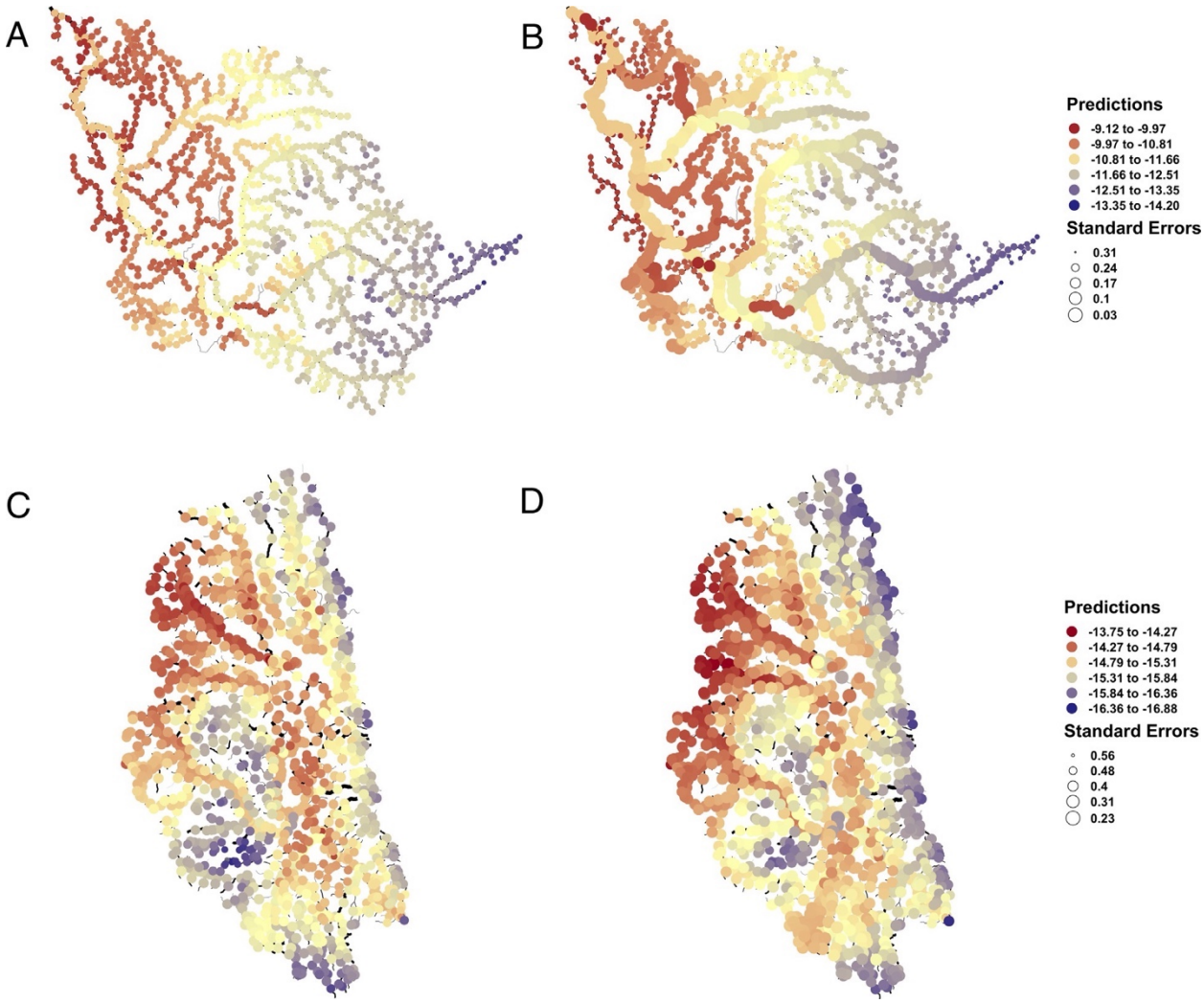

Figure 2.5. Isoscapes from the Snoqualmie best-fit linear model (A), Snoqualmie best-fit SSNM (B), Wenatchee best-fit linear model (C), and Wenatchee best-fit SSNM (D). Colors represent predicted δ18O values and the size of each point is inversely proportional to the prediction standard error.

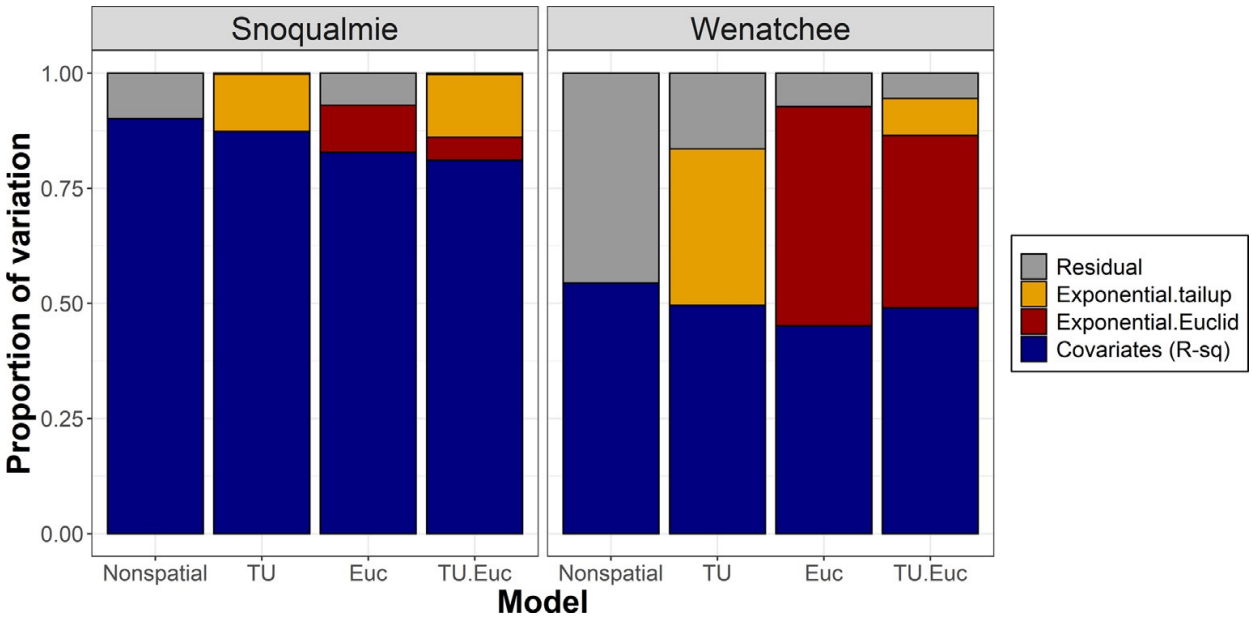

Figure 2.6. Variance decomposition into the proportion of variation explained by covariates (blue), tail-up covariance structure (yellow), Euclidean covariance structure (red), and the nugget (gray) for each of the SSNMs (categories on the x-axis) in the Snoqualmie and Wenatchee basins. TU = tail-up; Euc = Euclidean; TU.Euc = tail-up and Euclidean.

Table 2.1. Climate and physical characteristics for each basin.

		Snoqualmie	Green	Skagit	Wenatchee	Cowee
Mean Annual Temperature (C°)	Mean	8.16	8.25	6.36	6.15	1.76
	Maximum	11.55	11.84	10.68	11.13	5.09
	Minimum	1.77	4.04	-0.22	-0.12	-0.38
Mean Annual Precipitation (mm)	Mean	2,435	1,810	2,154	1,210	3,568
	Maximum	4,304	2,727	4,948	2,940	4,792
	Minimum	1,102	925	711	232	1,792
Elevation (m)	Mean	629	580	946	1,087	638
	Maximum	1,876	1,500	3,283	2,390	1,791
	Minimum	8	5	1	194	1
Basin Size (km^2)		1,793	1,185	8,163	3,440	118

Table 2.2. List of covariates considered for inclusion in each model. Here, "watershed" indicates the upstream area draining to a sample.

Covariate	Abbreviation	Description	Unit	Data Source
Elevation	MWE	Mean watershed elevation	m	NED DEM model
Mean Annual Precipitation	MAP	Mean watershed 30-year average (1981-2010) annual normal precipitation	mm	PRISM Climate Group, EPA StreamCat (Hill et al. 2015)
Mean Average Air Temperature	MAT	Mean watershed 30-year average (1981-2010) annual mean air temperature	C°	PRISM Climate Group, EPA StreamCat (Hill et al. 2015)
Area	Area	Log transformed watershed area	log(km^2)	NED DEM model
Latitude	Lat	Latitude of watershed centroid	degree	
Longitude	Lon	Longitude of watershed centroid	degree	
Soil Permeability	SoilPerm	Mean watershed soil permeability	cm/hour	STATSGO, StreamCat (Hill et al. 2015)
Bedrock Permeability	AqPerm	Mean watershed bedrock permeability	dimensionless; 1-7 based on lithology	USGS Hydrologic Landscape Regions (Wolock et al. 2004)

Table 2.3. Best fit linear models from the Snoqualmie, Green, Skagit, Wenatchee, and Cowee basins. The independent effect weight is the percentage of explained variance by each covariate.

Basin	Covariates	Covariate Coefficient (SE)	Independent Effect Weight (%)	R^2	RMSPE
Snoqualmie	MWE	-0.0025 (0.00013)	100	0.90	0.26
Green	MWE	-0.0022 (0.00020)	100	0.82	0.35
Skagit	MWE	-0.0018 (0.00051)	21	0.87	0.38
	MAP	0.00095 (0.00021)	33		
	Area	-0.00015 (0.000041)	26		
	Aquifer Permeability	0.40 (0.14)	20		
Wenatchee	Longitude	-2.99 (0.44)	70	0.47	0.42
	MWE	-0.0016 (0.00034)	30		
Cowee	MWE	-0.0017 (0.00028)	100	0.48	0.41

Table 2.4. Model fit statistics from SSNMs in the Snoqualmie and Wenatchee basins. Variance component values are the percentage of variance explained by fixed effects (covariates) and spatial error. Models in bold were selected as the best fit models.

	Model	Covariate	Covariate Coefficient (SE)	RMSPE	AIC	R^2	Variance Component	
							Fixed effects (%)	Spatial error (%)
Snoqualmie	Nugget	MWE	-0.0025 (0.00013)	0.26	25.80	0.90	90	-
	Tail-up	**MWE**	**-0.0026 (0.00015)**	**0.16**	**-5.97**	**0.96**	**87**	**9**
	Euclid	MWE	-0.0025 (0.00017)	0.23	19.35	0.89	83	6
	Euclid + Tail-up	MWE	-0.0026 (0.00019)	0.17	-4.18	0.96	81	15
Wenatchee	Nugget	Longitude	-2.99 (0.44)	0.42	61.07	0.47	47	-
		MWE	-0.0016 (0.00034)					
	Tail-up	Longitude	-3.24 (0.52)	0.37	53.29	0.61	45	16
		MWE	-0.0016 (0.00037)					
	Euclid	Longitude	-3.22 (0.58)	0.33	51.24	0.67	42	24
		MWE	-0.0013 (0.00033)					
	Euclid + Tail-up	**Longitude**	**-3.73 (0.62)**	**0.31**	**51.67**	**0.71**	**45**	**26**
		MWE	**-0.0015 (0.00034)**					

Chapter 3. SPATIOTEMPORAL DYNAMICS OF WATER SOURCES IN A MOUNTAIN RIVER BASIN INFERRED THROUGH Δ2H AND Δ18O OF WATER

A version of this paper is published as: *McGill, L.M., Brooks, J.R., Steel, E.A. 2021. Spatiotemporal dynamics of water sources in a mountain river basin inferred through δ2H and δ18O of water, Hydrological Processes. DOI: 10.1002/hyp.14063*

3.1 ABSTRACT

In mountainous river basins of the Pacific Northwest, climate models predict that winter warming will result in increased precipitation falling as rain and decreased snowpack. A detailed understanding of the spatial and temporal dynamics of water sources across river networks will help illuminate climate change impacts on river flow regimes. Because the stable isotopic composition of precipitation varies geographically, variation in surface water isotope ratios indicates the volume-weighted integration of upstream source water. We measured the stable isotope ratios of surface water samples collected in the Snoqualmie River basin in western Washington over June and September 2017 and the 2018 water year. We used ordinary least squares regression and geostatistical Spatial Stream Network models to relate surface water isotope ratios to mean watershed elevation (MWE) across seasons. Geologic and discharge data was integrated with water isotopes to create a conceptual model of streamflow generation for the Snoqualmie River. We found that surface water stable isotope ratios were lowest in the spring and highest in the dry, Mediterranean summer, but related strongly to MWE throughout the year. Low isotope ratios in spring reflect the input of snowmelt into high elevation tributaries. High summer isotope ratios suggest that groundwater is sourced from low elevation areas and

recharged by winter precipitation. Overall, our results suggest that baseflow in the Snoqualmie River may be resilient to predicted warming and subsequent changes to snowpack in the Pacific Northwest.

3.2 INTRODUCTION

Climate change is projected to alter river hydrology across the Pacific Northwest. Within this region, the majority of precipitation occurs between October and March. Winter hydrology is therefore governed by the timing and form of precipitation, and summer hydrology is governed by snowpack melt and groundwater discharge. Seasonal asynchrony between precipitation largely occurring during winter and summer water demand makes water supplies scarce and vulnerable (Jaeger et al. 2013). Climate models predict an exacerbation of this vulnerability (Elsner et al. 2010, Hamlet et al. 2010). Substantial winter warming will lead to increased precipitation falling as rain, decreased amount and earlier onset of snowmelt, and increased evapotranspiration (Stewart et al. 2005, Nolin and Daly 2006).

Pacific Northwest rivers with both significant winter rain and spring snowmelt, referred to as transient basins, are particularly climate sensitive and expected to experience substantial changes in the timing of runoff and stream flow (Wu et al. 2012, Vano et al. 2015). However, the impacts of climate induced changes to seasonal streamflow will be mediated by subsurface drainage processes that translate water inputs into streamflow, such as the capacity for the landscape to retain and release precipitation as groundwater. Although several studies have predicted future streamflow based on climate mediated shifts in precipitation and snowpack regimes, few have highlighted the role of underlying geology in controlling hydrologic responses to climate change (Tague and Grant 2004, 2009, Mayer and Naman 2011, Safeeq et al. 2013). Furthermore, much of river management occurs at localized scales, and therefore demands an

understanding of within basin spatial patterns of climate and geologic influence on streamflow processes. To identify streamflow vulnerability in a changing climate, approaches that take into account both climatic and geologic controls on water source are needed.

Previous approaches used to understand and assess climate risk have predominately relied on large, physically based runoff models coupled with general circulation models or statistical hydrologic classification schemes based on physical attributes or discharge metrics. Coupled climate-hydrology models have the benefit of simulating hydrologic processes under multiple climate scenarios and explicitly forecasting future hydrographs; however, many either do not explicitly simulate streamflow contributions from deep groundwater or approximate deep groundwater by extended soil profiles (Vano et al. 2010, Wenger et al. 2010). This can underestimate or inaccurately characterize groundwater contribution to streamflow and bias subsequent estimations of streamflow vulnerability (Safeeq et al. 2014). Statistical hydrologic classification approaches either classify locations according to attributes describing interactions of climate, geomorphology, and geology (Tague and Grant 2004, Wigington et al. 2013, Safeeq et al. 2014) or utilize emergent properties of discharge time series (Wolock et al. 2004, Olden et al. 2012, Reidy Liermann et al. 2012). Limitations of classification include poor data quality (e.g. soil and bedrock geology), incomplete understanding of hydrologic processes (e.g. groundwater–surface water connectivity), limited spatial coverage of stream gauges mostly restricted to large, downstream tributaries, and variable quality and quantity of discharge data available for each gauge (Kennard et al. 2009, Ruhi et al. 2018). Although physically based hydrology models and hydrologic classification provide a useful framework for expected streamflow behavior and advance our ability to make predictions in unmonitored catchments, additional tools for understanding future streamflow will help address uncertainty around these approaches. For

example, an understanding about spatial and temporal dynamics of where water originates in a basin will inform mechanisms of runoff generation and aid in predictions of where and how streamflow patterns are likely to shift.

A number of studies have used spatial variation in stable isotopes of input precipitation (Bowen et al. 2011) or in surface water across a basin (Brooks et al. 2012, Nickolas et al. 2017) to draw insights about variation in river water sources throughout the year. Water stable isotope ratios exhibit systematic spatial and temporal variation resulting from the process of isotope fractionation that accompanies water cycle phase changes and diffusion (Gat 1996, Araguas-Araguas et al. 2000). An example of this process is the Rayleigh rainout effect, wherein progressive isotopic depletion of a vapor cloud occurs as it moves along its storm trajectory. Rayleigh rainout occurs because heavy isotopes preferentially fall as precipitation (Dansgaard 1964, Clark and Fritz 1997). As a result, both precipitation and surface water isotopic ratios of oxygen and hydrogen, expressed as $\delta^{18}O$ and $\delta^{2}H$, are highly correlated with changes in elevation, latitude, and longitude (Ingraham and Taylor 1986, Yonge et al. 1989, Dutton et al. 2005, Lechler and Niemi 2011), although the strength and presence of these relationships can vary among river basins due to local processes such as evaporation (Bowen and Good 2015).

Previous work has shown that river water isotopes in windward basins draining the Cascade Range display a strong elevation gradient (Brooks et al. 2012, McGill et al. 2020). Here we explore how this elevation gradient can be used to understand how various portions of the watershed contribute to flow seasonally throughout a mid-size river basin and what the implications of source variation are for river flow dynamics in the future. We aim to understand potential watershed vulnerability to changes in precipitation type, timing, and location through understanding how water sources change seasonally and impact water supply across one river

network. Specifically, our objective was to characterize spatial and temporal isotopic variation of surface waters within the Snoqualmie River, Washington to understand the vulnerability of river flow to source water dynamics across space and time. To complete this objective, we (1) measured and modeled surface isotope ratios across a network of sampling stations throughout the year, and (2) developed a conceptual framework of streamflow generation to understand how changing water storage reservoirs (e.g. snow and groundwater) contribute to streamflow.

3.3 METHODS

3.3.1 *Study site*

The Snoqualmie River drains a 1,813 km^2 watershed on the west side of the Cascade Range, Washington (Figure 3.1). Major tributaries to the Snoqualmie River are the North Fork, Middle Fork, South Fork, Tolt River, and Raging River (Table 3.1). Headwaters lie primarily in forested public land. After the convergence of the North, Middle, and South Fork Rivers, the Snoqualmie River flows over Snoqualmie Falls then runs through a wide floodplain dominated by agricultural, residential, and commercial land use. The Snoqualmie River is home to ecologically and economically important runs of Coho, Chinook, pink, chum and steelhead salmon, including Endangered Species Act (ESA) listed Chinook and steelhead salmon. A dam and reservoir on the Tolt River provide approximately 30% of Seattle's drinking water.

The Snoqualmie River has a humid Mediterranean climate with dry summers and wet, mild winters influenced by its proximity to the Pacific Ocean (Figure 3.2). Precipitation occurs predominately from October to March. Precipitation isotope patterns were inferred from a 15-year record of precipitation isotopes collected in Corvallis, Oregon from 2003 to 2018 that represents the only available long-term precipitation stable isotope time series in a location with a similar climate to the Snoqualmie basin. Precipitation weighted means of weekly precipitation

isotopes do not show evidence of variation with season (ANOVA P> 0.1), although summer precipitation values are characterized by the lowest values of d-excess. The coldest month is typically January, whereas the warmest is July. The Snoqualmie River has a mixed rain-snow hydrology, with both substantial winter rain and spring snowmelt. The strong elevational temperature gradient controls the phase of precipitation. Areas of the basin below 300 m receive winter rain, while seasonal snow accumulates in areas above 900 m (Jefferson 2011). Intermediate elevations (300-900 m) are occupied by a transient snow zone, where snow falls and melts more than once per winter (Table 3.1).

Geology of the Snoqualmie River basin includes parts of two major physiographic provinces: the Puget Lowland and the Middle Cascade Range (Buffington et al. 2003; Figure 3.1). In the lowland portion of the watershed, geology and topography are primarily products of repeated continental glaciations. Glacial and interglacial deposits underlay the Snoqualmie and Tolt Valleys (Bethel 2004). In the alpine area, much of the ground surface is directly underlain by bedrock, and the bedrock units do not contain significant fracture systems (Debose and Klungland 1964, Nelson 1971, Goldin 1973, 1992, Turney et al. 1995).

3.3.2 *Data collection*

We collected water samples across 49 sites within the Snoqualmie River basin during June 2017, September 2017, November 2017, February 2018, May 2018, June 2018, and September 2018 for a total of 364 samples (Figure 3.1). Sampling dates represent five major hydrologic periods: fall wet-up (November), winter wet period (February), spring snowmelt (May), early summer (June), and summer baseflow (September). Sampling sites within the basin were selected to include a mix of mainstem and tributary locations and to span the elevation range found within the basin. We also collected biweekly water samples at the outlet of each

major tributary and the Snoqualmie mainstem for a total of 181 samples (Figure 3.1). Sampling sites were selected to coincide with a long-term water temperature monitoring program described in Steel et al. 2016. Seasonal samples were collected to understand basin-scale patterns in isotope ratios throughout the year whereas biweekly samples were collected to understand fine scale temporal patterns of source water change within each major tributary. Water samples were collected within wading distance from the stream edge, but in flowing current. Samples were collected in 20 ml vials with conical plastic cap inserts to prevent evaporation, and duplicates were collected for every 20th sample.

Water isotopes analysis was performed on a Laser Absorption Water-Vapor Isotope Spectrometer (Model 908-0004, Los Gatos Research, Mountain View, CA) located at the Integrated Stable Isotope Research Facility at the Pacific Ecosystems Systems Division of the Environmental Protection Agency, Corvallis, Oregon. Samples were run under high precision analysis mode using a 10 μL syringe for a total of six injections per sample, with the first three discarded to eliminate memory effects. All δ^2H and δ^{18}O values were expressed relative to Vienna-Standard Mean Ocean Water (V-SMOW) using δ notation:

$$\delta^2 H \text{ or } \delta^{18} O = \frac{R_{sample}}{R_{standard}} - 1 \quad (3.1)$$

Where R is the ratio of ^{2}H to ^{1}H atoms or ^{18}O to ^{16}O atoms and the standard V-SMOW. Values were reported in parts per thousand (‰) by multiplying by 1,000. Samples were calibrated to the VSMOW-SLAP scale using three laboratory standards spanning the range of sample values and calibrated annually to the IAEA certified standards. In addition, a separate QC standard was used to independently check the calibration and determine accuracy. Accuracy was 0.06 ± 0.11 ‰ for δ^{18}O and 0.1 ± 0.27 ‰ for δ^2H over the sample sets analyzed for this study. Measurement precision estimates (± 1 standard deviation) were determined on repeated

measures of both field and lab duplicates and were 0.11 ‰ for $\delta^{18}O$ and 0.25 ‰ for $\delta^{2}H$. Samples that experienced significant evaporation prior to sample collection (e.g., water impounded by beaver ponds) may not reflect the spatial pattern of input precipitation and so were removed from analysis. Based on d-excess variance in Corvallis precipitation isotope data, we removed 14 samples with d-excess values below 5 ‰, all in low gradient rivers sampled in spring and summer.

Watersheds for each sampling point were delineated and landscape variables describing the watersheds were derived from commonly available geostatistical products. Watershed area and mean watershed elevation (MWE), watershed relief, and proportion of area above 900 m were calculated using the National Elevation Dataset, a 30-meter resolution digital elevation model (Gesch et al. 2018). Mean watershed 30-year average mean annual precipitation (MAP) and precipitation weighted mean elevation for the period 1981-2010 were calculated (Hill et al. 2016). Geologic information was collected from the Washington DNR Division of Geology and Earth Resources (Frizzell et al. 1984, Yount and Gower 1991, Tabor et al. 1993). Detailed lithology of the Snoqualmie basin was summarized into three major groups, bedrock, glacial, and recent lithology, based on the classification scheme of Bethel (2004). Precipitation, snow water equivalent (SWE), and air temperature were collected from four Snowpack Telemetry (SNOTEL) stations within or extremely close to the Snoqualmie basin (US Department of Agriculture 2020). We obtained daily annual streamflow data from the U.S. Geologic Survey (USGS, 2001) and the King County Hydrologic Information Center for 11 sites within the Snoqualmie basin having data for the 2017 and 2018 water year (Figure 3.1).

3.3.3 *Analysis*

Two modeling approaches were used to understand how the relationship between MWE and stream water isotope ratios varied through time. We first used ordinary least squares regression to fit a linear model with MWE to $\delta^{18}O$ and $\delta^{2}H$ for each month separately, and then with month as a factor to determine if slopes were statistically different from one another. Slopes, intercepts, and R^2 values were compared among models. We further modeled the spatial relationship between $\delta^{2}H$ and MWE using a class of geostatistical models, spatial stream network models (SSNMs), which account for spatial dependencies across stream networks (Ver Hoef and Peterson 2010). As $\delta^{18}O$ and $\delta^{2}H$ values are highly correlated (Clark & Fritz, 1997), SSNM regression analyses considered only $\delta^{2}H$ values. SSNMs are similar to conventional linear mixed models in that the deterministic mean of the dependent variable is modeled as a linear function of explanatory variables; however, the assumption of independent errors is relaxed and an autocovariance model is used to account for spatial autocorrelation in the errors (Ver Hoef et al. 2006, Peterson and Ver Hoef 2010, Ver Hoef and Peterson 2010). We compared slopes and variance decomposition results from these SSNMs.

We also visualized spatial autocorrelation in model residuals using semivariograms. Semivariograms depict how semivariance, or average variation between measurement values separated by some distance, changes in relation to the distance separating them. Low semivariance values indicate that sample pairs within some distance are similar, whereas high values indicate dissimilar sample pairs. We displayed and compared two measures of distance between points: flow-connected distance (a network-based measure) and Euclidean distance (a straight-line measure). Semivariance was calculated using the robust estimator (Cressie 1993). We estimated the semivariogram at lag distances whose bins contained greater than 10 site-pairs

and that were less than half the maximum flow-connected distance between sites (Zimmerman and Ver Hoef 2017). We examined semivariograms to visualize dependencies in residuals from linear models that include MWE as a covariate. Semivariograms were compared to one another to identify scales of spatial autocorrelation (McGuire et al. 2014, Brennan et al. 2016).

We also examined the relationship between streamflow, geology, and water source. For each streamflow gaging station, we calculated two streamflow statistics based on the period of record to characterize individual stream hydrology: unit discharge at baseflow and baseflow index. Unit discharge, or specific discharge, was calculated by dividing average streamflow for the month of September by the upstream contributing area for each gage location (Tague and Grant 2004, Floriancic et al. 2019). Baseflow index is the ratio of annual baseflow to total streamflow and it represents the contribution of groundwater to river flow (Smakhtin 2001, Beck et al. 2013). Baseflow unit discharge and baseflow index were calculated for both the 2017 and 2018 water years. For each streamflow gaging station, we also identified the seasonal isotope sampling location closest to each site and calculated two isotope statistics to characterize water source: water source variability and baseflow isotope value. Water source variability is the standard deviation of all δ^2H values from a site and reflects how water sources shift throughout the year (δ^2H_{SD}). Baseflow isotope value is simply the September δ^2H value from a site, which varies with the mean elevation of source water at that time and place. Water source variability was calculated as one value across our sampling period, whereas the baseflow isotope value was calculated separately for September 2017 and 2018. We examined the relationship between baseflow index and water source variability and baseflow unit discharge and baseflow isotope value and the relationships between generalized geology, unit discharge, and baseflow index for each gage site.

All data analyses were conducted in R (http://cran.r-project.org) using the Spatial Stream Network (SSN) and lfstat packages (Koffler et al. 2013, Ver Hoef et al. 2014) and the Spatial Tools for the Analysis of River Systems (STARS) toolbox in ArcGIS 10.6 (Peterson and Ver Hoef 2014).

3.4 RESULTS

3.4.1 *General patterns in isotope ratios*

Drainage areas of seasonal sampling sites ranged in size from 3-1780 km^2. Surface water isotope ratios for all seasonal samples within the Snoqualmie ranged from -13.7 to -8.7 ‰ for $\delta^{18}O$ and from -98.4 to -63.9 ‰ for δ^2H over the sampling period (Figure 3.3).

Samples with d-excess values substantially below 10 ‰ have been likely influenced by evaporation since falling as precipitation. Most surface water samples fell on the Global Meteoric Water Line (GMWL) indicating no evaporative influence (Figure S3.1). D-excess values ranged from -3.75 ‰ to 14.74 ‰ over the course of the year. Low elevation sites, such as those found in the Raging, Tolt, and Mainstem Snoqualmie tended to have the lowest d-excess values, regardless of season.

3.4.2 *Relationship between isotope ratios and MWE*

$\delta^{18}O$ and δ^2H of water decreased linearly with MWE, although the strength of the relationship is stronger for $\delta^{18}O$. R^2 values from regressions of seasonal samples for individual months range from 0.77 to 0.87 for $\delta^{18}O$ and from 0.71 to 0.82 for δ^2H (Figure 3.3; Table 3.2). When all months were considered simultaneously, R^2 values were 0.73 for $\delta^{18}O$ and 0.65 for δ^2H. R^2 values increased to 0.83 for $\delta^{18}O$ and 0.77 for δ^2H when month was included as a factor in the linear regression because slopes varied significantly among months.

The relationship between MWE and isotope ratios changed through time (Figure 3.3). Slopes for isotope-MWE relationships were smallest in November (-1.9 ‰ km^{-1}, -11 ‰ km^{-1}) and February (-2.1 ‰ km^{-1}, -13 ‰ km^{-1}; Table 3.2) for $\delta^{18}O$ and $\delta^{2}H$, respectively. Slopes in May (-3.3 ‰ km^{-1}, -22 ‰ km^{-1}) and June (-2.8 ‰ km^{-1}, -17 ‰ km^{-1}) were the largest for $\delta^{18}O$ and $\delta^{2}H$, respectively. Slopes for $\delta^{18}O$ and $\delta^{2}H$ in September were intermediate (-2.3 ‰ km^{-1}, -14 ‰ km^{-1}). Sites below 550 m had little relationship between MWE and isotope ratios. We did not observe any clear seasonal variation in d-excess (Figure 3.3).

To examine how spatial autocorrelation impacted the relationship between MWE and isotope ratios, we compared model fit and variance decomposition for SSNMs for $\delta^{2}H$ isotope ratios for each month. Proportion of variation explained by spatial structure is fairly consistent among months, ranging from 15-30 %. All SSNMs had better predictive ability than non-spatial models, with R^2 values ranging from 0.86 to 0.94 (Table 3.3).

Spatial dependencies within the Snoqualmie basin varied with month for $\delta^{2}H$ residuals after accounting for effects of MWE (Figure 3.4). For the Snoqualmie basin residual $\delta^{2}H$ values, semivariance for Euclidean distance (i.e. the straight line distance between all sites) and for flow-connected sites (i.e. the network distance between sites that share flow) increased rapidly and linearly before leveling off around 10 km for May 2018 and June 2017 and 2018 and around 25 km for September 2018. This change in semivariance suggests that residuals from sites beyond 10 or 25 km apart were uncorrelated, whereas residuals from sites closer together were more highly correlated with one another after accounting for effects of MWE. November 2018, February 2018, and September 2017 overall had much smaller semivariance values that do not observably level off indicating that basin $\delta^{2}H$ residuals are overall more similar.

3.4.3 *Seasonal variance in isotope ratios*

Surface water isotope ratios varied seasonally in all surface water sampling sites, but low elevation (LE) sites (below 550 m) and high elevation (HE) sites (above 550 m) had distinctly different patterns (Figure 3.5). For both LE and HE sites, isotope values were highest in September (δ^2H_{LE} = -70.3 ± 1.2 ‰, δ^2H_{HE} = -78.6 ± 3.9 ‰) at the end of the long dry summers. Isotope ratios declined with winter precipitation inputs and were lowest at LE sites in February (δ^2H_{LE} = -77.7 ± 0.8 ‰). However, HE sites continued to decline and were lowest in May (δ^2H_{HE} = -87.9 ± 5.7 ‰), while LE isotopic values increased in May causing May to have the greatest variability observed across sites. By June, isotopic ratios at all sites had increased.

Outlets of major tributaries and the mainstem sampled biweekly show similar seasonal patterns (Figure 3.6). Sites with a substantial proportion of the basin above 900 m (Table 3.1), including the Mainstem, North Fork, Middle Fork, and South Fork, showed a decrease in isotopes beginning in late April through May. Although little precipitation occurred after May, discharge remains relatively high, as compared to the low elevation tributary (Raging). The drop in isotopic ratios and sustained flow in these tributaries likely reflects the input of snowmelt. For all sites except the regulated Tolt, isotope ratios increase throughout the summer as flow drops to its lowest annual value and with little new precipitation falling. The increase began in January for the Raging and in May after the spring freshet for the Mainstem, North Fork, Middle Fork, and South Fork. In addition to broad seasonal patterns, two basin-wide shifts in surface water isotope ratios occurred during storm events. The first occurred on December 30th, 2017 and resulted in a decrease in isotope ratios ranging from 3.1 - 6.2 ‰. The second occurred on November 6th, 2018 and resulted in an increase in isotope ratios ranging from 3.3 - 10.5 ‰ compared to the previous sampling event.

3.4.4 *Relationship between discharge and geology*

Baseflow index for all sites ranged from 0.43 – 0.98 with a mean of 0.63 and unit discharge at baseflow ranged from 0.03 – 0.70 $m^3 s^{-1} km^{-2}$ with a mean of 0.36 $m^3 s^{-1} km^{-2}$. δ^2H_{SD}, e.g. water source variability, ranged from 0.50 – 6.54 ‰ with a mean of 3.50 ‰. September 2017 and 2018 δ^2H values ranged from -84.91 to -69.77 ‰ with a mean of -77.39 ‰.

Unit discharge at baseflow increased positively and linearly with δ^2H values; however, two separate groups with similar patterns emerged (Figure 3.7A). Watersheds with a mean elevation above 550 m generally increase unit baseflow with increasing baseflow isotopic values up to -75‰ indicating more lower elevation water leads to greater baseflow. However, three relatively small watersheds with mean elevations lower than 550 m fall in a separate line with much lower unit discharge values (0.04 - 0.16 $m^3 s^{-1} km^{-2}$). Within these low elevation basins, baseflow unit discharge also increases with higher water isotope values.

Baseflow index was not related to water source variability (Figure 3.7B). The two sites with the lowest water source variability have the largest baseflow index, however the remaining sites are clustered between baseflow index values of 0.43 - 0.69 and display no relationship with water source variability.

Generally, baseflow index increases linearly with the proportion of low elevation glacial deposits underlying the catchment (Figure 3.8). A notable exception to this is the Raging, which is underlain by a large percentage of glacial deposits (69%) but has a low baseflow index (BFI_{2017} = 0.48, BFI_{2018} = 0.43). The relationship between the proportion of glacial deposits and unit discharge is less clear (Figure 3.8). Streams underlain by a higher proportion of glacial deposits do not necessarily have a higher unit discharge at baseflow. Notably, all streams with

greater than 50% of their catchment underlain by glacial deposits, including the Raging and two additional low elevation tributaries, have very low unit discharge.

3.5 DISCUSSION

3.5.1 *Isotope ratios vary strongly with MWE*

Surface water isotopes in the Snoqualmie basin primarily varied with MWE (Figure 3.3). The strong observed elevation gradient can be attributed to the rainout effect, or Rayleigh distillation (Dansgaard 1964, Clark and Fritz 1997). Storms bringing precipitation to western Washington basins originate from the Pacific Ocean and move eastward. Continued rainout as storms move inland and up the Cascade Mountains produces ^{18}O and ^{2}H depleted precipitation at higher elevations. Close proximity to the Pacific Ocean exacerbates the rainout process. As the warm, wet air mass travels up the Cascade Mountains, it experiences orographic lifting and adiabatic cooling, resulting in increased precipitation strengthening the observed isotopic trends with elevation. Results are consistent with previous studies, which found that in coastal proximal settings precipitation $\delta^{2}H$ variability follows an open-system behavior in which precipitation is not recycled by evaporation, and the isotopic fractionation is compatible with a Rayleigh distillation process as the air rises and cools over mountains (Ingraham and Taylor 1986, 1991). In surface water samples, studies across western Washington river basins have found that MWE is the dominant predictor of isotope ratios, but basin scale factors such as geology, geographic location, and landscape attribute configuration can substantially influence isotope ratios (Brooks et al. 2012, McGill et al. 2020). For the Snoqualmie River, MWE explained most of the variation in isotope ratios across seasons (Table 3.2), indicating that elevation-induced rainout is the greatest control on surface water isotope ratios. We use this observed elevation gradient in

conjunction with seasonality in surface water isotopes to make inference on how various catchments across the basin contribute to river flow in the Snoqualmie River throughout the year.

3.5.2 *Seasonality in isotope ratios reflects hydrological processes*

Seasonality in Snoqualmie basin surface water isotopes can be explained by both changes in the isotopic ratio of input precipitation entering the watershed and changes in contributing catchments. Within the Pacific Northwest, precipitation isotope ratios are highly variable, with little distinct seasonality (Ersek et al. 2010, Brooks et al. 2012, Nickolas et al. 2017). Therefore, the majority of variability in precipitation isotope ratios is storm specific. Although the exact causes of inter-storm variability are still uncertain, moisture source, temperature at condensation, air parcel trajectory, and the extent of the rainout process have all been shown to contribute to variability in precipitation isotope ratios (Ersek et al. 2010, Yoshimura et al. 2010, Berkelhammer et al. 2012, McCabe-Glynn et al. 2016). Biweekly timeseries data shows two large, basin-wide shifts in surface water isotope ratios, even in the regulated Tolt basin, that reflect variability in incoming precipitation isotopes (Figure 3.6). Both of these samples were taken on the rising limb of storms, where recent precipitation likely made up a larger percentage of streamflow. Large shifts in isotope ratios may therefore be the result of precipitation with isotopic ratios distinct from that of stream water entering the watershed and contributing to streamflow.

Isotope ratios from biweekly samples of major tributaries indicate that streamflow in fall and winter is predominately sourced from recent and lower elevation precipitation. In the humid Mediterranean climate western Washington experiences, winter precipitation begins in October and continues through March. This is typically the wettest and coldest time of the year (Figure 3.2). These conditions lead to snow accumulating in the high elevation mountains within the

Snoqualmie basin. Subsequently, lower elevation portions of watersheds are contributing more flow than higher elevation portions of the watersheds located in the transient (300-900 m) and seasonal (above 900 m) snow zones at this time, and the δ^2H-MWE slope is shallowest (Jefferson, 2011; Figure 3.3; Table 3.2). High variability in early winter isotope ratios corresponding to changes in river discharge (Figure 3.6) suggest that most stream water is derived from recent precipitation in winter. Results from spatial modeling are consistent with this finding. In November and February samples, spatial autocorrelation not explained by MWE is low (Table 3.2; Figure 3.4). This occurs because precipitation amount, type, and isotopic signature are controlled by orographic processes that vary strongly with elevation, and during the wet winter a larger fraction of stream water derives directly from recent precipitation. Previous studies have found similar patterns, wherein during the winter rainy season and wetter-than-average summers the isotope ratios of surface water across Pacific Northwest river basins are consistent with recent precipitation, and differences in isotope ratios due to physical watershed characteristics are limited (Blumstock et al. 2015, Nickolas et al. 2017, Segura et al. 2019).

Lower surface water isotope ratios in high elevation sites and large δ^2H-MWE slopes in May and June reflect the input of spring snowmelt to high elevation sites (Figure 3.4; Figure 3.6). According to SNOTEL data from across the basin, snowmelt in 2018 began in some locations as early as April and persisted until late June (Figure 3.2). However, SWE estimates at SNOTEL stations represent only a small subset of conditions within an area. SNOTEL stations are typically located at higher elevations and in areas that accumulate deeper snowpack than a majority of the surrounding landscape (Daly et al. 2000, Molotch and Bales 2006). Therefore, the majority of realized snowmelt in the Snoqualmie basin likely began and ended earlier than SNOTEL data suggest. Slopes for δ^2H-MWE relationships are largest in May and June (Table

3.2) and high elevation sampling sites show low isotope ratios compared to February (Figure 3.5). Snowmelt is typically ^{18}O and ^{2}H depleted relative to stream water and rain due to a combination of accumulating at high elevations and cold temperatures during fractionation (Beria et al., 2018). Furthermore, biweekly samples show a distinct drop in isotope ratios beginning in March that lasts until early June for the Mainstem, North Fork, Middle Fork, and South Fork, all tributaries with a substantial portion of the basin above the 900 meter snowline (Figure 3.6).

Water isotope values within the regulated Tolt River were more stable over time than other tributaries similarly positioned in the watershed (Figure 3.6). The Tolt Reservoir is operated for flood control in winter, flow augmentation in summer, and provides drinking water to the City of Seattle year-round. The reservoir fills in late winter and spring, potentially holding back winter precipitation and high elevation snowmelt and releasing it during summer low flow. The isotope ratio of water within the Tolt Reservoir likely reflects the long-term average of river water input, which may explain the relatively flat isotope time series and lack of a discernable snowmelt signal in spring (Figure 3.6). Previous studies have found muted temporal isotopic variation below artificial impoundments and natural lakes, reflecting extended retention times and elevated river water mixing (Kendall and Coplen 2001, Wassenaar et al. 2011, Brooks et al. 2012, Trinh et al. 2017). We did not observe d-excess values below 5 ‰, which indicated no appreciable evaporation within the reservoir (Figure 3.3).

3.5.3 *Catchment geology controls summer baseflow*

We found that summer baseflow within the Snoqualmie basin was derived from low elevation sources. In our biweekly sampling, water isotope values slowly increased throughout the dry summer as flows decreased at outlets of the mainstem and major tributaries (Figure 3.6).

The highest surface water isotope ratios were found in September. In Mediterranean climates without significant summer precipitation, water isotopes in precipitation infiltrating into mountain blocks with different residence times determine the isotopic composition of river water at baseflow. Shallow groundwater isotope ratios do not deviate significantly from the mean weighted annual composition of precipitation in temperate climates in areas without seasonal or spatial bias in recharge (Clark and Fritz 1997, Bowen et al. 2011). As the vast majority of precipitation within the Snoqualmie basin falls in winter (Figure 3.2) and Pacific Northwest precipitation isotope ratios have little distinct seasonal pattern (Ersek et al. 2010, Brooks et al. 2012), a temporal bias in groundwater recharge is unlikely. The relatively high summer baseflow isotope ratios in the Snoqualmie basin therefore suggest a spatial bias in recharge towards lower elevation sources, given the strong δ^2H-MWE relationship we observed in Figure 3.3.

Lower elevations of the Snoqualmie basin are dominated by a deep permeable, productive glacial aquifer that we presume is the source of baseflow (Turney et al. 1995, Bethel 2004). Glacial and interglacial deposits in the valley bottom contain several geohydrologic units, each with differing lithological and hydrologic characteristics that control aquifer potential. Deposits consist of a mix of unconsolidated gravel, sand, silt, clay, and peat and include geologic features of alluvium, recessional and advance outwash, till, ice-contact deposits, and confining beds (Bethel, 2004; Turney et al., 1995; Figure S3.2). Features such as alluvium and advance outwash consist of sand and gravel on average hundreds of feet thick and have better aquifer properties than units such as till or transitional beds (Turney et al. 1995). However, most glacial and interglacial deposits can form small but useable aquifers that may help sustain baseflow in summer months (Turney et al. 1995, Soulsby et al. 2004, Blumstock et al. 2015). In the Pacific Northwest more specifically, geology is critical in determining baseflow patterns. In Oregon,

Nickolas et al. (2017) found that baseflow was sustained by permeable sandstone portions of the Marys River watershed, and Segura et al. (2019) found that during drought conditions water stored in deep seated earthflows, other Quaternary deposits, and porous volcanic bedrock supported baseflow. Furthermore, baseflow in the Oregon Cascades is supported by high elevation snowmelt that travels through extensive subsurface flow paths within highly porous and permeable young volcanic bedrock (Tague and Grant 2004, Tague et al. 2013). Such studies of streamflow show that Pacific Northwest rivers will not respond uniformly to the same climate signal and illustrate the importance of subsurface geology in controlling baseflow.

The ^{18}O and ^{2}H enriched summer baseflow in the Snoqualmie also suggests that snowmelt does not recharge groundwater or contribute substantially to late summer baseflow, but rather comes out as a pulse during the spring freshet. We observed a distinct decrease in water isotope ratios during spring in the mainstem and major tributaries with area above 900 m (Jefferson 2011), quickly followed by a continual increase in isotope ratios throughout summer (Figure 3.6; Table 3.2). Snowmelt enters and moves through the system in a quick pulse, and as the year progresses lower elevation water sources sustain streamflow. The upper portion of the Snoqualmie basin is covered by thin soil over impermeable bedrock lacking extensive fracture networks, meaning that rain and snowmelt are not retained in the mountains but are rapidly transmitted to the stream system (Bethel, 2004; Turney et al., 1995). Recharge in mountain areas such as the Snoqualmie basin can be permeability-limited rather than recharge-limited due to thin soils overlying low-permeability crystalline bedrock (Debose and Klungland 1964, Nelson 1971, Goldin 1973, 1992, Flint et al. 2008). When the rate of snowmelt infiltration into soils exceeds percolation into bedrock, lateral flow occurs and water drains to streams or wetlands. Furthermore, in the Pacific Northwest, spring snowmelt may substantially exceed unsaturated

zone storage capacity due to high antecedent soil moisture from winter rains (Blankinship et al. 2014). Therefore, upper elevation bedrock is not an important source of runoff control and groundwater storage.

Hydrologic evidence supports the assertion that low elevation glacial deposits are the main source of summer baseflow. Unit discharge for baseflow increased when water originated from lower elevation (Figure 3.7B), supporting the idea that baseflow was sourced from a glacial aquifer within the Snoqualmie valley. Interestingly, three watersheds with mean elevations below 550 m, including the Raging River, had the smallest unit discharge values despite having a low water source elevation, high baseflow index and a large proportion of glacial deposits (Figure 3.7; Figure 3.8). These watersheds may have these unexpected attributes because less precipitation is entering the catchment or because their subsurface catchment is smaller than their topography delineated catchment (Nickolas et al., 2017). In addition, groundwater upwelling generally occurs at breaks in the landscape (Neff et al. 2019), and all these basins are below the break related to the Snoqualmie falls potentially limiting groundwater discharge points. A mass balance calculation using river discharge data also suggests that during summer, proportionally more water enters the basin from low elevation sources such as mainstem tributaries.

For all sites except the Raging River, as the proportion of glacial deposits within a catchment increases, the baseflow index increases linearly (Figure 3.8) meaning groundwater comprises a larger percentage of annual streamflow. The lack of a relationship between water source variability and baseflow index is surprising (Figure 3.7). We expect groundwater to have a relatively constant isotope ratio through time (Clark & Fritz, 1979), and therefore anticipate that sites dominated by groundwater have a low water source variability. We hypothesize that the weak pattern is partially due to our limited temporal sampling, which captures events on long

time scales (e.g. snowmelt) better than on short timescales (e.g. storm driven events). Therefore, our metric of water source variability is correlated with elevation and snowmelt and may not capture the true water source variability for a site like the Raging River, which is a flashy system that lacks snowmelt.

Alternative explanations for ^{18}O and ^{2}H enriched summer baseflow, such as enriched precipitation falling in summer or displacement of evaporated soil water with an enriched isotopic composition, are unlikely. Very little rain falls in summer within the Snoqualmie basin; stream discharge response to summer precipitation is limited (Figure 3.2), likely because dry soils and plant transpiration adsorb and utilize these small summer events. In addition, evaporatively enriched soil water was not the cause of the increase in stream water isotope values as seen in some other studies (Tetzlaff et al. 2015, Peralta-Tapia et al. 2015, Sprenger et al. 2017), because September samples had a similar d-excess as June samples. Brooks et al. (2010) found tightly bound soil water with an evaporatively enriched isotopic signal remained stationary throughout summer unless utilized by plants, and mobile water without an evaporated signal contributed to streamflow in a similar Mediterranean climate. Good et al. (2015) suggested that globally this process is more widespread than previously thought. The observed isotopic increase in baseflow was therefore likely due to a decrease in elevation of the water origin, indicating that ^{18}O and ^{2}H enriched lower-elevation groundwater is contributing more to streamflow in late summer. Additionally, residual snowmelt, which may be present in June, did not sustain streamflow into September.

3.5.4 *Caveats and limitations*

Our ability to generalize results is limited by our sampling design and dataset. Our sampling design involved intensive temporal and spatial sampling over June and September 2017

and the 2018 water year. The coupling of widespread and frequent water sampling provided information about regional, geologic, and climatic controls on the spatial and temporal variability of water sources relevant to management. Given that our study only spanned a single year, our results may be a reflection of specific conditions during the 2018 water year. However, as 2018 was a relatively average year in terms of temperature and precipitation (Figure S3.3), this seems unlikely. Precipitation samples were not collected within the Snoqualmie basin due to logistical restrictions, although we obtained precipitation samples from nearby locations.

3.5.5 *Climate and management implications*

A critical challenge for resource managers seeking to prioritize restoration or research actions is in identifying streamflow sensitivity to climate change. Our results show that in the Snoqualmie basin, summer streamflow is sustained primarily by groundwater recharged by low elevation precipitation, and snowmelt does not substantially contribute to summer streamflow. This suggests that the Snoqualmie River may be less sensitive to predicted warming than Pacific Northwest rivers that rely on snow or glacial melt to sustain summer streamflow (Riedel and Larrabee 2016). However, it is important to note that although groundwater discharge may remain constant, warmer air temperatures could lead to warmer water temperatures and a reduction in baseflow discharge due to increased evaporation and evapotranspiration. Furthermore, groundwater likely integrates several years of storage; amount of storage and timing of release to the stream are key considerations for drought resiliency. Although several studies have highlighted the role of underlying geology in controlling hydrologic responses to climate change (Tague and Grant 2004, 2009, Tague et al. 2008, Mayer and Naman 2011), future streamflow predictions for Puget Sound continue to focus predominately on climate mediated changes in snowpack regimes (Elsner et al. 2010, Mantua et al. 2010, Wu et al. 2012).

An increased focus on basin-scale attributes that impact timing and magnitude groundwater discharge to rivers could improve future streamflow predictions (Tague et al. 2013).

Recognizing that subsurface geology plays a major role in controlling the hydrology of the Snoqualmie River can be used to advise management decisions relating to restoring floodplain functions that recharge aquifers. Understanding major groundwater recharge areas may enable managers to target restoration actions such as placing engineered logjams or reintroducing beavers in areas underlain by permeable glacial deposits where recharge is greatest (Abbe and Brooks 2013, Pollock et al. 2014). Similarly, by combining climate predictions with our water source estimates we can estimate areas of the basin and times of year that will undergo the greatest shifts in streamflow timing and magnitude. For example, Figure 3.6 illustrates that recent precipitation from incoming storms can dominate streamflow across the Snoqualmie River. Climate models predict more intense and frequent winter storms, which have the potential to cause flooding across all areas of the basin. Impacts from flooding could be particularly severe in the Raging River due to its flashy hydrology and low elevation. Several species of Pacific Salmon spawn in the Raging River and flooding here may negatively impact egg-to-fry survival rates (Mantua et al. 2010, Isaak et al. 2012). Resource managers may therefore decide to preemptively focus management efforts such as wetland restoration and riparian planting within this and other low-elevation tributaries to provide fish habitat complexity and mitigate flood risk.

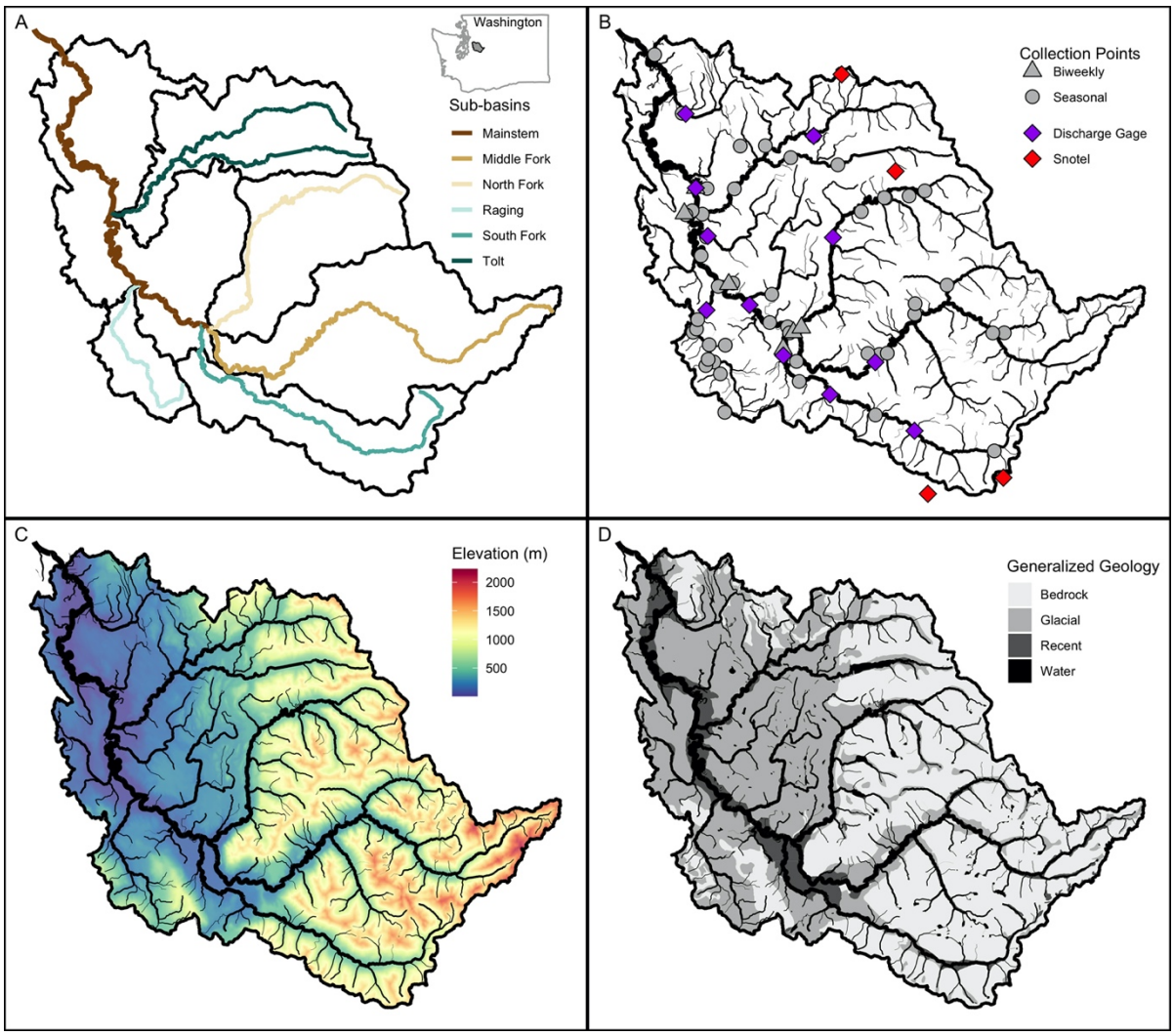

Figure 3.1. The Snoqualmie River basin and sub-basins, and the Snoqualmie's location in Washington, USA (A), water sample, USGS gage, and SNOTEL site locations (B), elevation of the Snoqualmie basin (C), and generalized geology of the Snoqualmie basin (D).

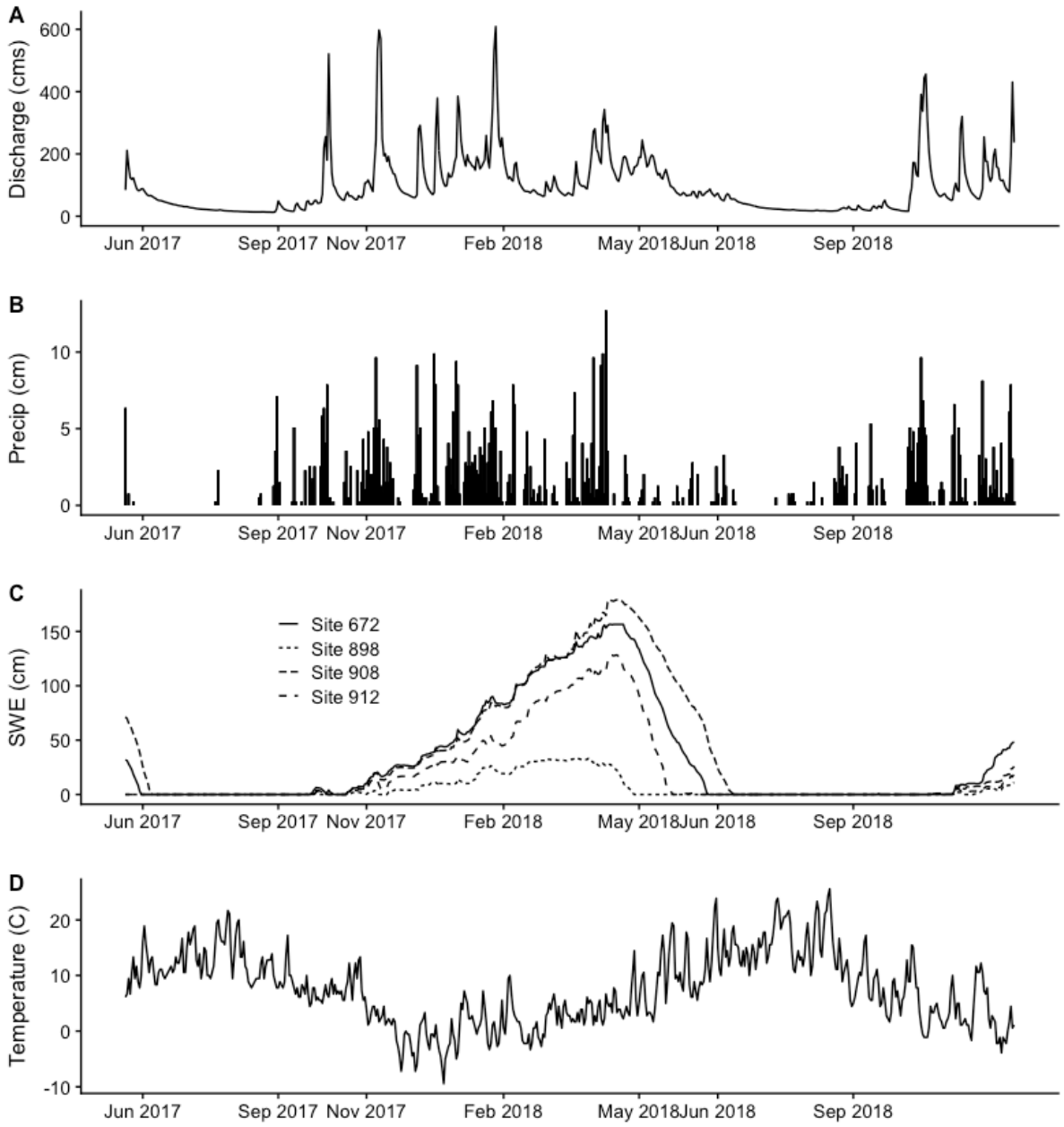

Figure 3.2. Climatic time series over our study period. Mainstem Snoqualmie discharge from USGS station 12149000 (A), total daily incoming precipitation from SNOTEL site 908 (Alpine Meadows) (B), snow-water-equivalent (SWE) from all SNOTEL sites within the basin (C), and mean daily air temperature from SNOTEL site 908 (Alpine Meadows) (D). The ticks on the x-axis are the median date of our whole basin, seasonal sampling events.

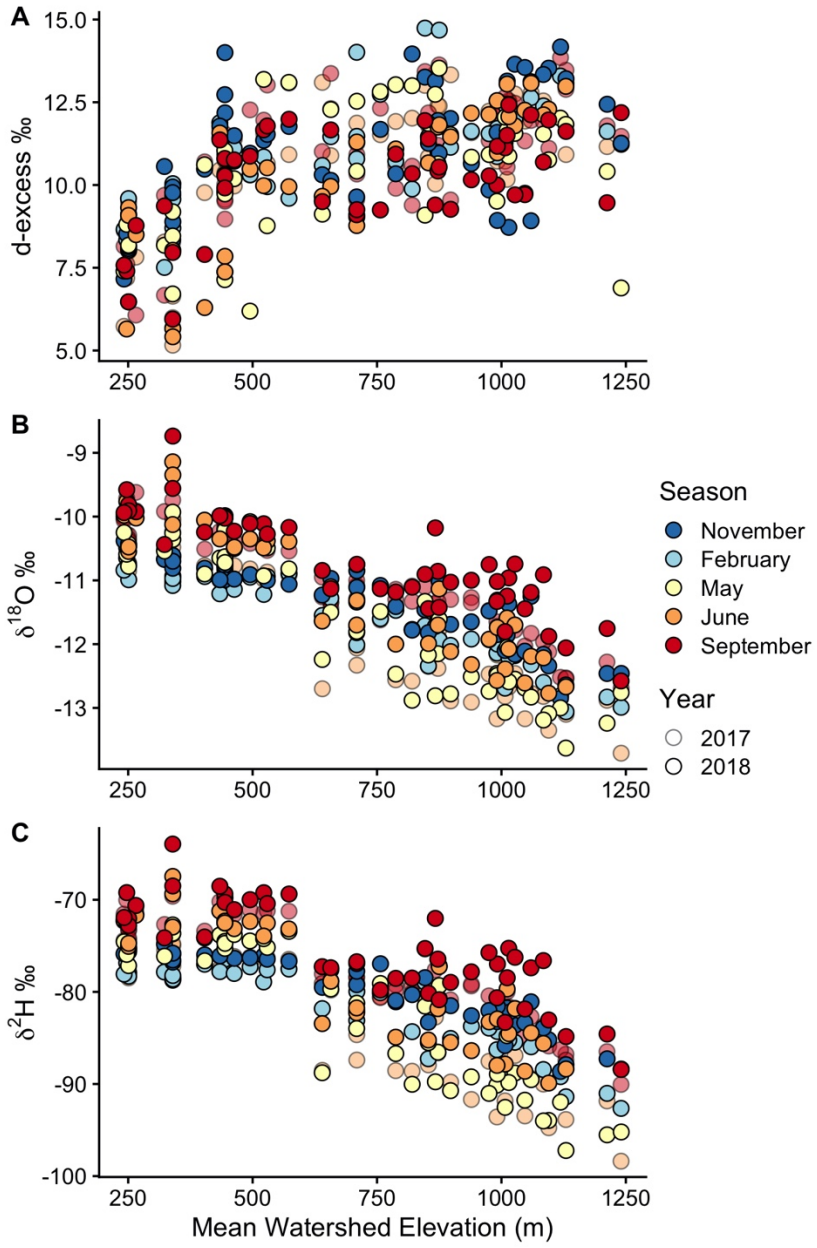

Figure 3.3. Relationships with elevation for d-excess (A), $\delta^{18}O$ values (B), and $\delta^{2}H$ values, (C) for all seasonal sampling events. Color indicates the month that each water sample was collected. For September and June, there are two sets of sampling events shown (2017 and 2018), with 2017 having a faded color.

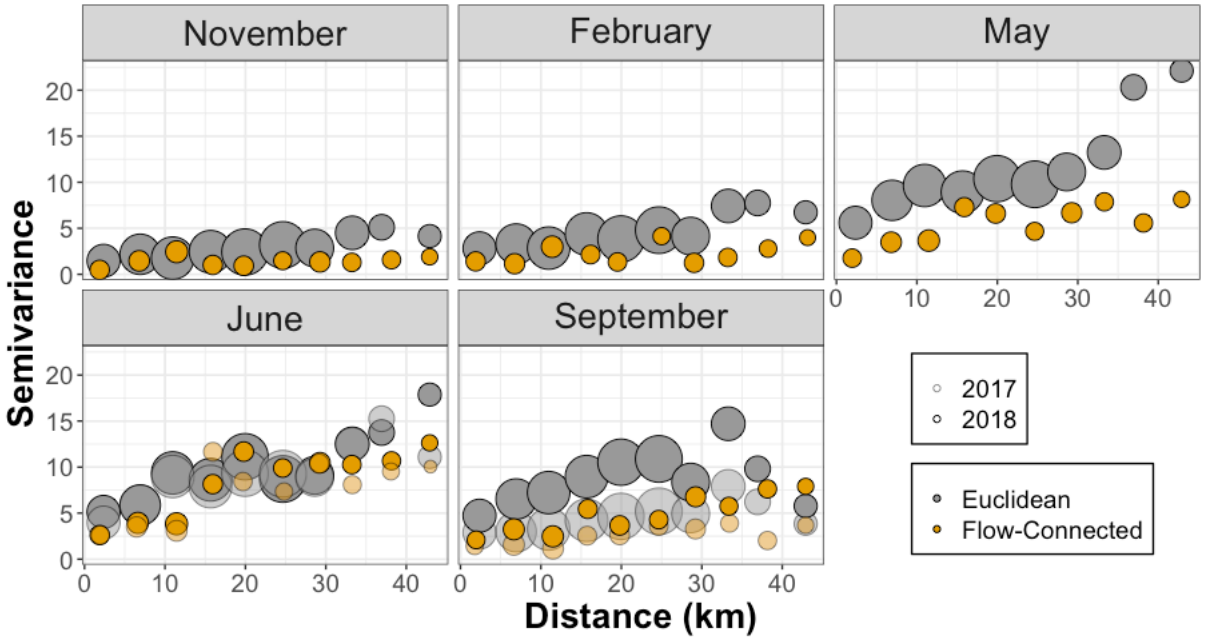

Figure 3.4. Semivariograms for the residuals from the δ2H-MWE linear regression. Circles are proportional to the number of sites used to estimate each bin value.

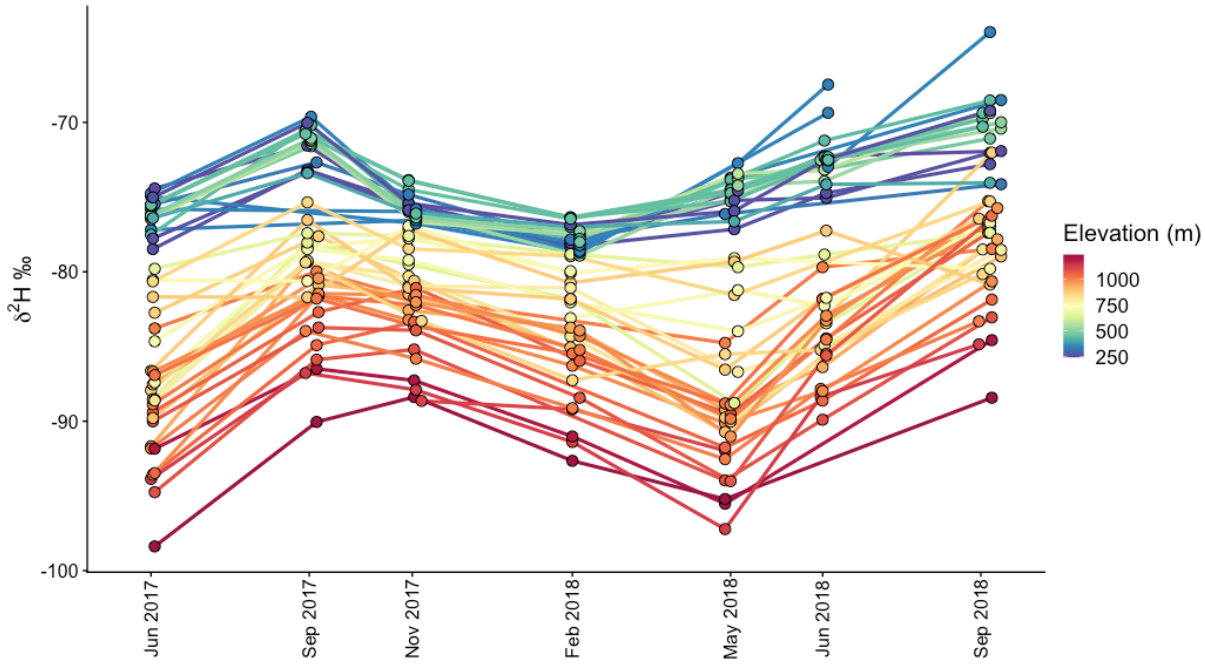

Figure 3.5. The δ^2H values for all seasonal sites throughout the year. Color indicates the MWE of the basin.

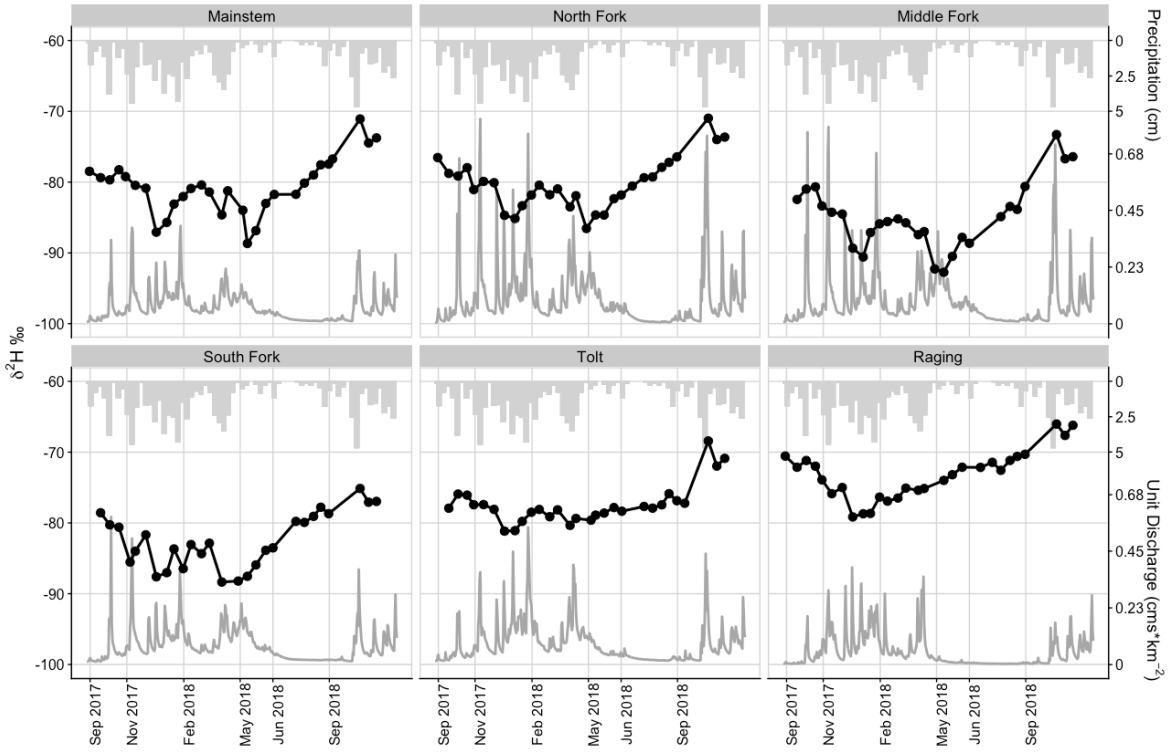

Figure 3.6. Black lines are δ^2H values for biweekly samples collected at the mouth of the mainstem Snoqualmie and each major tributary over WY 2018. Dark gray lines along the bottom are daily streamflow hydrographs from nearby USGS gages, normalized by drainage area. Gray bars along the top are weekly averages of precipitation.

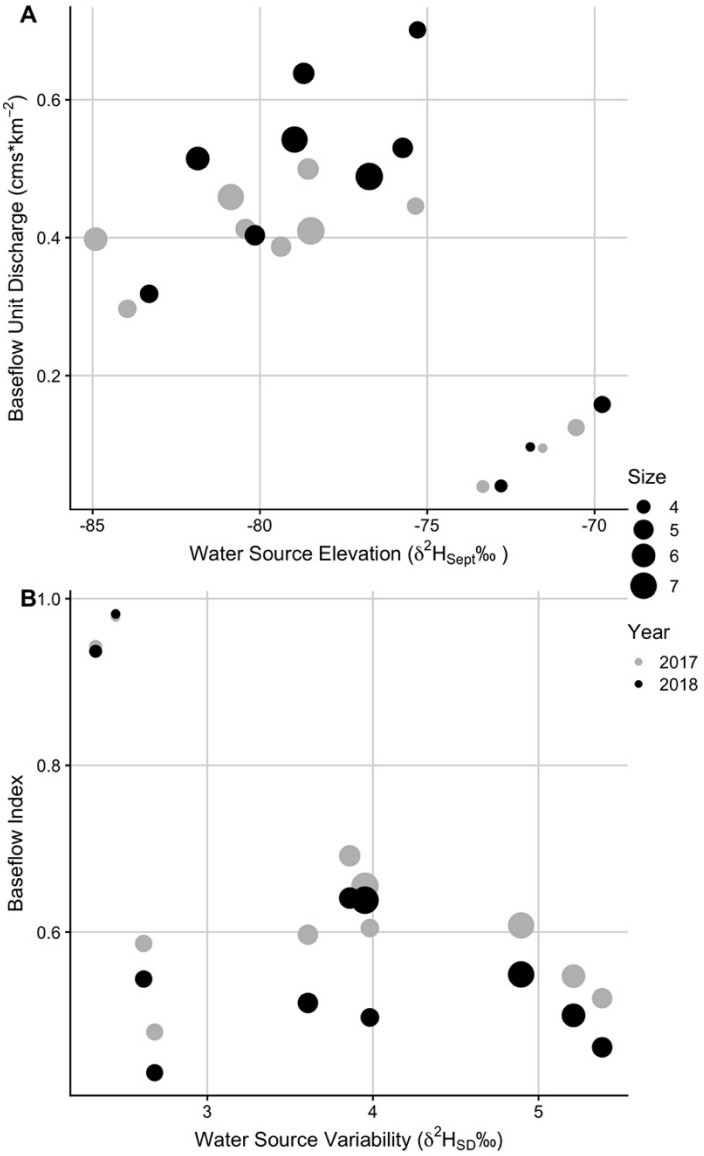

Figure 3.7. Relationships between water source variability and the baseflow index (A) and water source elevation and average unit discharge at baseflow (B) for all streamflow gages within the basin. Points are colored by year. Point size is related to the log watershed area for each site.

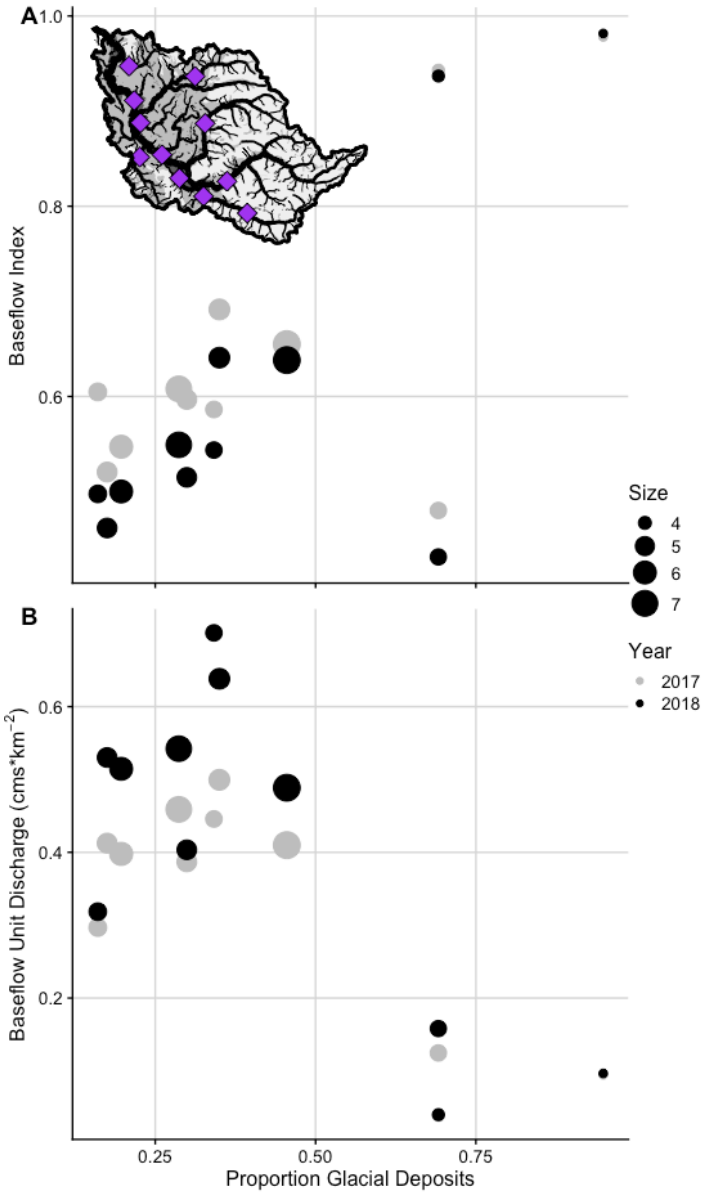

Figure 3.8. Relationships between the proportion of glacial deposits within a watershed and the average unit discharge at baseflow (A) and baseflow index (B) for all streamflow gages within the basin. Points are colored by year. Point size is related to the log watershed area for each site. The inset panel shows the Snoqualmie basin generalized geology (see Figure 1A for legend colors) and streamflow gage locations.

Table 3.1. Watershed characteristics for the Snoqualmie River and each of its major tributaries. The "snow zone" in the Snoqualmie is considered to be areas greater than 900 m (Jefferson 2011). Mean Annual Precipitation was calculated over the period 1980-2010.

Subwatershed	Drainage Area (km^2)	Mean Watershed Elevation (m)	Relief (m)	Mean Annual Precipitation (cm)	Mean Slope (%)	Proportion of basin >900 m	Proportion of basin w/ bedrock geology	Precip Weighted Elevation (m)
Mainstem	1781	637	2,295	236	36.3	0.34	0.49	781
Middle Fork	442	988	2,176	325	58.0	0.65	0.77	1043
South Fork	218	814	1,771	267	44.1	0.46	0.65	890
North Fork	268	869	1,667	281	47.9	0.53	0.71	919
Tolt	263	610	1,801	217	33.9	0.25	0.46	710
Raging	84	442	1,035	196	21.7	0.00	0.31	472

Table 3.2. Model fit statistics from linear regressions with mean watershed elevation in the Snoqualmie River basin. Units for the coefficients are ‰/m. Numbers in parentheses are the standard error (SE) for model parameters.

		$\delta^{18}O$			**$\delta^{2}H$**	
	R^2	Coefficient (SE)	Intercept (SE)	R^2	Coefficient (SE)	Intercept (SE)
November (n=48)	0.81	-0.0019 (0.00019)	-9.98 (0.14)	0.81	-0.011 (0.0011)	-71.74 (0.81)
February (n=45)	0.87	-0.0021 (0.00014)	-10.16 (0.099)	0.77	-0.013 (0.0012)	-73.03 (0.84)
May (n=47)	0.84	-0.0033 (0.00026)	-9.26 (0.19)	0.82	-0.022 (0.0021)	-66.26 (1.56)
June (n=90)	0.83	-0.0028 (0.00018)	-9.29 (0.13)	0.78	-0.017 (0.0014)	-68.10 (0.96)
September (n=92)	0.77	-0.0023 (0.00018)	-9.24 (0.13)	0.71	-0.014 (0.0013)	-66.05 (0.96)
All Months	0.73	-0.0025 (0.00012)	-9.50 (0.82)	0.65	-0.015 (0.00088)	-68.49 (0.63)
All Months (with month as a factor)	0.83	-0.0025 (0.000095)	-9.95 (0.10)	0.77	-0.015 (0.00071)	-71.15 (0.79)

Table 3.3. Spatial stream network model (SSNM) statistics for each month. All sites were included in these regressions. Units for the coefficients are ‰/m.

	δ^2H				
				Variance Component	
	R^2	Coefficient (SE)	RMSPE	Fixed (%)	Spatial (%)
November (n=48)	0.93	-0.019 (0.0016)	1.04	72	21
February (n=45)	0.93	-0.013 (0.0013)	1.16	72	21
May (n=47)	0.89	-0.016 (0.0018)	2.57	69	20
June 2017 (n=48)	0.94	-0.021 (0.0015)	1.64	74	20
June 2018 (n=42)	0.91	-0.013 (0.0011)	1.91	69	22
September 2017 (n=46)	0.94	-0.021 (0.0021)	1.29	79	15
September 2018 (n=46)	0.86	-0.013 (0.0017)	1.93	56	30

Chapter 4. SPATIAL COVARIANCE OF HYDROLOGIC CHANGE AMONG RIVER DISCHARGE TIME SERIES ACROSS WESTERN NORTH AMERICA

4.1 ABSTRACT

Seasonal flow regimes support both physical and ecological river processes such as disturbance regimes, habitat provisions, and native species life history cues. In western North America, many rivers rely on winter precipitation and the resulting snowpack to sustain spring and summer streamflow. Warmer winter temperatures have led to increased precipitation falling as rain and decreased mountain snowpack; subsequent changes to the timing, duration, and magnitude of streamflow over the course of the year are already occurring. We mapped the magnitude and extent of historical changes to peak, baseflow, and recession hydrology metrics to resolve the relative influence of local-scale morphological and regional-scale climactic processes in governing patterns of change. Across all hydrologic metrics, relatively few basins displayed significant monotonic trends. However, baseflow metrics showed more substantial and widespread changes than peak or recession flow metrics. For all hydrologic metrics, geographically localized interannual variation was the dominant control on observed changes to streamflow, rather than variability corresponding to river type or monotonic changes. Additionally, study results illustrate that mean annual precipitation that falls in a catchment has historically been the dominant control on measured facets of river hydrology, compared to air temperature and global circulation metrics. Lower and longer baseflow and high interannual variability coupled with even modest trends portends challenges for both water resource management and native fish species such as Pacific salmon.

4.2 INTRODUCTION

Anthropogenic climate change is altering water resources in western North America, resulting in increasing temperatures, decreasing mountain snowpack, and sharpened seasonal precipitation (Whitfield and Cannon 2000, Barnett et al. 2008, Cayan et al. 2008, Mote and Salathé 2010, Hagos et al. 2016, Swain et al. 2018). The rate and intensity of these changes will be mediated by latitude, with northern latitudes expected to see faster warming, and southern latitudes expected to see greater variability in precipitation (Diffenbaugh et al. 2015, Swain et al. 2018). River runoff within western North America is particularly sensitive to changes in climate due to strong seasonality in precipitation (October through March) and dependence on mountain snowpack from the Cascades, Sierra Nevadas, and coast ranges to sustain warm season stream flow (April through September; Stewart et al. 2005, Elsner et al. 2010, Safeeq et al. 2016, Dierauer et al. 2018). A changing climate affects the timing and balance of precipitation falling as rain and snow, and therefore the timing and magnitude of streamflow over the course of the year (Knowles et al. 2006, van Vliet et al. 2013). Anticipated shifts in these climatic drivers have implications for ecologically and economically relevant components of river discharge. As changes will not be uniform across rivers, there is an urgent challenge and opportunity to identify how climate and catchment parameters influence individual river response.

Process-based hydroclimate modeling suggests several directional shifts in river discharge metrics are expected with a changing climate. Less intense and earlier snowmelt should modify spring recession characteristics to produce an earlier timing, smaller magnitude, and shorter duration for spring recession flows (Stewart et al. 2005). Snowpack acts as a natural water reservoir that sustains streamflow throughout the summer, and its loss will likely lengthen the dry season duration and decrease dry season magnitude (Wu et al. 2012). Additionally, the

intensification of the water cycle due to a warming climate and a greater proportion of winter precipitation falling as rain may increase the number and intensity of river floods (IPCC 2014; Hamlet and Lettenmaier 2007). These changes will likely strain human water resource systems where the seasonal asynchrony between runoff from winter precipitation and summer water demand (i.e., the combination of atmospheric demands, ecological requirements, and consumptive use) already makes water supplies scarce and vulnerable (Barnett et al. 2005, Jaeger et al. 2017). Furthermore, aquatic and riparian species that are highly adapted to seasonal flooding and drought disturbances (Gasith and Resh 1999, Bonada et al. 2007) may have difficulty adapting to the changes in the timing or intensity of these signals; when coupled with high interannual variability, even modest trends may push species outside their tolerance limits. Thermal and hydrologic conditions outside the tolerance of species, such as warm water temperatures and low summer baseflows, are expected to prove challenging for species such as Pacific salmon (Mantua et al. 2010, Steel et al. 2019). Understanding the mechanisms driving past and predicted future river response to these climatic changes is therefore critical for resource planning and management.

River streamflow is influenced by myriad factors at multiple spatial scales, including oscillations in ocean circulation patterns, regional precipitation and temperature, and basin morphology. Understanding an individual river's hydrologic change requires a macrosystems context for comparing river responses. On a global scale, river hydrology is impacted by variability in sea surface temperatures over the Pacific Ocean characterized by the Pacific Decadal Oscillation (PDO) and the El-Niño Southern Oscillation (ENSO) indices. Both PDO and ENSO phenomenon contribute to decadal and inter-decadal scale oscillations in temperature and extreme precipitation across western North America (Mantua et al. 1997, Gershunov et al. 2019)

which govern regional patterns in hydrology. Western hydrology has largely been influenced by winter precipitation, but increasingly warmer temperatures are expected to play a role in water year runoff through changes to snowmelt timing and drought (Diffenbaugh et al. 2015, Williams et al. 2015, Woodhouse et al. 2016). Basin morphological characteristics are the local-scale lens through with climatic changes will be filtered and translated into discharge.

Western rivers have been broadly categorized into three discharge regimes, rain-dominated, mixed, and snow-dominated, based on the predominant form of winter precipitation. These classifications closely correspond to watershed latitude and elevation (Hamlet and Lettenmaier 2007, Jefferson 2011). Rain-dominated flow regimes are controlled by the intensity of winter rainfall and characteristics of individual storm events. Snow-dominated flow regimes are largely controlled by the timing and rate of snowmelt, which are driven by seasonal patterns of precipitation and temperature. Mixed source streams experience both rainfall driven flows in the winter and a snowmelt pulse in the spring, or they occur in large drainages that receive both snowmelt and rainfall contributions from upstream. With the transition towards warmer temperatures, many snow-dominant watersheds are expected to become mixed, and mixed watersheds will shift toward rain-dominance (Hamlet et al. 2005, Barnett et al. 2008, Elsner et al. 2010, Shrestha et al. 2012, Schnorbus et al. 2014).

Numerous studies have examined projected changes in climate and hydrology at multiple scales across western North America (Elsner et al. 2010, Vano et al. 2010, Wu et al. 2012). Western North American river hydrology is often characterized by often extreme hydrologic variability and widespread human intervention, which can make the detection and attribution of monotonic (consistently increasing or decreasing) trends a difficult task. Despite this, studies to detect the presence of these climate-driven trends in river discharge have occurred at the local,

regional, and national scale, resulting in a large body of literature with mixed results (Whitfield and Cannon 2000, Stewart et al. 2005, Burn et al. 2012, Ficklin et al. 2018). Some studies have found a shift in timing of discharge with an increase in winter and early spring and a decrease in late spring and summer (Zhang et al. 2001, Burn and Hag Elnur 2002, Ehsanzadeh and Adamowski 2007, Khaliq et al. 2008, Cunderlik and Ouarda 2009), trends towards earlier and less intense snowmelt (Stewart et al. 2005, Déry et al. 2009, Cunderlik and Ouarda 2009), decreases in summer low flows (Ehsanzadeh and Adamowski 2007, Déry et al. 2009, Dierauer et al. 2018), and decreases in surface water supplies (Déry and Wood 2005, St. Jacques et al. 2010). Other studies, however, have failed to detect trends when attempting to assess changes in hydrologic metrics such as median discharge and extreme events (Ficklin et al. 2018).

Despite the breath of research examining historical trends in discharge across a range of hydrologic metrics and river types, few studies have quantified the relatively balance of interannual variability to directional change across western North America. Furthermore, while regional cohesion in hydrologic trends is common (Burn and Hag Elnur 2002, Ehsanzadeh and Adamowski 2009, Ficklin et al. 2018), formal clustering is rarely done (but see Pournasiri Poshtiri et al. 2019). Our study aims to comprehensively map the magnitude and extent of changes to hydrologic metrics using recently updated discharge data from British Columbia, Alaska, and the western conterminous United States, and to resolve the relative influence of local-scale morphological versus regional-scale climactic processes in governing overall patterns of hydrologic change. We utilize dynamic factor analysis (DFA), a dimension-reduction technique designed for time series data (Zuur et al 2003), to characterize non-monotonic temporal and spatial patterns in river discharge metrics and examine the influence of climatic forcing in the form of precipitation, temperature, soil moisture, and Pacific climate indicators

(PDO and ENSO). We also examine how basin characteristics such as river type and latitude mediate river response to climatic forcing.

4.3 METHODS

4.3.1 *Watershed selection*

Mean daily discharge observations were downloaded from gauges located in the western United States and Canada from the United States Geologic Survey and Environment Canada respectively. We identified reference stream gages with at least 40 years of data using the Geospatial Attributes of Gages for Evaluating Streamflow (GAGES-II) dataset (Falcone et al. 2010) within the United Sates and the Environment Canada Reference Hydrometric Basic Network (RHBN, Brimley et al. 1999, Lins 2012) within Canada. Reference stream gages are sites for which discharge reflects the prevailing meteorological conditions and are screened to exclude sites where human activities (e.g., impoundments, withdrawals, diversions, land use change) affect natural streamflow. We included two gages on the same river if the downstream gage had a contributing watershed area at least twice that of the upstream gage. If the two watersheds were closer in size, only data from the larger watershed was used. In total, we obtained discharge data from 185 gauges: 55 from California, 33 from Oregon, 51 from Washington, 3 from Southeast Alaska, and 43 from British Columbia.

Basins were *a priori* categorized into three hydrologic classes (rain, mixed, or snow) based on the average ratio of maximum snow water equivalent (SWE) to cumulative wet season precipitation (October to March) from 1981-2010 (Hart and Bell 2015, Arsenault et al. 2020). These classes can be considered nodes along a complex continuum of discharge response to mixed flow drivers. The SWE to winter precipitation ratio can range from 0 to 1 and provides a continuous estimate of the degree of snow influence.

4.3.2 *Hydrograph metrics*

We calculated six hydrologic metrics that describe ecologically and climatically relevant aspects of discharge to obtain annually resolved time series for each river-metric combination. The first pair of metrics deal with peak flows and include the magnitude and duration of peak flow conditions for each site. Peak flow magnitude was calculated as the maximum annual discharge value, and the peak flow duration was calculated as the number of days with discharge above the 80th percentile of flow. The second pair of metrics deal with spring recession flows, which mark the seasonal shift from high magnitude winter flows to the dry season baseflow and include the magnitude and timing of the spring recession for each site. The timing metric was developed with the eFlows software (Lane et al. 2017, 2018, Patterson et al. 2020), which uses an iterative smoothing, feature detection, and windowing methodology to identify and characterize seasonal flows across highly variable natural flow regimes. Spring recession magnitude was calculated as the discharge value at the onset of spring recession. The last pair of metrics deal with summer low flows and include the magnitude and duration of summer baseflow conditions. The dry season baseflow period represents the low magnitude, low variability portion of the water year, which occurs in summer for Western North American rivers that experience a Mediterranean climate. Low flow magnitude was calculated as the minimum 7-day average discharge value, and the low flow duration was calculated as the number of days from May 1st – September 30th with discharge below the 20th percentile of flow.

4.3.3 *Climate covariates*

We explored a suite of candidate climatic variables (covariates) related to seasonal climate and ocean circulation patterns. For each individual watershed, we calculated time series of mean annual temperature (MAT), total annual precipitation (TAP), maximum annual monthly

temperature (MAT), maximum annual weekly precipitation (MAP), and both winter (October to March) and summer (April to September) soil moisture. We also calculated a single time series for the entire region of annual winter and summer anomalies of the Pacific Decadal Oscillation (PDO) and the El-Niño Southern Oscillation (ENSO). Daily mean temperature and precipitation data for each watershed were extracted through the Hydrometeorological Sandbox dataset (HYSETS; Arsenault et al. 2020). The meteorological data in the HYSETS are based on the Global Historical Climate Network Daily (GHCN-Daily) dataset (Menne et al. 2012). Arsenault et al. (2020) averaged the meteorological data from the GHCN-Daily dataset within each watershed with 1°extension using the Thiessen polygons method to obtain watershed-averaged time series. We used the watershed-averaged meteorological data in the HYSETS dataset for the analysis in this study. Soil moisture data was obtained from the TerraClimate dataset (Abatzoglou et al. 2018). The data consists of simulated monthly gridded soil moisture data with a spatial resolution of 1/24° by 1/24°. Covariate data spans 1958-2018 and contains no missing values. Pacific Decadal Oscillation (PDO) and the El-Niño Southern Oscillation (ENSO) indices, which characterize variability in sea surface temperatures over the Pacific Ocean, were obtained by year for all years in which we had data from the NOAA National Centers for Environmental Information, and average winter (October – March) and summer (April – September) anomaly values were used as covariates. Although some relationship between ENSO, PDO, and climate conditions is expected (e.g., McCabe and Dettinger 2002), we found relatively weak correlations among covariates within our model.

4.3.4 *Directional trend tests*

Monotonic (i.e., strictly increasing or decreasing) trend tests for all hydrologic metrics were performed for the entire period of record for each gage. Trend magnitudes were assessed

using the Theil–Sen slope estimator. The Theil–Sen slope is a robust estimator for trend analysis, as it uses the median slope of all data pairs (Thiel 1950; Sen 1968). It is more accurate for skewed or heteroskedastic data and comparable to least squares regression for normally distributed data (Wilcox 1998). Statistical significance was evaluated using the Mann–Kendall trend test with a threshold p-value of 0.05 (Mann 1945; Kendall 1975).

4.3.5 *Non-monotonic trend dynamics*

Non-monotonic trends in response time series (hydrologic metrics) were then modeled using dynamic factor analysis (DFA; Zuur et al. 2003), a multivariate technique partly analogous to principal component analysis in the time domain. At the extremes, hydrologic metrics among rivers can range from one synchronous time series to *n* individual and uncorrelated time series. The DFA approach fits each response time series (i.e., discharge metric for a given river) with linear combinations of covariates, latent trends modeled as random walks, and random error. Covariates are pre-specified times series that are *a priori* expected to correlate with the response times series, while each latent trend represents unspecified but shared sources of variation. Both covariates and latent trends explain variation in multiple response series, such that the number of covariates + latent "shared" trends required to model each response is much smaller than the number of observed time series. The influence of each covariate or latent trend on a given response time series is quantified through model coefficients, which can be thought of as the effect size of the covariate or trend on the response. All models were fit using maximum likelihood estimation by automatic differentiation, with Template Model Builder software, which we called using package TMB in R (R Core Team 2021, Kristensen et al. 2016).

DFA models include both observation and process uncertainty and are described by two parts. The process model, describes changes in the true, unobserved states of nature over time:

$$x_t = \mathbf{x}_{t-1} + \mathbf{w}_t \text{ where } \mathbf{w}_t \sim \text{MVN}(0, \mathbf{Q}) \quad (4.1)$$

$\mathbf{x_t}$ is the vector of latent trend values at time t and $\mathbf{w_t}$ is some random process error at time t, which is distributed as a multivariate normal with mean 0 and covariance matrix **Q**. **Q** is an identity matrix for model identifiability (Harvey 1990).

The second part of the DFA model is the observation equation, which relates observed data to the unobserved states:

$$y_t = \mathbf{Z}\mathbf{x}_t + \mathbf{D}\mathbf{d}_t + \mathbf{v}_t \text{ where } \mathbf{v}_t \sim \text{MVN}(0, \mathbf{R}) \quad (4.2)$$

$\mathbf{y_t}$ is the vector of observed hydrologic metrics for each river in year t. The matrix **Z** contains factor loadings that map each of the observed time series onto each of the latent variables in $\mathbf{x_t}$. **D** is the matrix of covariate coefficients, $\mathbf{d_t}$ is the vector of values at time t. The vector $\mathbf{v_t}$ contains the observation errors, which are distributed as a multivariate normal with mean vector **0** and covariance matrix **R**. Both the observed data and the covariates were standardized to have a mean of 0 and standard deviation of 1 to facilitate model comparisons and interpretation across states and spatial scales. Each hydrologic metric was modeled as a separate response variable.

For each response variable, we used the small sample Akaike information criterion (AICc; Burnham and Anderson 2004) to find the most parsimonious combination of covariates, latent trends, and the error structure. Starting with the hypothesis that all rivers (n = 185) effectively operate as a small number of synchronous time series, we fit models having from m = 1 up to a maximum of 6 latent trends. We chose to limit the possible number of shared trends to limit the number of models tested and allow for greater inferential parsimony. For the **R** matrix we explored two competing structures: same variance, zero covariance (implies that the same process variance is affecting all the time series) and same variance and covariance (assumes rivers covary, allowing joint information among time series to be modeled). Details on these

structures and their implications can be found in Holmes et al. (2012). After identifying a range of the more supported number of latent variables, we added environmental covariates in a modified forward stepwise procedure based on ΔAICc scores to determine whether any of the underlying patterns and latent variables in the time series data could be better represented by including environmental drivers as computational constraints prevented an exhaustive model search (Jorgensen et al. 2016; Table 4.1). We required that each additional factor or covariate explain at least 5% of total explained variance and reduce AICc. This strategy was intended to allow analysis of very large datasets, while only adding factors that explain a substantial portion of streamflow variance. We examined model fits to data and potential problems with residuals after ensuring that parameter estimation converged.

4.4 RESULTS

4.4.1 *River classification*

River hydrologic regime classification based on SWE to winter precipitation ratios resulted in 59 gages classified as rain-dominated hydrology, 61 gages classified as mixed hydrology, and 65 gages classified as snow-dominated hydrology (Figure 4.1; Figure 4.2). The ratio between SWE and winter precipitation varied strongly with both latitude and mean watershed elevation (Figure S4.1). Rivers in the rain-dominated class mostly occurred in southern California and coastal Washington and Oregon. High annual precipitation, mean winter temperatures above freezing, and mean elevations generally below 1000 m facilitated rain-dominance. Rivers in the snow-dominated class predominately occurred in British Columbia or high elevation areas of Washington and California (Figure 4.1). Snow-dominated rivers rarely had elevations below 1000 m. Glaciers provided additional summer melt-based flow in select snow-dominated class basins in British Columbia and Alaska (Curran and Biles 2021). Mixed

class rivers show the most variable hydrologic patterns. Although rainfall and snowmelt, on average, formed a primary and secondary high-flow mode in all mixed subclasses, rainfall and snowmelt timing and relative influence greatly varied across individual basins (Figure 4.2).

Hydrologic metrics differed across the river types. Generally, snow-dominated watersheds displayed a larger minimum flow magnitude, smaller peak flow magnitude, and later recession timing than either mixed or rain basins. Rain-dominated watersheds did not consistently differ from mixed watersheds, except for spring recession metrics. Rain-dominated watersheds experienced a larger and earlier recession than mixed watersheds. Watersheds at low latitudes experienced both shorter periods of high flow and longer periods of low flow (Figure 4.3). Furthermore, for all metrics except minimum flow magnitude, snow-dominated watersheds had a smaller standard deviation than mixed or rain-dominated watersheds across the period of record. Mixed basins were more variable than rain-dominated basins at comparable latitudes for minimum and peak flow duration and recession timing (Figure 4.3).

4.4.2 *Mann-Kendall trend results*

A relatively low proportion of rivers showed significant monotonic trends over time to suggest consistent shifts in hydrologic metrics (Figure 4.4). Minimum hydrologic metrics generally exhibited the largest trend estimates and highest rates of statistical significance. For minimum flow magnitude, 45% of gages showed significant trends, with over two thirds of those trends (68%) decreasing (smaller minimum flows through time). Minimum flow duration exhibited fewer significant trends (33% of gages), but with the vast majority showing longer minimum flow duration over time (84% of gages). Trends in peak flow and recession flow were generally not as large or significant (Figure 4.4). For peak flow magnitude, 18% of gages showed significant trends with 70% of significant trends decreasing (smaller peak flows through time).

Peak flow duration showed fewer significant trends (10% of gages), with the vast majority decreasing (81% of gages). For recession flow magnitude, 6% of gages showed significant trends with exactly half of them increasing (smaller recession magnitude through time). Recession flow timing displayed slightly more significant trends (7% of gages). Most gages exhibited earlier recession flows (75% of gages). The hydrologic metrics in this work do not exhibit strong temporal autocorrelation.

The monotonic trend analyses identified regionally distinct changes in discharge throughout the western United States and Canada that were somewhat consistent across all hydrologic metrics (Figure 4.4). For example, mid-latitude river basins (e.g., Washington and Oregon) showed the largest changes through time, indicated by generally large trend estimates. River class also loosely correlated with trend estimates. Trends in minimum flow magnitude, minimum flow duration and, to a lesser extent recession timing, all showed relationships with the ratio of SWE to winter precipitation (Figure 4.4). Typically, high latitude, snow-dominated watershed displayed increases in minimum magnitude, smaller decreases in minimum duration, and earlier spring recession. Nearly all gages with increasing flood magnitudes over time were snow-dominated basins.

4.4.3 *Dynamic factor analysis results*

The data best supported models with 3 to 4 common latent variables among the six hydrologic metric time series (Table 4.1). The best-fit model structure varied by metric, although most included TAP as a covariate (Table 4.1). Model structures are described in Table 4.1.

The covariate coefficients for the best-fit DFA model for each hydrologic metric are presented in Figure 4.5. Covariate coefficients varied with both latitude and river type. Summer soil moisture and winter ENSO anomalies were positively related to minimum flow magnitude,

particularly for mid-latitude rain-dominated basins. TAP was also positively related to minimum flow magnitude. Generally, covariates explained a large proportion of interannual variation for minimum flow duration. Covariate coefficients indicated that summer soil moisture and TAP exhibited inverse relationships with minimum flow duration: low summer soil moisture correlated with long minimum flow durations and high TAP correlated with short minimum flow durations. Precipitation metrics coefficients for peak flow duration and magnitude and recession magnitude were universally negative, with low latitude gages displaying larger coefficients. For peak flow duration, rain-dominated watersheds had larger coefficients for MAP than mixed watersheds for similar latitudes. Covariates explained relatively little variation in recession timing, although snow and mixed watersheds exhibited generally positive TAP coefficients.

The DFA analysis identified regionally distinct changes in discharge not accounted for by climate covariates throughout the United States and Canada (Figures 4.6-4.8). These regions were not necessarily consistent across hydrologic metrics. Latent variable factor loadings for peak flow magnitude clustered in narrow geographic areas, for example Southern British Columbia and Washington for trend 1, and Northern California and Oregon for trend 2 (Figure 4.6). Clusters were relatively small and there was no coherent response associated with basin type. Alternatively, latent variable factor loadings for minimum magnitude flow were much more dispersed, with relatively similar loadings over broad geographic areas and the latent variables themselves varying more smoothly though time (Figure 4.7). The latent variable factor loadings for recession timing exhibited the greatest cohesion across river type (i.e., Trend 1, Figure 4.8).

4.5 Discussion

River hydrology in western North America is driven by seasonal periods of wet and dry conditions over an annual cycle. The strong latitudinal gradient in both temperature and

precipitation, interannual fluctuations in global-scale atmospheric circulation processes, and large elevation gradients make the West Coast of North America an interesting region to study the relative influence of local-scale morphological versus regional-scale climactic in governing patterns of hydrologic change.

4.5.1 *Metrics capture important facets of the hydrologic regime*

Dynamic, seasonal flow regimes support critical ecosystem processes such as disturbance, habitat provisions, and native species life history cues. Distilling discharge regimes down into key elements is a complex task, and as a result hundreds of metrics describing flow regime have been proposed (Poff et al. 1997, George et al. 2021), many of which lack biological relevance (Carlisle et al. 2017) or are redundant (Olden and Poff 2003) and lack consistent relationships between flow and ecologic response (Webb et al. 2013). Here we selected a series of discharge metrics that describe facets of the hydrograph timing, magnitude, and duration and which have documented relationships with ecological, geomorphic, or biogeochemical processes in riverine systems or socio-economic needs for water.

Overbank (flood) flows are a well-recognized functional flow component that supports a broad suite of physical and ecological processes, including the maintenance of habitat heterogeneity in space and time (Ward et al. 1998), providing cues for fish migration and reproduction (Jeffres et al. 2008) and controlling patterns of riparian succession (Ward and Stanford 1995). The baseflow, or low flow, period coincides with peak demand and the agricultural growing season, and drought years can pose severe economic consequences for farmers because of decreased crop yields (Jaeger et al. 2017, Banerjee et al. 2018, Al-Kaisi and Kwaw-Mensah 2020). Low river flows and associated warm stream temperatures have a range of ecological consequences for native fish such as Pacific salmon, including range contractions

(Isaak and Rieman 2013), accelerated emergence of fry and an associated phenological mismatch with available food resources (Steel et al. 2012), higher rates of metabolic stress, and increased susceptibility to pathogens and disease (Goniea et al. 2006). Finally, spring recession flows can provide cues for migration for native fish species, and Pacific salmon use high flows to migrate upstream to areas suitable for spawning (Quinn and Adams 1996). Previous studies have largely used Spring Pulse Onset (SPO) or Center of Timing (CT) to describe spring recession changes (Stewart et al. 2005). This study, on the other hand, uses a flexible metric that describes the transition timing from winter high flows to summer baseflows, and maintains ecological significance across river class.

4.5.2 *Trends in peak flows are driven by interannual variability in precipitation*

Peak flow metrics showed limited monotonic change (Figure 4.4), strong regional cohesion, and high interannual variability through time (Figure 4.6). Results for peak flow metrics were closely tied to changes in TAP and MAP, with wetter conditions and larger individual storms producing longer duration and larger magnitude peak flows (Table 4.1; Figure 4.5). The absence of monotonic changes is consistent with recent work that found limited change to maximum flows (Kundzewicz et al. 2005, Burn et al. 2010, Kormos et al. 2016), despite consistent model-based projections of increased flood magnitudes in western rivers (Wrzesien and Pavelsky 2020, Chegwidden et al. 2020). Clustering of time series in particular geographic regions of the domain (for example, coastal areas of WA, OR, and northern CA), the lack of a coherent response associated with basin type, and the importance of MAP as a covariate suggest that the primary mechanism that determines flood risks in certain climate categories is the spatial distribution of winter storms. This is not to say that variability in catchment properties does not play some role in determining flood risks. For example, for peak magnitude flows, snow-

dominated and mixed basin MAP coefficients were smaller than those of rain-dominated basins at similar latitudes (Figure 4.5). Additional regional conditions such as elevated soil moisture or enlarged contributing basin area due to high temperatures likely account for the spatial cohesion that exists even after accounting for precipitation effects (Ralph et al. 2013; Nied et al. 2013). Such effects, however, appear secondary to storm track behavior affecting precipitation (Hamlet and Lettenmaier 2007).

The dominance of precipitation variability as a driver of discharge across western North America has been well documented (Nash and Gleick 1991, McCabe and Wolock 2011), although relatively few studies have examined spatial variation in the role of precipitation driving magnitude and duration of peak flows. Predictably, covariate coefficients in our study illustrate that higher total and maximum precipitation led to larger maximum and longer duration peak flows, with the largest precipitation coefficients in low latitude, rain-dominated basins (Figure 4.5). Atmospheric rivers (AR) have been shown to be an important source of intraseasonal and interannual variations in precipitation and discharge in the western United States and contribute most of the total wet season precipitation (Dettinger 2013, Rutz et al. 2014). The effect of AR storms is particularly pronounced in low latitudes, with the majority of winter precipitation occurring in just a few AR storms (Dettinger 2011, Rutz et al. 2014, Gershunov et al. 2019). For California, year-to-year fluctuations in precipitation strongly reflect year-to-year fluctuations of contributions from the largest storms, with the large-storm contributions explaining about twice as much precipitation fluctuation as do contributions from all remaining storms combined (Dettinger 2016). The small number of intense storms may indicate that California river basins are less dependent on antecedent conditions such as soil moisture (Ralph et al. 2013, Berghuijs et al. 2019) or total winter precipitation in generating

flood conditions, and therefore flood events more closely vary with the single largest annual precipitation event. Relatively low MAP coefficient estimates for mixed and snow-dominated basins for peak magnitude likely occurred because, while correlated with total winter precipitation, MAP does not account for temperature mediated cycles of melt and accumulations that often contribute to maximum flows in snowmelt influenced basins (Fritze et al. 2011, Gangopadhyay et al. 2019).

4.5.3 *Trends in recession flow cluster by river type*

Numerous studies have examined changes in snow over the western United States due human-induced climate change using both empirical observations and model-based projections (e.g., Cayan et al. 2001, Mote 2003, Regonda et al. 2005, Knowles et al. 2006, Das et al. 2009). Formal detection and attribution studies have shown that anthropogenic climate change has already increased winter temperatures and reduced the fraction of cold-season precipitation retained in the spring snowpack (e.g., Barnett et al. 2008, Bonfils et al. 2008, Pierce et al. 2008). Despite these clear climactic shifts, recession flow metrics in our study showed relatively limited directional change through time (Figure 4.4). The paradox of clearly detectable trends in snowpack but a limited discharge response is easily explained. Pierce and Cayan (2013) found that snowpack metrics closely tied to precipitation (e.g., total cold-season snowfall) take decades longer than those tied to temperature (e.g., fraction of snow in winter precipitation) to achieve a statistically significant linear trend because precipitation has large natural variability and only a weak anthropogenic trend in the western United States (Siler et al. 2013, Marshall et al. 2019). Recession metrics included in this study are similarly tied to variable precipitation dynamics (Figure 4.5). Recession timing, which is more strongly linked to temperature induced snowpack melt in snow-dominated and mixed basins, exhibited relatively stronger trends as a result. These

results mirror a recent study looking at trends in SWE across western North America, which found that changes in melt timing have occurred more frequently and observably than changes in total SWE accumulation (Musselman et al. 2021). The recession timing metric used in this study represents the transition timing from the wet to dry season, characterized by a steady decline of flows over a period of weeks to months. This metric differs from previous studies, which have largely examined the start of snowmelt or center of streamflow timing to describe spring recession changes in snow-dominated watershed and found more robust trends (Stewart et al. 2005). Taken together, these results indicate that spring recession characteristics are not changing uniformly; new paradigms, such as a large snowpack that melts early, may develop as a result.

4.5.4 *Trends in minimum flows show large, widespread decreases*

Trend analyses indicated large, widespread declines in low flow metrics across western North America over our period of record. Nearly half of all gages showed significant changes to minimum flow magnitude and a third showed significant change to minimum flow duration (Figure 4.4). Widespread declines in summer discharge and lengthened duration of dry conditions are consistent with previous trend analyses of regional hydrology (Luce and Holden 2009 p. 20, Kormos et al. 2016). Overwhelmingly, rain-dominated and mixed rivers shifted to smaller magnitude and longer duration baseflow conditions. High latitude snow-dominated basins generally experienced higher minimum flow magnitude, which can be explained by both an increased contribution from melting glacial and permanent snow (Nolin et al. 2010) or, for a select number of sites where minimum flow occurs in winter, an increase in precipitation falling as rain rather than snow during these periods (Dierauer et al. 2018).

Nearly all sites experienced a longer summer baseflow period, although trends are largest where snowmelt is a negligible component of discharge. Generally, changes in minimum flow duration and magnitude covaried with one another; indicating that when low flows were lower (higher) than average, the duration of low flows also, in general, were longer (shorter) than average. Similar to other metrics, minimum flow metrics showed regional cohesion in latent trend loadings. However, the spatial extent of loadings was much larger than for peak magnitude metrics. The broad spatial loadings of baseflow metrics indicates that mechanisms impacting hydrological droughts occur over a larger spatial scale, with small-scale variations in precipitation characteristics (e.g., individual storm events) not nearly as important as long-term variability (Gaál et al. 2012).

Changes to baseflow metrics were closely tied to both summer soil moisture and TAP, with the highest soil moisture loadings in mid-latitude rain-dominated basins and the role of TAP most pronounced in snow-dominated, mixed, and low latitude, California rain-dominated basins (Figure 4.5). Previous studies have largely found that the interannual variability in low flows is dominantly controlled by precipitation, with higher annual precipitation leading to shorter, less severe low flows (Godsey et al. 2014, Jenicek et al. 2016, Kormos et al. 2016). The role of temperature is thought to be secondary; however, recent studies illustrate that droughts in western watersheds can be amplified by warm temperatures that exacerbate the effects of precipitation deficits (Diffenbaugh et al. 2015, Woodhouse et al. 2016). Our results align with this framework for snow-dominated and mixed basins, wherein baseflow conditions and TAP covary strongly. On the other hand, the importance of soil moisture in mid-latitude rain-dominated basins potentially reflects the role of geology in mediating baseflow conditions in the absence of snowpack. Soil moisture represents the combined influence of temperature,

precipitation, and geologic context (Abatzoglou et al. 2018) and is recognized as an important variable for land-climate interactions and extreme events (Seneviratne et al. 2010, Hirschi et al. 2011) as well as for hydrology and its extremes in the landscape (Van Loon 2015, Orth and Destouni 2018). Mechanistically, the importance of soil moisture is explained by soil moisture changes imply corresponding changes in groundwater table depth (Destouni and Verrot 2014). It is also likely that soil moisture represents an integrated metric of precipitation and temperature over a more representative period (i.e., summer) rather than the total or maximum metrics calculated for temperature and precipitation and is therefore more reflective of summer water availability in basins without snowpack as storage.

In our results, we saw that summer ENSO anomalies most strongly affect minimum flow magnitude and PDO correlated with peak flow magnitude (Table 4.1). Both PDO and ENSO phenomenon are defined by sea surface temperature anomalies, with the extreme phases classified as being either warm or cool, as defined by ocean temperature anomalies in the Northeast and tropical pacific. A primary difference between the two is that PDO captures decadal-scale variability, whereas ENSO events tend to persist on the order of one year (Zhang et al. 1997). Additionally, although both processes influence the entire Pacific, ENSO primarily affects the climate of lower latitudes and PDO primarily affects the North Pacific region (Mantua et al. 1997, Mantua and Hare 2002). Previous studies have found more widespread impacts, including that during warm PDO and ENSO years, flood risks are generally lower in the Pacific Northwest and northern California, and higher in southern California and the Columbia River basin (Piechota et al. 1997, Dettinger et al. 1998, Gershunov and Barnett 1998).

4.5.5 *Caveats and limitations*

We note several considerations when evaluating our results. In this study, we use the ratio of SWE to winter precipitation to capture basin-specific differences in catchment properties. Using this ratio ignores processes such geologic controls on groundwater discharge, which have been shown to be an important influence across the study area in controlling both high and low flows (Safeeq et al. 2013, 2014). Geologic data such as subsurface permeability and porosity is available for all watersheds within the study area (Gleeson et al. 2014), and future work should examine to role of geology in mediating river response to climatic drivers. Understanding the role of basic characteristics such as vegetation cover may also be important, as increases in evapotranspiration associated with increased longwave radiation are expected to contribute to decreases in summer low flows in the region (Roderick et al. 2013). Furthermore, the long study period, combined with a broad geographic region, limited covariate data availability to totals, averages, or maximums across seasons and years. Conducting additional analyses with targeted questions and nuanced metrics of climate signals may further elucidate mechanisms driving streamflow and explain additional variability currently modeled by DFA latent trends.

At the scale of western North America, gridded datasets provide a rough approximation of key hydroclimate variables such as soil moisture, precipitation, and temperature. However, gridded data are averaged over considerable spatial heterogeneity, including complex topography, and as a result estimated values may not always reflect local catchment conditions. Simulated soil moisture is a highly simplified representation of actual conditions and will not always accurately represent event-scale catchment conditions (Abatzoglou et al. 2018). More complex, process-based models can be used to infer the importance of various drivers to hydrological events, however, these models still come with substantial uncertainties (Zaherpour

et al. 2018). Our decision to use relatively simple covariates averaged across a single year and examine relative changes rather than absolute values enables detections of large-scale patterns but likely smooths over watershed specific nuances at the event scale.

Lastly, it is important to note that this analysis was designed to identify major climatic drivers of discharge across western North America, not to identify the most important individual drivers within each basin. The DFA model selection process included covariates based on average importance across all basins. Therefore, a covariate's lack of inclusion in a best fit model or poor overall fit (indicated by a high AIC value) does not necessarily indicate that this process is unimportant to all rivers included in this study. Rather, it indicates that over the average of all basins examined in this study, including the covariate did not produce the necessary increase in overall model fit to warrant inclusion. Future studies could examine the relative importance of various flood, drought, or recession generating mechanisms at an individual site scale, to determine if results are consistent with our findings. Future work could also examine shifts in the importance of different mechanisms over time, as our study assumes a constant relationship through time (Milly et al. 2008).

4.5.6 *Management implications*

Our study provides an approximation of how physical and climate driver importance varies across spatial scales and highlights that geographically localized interannual variation is the dominant control on observed changes to discharge. Hydrologic research often considers mean changes or trends through time (e.g., Cayan et al. 2008; Mote and Salathe 2010), however, extreme events and interannual variability often affect natural systems more than mean changes, particularly on local-to-regional scales. Water resources infrastructure must accommodate such variability; however, aspects of the water supply system such as dams and reservoirs, are

designed for present-day climate patterns and generally assume the probability of precipitation or discharge extremes are statistically stationary (Milly et al. 2008). Additionally, although organisms native to western North America may be adapted to seasonal disturbance regimes, when coupled with high interannual variability even modest trends may push species outside their tolerance limits. Looking forward, information on climate sensitivities of hydrologic processes and patterns of clustering across rivers can be used as a tool to identify regions with potential vulnerabilities to future climatic conditions and prompt additional research towards understanding the complexity of river discharge regimes (Dettinger et al. 2015).

Shifts in hydrologic metrics across western North America have major implications for the health of aquatic ecosystems. Our study identifies large, widespread decreases in baseflow magnitude and increases in baseflow duration. These trends are likely to continue with climate change. Dry spells are projected to lengthen in most regions, especially across the southern and northwestern parts of the contiguous United States (Walsh et al. 2014), with the most consistently projected increases being for the numbers of dry days in the southwest and up the coast (Polade et al. 2014). Given the joint influence of precipitation and summer soil moisture in our study, the most severe droughts will likely occur due to the combination of warm and dry conditions, with temperature mediated decreases in soil moisture playing a more important role in mid-latitude basins (Figure 4.5). Increased duration and severity of the summer baseflow period portends difficulties for native fish and water resource management. Reduced summer baseflow could lead to increased stream temperature that exceed the tolerance of native species (Steel et al. 2019; Isaak et al. 2010), decreased habitat connectivity and reduced total habitat availability (Lake 2003), and increased pollutant concentrations through decreased dilution capacity (Mosley 2015). Furthermore, summer is the period of peak water consumption (Jaeger

et al. 2017), and a reduction in summertime discharge will increase competition between instream flow requirements and out-of-stream demands (Jaeger et al. 2013, 2017, Averyt et al. 2013).

Our results also indicated that precipitation that falls in a catchment has historically been the dominant control on peak flows, compared to air temperature and global circulation metrics. Across the west, climate models predict increasing year-to-year variability of precipitation, whereas change in total precipitation is not projected with confidence (Luce et al. 2013, Gershunov et al. 2019). Some studies project intensification of precipitation in the Pacific Northwest and decreased precipitation in the southwest United States, consistent with a projected poleward shift of mid-latitude storm tracks (Baker and Huang 2014, Wrzesien and Pavelsky 2020, Salathé 2006, Mbengue and Schneider 2013, 2017). Increase in heavy and extreme precipitation have almost entirely been due to AR dynamics: years with many AR episodes, ARs with higher-than-historical water-vapor transport rates increase, and AR storm-temperatures are all projected to increase (Dettinger 2016). Due to their role in extreme precipitation generation, ARs have been identified as the primary source of hydrologic flooding across western United States, particularly along the Pacific Coast (Barth et al. 2017, Konrad and Dettinger 2017). Given projected changes to precipitation variability, the high sensitivity of peak flow magnitudes to MAP, as is supported by this study, suggests an increase in flooding despite limited monotonic change in peak flow magnitude. Areas such as California and coastal Oregon, which exhibited the largest MAP covariate coefficients in our analysis, may experience particularly severe and frequent flooding, resulting in substantial ecological and economic impacts (Corringham et al. 2019).

Our study also offers insights into best practices for hydrologic trend analyses. The analysis of historical data to extract trends in hydroclimate data is a common practice in hydrology (Burn and Hag Elner 2002). In this study, we first utilized the most common trend analysis method, the Mann-Kendall test and Thiel-Sen slope estimator, to examine monotonic changes in ecologically relevant hydrologic metrics. Our results, like many others, show patterns of change consistent with theoretical predictions, but relatively few significant trends (Zhang et al. 2001, Ehsanzadeh and Adamowski 2007, Ficklin et al. 2018). Several factors likely contribute to this outcome. The Mann-Kendall and Theil-Sen trend tests are sensitive to oscillations within the data, particularly for time series that are short relative to the cycle length of the oscillation (Chen and Grasby 2009). Such oscillations are common in hydroclimate data influenced by decadal and inter-decadal global circulation processes, and these patterns are particularly pronounced for western North America. Furthermore, relatively weak trends, short time series, and high interannual variability can contribute to the lack of detectability (Kundzewicz 2005). Additionally, our analysis and others that utilize the Mann-Kendall trend test necessitate many statistical tests. Multiple testing increases the chance of finding a statistically significant result by chance alone. Estimates of significance should therefore be assessed in terms of general patterns across all time series, rather than focusing on individual site results. DFA analysis overcomes many of the limitations of the Mann-Kendall test by allowing for greater flexibility in trend form and number. Individual trend tests consistent with the DFA framework can also be conducting by modeling time series as biased random walks, with the bias term equivalent to the Thiel-Sen slope estimator. Moving beyond monotonic trend analyses to detect regional patterns and changes will be an essential step for western water management.

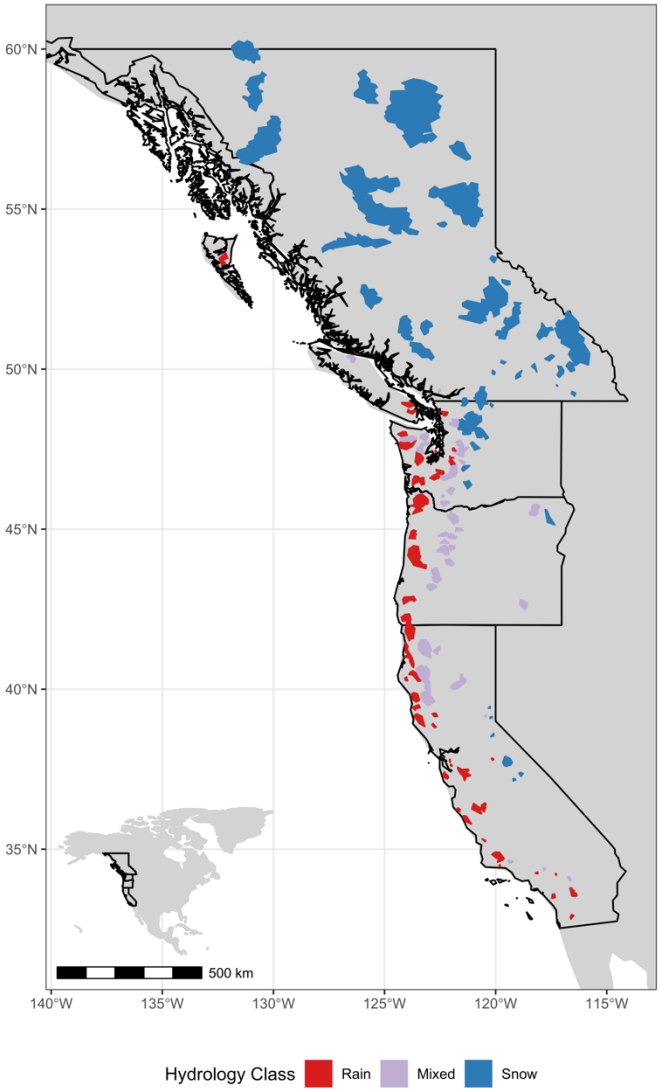

Figure 4.1. Locations and upstream watershed area of gages in each of the three seasonal flow regime classes.

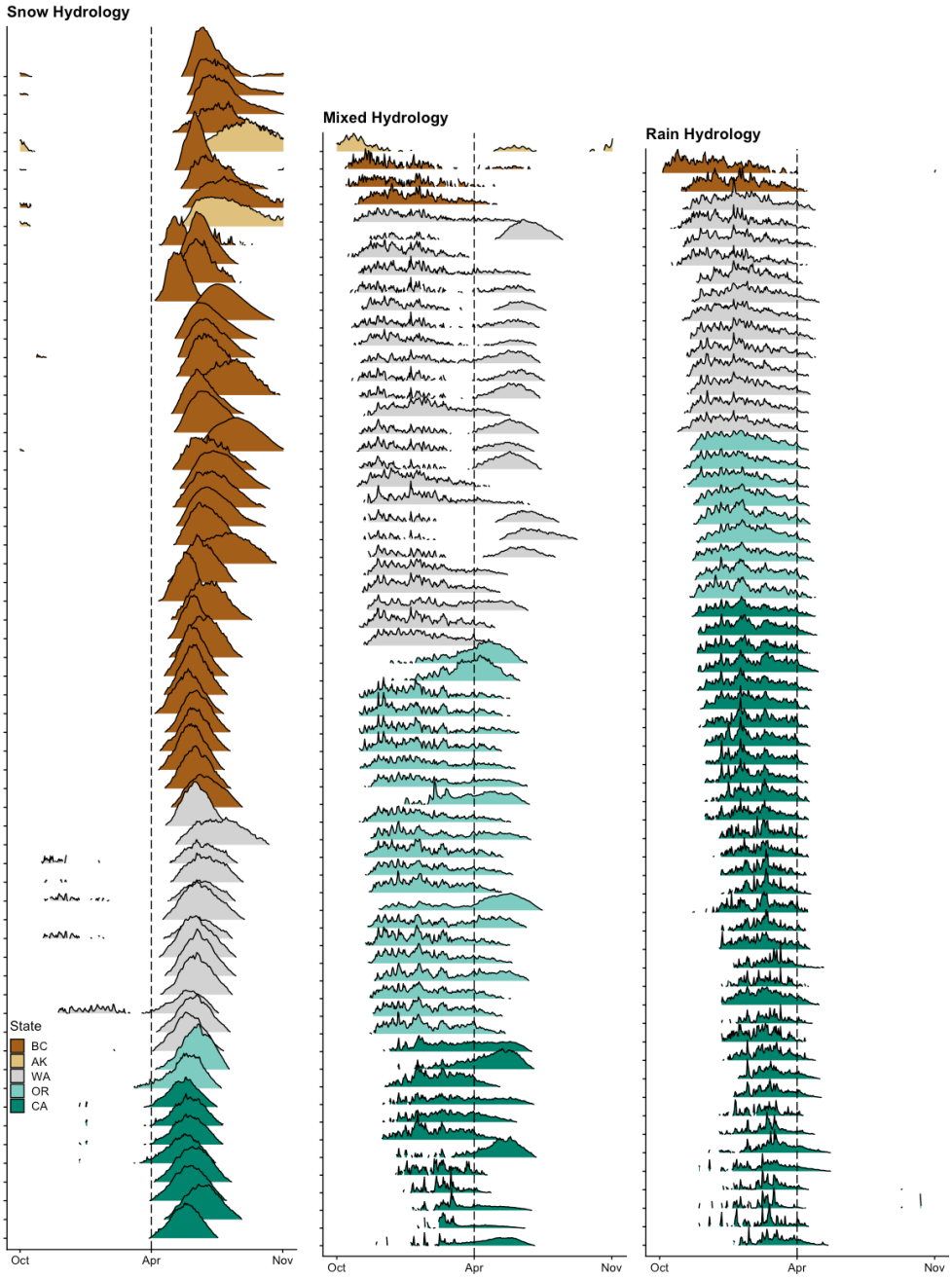

Figure 4.2. Hydrographs of normalized mean daily streamflow for three seasonal flow regime classes: snow, mixed, and rain, colored by state and ordered by latitude. Normalized mean daily streamflow is shown on a linear scale. The black dotted line shows April 1st, which is commonly considered the date of peak SWE across western North America.

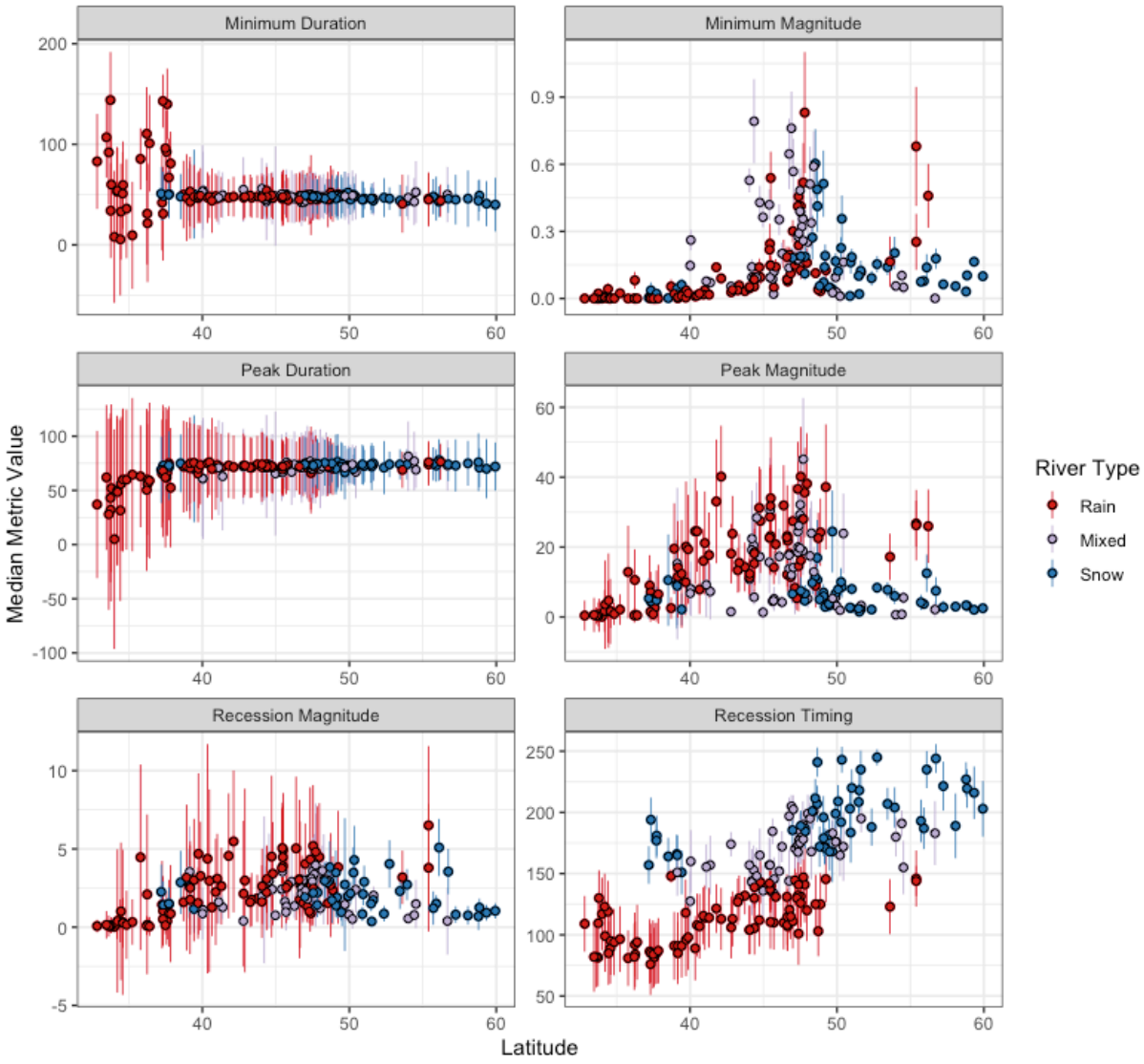

Figure 4.3. Median values and standard deviation across each site's period of record for each of the six metrics versus latitude. Points are colored by river basin type. All magnitude metrics are standardized by watershed area to facilitate comparison.

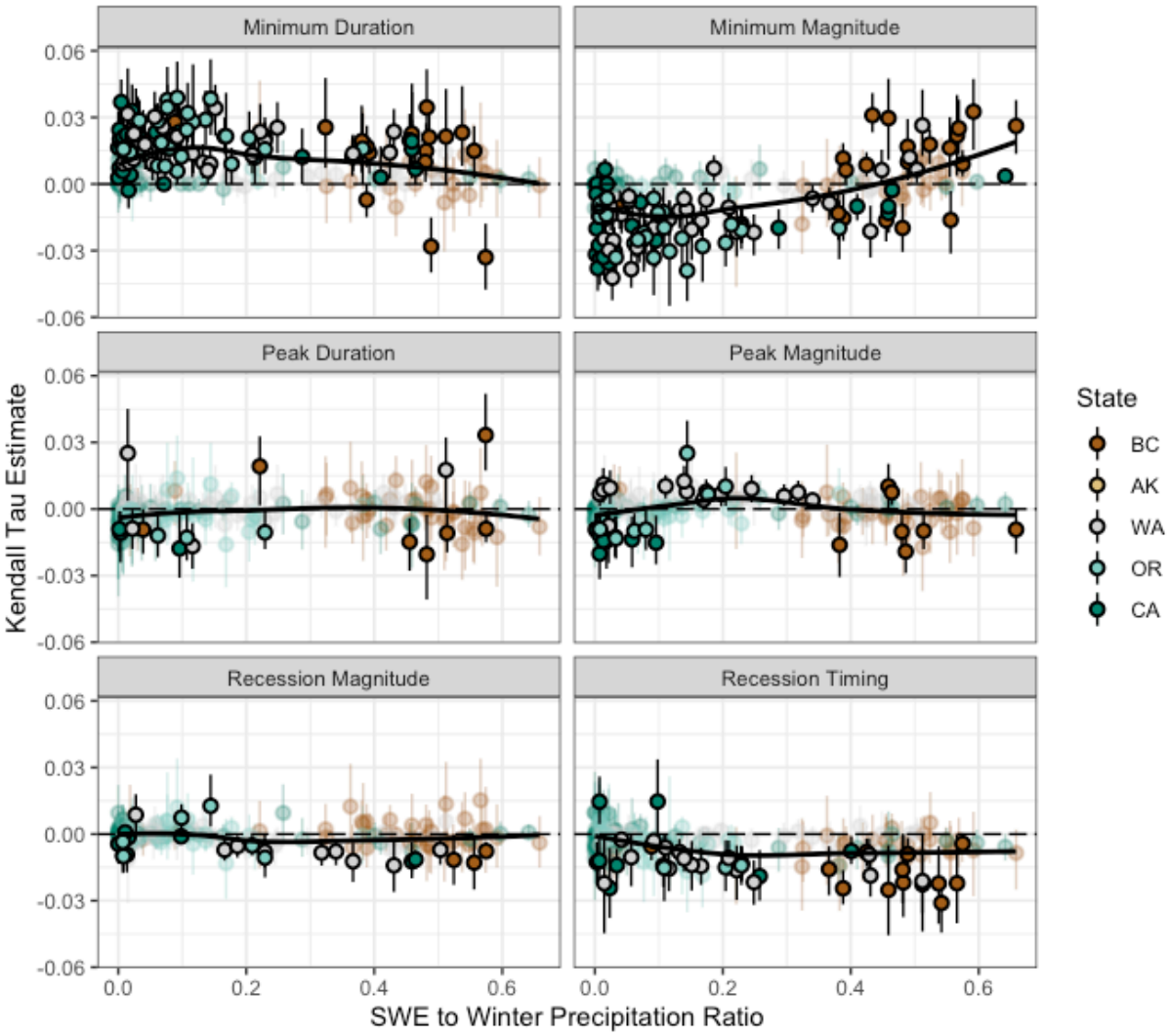

Figure 4.4. Mann-kendall trend test tau estimates, representing the monotonic trends through time, for each of our six metrics versus SWE to winter precipitation ratios. Colored by state. Significant results are shown in color. A loess smoothing line using all trend estimates is shown in black.

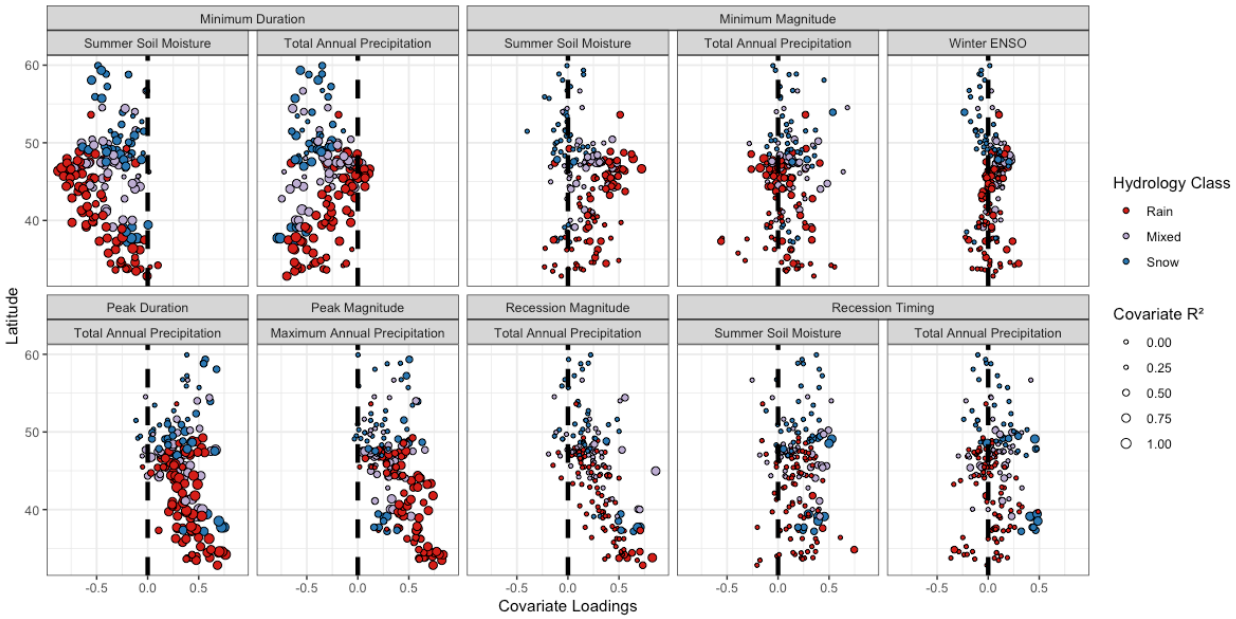

Figure 4.5. Covariate coefficients for all flow magnitude metrics from best fit DFA models. The size of each circle indicates the proportion of variance explained by all covariates within the best-fit model.

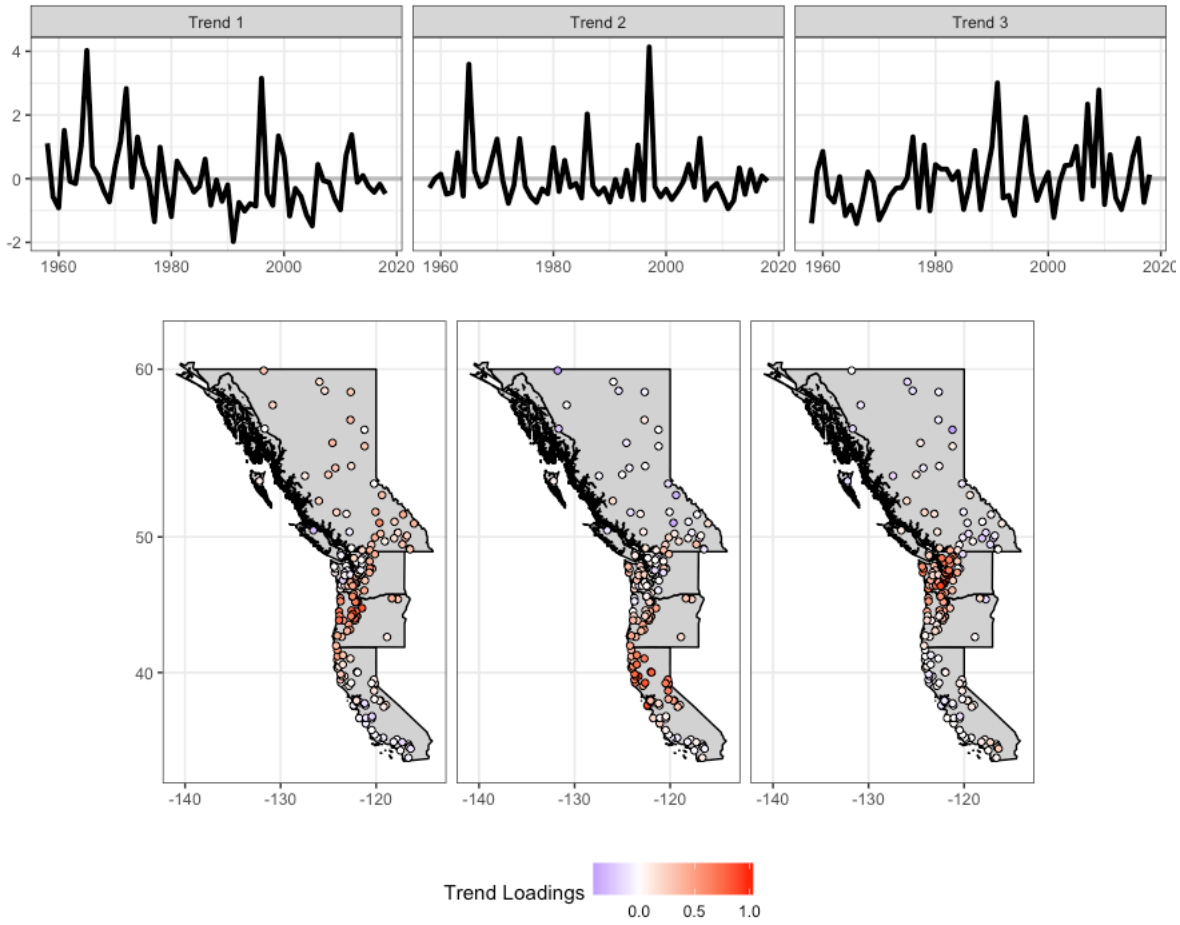

Figure 4.6. Latent variables (top row) and factor loadings per latent variable for the best-fitting model for peak flow magnitude. Points are colored by their factor loading, where their values indicate strength of latent variable association.

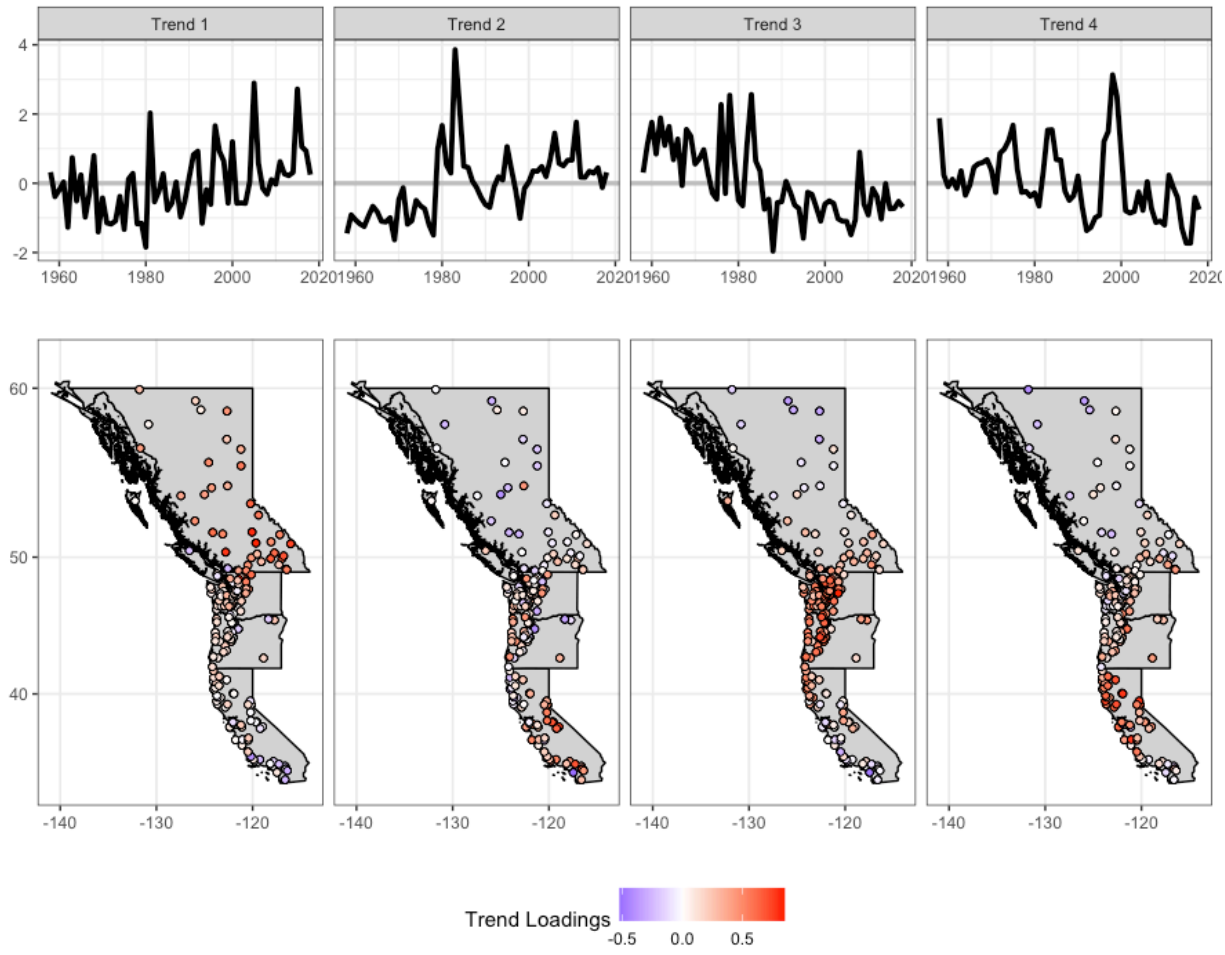

Figure 4.7. Latent variables (top row) and factor loadings per latent variable for the best-fitting model for minimum flow magnitude. Points are colored by their factor loading, where their values indicate strength of latent variable association.

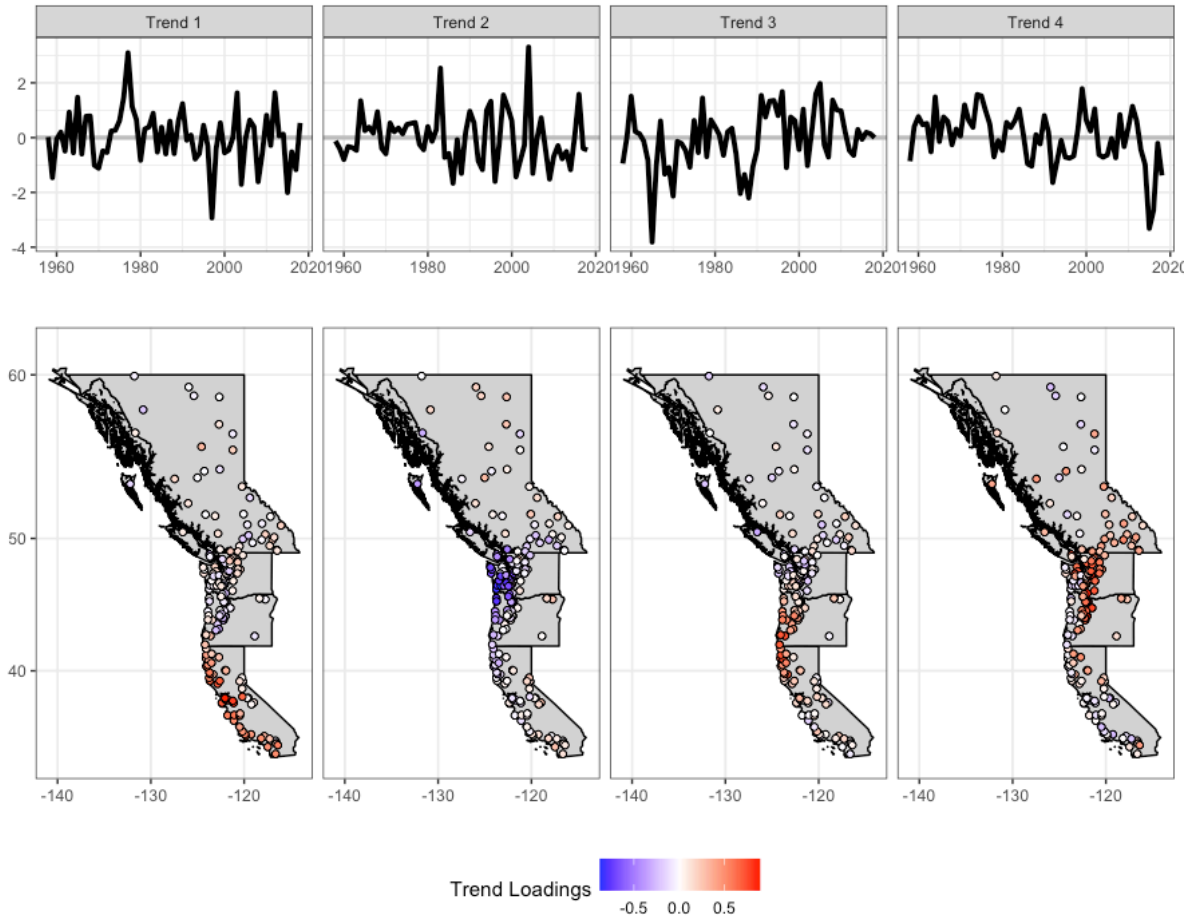

Figure 4.8. Latent variables (top row) and factor loadings per latent variable for the best-fitting model for recession flow timing. Points are colored by their factor loading, where their values indicate strength of latent variable association.

Table 4.1. Delta AIC values for each of the DFA models with covariates. The covariates included in each final best-fit model are shown in bold.

	Hydrology Metrics					
	Peak Flow Magnitude	Peak Flow Duration	Min Flow Magnitude	Min Flow Duration	Recession Magnitude	Recession Timing
Latent Trends	3	3	4	4	4	4
No Covariates	1494.7	1482.4	231.7	1452.3	324.0	378.7
T_{mean}	1590.3	1401.3	226.5	510.5	437.8	242.2
T_{max}	1647.6	1336.8	198.1	1251.2	426.8	417.7
P_{MEAN}	290.7	**0.0**	**62.9**	**297.6**	**0**	**109.1**
P_{MAX}	**0.0**	839.3	209.7	1175.1	238.5	158.3
$Soil_{SUMMER}$	1981.5	1068.0	**0.0**	**0.0**	316.0	**0.0**
$Soil_{WINTER}$	2084.2	1469.6	241.4	1474.6	457.5	387.7
PDO_{WINTER}	671.9	1500.5	234.4	1590.2	496.3	528.8
PDO_{SUMMER}	684.6	1622.2	272.6	1502.5	466.6	514.2
SOI_{Winter}	1661.3	1486.3	**140.5**	1590.2	453.3	556.7
SOI_{Summer}	1645.2	1645.7	374.9	1502.5	473.1	519.1

Chapter 5. EMPIRICAL STREAM THERMAL SENSITIVITIES CLUSTER ON THE LANDSCAPE ACCORDING TO GEOLOGY AND CLIMATE

5.1 ABSTRACT

Climate change is modifying river temperature regimes across the world. To apply management interventions in an effective and efficient fashion, it is critical to both understand the underlying processes causing stream warming and identify the streams most and least sensitive to environmental change. Empirical stream thermal sensitivity, defined as the change in water temperature with a single degree change in air temperature, is a useful tool to characterize historical stream temperature conditions and to predict how streams might respond to future climate warming. We measured air and stream temperature across the Snoqualmie and Wenatchee basins, Washington during the years 2014-2021. We used ordinary least squares regression to calculate seasonal summary metrics of thermal sensitivity and time-varying coefficient models to derive continuous estimates of thermal sensitivity for each site. We then applied classification approaches to determine unique thermal sensitivity regimes and to establish a link between environmental covariates and thermal sensitivity regime. We find a diversity of thermal sensitivity responses across our basins that differ in both timing and magnitude of sensitivity. We also found that covariates describing underlying geology and snowmelt were the most important in determining cluster membership. Our findings can be used to inform strategies for river basin restoration and conservation in the context of climate change, such as identifying climate insensitive areas of the basin that should be preserved and protected.

5.2 INTRODUCTION

Climate change is modifying river temperature regimes across the world. As water temperature is a critical component of aquatic ecosystems, these changes will alter the thermal habitat of many lotic organisms (Daufresne and Boët 2007). To apply management interventions in an effective and efficient fashion, it is critical to both understand the underlying processes causing stream warming (Arismendi et al. 2014, Steel et al. 2017) and identify the streams most and least sensitive to environmental change (Parkinson et al. 2016, Pyne and Poff 2017, Jackson et al. 2018).

Empirical stream thermal sensitivity, defined as the change in water temperature with a single degree change in air temperature, or the slope of the statistical relationship between air temperature and water temperature, has been widely used to characterize historical stream temperature conditions and to predict how streams might respond to future climate warming. Thermal sensitivities reflect the combined influence of both spatially and temporally varying meteorological and hydrological factors. Variation in solar radiation is the most important driver of both air and river temperature, and as a result, air and river temperatures are typically correlated (Johnson 2003). Stream temperature is also influenced by runoff composition where snowmelt, surface runoff, or groundwater inflow entering the stream have different temperature signatures than the stream itself (Webb and Zhang 1997, Mohseni and Stefan 1999). Inputs from water sources such as snowmelt and groundwater upwelling decouple air and water temperatures and result in a decreased thermal sensitivity of water temperature to air temperature (Tague et al. 2007, Mayer 2012, Johnson et al. 2014).

Generally, larger thermal sensitivities indicate that water temperatures are more likely to track changes in air temperature (Isaak et al. 2016, Mauger et al. 2017, Isaak et al. 2018b);

however, there are concerns about employing this approach to predict future stream temperatures. Past studies have found that using empirical relationships for extrapolating to future climate scenarios without accounting for underlying processes such as snowmelt, groundwater, and thermal memory may provide inaccurate predictions of future stream temperatures (Leach and Moore 2019, Steel et al. 2019). Furthermore, under changing climatic conditions, the interrelations between air temperature and the other processes controlling stream temperature may not remain stable (Arismendi et al. 2014). Despite these shortcomings, thermal sensitivity remains a commonly used and straightforward tool that allows for comparison between locations within rivers and has the potential to guide management.

The relationship between air and water temperature can also be a useful predictive tool for hydrological processes. Thermal sensitivity has been used in the past to estimate areas of shallow and deep groundwater influence (Snyder et al. 2015, Briggs et al. 2018) and understand the role of snowmelt in modulating river temperature (Lisi et al. 2015, Winfree et al. 2018). Furthermore, physical characteristics of basins can mediate how meteorological (e.g., solar radiation, air temperature and precipitation) and hydrological (e.g., discharge and water source) processes impact thermal sensitivity. For example, stream networks can exhibit patchy thermal conditions due to spatially heterogeneous landscape attributes such as riparian shading, valley form and aspect, and geology (Bogan et al. 2003, Benyahya et al. 2010). The thermal sensitivity of stream may vary substantially over relatively small spatial extents, and large-scale models that do not incorporate fine-scale variation in thermal sensitivity may not accurately predict thermal habitat at ecologically relevant scales.

Both deterministic and statistical models have been used to study the relationship between air and water temperature (Caissie 2006, Dugdale et al. 2017, Ouellet et al. 2020).

Physical processes-based models are based on the balance of energy (heat) and mass (flow) fluxes in a water body (Glose et al. 2017). Process-based approaches allow the identification of the most important drivers in the heat budget of streams across timescales, improving the resolution and accuracy of stream temperature predictions (Stefan and Sinokrot 1993, van Beek et al. 2012, Wondzell et al. 2019). Issues exist with process-based modeling, including intensive data and computational efforts, limited ability to generalize across basins, and difficulty representing groundwater and subsurface flow paths. Statistical models are computationally simpler with potentially minimal data requirements (Benyahya et al. 2007) facilitating prediction at ecologically relevant spatial grains and extents. These models are appealing because of their simplicity and limited requirement of meteorological and hydraulic data, while still being characterized by high levels of explained variance in some basins. However, it can be difficult to derive insights about river response to perturbations from statistical models as statistical approaches rely on relationships that may not extrapolate well to future conditions (e.g., relationships may change between water temperature and covariates such as flow or the composition and coverage of riparian vegetation and land use). Statistical models currently lack a clear understanding of the relationships between derived model coefficients and important watershed processes, potentially limiting their utility.

There is a need to better understand how thermal sensitives evolve throughout the year and on river networks. A clearer vision of how thermal sensitivities vary will allow managers to understand what a single snapshot in time or space may indicate. Identification of groups of streams that share similar patterns of thermal sensitivity will also have management relevance. Clusters of streams with similar thermal sensitivities will likely also share similar risk profiles; managers may therefore tailor investment by streams within groups based on watershed specific

influences (Mayer 2012). Examining whether these clusters are stable through time and season can provide insight into how river thermal sensitivity may evolve under nonstationary air temperature and precipitation regimes. This study aims to answer three questions across two river basins: **1)** What is the spatial and temporal distribution of commonly used air-water temperature metrics across each basin? **2)** What are the characteristic regimes of air-water temperature correlations and how do they cluster on the landscape? And **3)** What are the landscape or climate factors that drive the decoupling between air and water temperature across each basin?

5.3 METHODS

5.3.1 *Study area*

The Snoqualmie River begins as three distinct forks in the Mt. Baker Snoqualmie National Forest and drains a 1,813 km^2 watershed on the west side of the Cascade Range, Washington. The three forks originate in forested public land before converging and flowing through a mix of agricultural, residential, and commercial land use. On one major tributary, the Tolt River, a dam and a large reservoir provide drinking water for the City of Seattle. The Wenatchee River drains 3,440 km^2 of the eastern Cascades before flowing into the Columbia River. Although land use is similar to the Snoqualmie basin, wherein the headwaters originate in forested public lands before flowing through a mix of agricultural, residential, and commercial land use, forest density is generally lower in the eastern Cascades.

Both the Snoqualmie and Wenatchee basins have a Mediterranean climate with dry summers and wet, mild winters influenced by proximity to the Pacific Ocean. The climate on the east side of the Cascades is drier than that of the west side; however, the prevailing westerly winds, which cross the Cascades, create temperature and precipitation gradients that vary widely

across the Wenatchee basin. Precipitation occurs predominately from October to March. The coldest month is typically January, whereas the warmest is July. Rivers have a mixed rain-snow hydrology with substantial winter rain and spring snowmelt, although the Wenatchee basin receives a greater proportion of winter precipitation as snow. Peak flow generally occurs during winter in the Snoqualmie River and spring in the Wenatchee River. The Snoqualmie and Wenatchee basins both have reaches where water temperature exceeds regulatory thresholds established for salmonids that are protected by the U.S. Endangered Species Act (ESA). Both basins support ESA-listed Chinook Salmon (*Oncorhynchus tshawytscha*) and Steelhead Trout (*Oncorhynchus mykiss*) and the Wenatchee basin additionally supports populations of Bull Trout (*Salvelinus confluentus*) and Sockeye Salmon (*Oncorhynchus nerka*).

Water temperature loggers (N_{SNO}=42, N_{WEN}=31) were installed throughout the mainstems, on major tributaries and on a selection of minor tributaries for both the Snoqualmie and Wenatchee rivers (Figure 5.1). Practical limitations forced sites to be publicly accessible, or on private property with landowner permission, and within 1 km of a road. For this study, water temperature was recorded using Onset Tidbit loggers every hour from October 1, 2014 through September 30, 2021 in both basins. We hereafter use hydrologic years (1 Oct – 30 Sep) instead of calendar years with the year of summer data as the year of reference. Air temperature data was recorded using Onset Pendant loggers at all water temperature monitoring sites. Air temperature was logged for subset of 11 (6) sites in the Snoqualmie (Wenatchee) basin beginning October 1, 2014, and for all sites beginning October 1, 2016 (October 1, 2018). Air loggers were placed on trees along the stream bank, as close to the stream temperature loggers as possible. The air temperature loggers were secured at approximately breast height on the north side of the trees and solar shields were fashioned to house the loggers.

5.3.2 *Exploration of air-water correlation summary metrics*

We calculated two summary metrics to characterize the relationship between air temperature and water temperature. For each site, summary metrics are derived from linear regressions between mean daily values of air and water temperature. The slope of this relationship, the thermal sensitivity, indicates how sensitive a given stream's water temperature is to changes in air temperature. The strength of this relationship (R^2) is an indicator of how well water temperature can be approximated by air temperature and is calculated as the Pearson correlation value between air and water temperature. Summary metrics were calculated separately for each season. Seasons were defined as fall (October, November, December), winter (January, February, March), spring (April, May, June), and summer (July, August, September).

We explored the relationship between warm-season (spring and summer) thermal sensitivity and climatic variables including mean daily air temperature, total daily precipitation, and snowmelt (defined as the snow water equivalent for a given day). Climatic variables were obtained from gridded DAYMET data products (Thornton, M.M. et al. 2020) and calculated for the upstream catchment of each monitoring station. In addition to climate variables, we explored the relationship between thermal sensitivity metrics and basin properties, including mean watershed elevation (MWE), watershed slope, distance upstream, percent riparian forest cover, and substrate hydraulic conductivity. Covariate descriptions and sources are found in Table 5.1.

5.3.3 *Spatially weighted clustering of thermal sensitivity*

We obtained continuous estimates of thermal sensitivity using a varying coefficient linear model. We used agglomerative hierarchical clustering to identify groups of stations where the patterns in thermal sensitivity are similar over time. To estimate the spatial correlation while

accounting for the directed river network structure, we weighted the distance matrix by a stream distance-based covariance metric. Details of each step are provided in the following sections.

5.3.3.1 Varying coefficient linear model for the air-water relationship

To derive a continuous thermal sensitivity metric, we fit a time-varying coefficient model (TVCM) to the original air and water temperature data. The TVCM is an effective tool for exploring dynamic features of the sensitivity of water temperature with changes in air temperature and uses a parametric linear model but with time-varying coefficients (Li et al. 2014, 2016). For a given site, we described the varying coefficient model for the air–water temperature relationship as:

$$y_t = \beta_{0,t} + x_t\beta_{1,t} + \epsilon_t, t = 1, \dots, T \quad (5.1)$$

Where $\beta_{0,t}$ and $\beta_{1,t}$are varying intercept and slope coefficients. To estimate the time-varying coefficients, we adopted an ordinary least squares kernel regression with the Nadaraya–Watson estimator, where we fit a set of weighted local regressions with an optimally chosen window size defined by the bandwidth, *b*, and the weights given by the kernel function (Hoover 1998, Casas and Fernandez-Casal 2019). The kernel and its bandwidth control the level of smoothing by adjusting the weight that the neighboring time points have on estimates at ***t***. The bandwidth was set a priori to ensure consistency across time series. We used the Gaussian kernel that is of the form $k(x) = \frac{1}{2}\pi\, \mathrm{e}^{-\frac{x^2}{2}}$. The varying intercept term represents the mean water temperature at time *t* and the varying slope term represents the local sensitivity of water temperature to changes in air temperature at time *t*. We used the R package tvReg (Casas and Fernandez-Casal 2021) for implementing the model.

We filtered subsequent temperature time series for site-years with >218 days (60% of the year) and gaps of <8 days, yielding 250 site-years from 74 sites across both the Snoqualmie and

Wenatchee basins. To capture the typical range and timing of thermal sensitivity at each site, we created a single representative time series of thermal sensitivity at each site by calculating the mean daily thermal sensitivity for each day of the year across all years of filtered data. We use this average annual time series for subsequent clustering analyses.

5.3.3.1 Estimating a spatially weighted dissimilarity matrix

We developed a distance measure for our time series of thermal sensitivity and incorporate spatial correlation between streams into the distance (Haggarty et al. 2015). The general form of the proposed distance between sites *x* and *y* can be written as:

$$d_{xy}^{c} = d_{xy}\widehat{cov}(h_s) \tag{5.2}$$

where $d_{xy}$is the Canberra distance (Lance and Williams 1967) and $\widehat{cov}(h_s)$ is a valid stream distance-based covariance matrix. The Canberra distance is used to measure the distance between stream time series based on the time-varying slope time series and is defined below.

$$d_{xy} = \sum_{t=1}^{T} \frac{|\mathrm{x_t} - y_t|}{|x_t| + |y_t|} \tag{5.3}$$

To estimate a stream distance-based covariance matrix for stations on a river network, we used the tail-down model that was introduced by Ver Hoef and Peterson (2010). Due to the complex structure of the tail-down model, it is necessary to model spatial correlation on a river network with a covariogram. To fit the tail-down model, we first computed the observed pairwise covariances for all pairs of stations. Subsequently, we plotted these covariances against lags (measured as stream distance) and binned at regular intervals to obtain an empirical stream distance-based covariogram. To estimate the covariance between time series at each site, we adopted a classic formula from Cressie (1993), which states that the estimated covariance between stations *x* and *y* is given by

$$\widehat{cov}(x, y) = \sum_{t=1}^{T} \frac{\{x_t - \bar{x}\}\{y_t - \bar{y}\}}{T} \quad (5.4)$$

where x_t and y_t are the values of the variable (thermal sensitivity) at stations x and y at time t and T is the total number of discrete times. This results in a single value which summarizes the covariance between the time series at the two stations over the period of interest.

We then used these point summaries of the covariance between pairs of curves to create an adjusted covariogram cloud. We fit an exponential covariance function to this empirical covariogram. Evaluating this model at the relevant stream distances resulted in an estimated stream distance-based covariance matrix $\widehat{cov}(h_s)$. We used this new covariance matrix to weight the dissimilarity matrix developed in Equation 5.2.

5.3.3.1 Agglomerative hierarchical clustering

We used agglomerative hierarchical clustering (AHC) to identify groups of stations where the patterns in thermal sensitivity are similar over time using the hclust function in R (R Core Team 2020). AHC is one of the most common clustering methods and has been used to cluster river regimes (Olden et al. 2012, Maheu et al. 2016, Savoy et al. 2019, Isaak et al. 2020). Each time series starts in its own cluster, and the hierarchy is built by repeatedly merging pairs of similar clusters separated by the shortest distance (i.e., measured as the similarity between individual times series) until all points are contained in a single cluster. To decide which clusters are merged in every iteration, AHC uses a distance metric and a linkage criterion. We used Ward's minimum variance linkage method for clustering, where the distance between two clusters is computed as the increase in the sum of squared differences after combining two clusters into a single cluster. The shortest of these links (minimum increase in the sum of squared

differences) that remains at any step causes the fusion of the two clusters whose elements are involved.

A difficulty associated with cluster analysis is determining the most appropriate number of clusters given the data because no a priori optimal number of clusters exists. Clusters can be validated through internal cluster validity indices (CVI); there are a variety of CVIs, most of which combine within cluster cohesion (intra-cluster variance) or between cluster separation (inter-cluster variance) to compute a quality measure. There is no universally best CVI (Arbelaitz et al. 2013), therefore we calculated a suite of five CVIs, including the Silhouette, Gap, Davies–Bouldin, Calinski–Harabasz, and generalized Dunn indices, using the NbClust R package (Charrad et al. 2014). A final number of clusters was determined by a majority rules approach based on the optimal number of clusters suggested by each index (Table S5.2).

The stability of clusters was assessed by a bootstrapping approach where sites were sampled with replacement and then AHC was performed on the resampled data using the fpc R package (Hennig 2020). For each bootstrapped cluster, we assessed the similarity between each new cluster and the most similar original cluster with the Jaccard index. The Jaccard coefficient ranges from 0 to 1. Clusters with a coefficient larger than 0.75 were considered stable and clusters with a mean Jaccard coefficient of less than 0.5 were considered unstable and may not reflect a true pattern in the data (Maheu et al. 2016, Savoy et al. 2019). We repeated the bootstrapping procedure 10,000 times; the mean Jaccard coefficient for each cluster is reported in Table 5.2.

5.3.3.1 Identification o\f environmental drivers in thermal sensitivity

We used classification and regression trees (CART; Breiman et al. 1984) to investigate the relative importance of climatic and physical drainage basin attributes for predicting each

site's degree of membership to each cluster. CART is typically used to attempt to predict membership to clusters using environmental attributes, and it allows the modeling of nonlinear relationships among mixed variable types and facilitates the examination of intercorrelated variables in the final model (De'ath and Fabricius 2000, Olden et al. 2008). We took an exploratory approach to this analysis due to our relatively small sample size ($n_{Wenatchee} = 31$, $n_{Snoqualmie} = 42$), which limited our ability to conduct statistical tests. Therefore, we calculated variable relative importance, defined as the sum of squared improvements at all splits determined by the predictor. These values are scaled to sum to 100 (rounded). We used the R package rpart (Therneau and Atkinson 2019) for implementing the CART model. Covariates examined are described in Table 5.1.

5.4 RESULTS

5.4.1 *General patterns in temperature, precipitation, and thermal sensitivity*

The long-term average annual precipitation was 1874 mm (939 mm) for the western (eastern) Cascades time series. For the western (eastern) Cascades, all years have average annual temperatures higher than the long-term average of 8.6 °C (5.3 °C), although individual seasons may be slightly cooler than average. Generally, the years spanned by our dataset were warmer than the historical average, with wetter than historical average winter and fall months and drier spring and summer months (Figure S5.1; Figure S5.2). The year 2015 stands out as a year with an exceptionally warm winter, low snowpack, and dry spring. Temperature and precipitation patterns in the western and eastern Cascades are generally similar, however, precipitation anomalies are typically smaller in the eastern Cascades due to the overall lower precipitation in this region (Figure S5.2).

Summary metrics describing air-water temperature relationships exhibited substantial variation across time (season and year) and space. Thermal sensitivities for all seasons and years ranged from 0.05 to 0.97 with a median of 0.56 in the Snoqualmie basin and from 0.06 to 0.74 with a median of 0.42 in the Wenatchee basin over the sampling period (Table 5.2). Although there was substantial overlap in thermal sensitivities across seasons, the overall distribution varied (Figure 5.1). Thermal sensitivities for sites with consistent data coverage generally followed the same trends across years (i.e., two sites will both be higher and lower in the same years), patterns in thermal sensitivity estimates were not entirely consistent, highlighting the importance of local influences that may shift year-to-year (Figure 5.2). Overall, weak and inconsistent patterns emerge in summer between thermal sensitivity and landscape and climate variables (Figure 5.3; Figure 5.4). Of the climate variables, precipitation and air temperature display no relationships with thermal sensitivity (Figure 5.3). Snowmelt, however, appears to play an important role in mediating thermal sensitivity. Generally, in years with a smaller snowpack, thermal sensitivities are higher, although there is an asymptotic pattern where even during very high snowmelt thermal sensitivities do not fall below 0.25 (Figure 5.3). For landscape variables, a consistent negative relationship between thermal sensitivity, distance upstream and mean watershed elevation exists (Figure 5.4). Riparian forests and thermal sensitivity show no relationship for either basin. Hydraulic conductivity is weakly positive in the Snoqualmie basin, and similar to watershed slope and elevation, the relationship appears parabolic rather than strictly linear.

Time-varying thermal sensitivities can have periods of both high and low thermal sensitivity within a season, which is not necessarily represented when looking only at seasonal summary metrics. The thermal sensitivity varies strongly with water and air temperature within

the Snoqualmie and Wenatchee basins (Figure 5.5 and Figure 5.6). Generally, thermal sensitivity rises sharply in late spring, is highest in summer, declines slowly throughout the fall, and remains depressed through winter and early spring. Sites in the Wenatchee appear to have a more consistent seasonal signal than those in the Snoqualmie (Figure S5.4).

5.4.2 *How do water temperature, air temperature, and thermal sensitivity cluster?*

Spatially weighted AHC yielded four clusters for thermal sensitivity and two clusters for air and water temperature in the Snoqualmie basin, and five clusters for thermal sensitivity and two clusters for air and water temperature in the Wenatchee basin (Figure 5.5; Figure 5.6; Table S5.2). For both basins, clusters of air and water temperature correspond closely with elevational gradients. Higher elevation sites exhibit generally lower magnitudes but similar patterns in air and water temperatures. In the Snoqualmie, air temperature clusters were stable, with a mean Jaccard index of 0.91 for high elevation sites and 0.73 for low elevation sites. Water temperature clusters were slightly less stable, with a mean Jaccard index of 0.65 for high elevation sites and 0.89 for low elevation sites. Air and water temperature clusters in the Wenatchee basin were more stable than the Snoqualmie clusters. In the Wenatchee basin, air (water) temperature clusters had a mean Jaccard index of 0.85 (0.86) for high elevation sites and 0.95 (0.73) for low elevation sites.

Clustering patterns for thermal sensitivity were more complex (Figure 5.5; Figure 5.6). Like clusters of air and water, clusters of thermal sensitivity were generally less stable in the Snoqualmie basin than in the Wenatchee basin (Table 5.3). In the Snoqualmie basin, Cluster 1 consisted primarily of low elevation tributaries to the mainstem and Raging River that displayed relatively stable thermal sensitivities throughout the year (Figure 5.5). This cluster was moderately stable with an average Jaccard index of 0.68. Relatively few sites belonged to Cluster

2 (n=5) and the distribution of sites within this cluster included three mainstem Snoqualmie sites and two high elevation tributaries. Despite the large geographic distances separating sites, this cluster was highly stable with an average Jaccard index of 0.88. Annual thermal sensitivity patterns within Cluster 2 are defined by somewhat high mean thermal sensitivities and moderate variability. Cluster 3 contained the largest number of sites (n=15), and sites were generally located within the three forks of the Snoqualmie River. Sites in this cluster had the lowest average annual thermal sensitivity. Lastly, Cluster 4 had the lowest stability of any cluster in the Snoqualmie basin. Sites within this cluster were characterized by overall high thermal sensitivity and relatively low variability. All five thermal sensitivity clusters in the Wenatchee basin were relatively stable. Cluster 1, 2, and 3 all displayed similar seasonal patterns in thermal sensitivities and moderate to high stability (mean Jaccard indices of 0.79, 0.86, and 0.79). Cluster 2 had the lowest annual thermal sensitivities and primarily contained high elevation sites in the Chiwawa, White, and Little Wenatchee rivers, while sites in Cluster 3 had the greatest variability in thermal sensitivity through time. Cluster 2 consisted of a single site (Chumstick Creek) that was nearly always assigned to a unique cluster when included in the bootstrapping procedure, therefore the mean Jaccard index is 0.62. The thermal sensitivity for this site was quite low and virtually flat throughout the year. Cluster 3 was very stable with a mean Jaccard index of 0.94. This cluster contained primarily sites from tributaries lower in the basin (Peshastin and Mission Creek) and waws defined by relatively high winter and spring thermal sensitives.

CART analysis indicated that basin topography and geology are the principal discriminators of thermal regime clusters. The top predictors of cluster membership with a greater than 10% increase in mean standard error if removed from the model were watershed elevation and baseflow index in the Wenatchee basin and mean slope, watershed elevation, and

soil depth in the Snoqualmie basin (Figure 5.7). The distribution of variable importance varied between the Wenatchee and Snoqualmie basins, although in both basins many covariates had similar relative importance values. Covariate distributions also varied across clusters. In the Snoqualmie basin, Cluster 1 rivers were generally below an elevation of 600 meters, whereas Cluster 3 rivers were generally mid-sized, high elevation sites with a low baseflow index. In the Wenatchee basin, Cluster 4 sites were predominately located at high elevations and had steep slopes and a large proportion of precipitation falling as rain. Sites in Clusters 2 and 3 were generally low elevation sites with a high baseflow index and soil depth.

5.5 DISCUSSION

Study results illustrate that thermal sensitivity should not be treated as a static value, as it varies throughout the year and reflects hydrologic conditions at a given time and place within a watershed. Annual patterns in thermal sensitivity are largely controlled by underlying geology and climate across two Pacific Northwest river basins. Overall, this study provides a framework for utilizing thermal sensitivity regimes to improve understanding of factors contributing to stream temperatures and will enable managers to target mitigation and adaptation activities to work best with local conditions within a watershed.

5.5.1 *Patterns of thermal sensitivity clustering*

Our analysis of stream air and water temperatures supports the presence of distinct thermal sensitivity regimes, providing an organizing framework for river research and management by identifying sites with similarities across space. We identified four annual thermal sensitivity clusters from 42 sites in the Snoqualmie basin, and five clusters form 31 sites in the Wenatchee basin. Identified regimes differ in both timing and magnitude. Within both the

Snoqualmie and Wenatchee basins, winter thermal sensitivities were low and varied strongly with elevation (Figure 5.1). Low thermal sensitivities in winter are likely due to the non-linear relationship between air and stream temperature at cold temperatures when air temperatures can dip below the water temperature-freezing limit (Mohseni et al. 1998, 1999). Air temperature covaries strongly with elevation in Pacific Northwest basins, and sites that are high in the watershed will experience a greater number of sub-freezing days. Fall thermal sensitivities were relatively homogeneous, whereas spring and summer thermal sensitivities varied substantially. We expect thermal sensitivities to be similar during periods of heavy precipitation, when water sources with thermal characteristics distinct from air temperature, such as groundwater and snowmelt, contribute relatively less flow. The greater variability of responses in spring and summer indicates that the processes controlling river temperatures are more diverse than in fall or winter (Hrachowitz et al. 2010).

Thermal sensitivity regimes reflect non-redundant aspects of river dynamics. Air temperature and water temperature clusters closely corresponded to one another and were almost entirely determined by elevation of the temperature loggers, whereas thermal sensitivity clusters showed more variability in annual patterns and were intermixed spatially (Figure 5.5; Figure 5.6). Air and water clustering results are consistent with previous studies that observed broad temporal correspondence of air and river temperature dynamics with differing magnitudes of response (Bower et al. 2004, Chu et al. 2010, Garner et al. 2014, Isaak et al. 2018a). More locally, Isaak et al. (2020) found that across western rivers, much of the information in stream temperature records could be summarized by a relatively limited number of distinct regime components primarily driven by differences in elevation and latitude.

Viewing thermal sensitivity as a continuous parameter adds novel insights to our understanding of river basin functioning. Studies have highlighted the importance of changes in the processes that drive heat budgets as well as the non-stationarity of the resulting statistical relationships (Arismendi et al. 2014, Boyer et al. 2021). Our clustering analysis overcomes these issues by utilizing a varying coefficient model that treats thermal sensitivity as a continuous function through time, rather than a series of discrete summary metrics, and allows clustering based on the entirety of annual average annual patterns. Varying coefficient models are useful in situations where there is a substantial amount of variability in water temperature that is not accounted for by air temperature but might be related to unmeasured factors that shift over time (Li et al. 2014, 2016). The observed complexity in thermal sensitivity response hints at the diversity of physical processes controlling stream temperature response and the large, clear shifts in thermal sensitivity magnitude across the year calls into question the common practice of summarizing a river's sensitivity as a static value. The ability to directly observe shifts in the air-water temperature relationships also opens the possibility of using thermal sensitivity as a diagnostic tool to examine gradual changes in the importance of drivers of water temperature, such as dynamic changes in riparian shading or snowmelt.

5.5.2 *Importance of underlying geology for thermal sensitivity*

Geologic characteristics shaped the relationship between air and water temperatures across the Wenatchee and Snoqualmie basins. The inclusion of baseflow index, hydraulic conductivity, and soil depth in determining cluster membership (Figure 5.7) implies the importance, and detectability, of groundwater as a key mediator of thermal sensitivity regimes in Pacific Northwest basins. Clusters with high baseflow index, hydraulic conductivity, and soil depth values generally had lower summer and less variable thermal sensitivities (Figure 5.5;

Figure 5.6; Figure 5.7), implying greater groundwater influence (Kelleher et al. 2012). Interestingly, despite the clear importance of groundwater metrics in the clustering analysis, results from summary metric regressions were mixed and, in the Snoqualmie basin, did not align with expectations of a negative relationship between thermal sensitivity and groundwater influence (Figure 5.4). Although it is possible to infer broad patterns in surface-groundwater connectivity based on the geologic context of a basin and datasets of interpolated metrics describing properties of geology (i.e., hydraulic conductivity, soil depth) or water source (i.e., baseflow index), individual metrics often have substantial uncertainty, do not covary perfectly, and may be particularly unconstrained for mountain headwater streams (Wolock et al. 2004, Patton et al. 2018, Briggs et al. 2022). Additionally, the influence of these processes can be localized and variable across space (Johnson et al. 2017). The ability to use thermal sensitivity as an empirical measure of groundwater influence, therefore, shows great promise for understanding catchment processes and informing management and restoration actions at ecologically relevant scales.

Geology across the Snoqualmie and Wenatchee basins supports our conclusion that low thermal sensitivities are indicative of groundwater inputs. The lowland portion of the Snoqualmie watershed contains a deep, permeable, productive glacial aquifer that is presumed to be the source of summer baseflow to much of the river (Bethel 2004, McGill et al. 2021, Turney et al. 1995). Glacial and interglacial deposits in the valley contain several geohydrologic units with differing aquifer potential (Bethel 2004); however, most deposits can form small but useable aquifers that could be helping to sustain baseflow in summer months (Turney et al. 1995, Soulsby et al. 2004, Blumstock et al. 2015). Soil depth, hydraulic conductivity, and baseflow index were correspondingly high in streams that overlay the lower portion of the watershed

(Figure 5.7). Thermal sensitivities reflected this pattern, wherein generally sites draining low elevation tributaries (Cluster 1) had relatively constant thermal sensitivities throughout the year (Figure 5.5). Conversely, the upper portion of the Snoqualmie basin is covered by thin soil over impermeable bedrock lacking extensive fracture networks, meaning that rain and snowmelt are not retained in the mountains but are rapidly transmitted to the stream system (Debose and Klungland 1964, Nelson 1971, Goldin 1973, 1992). Sites with catchments predominantly within this upland area tended to belong to Clusters 2 and 3 and displayed high summer thermal sensitivities, indicating limited groundwater influence.

Geology in the Wenatchee basin is predominated by low permeability igneous and metamorphic bedrock in the upland perimeter areas and by sedimentary bedrock deposited within the Chiwaukum Graben structure that forms the more central and lowland areas (Wildrick 1979, Montgomery Water Group 2003). Two major aquifers exist in the Wenatchee basin: an aquifer within the sedimentary bedrock of the central and lowland areas and an overlying unconsolidated alluvial and outwash aquifer located primarily in river valley bottoms across the basin (Montgomery Water Group 2003). The bedrock aquifer consists of sandstones and shales, which tend to have moderately low permeability. Folding and faulting have caused the shale to break up or fracture and groundwater moves preferentially within these zones of higher secondary permeability. The alluvial and outwash aquifers, on the other hand, exhibit relatively high permeability where groundwater can move easily and are considered the primary groundwater source (Wildrick 1979, Montgomery Water Group 2003). Cluster 2 in the Wenatchee basin, consisting of a single site located at the mouth of Chumstick Creek, stands out for having a unique, nearly flat pattern compared to patterns in other sites (Figure 5.6). Covariate distributions for the clustering results showed that Chumstick Creek has a relatively high

hydraulic conductivity and baseflow index (Figure 5.7; Figure S5.5). A transition from low to high permeability glacial material occurs near the mouth of Chumstick Creek (Montgomery Water Group 2003), and it is possible that substantial groundwater discharge occurs near this discontinuity (Neff et al. 2019). Similarly, sites within Cluster 3 showed low variability in thermal sensitivity and had high soil depth and baseflow index values. Streams within this cluster are situated on top of predominantly sandstone bedrock (Frizzell 1979, Gendaszek et al. 2014).

Overall, the importance of groundwater is consistent with previous studies, which broadly find that thermal sensitivity decreased with increasing groundwater contribution (O'Driscoll and DeWalle 2006, Chang and Psaris 2013, Beaufort et al. 2020, Georges et al. 2021). The degree to which groundwater decouples trends in stream and air temperature depends on stream depth, the rate of groundwater inflow, and the depth of groundwater source. Although not examined in this study, aquifer source and groundwater depth likely influence thermal sensitivity estimates, with runoff sourced from deep groundwater being less variable and less sensitive in comparison with groundwater sourced from shallow sub-surface flows (Tague et al. 2007, Johnson et al. 2021, Hare et al. 2021). Shallow groundwater temperatures are already responding to climate change (Menberg et al. 2014). As warming continues, the summer cooling capacity of groundwater may be reduced, limiting the availability of cold-water refugia patches sourced by groundwater (Brewer 2013, Briggs et al. 2013).

5.5.3 *Climate controls on thermal sensitivity*

Although the ratio of precipitation falling as snow showed limited variable importance, elevation and slope covary closely with snow accumulation and were among the most important predictors of cluster membership, perhaps masking a statistical signal of snowfall (Figure 5.7). In both the Snoqualmie and Wenatchee basins, clusters with higher elevation, steeper slope, and

greater snowmelt within the catchment had thermal regimes that were less sensitive to changes in air temperature during spring and early summer. Generally, the relationship between snowmelt and thermal sensitivity formed a wedge-shaped pattern, wherein sites with limited snowmelt displayed both high and low thermal sensitivity, but sites with extensive snowmelt always display low thermal sensitivity (Figure 5.3). Importantly, snowmelt buffering diminishes throughout the summer, and by late summer high elevation, snowmelt influenced sites were often more sensitive to air temperatures than their low elevation counterparts (Figure 5.5; Figure 5.6). Sites within Cluster 4 in the Wenatchee basin were an exception to this pattern and maintained summer thermal sensitivities that were substantially depressed relative to adjacent locations (e.g., Clusters 1 and 5). This is likely due to glacial inputs within these catchments, and points to the importance of high elevation glacial and late-summer snowpack melt as a significant source of summer baseflow and control on water temperatures during the months of greatest heating within these watersheds.

Numerous studies have examined the buffering impact of snowmelt on water temperature due to advective flux from cooler meltwater entering the river. Studies in Alaskan rivers found a linear, negative relationship between summer thermal sensitivity and snowmelt (Lisi et al. 2015, Cline et al. 2020) and a recent study in the Snoqualmie basin found that snowmelt can reduce basin-wide peak summer temperatures, particularly at high elevation tributaries, and the thermal impacts of melt water can persist through the summer (Yan et al. 2021). Our results suggest that snowpack offers substantial buffering to changes in air temperature across mountain river basins, but that the largest impacts are localized across space and time. Climate change is expected to shift snowmelt earlier and reduce snow water resources (Barnett et al. 2005, Musselman et al. 2021). The loss of snow may result in warming in snow-influenced systems and the subsequent

homogenization of thermal conditions across basins (Winfree et al. 2018). Homogenization of thermal conditions likely leads to important changes in ecological functions and ecosystem services supported by lost thermal heterogeneity, such as a loss of cold-water patches for Pacific salmon (Brennan et al. 2019).

5.5.4 *Landscape controls on thermal sensitivity*

Variable relationships between thermal sensitivities and site characteristics highlight complexities in stream thermal regimes. Steeper channel slopes and greater stream velocities limit warming in streams by decreasing the time for equilibration with local heating conditions (Donato 2002, Webb et al. 2008, Isaak et al. 2012). Topographic shading associated with steep watersheds can suppresses stream temperature by reducing exposure to solar radiation (Webb and Zhang 1997). In the Wenatchee basin, the Cluster 3 site, Chumstick Creek, drains a steep canyon. This may contribute to observed low, stable thermal sensitivities throughout the year. Additionally, watershed size and distance upstream covary closely and displayed relatively consistent relationships with summer thermal sensitivity summary metrics despite ranking moderately in variable importance. We expected thermal sensitivity to increase with river size; groundwater influence should be more visible on smaller streams because the volume of water is small and the travel time of the water from the source is short and not sufficient to equilibrate water temperature with the atmosphere (Mohseni and Stefan 1999, Tague et al. 2007, Beaufort et al. 2016). Reduced sensitivity of headwater streams to air temperature was observed in the Aberdeenshire Dee, Scotland (Hrachowitz et al. 2010), and River Danube, Austria (Webb and Nobilis 2007), and small Pennsylvanian streams were shown to be less sensitive to changes in air temperature than larger streams (Kelleher et al. 2012). However, Hilderbrand et al. (2014) found no relationship between thermal sensitivity and watershed size.

We expected land cover characteristics such as open water and forest cover to be important predictors of thermal sensitivity regimes, however, land use was of limited variable importance and showed inconstant relationships with summary metrics (Figure 5.4; Figure 5.7). Several factors may account for this. Inherent covariation in river basins can hinder statistical efforts to identify mechanistic links between landscape gradients and features of aquatic ecosystems (Lucero et al. 2011); land cover characteristics may have a small impact that went undetected due to noisy observations. It is also possible that land cover metrics may not adequately describe the intended process. For example, the relative unimportance of shading may be due in part to our metric of shade, which was limited to riparian and catchment forest cover and ignored topographic shading or vegetation height. Lastly, human modifications to the river that are not captured by land cover statistics, such as channelization or the presence of dams and reservoirs, may alter thermal sensitivity and obscure natural gradients. For example, areas of the river that are degraded and subsequently disconnected from their floodplain may have artificially high thermal sensitivities, and the release of water from dams and reservoirs has the potential to either warm or cool downstream temperatures, depending on dynamics of where and how impounded water is released (Ahmad et al. 2021, Cheng et al. 2022). Future research could include covariates sinuosity or variance of thalweg depth to better capture these effects. Untangling exact controls will require additional research.

5.5.5 *Caveats and limitations*

Due to the nature of data collection, time series of both air and water temperature used in this analysis have periods of missing values that span weeks to months. Classical clustering techniques require complete datasets, limiting analyses to time series without gaps. To overcome this issue, we calculated a single representative time series at each site that captures the typical

range and timing of thermal sensitivity. Alternative options for dealing with missing values include removing data points that do not cover the target time period or imputing missing values by means of statistical procedures or summary metrics (e.g., Savoy et al. 2019, Beaufort et al. 2020). However, we chose not to use these approaches in our study due to the long and inconsistent periods of missing values across sites. We acknowledge that interannual variability in precipitation and temperature impacts river thermal sensitivity, and average time series calculated from differing years may exhibit differences in shape and timing for reasons outside of inherent characteristics. Future studies could use novel clustering methods capable of dealing with sparse datasets, which would provide more detailed information on clusters generated from time periods with robust values versus data scarcity (Carro-Calvo et al. 2021). Alternatively, recent advances in space-time imputation for river basins may prove a fruitful direction (Li et al. 2017).

Our calculation of time-varying thermal sensitives also necessitated decisions regarding what features of the time series to preserve. Selection of the bandwidth parameter and kernel function for the time varying model will impact estimation of thermal sensitivity and intercept. Generally, with larger bandwidth estimates or averaging periods (e.g., daily, weekly, monthly), intercept estimates increase and thermal sensitivity estimates decrease. Decisions of this nature should be approached carefully and with a clear question in mind. For this study, we were interested in seasonal to annual patterns in thermal sensitivity, and thus chose a relatively large bandwidth, resulting in a smooth time series. Previous studies have also used regression splines to estimate the time varying relationship between air and water temperatures (Haggarty et al. 2015). This approach smooths data and can account for missing data but may not preserve small-scale features of interest. We chose to use absolute values of our thermal sensitivity time series,

as we cared about differences in mean thermal sensitivity as well as correlated variability. Future work could normalize thermal sensitivity time series first to examine only patterns.

5.5.6 *Implications for management and future directions*

Classifying rivers based on thermal sensitivity could be a powerful tool when planning for global change. Our results show that annual patterns in thermal sensitivity are diverse and controlled by underlying geology and climate across two Pacific Northwest river basins. Climate change is decreasing snowpack in the region, resulting in earlier runoff and extended summer baseflow (Elsner et al. 2010, Wu et al. 2012), and may decrease groundwater discharge depending on sources and timing of recharge (Brooks et al. 2012, McGill et al. 2021). Furthermore, high thermal sensitivities in late summer, during the hottest part of the year, and in high elevation streams, which are typically thought to be climate refuges, is troubling for the conservation of native species such as Pacific salmon (Mantua et al. 2010; Isaak et al. 2016). Climate change will likely decrease juvenile rearing and spawning habitat quantity and quality, although it is important to note that streams with high thermal sensitivity may still provide adequate habitat in select portions of the year if stress-related thresholds are not exceeded (Armstrong et al. 2021). Examining thermal sensitivity regimes improves understanding of factors contributing to stream temperatures and may enable managers to target mitigation and adaptation activities to work best with local conditions, thus maximizing benefits given limited resources. For example, given the importance of subsurface geology within the Wenatchee and Snoqualmie basins, targeted actions to restore floodplain functions that recharge aquifers through actions such as placing engineered logjams or reintroducing beavers could be prioritized (Abbe and Brooks 2013, Pollock et al. 2014). Additionally, identification of particularly insensitive portions of the river could help to better constrain areas where coldwater patches exist that may

be used as refuges for coldwater fish (Snyder et al. 2020). This process-based approach will be particularly important as non-stationary relationships caused by climate change make it unreliable to use past regressions built under historical climate conditions (Boyer et al. 2021).

As longer, more spatially extensive air and water temperature time series become available (Isaak et al. 2017), we can begin to ask questions about 1) the spatial extent of different thermal sensitivity regimes, 2) how interannual variability shifts with climate conditions, and 3) detect changes in the drivers of thermal sensitivities with more precision than has previously been possible. Furthermore, we can also begin to ask questions about how commonly rivers shift between regimes, what external drivers lead to these shifts, and the extent to which shifts are periodic, sustained, or reversible. Such insights will vastly improve our understanding of lotic ecosystems while offering a suite of new tools for monitoring the impact of management decisions and climate change.

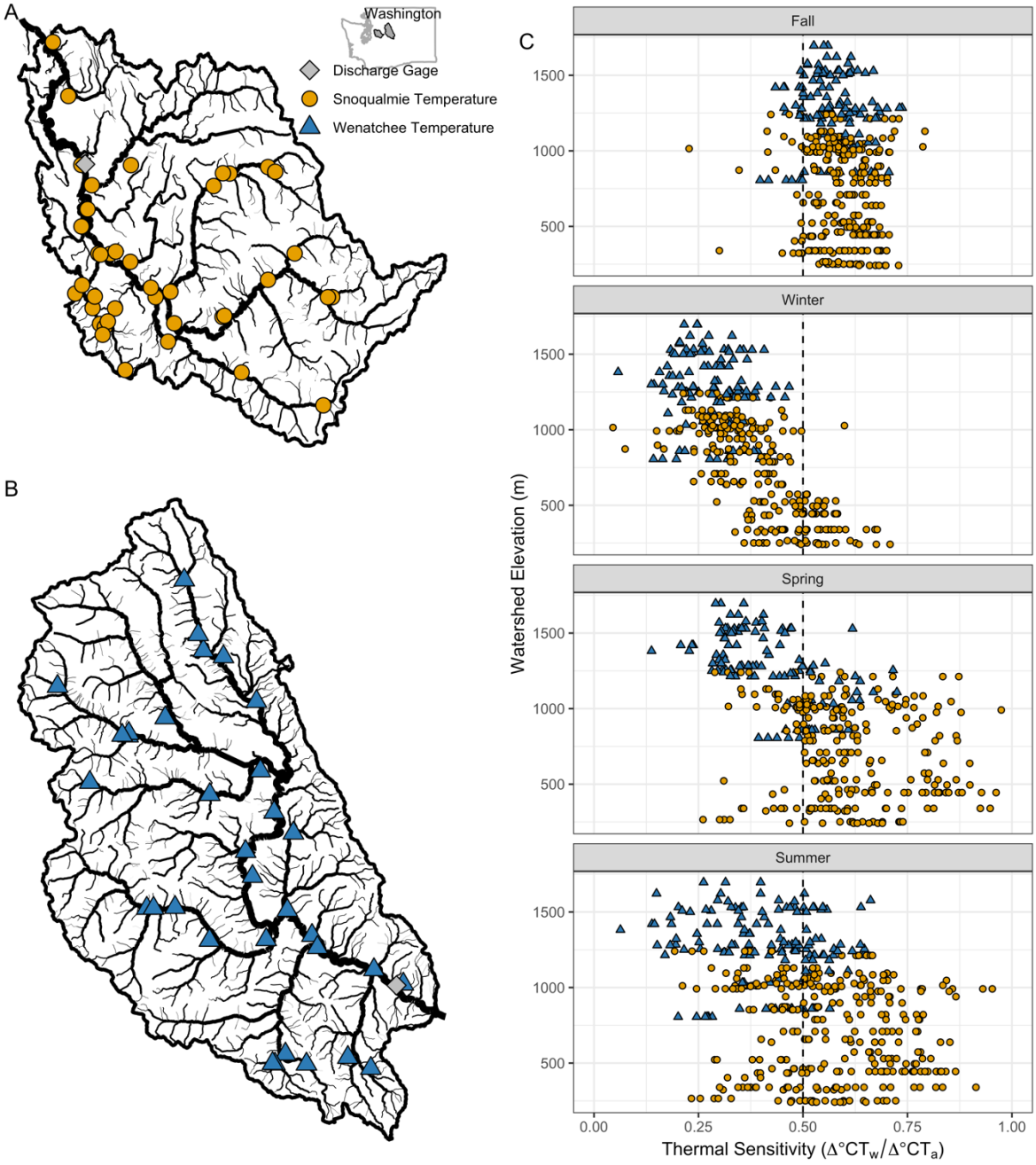

Figure 5.1. A map of the Snoqualmie (A) and Wenatchee (B) basins water and air temperature monitoring sites and the most downstream USGS gage for each basin. Thermal sensitivity, defined as the change in water temperature with a single degree change in air temperature, versus mean watershed elevation for each site-year combination (C).

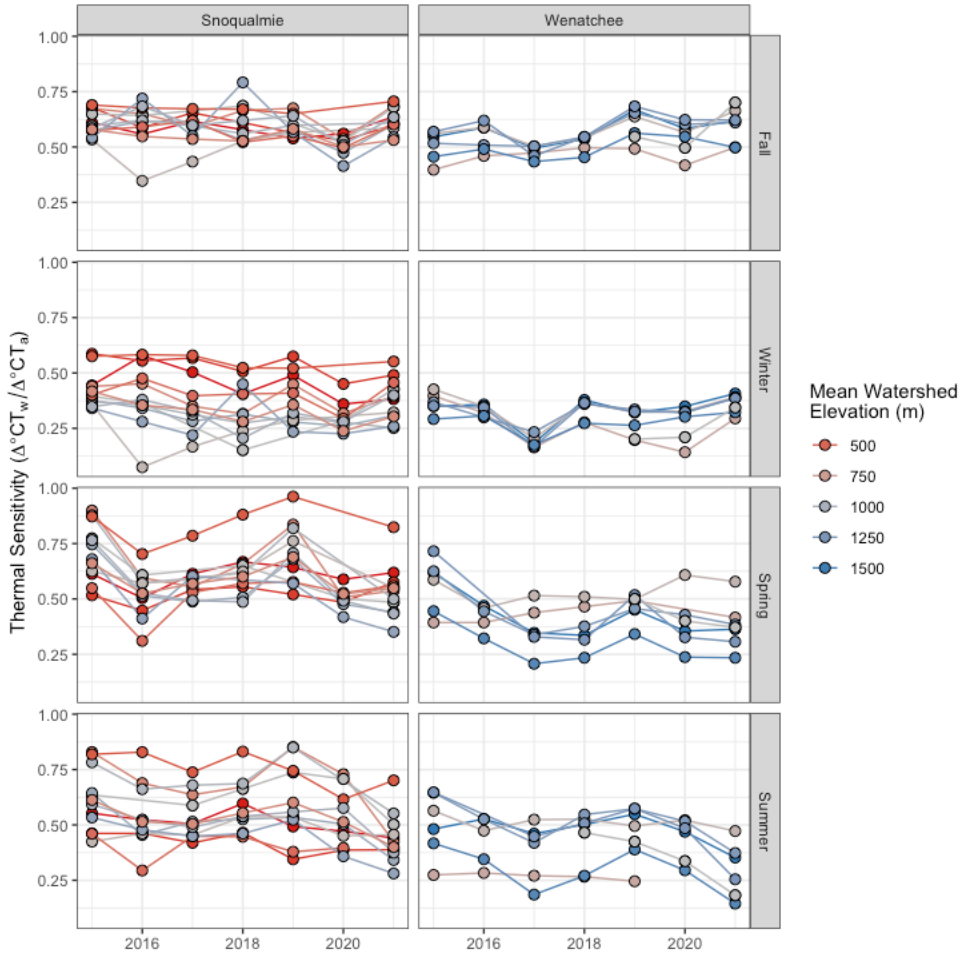

Figure 5.2. Thermal sensitivities for all seasons for sites with consistent data coverage (at least 6 years of data) for all seasons throughout the sampling timeframe. The color of each point corresponds to the mean watershed elevation

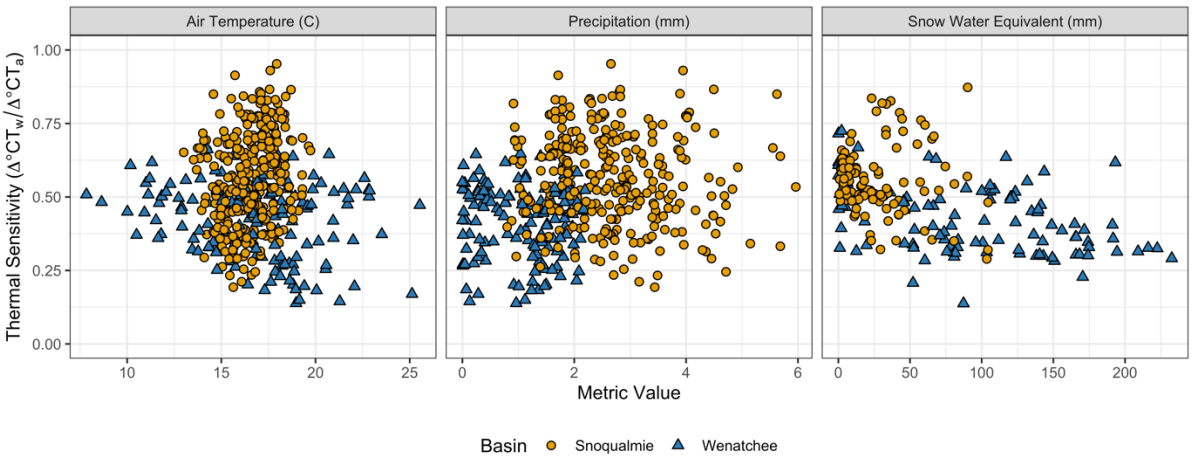

Figure 5.3. Spring thermal sensitivity values for all site-year combinations in the Snoqualmie and Wenatchee basins versus total snow water equivalent in spring and summer (A), precipitation (B), and air temperature (C) from gridded DAYMET data for each sampling point. Points are colored by basin. Basins that have no snowmelt in a given year are not shown on graph (A).

Stream or watershed attribute (covarying variables)	Theoretical relationship with thermal sensitivity	Explanation	Observed Relationship in Summer
Watershed slope +elevation +dist upstream – soil depth	Negative	• Increased snowmelt and cooling due to faster velocity water movement and shorter water residence time (Winfree et al. 2018). • Topographic shading associated with steep watersheds suppresses stream temperature by reducing exposure to solar radiation (Webb and Zhang 1997).	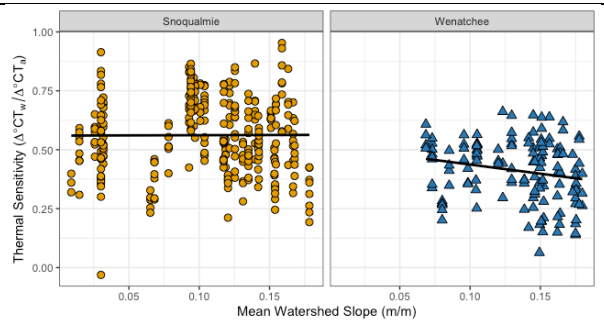
Watershed elevation +slope +dist upstream +% lake area – soil depth	Negative	• Higher elevations have higher snowmelt accumulation and greater proportion of snowmelt in spring. • The impact of elevation on spring and early summer stream temperature is diminished in years with low winter snow accumulation.	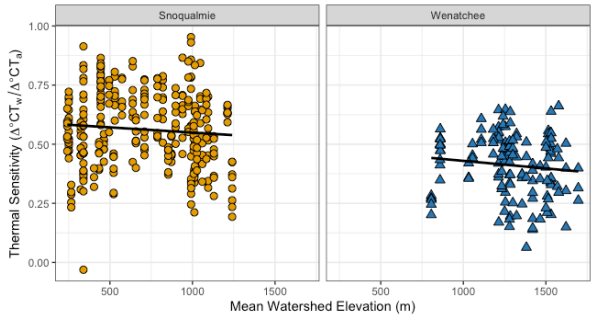
Distance upstream – watershed size +slope +elevation	Negative	• Duration of surface water's exposure to solar radiation and atmospheric energy flux is higher in low gradient watersheds with slower streamflow velocities (Poole and Berman 2001).	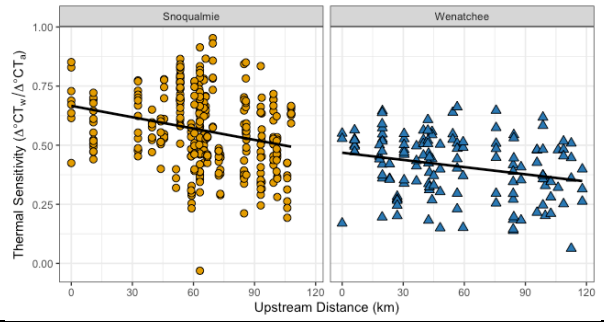

Percent riparian forest cover +% forest cover – watershed size	Negative	• Riparian vegetation provides shading to streams, reducing exposure to solar radiation (Webb and Zhang 1997), particularly during summer base flows. • Forest canopy can influence snow accumulation within a watershed and snowmelt contribution to streams. Low density forests accumulate more snow relative to high density forests (Varhola et al 2010). • Conversion of forested land area can accelerate runoff and reduce infiltration, warming surface flows before they reach stream channels (Naiman et al. 2005; Nelson and Palmer 2007).	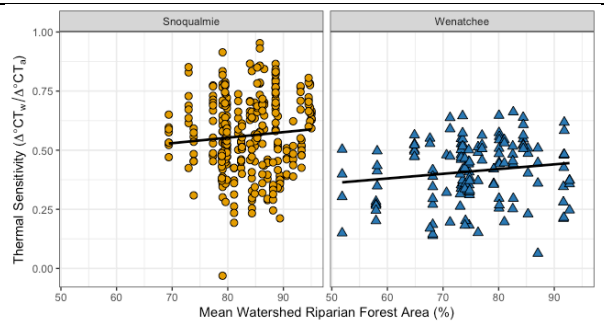
Hydraulic Conductivity +baseflow index	Positive	• Hydraulic conductivity refers to the ability of a geologic material to transmit water. • Relatively high hydraulic conductivity material would be represented by something like unconsolidated alluvial sands and gravels. • High hydraulic conductivity is typically associated with areas of greater groundwater activity and lower, more stable thermal sensitivity values.	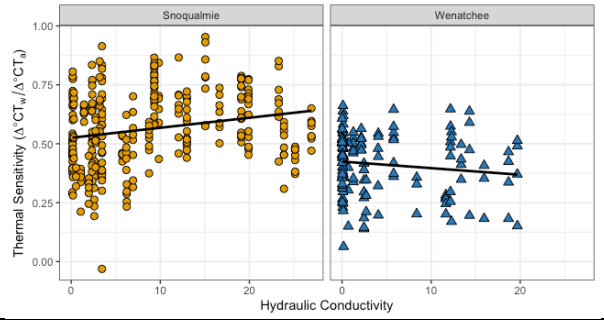

Figure 5.4. The relationship between landscape variables and thermal sensitivities in summer. See Figure S3 for a detailed description of how river attributes covary with one another.

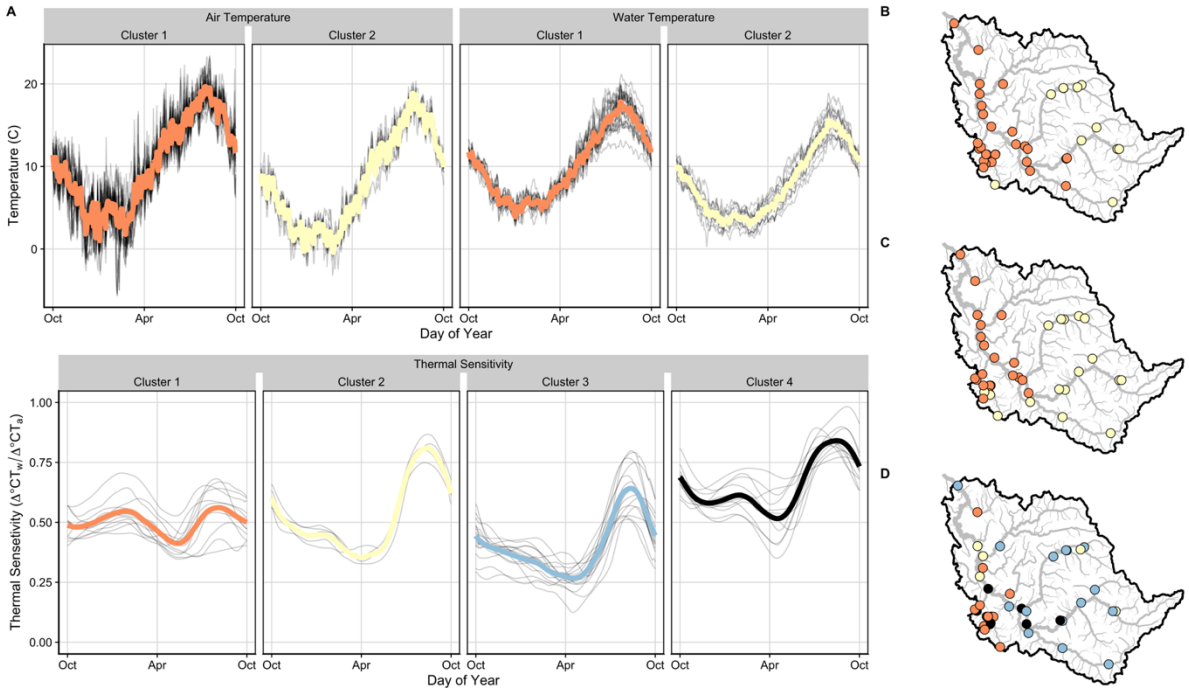

Figure 5.5. Average time series (A) and spatial clustering results (columns/colors indicate unique clusters) for average annual air temperature (B), water temperature (C), and thermal sensitivity (D) in the Snoqualmie basin. The spatial distribution for Colored lines indicates mean average annual values for each cluster, and gray lines denote average annual values for each site within a given cluster.

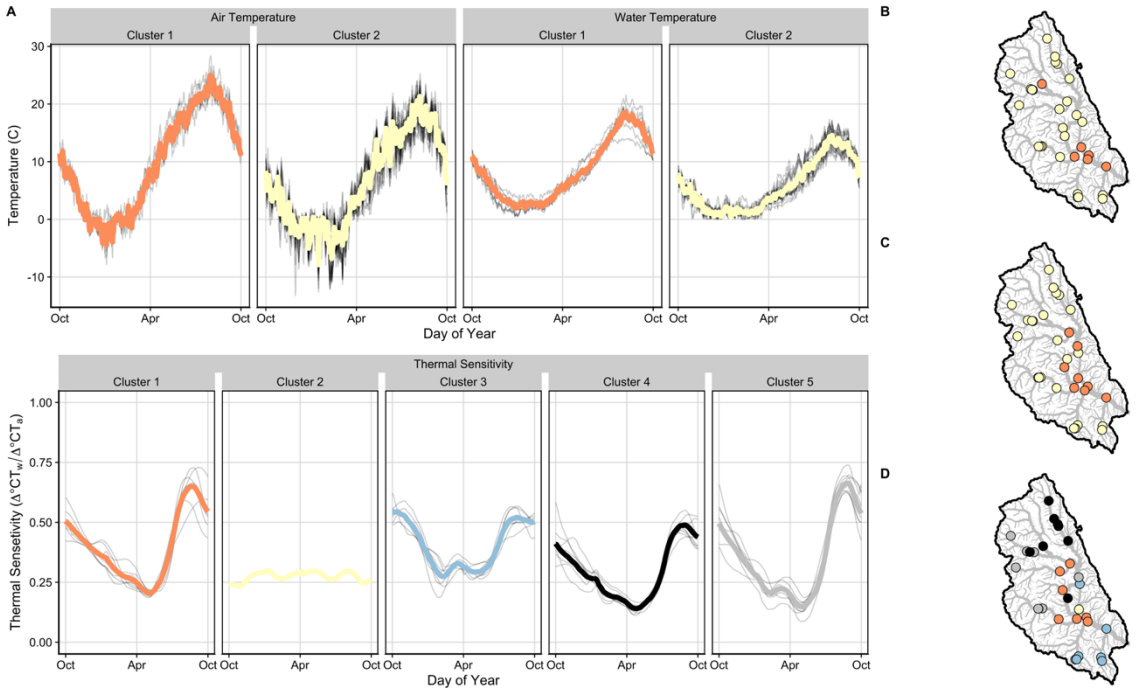

Figure 5.6. Average time series (A) and spatial clustering results (columns/colors indicate unique clusters) for average annual air temperature (B), water temperature (C), and thermal sensitivity (D) in the Wenatchee basin. The spatial distribution for Colored lines indicates mean average annual values for each cluster, and gray lines denote average annual values for each site within a given cluster.

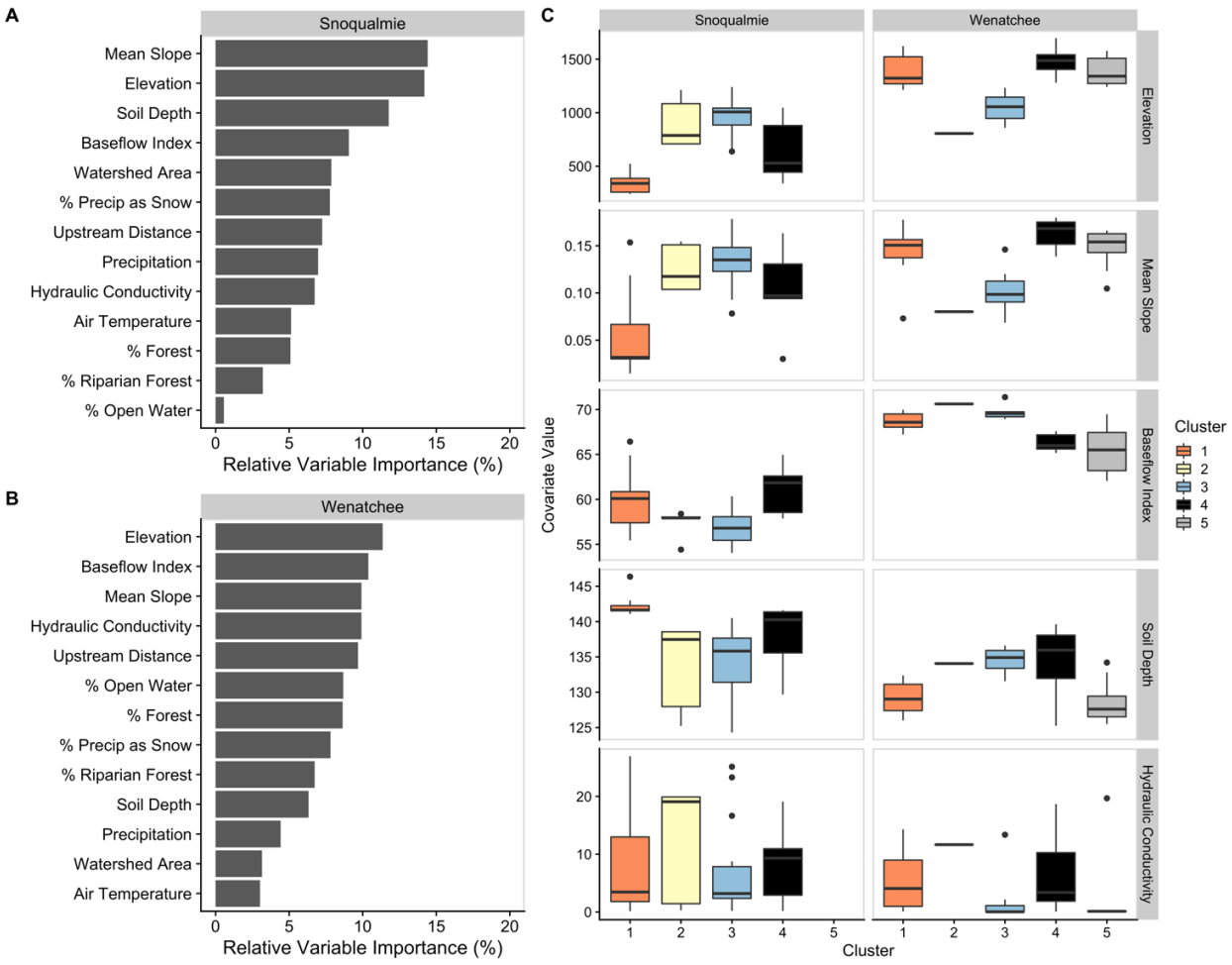

Figure 5.7. Relative variable importance for all covariates in the Snoqualmie (A) Wenatchee (B) basins, and the distributions of variables for the four most important variables (C) in the Snoqualmie basin (Mean Slope, Elevation, Soil Depth, and Baseflow Index) and in the Wenatchee basin (Elevation, Baseflow Index, Mean Slope, and Hydraulic Conductivity). Boxes are grouped and colored by cluster membership. See Figure S5 for plots of the remaining relative variable importances.

Table 5.1. Physical environmental data and basin characteristics used to predict air-water clusters.

Variable	Category	Units	Data Source
Watershed area	Basin Topography	km^2	Hill et al. 2016
Watershed elevation	Basin Topography	m	Hill et al. 2016
Avg. stream slope	Basin Topography	mm^{-1}	Hill et al. 2016
Distance upstream	Basin Topography	km	Hill et al. 2016
% Watershed forest	Land Use	%	Hill et al. 2016; Dewitz et al. 2019
% Riparian forest	Land Use	%	Hill et al. 2016; Dewitz et al. 2019
% Lake area	Land Use	%	Hill et al. 2016; Dewitz et al. 2019
Avg. Temperature	Climate	C	Hart and Bell 2015
Avg. Precipitation	Climate	mm	Hart and Bell 2015
Avg. % precip as snow	Climate	%	Hart and Bell 2015
Baseflow index	Geology	%	Hill et al. 2016; Wolock 2003
Hydraulic conductivity	Geology	%	Hill et al. 2016; Olson and Hawkins 2014
Soil depth to bedrock	Geology	cm	Hill et al. 2016; Carlisle et al. 2009

Table 5.2. Air water correlation summary metrics by basin and season.

		Thermal Sensitivity			R^2		
		Min	**Median**	**Max**	**Min**	**Median**	**Max**
Snoqualmie	Fall	0.22	0.59	0.79	0.58	0.93	0.99
	Winter	0.05	0.39	0.71	0.20	0.88	0.96
	Spring	0.26	0.59	0.97	0.67	0.90	0.98
	Summer	0.19	0.55	0.95	0.41	0.88	0.97
Wenatchee	Fall	0.40	0.56	0.74	0.74	0.92	0.98
	Winter	0.05	0.28	0.47	0.44	0.86	0.95
	Spring	0.14	0.40	0.72	0.59	0.90	0.98
	Summer	0.06	0.44	0.66	0.08	0.85	0.96

Table 5.3. Metrics averaged for all sites within each thermal sensitivity regime determined with the spatially weighted agglomerative hierarchical clustering.

Basin	Cluster	# Sites	Mean Thermal Sensitivity	Thermal Sensitivity Range	Cluster Stability
Snoqualmie	1	11	0.50	0.71 – 0.35 (0.36)	0.68
	2	5	0.52	0.86 – 0.32 (0.54)	0.88
	3	15	0.40	0.80 – 0.12 (0.67)	0.67
	4	11	0.65	0.98 – 0.35 (0.63)	0.55
Wenatchee	1	7	0.39	0.73 – 0.19 (0.54)	0.79
	2	1	0.27	0.30 – 0.23 (0.06)	0.62
	3	7	0.40	0.62 – 0.19 (0.44)	0.94
	4	8	0.29	0.58 – 0.11 (0.47)	0.86
	5	8	0.35	0.74 – 0.09 (0.65)	0.69

Chapter 6. CONCLUSION

River networks are complex systems. Their ecological and economic importance, particularly across the Pacific Northwest and western North America, necessitates careful treatment with considering potential future trajectories with respect to climate change, land use modification, and population growth. To simultaneously maintain ecosystem services and health in the face of anthropogenic impacts, we need to understand drivers and changes to hydrology and temperature regimes, and develop a suite of inexpensive, broadly applicable tools that resource managers can use to understand which river basins, which parts of those basins, and which times during the annual cycle may be at most risk in the future.

At its core, my dissertation research answers questions relating to how we understand, describe, and model current and future river hydrology at the local and regional scales. My dissertation strives to match mathematical and statistical methods to existing questions in hydrology, and to examine how multiple approaches can be integrated to reduce error and arrive at robust understanding and predictions. Although general conclusions can be drawn, any answer necessarily demands consideration of the specific context. There is no one size fits all approach in quantitative analyses of ecological systems; when creating management recommendations, it is necessary to acknowledge and embrace complexity and uncertainty.

6.1 CHAPTER CONCLUSIONS

Major conclusions of each chapter are as follows:

1. Across basin patterns in stable isotopes of surface water:

a. Elevation was the dominant predictor of isotope ratios across five Pacific Northwest basins, but the importance varied across basins and depended on geographic location, landscape attribute configuration, and basin size.
b. Incorporating spatial structure through the SSNM framework captured aspects of water isotopic variation even in basins where variance explained by covariates was high but was particularly important to consider in areas where covariates explained the least of the isotopic variation.
c. Basin-specific models that include spatial structure improve accuracy of surface-water isoscapes for understanding hydrologic function, interpreting source contributions downstream, or assisting in basin management.

2. River water sources throughout the year:
    a. Stable isotope ratios in river water related strongly to elevation throughout the year; seasonal variation in isotope ratios was present and reflected hydrologic processes.
    b. Relatively depleted isotope ratios in spring reflected the input of snowmelt into the river. Enriched baseflow isotope ratios suggest that groundwater is sourced from low elevation glacial deposits and recharged by winter precipitation.
    c. Stable isotopes of surface water can be used to understand water source dynamics and provide insights into management strategies. For example, in the Snoqualmie basin, management strategies could focus on actions to restore floodplain functions that recharge aquifers to preserve late summer baseflow.
3. Long term trends in hydrologic metrics:

a. Relatively few basins displayed monotonic trends in discharge metrics, although baseflow metrics showed more substantial and widespread changes.
b. Geographically localized interannual variation was the dominant control on observed changes to streamflow, rather than variability corresponding to river type or monotonic changes.
c. Mean annual precipitation that falls in a catchment has historically been the dominant control on measured facets of river hydrology, compared to air temperature and global circulation metrics.

4. Spatially-weighted clustering of thermal sensitivities:
    a. The sensitivity of stream temperatures to variation in air temperature exhibited substantial seasonal and interannual variation, calling into question the utility of the widespread practice of using stationary thermal sensitivity values to extrapolate to future climate conditions.
    b. Clustering results varied substantially between air temperature, water temperature and thermal sensitivities, illustrating that thermal sensitivity regimes reflect non-redundant aspects of river dynamics.
    c. Groundwater was an important and observable mediator of thermal sensitivity regimes in Pacific Northwest basins.

6.2 UNDERSTANDING DRIVERS OF RIVER REGIMES ACROSS SCALES

Drivers of physical river dynamics are numerous, with multivariate controls and process interactions spatially nested at macro (e.g., PDO, ENSO, latitude), regional (e.g., temperature, precipitation), and local (e.g., elevation, channel geometry, riparian shading, geomorphic context) scales. Findings in my dissertation are statistical in nature, however, whenever possible

I attempted to create a process-based understanding of causes of patterns in hydrologic regimes. Previous work in western North America identified elevation as it relates to snowpack dynamics as the primary control on streamflow sensitivity to warming. However, Chapter 4 shows that on the time scale of decades, interannual variability in mean annual precipitation has historically been the dominant control on measured facets of river hydrology. Chapters 3 and 5 illustrate the importance of geology, in addition to snowpack dynamics, in controlling patterns of water source and thermal sensitivity in Pacific Northwest river basins. River drainages may express a range of reactions to the same environmental forcing due to their geomorphic complexity, as basin morphological characteristics are the local-scale lens through with climatic changes will be filtered and translated into streamflow. My dissertation research emphasizes that along with changes in the timing of snowpack accumulation and melt, streamflow is also dependent on interannual variability in climate and intrinsic, geologically mediated differences in the efficiency of landscapes in storing and transforming recharge into discharge.

It is important to note that as climate change progresses, precipitation, temperature, and snowpack dynamics will continue to shift. Statistical relationships are not necessarily stationary in time, and hydrologic features that once existed may change or disappear entirely. Interactions between climate and landscape variables are complex and depend on spatial and temporal relationships of network location and water source dynamics. Integrating statistical insights with process-based modeling may provide an avenue forward for untangling these interactions.

6.3 Modeling spatial data within and across watershed

In this dissertation, I look across the scale of continents to kilometers, and spatial autocorrelation is present in every study. Autocorrelation within a variate (e.g., water temperature) is created by both atmospheric processes and landscape characteristics and can be a

powerful tool for resource management if properly accounted for. For example, Chapters 2 and 3 show that the combination of west-to-east movement of airmasses and orographic rainout create a consistent gradient of water isotope ratios in western Washington basins that can be used to understand seasonal water source dynamics. Similarly, Chapter 5 illustrates that individual storms generate regional synchrony in peak flows. In addition to spatial autocorrelation within a variate, correlation among landscape characteristics and human development also exists. This covariation can result in multicollinearity of covariates and hinder statistical efforts to identify mechanistic links between landscape gradients and features of aquatic ecosystems. For example, in watersheds within the Pacific Northwest, elevation and human development gradients often align so that valley bottoms are more developed than headwater areas. These correlation structures, although part of the functioning of the landscape, need to be accounted for due to their ability to undermine statistical estimation.

Large-scale studies such as Chapter 4 provide a framework for interpreting climate impacts to entire river basins and provide an indication of how regional water resources are likely to shift. However, much of river basin management occurs at the sub-basin scale, and current approaches are often insufficient for understanding how climate change will impact future streamflow across both space and time. Chapters 2, 3, and 5 capitalize on the unique dendritic and flow directed configuration of river networks, wherein upstream processes influence downstream patterns to predict stable isotope values and thermal sensitivity dynamics on the network. Despite the presence of spatial correlation, the response to climate can be diverse within an individual watershed. The results of this work highlight that ongoing climate change can have distinct impacts on stream hydrology and thermal regimes even on sites that are within

the same river basin due to differing physical characteristics of stream catchments. These results may help to further constrain stream response under warmer climate.

6.4 MODELING TEMPORAL DATA WITHIN AND ACROSS YEARS

Patterns in both river temperature and hydrology show variability at multiple time scales and are shaped by diverse processes. For example, in western North America evapotranspiration and the freeze-thaw cycle can result in diel fluctuations in discharge, whereas annual fluctuations occur due to seasonal precipitation and snowmelt dynamics. Measuring and modeling hydrologic patterns necessitates careful consideration and should be approached with a clear question in mind. In this dissertation, I examine thermal and hydrologic fluctuations spanning days to decades and wrestle with the question of how to divide and model environmental time series. Chapters 4 and 5 take complementary approaches to time series modeling. Chapter 5 utilizes regime-based classification to separate continuous time series into discrete clusters, while Chapter 4 distills time series data down into discrete metrics and utilizes regression-based approaches to explore continuous relationships. The overarching goal in both studies is to aggregate and simplify the data, retaining essential information without getting bogged down with unnecessary detail.

Metric-based approaches is to find the signal in the noise by changing the scale of description and moving from noisy, unpredictable time series into a collection of cases with behavior regular enough to allow generalizations to be made. To accomplish this task, key elements of the temperature of discharge regime need to first be identified. Given that there are an infinite number of potential metrics that could be calculated from a single time series, selected metrics should have documented relationships with the ecological, geomorphic, or biogeochemical facets of interest in riverine systems. Currently, river basin management utilizes

narrowly defined metrics often based on mean, minimum, or maximum summer temperatures or flows. However, managers and decision makers have begun to recognize the importance of thermal and hydrologic diversity across both season and space in supporting healthy rivers. As a result, metrics that describe portions of the year outside of summer are becoming more common, as are approaches such as frequency decomposition (i.e., wavelet or Fourier analysis), which can examine how variability at different time scales has shifted through time.

6.5 FUTURE DIRECTIONS

As with any scientific endeavor, my dissertation represents only a small piece of the overall scientific puzzle. A fruitful area of future research lies in linking variation in stream temperature and discharge to specific biological outcomes for organisms such as algae, macroinvertebrates, and fish species. Specifically, an understanding of the cumulative impacts of flow and temperature regime shifts remains elusive. Given the complexity of isolating specific organism responses to individual metrics or patterns, a comparative approach across rivers may be useful. Advances in data generation and sharing have led to an ongoing data revolution, with data freely available from satellite imagery, large scale collection programs, and published studies. For example, continent-wide datasets on stream organisms (e.g. RivFishTime, NEON, EPA NARS) and modeled temperature, precipitation, snowmelt, and streamflow are freely available. There is ample opportunity to integrate these historical datasets with remote sensing products to answer novel questions previously constrained by a lack of available data.

I hope that results from my dissertation can be used to develop mitigation and adaptation activities to work best with local conditions, thus maximizing benefits given limited resources. Development of appropriate conservation strategies depends on accurate understanding of the potential range of ecological response to future changes in the aquatic landscape. In the

Snoqualmie basin, for example, small headwater streams may be particularly susceptible to warming temperatures and reduced flows in the future (Chapters 3, 4, and 5). River basin managers may therefore look towards management actions such as increasing alluvial storage, restoring floodplain functions that recharge aquifers, and riparian planting to preserve essential aquatic habitat in the future.

BIBLIOGRAPHY

Abatzoglou, J. T., S. Z. Dobrowski, S. A. Parks, and K. C. Hegewisch. 2018. TerraClimate, a high-resolution global dataset of monthly climate and climatic water balance from 1958–2015. Scientific Data 5:170191.

Abbe, T., and A. Brooks. 2013. Geomorphic, Engineering, and Ecological Considerations when Using Wood in River Restoration. Pages 419–451 *in* A. Simon, S. J. Bennett, and J. M. Castro, editors. Geophysical Monograph Series. American Geophysical Union, Washington, D. C.

Ahmad, S. K., F. Hossain, G. W. Holtgrieve, T. Pavelsky, and S. Galelli. 2021. Predicting the Likely Thermal Impact of Current and Future Dams Around the World. Earth's Future 9.

Al-Kaisi, M. M., and D. Kwaw-Mensah. 2020. Quantifying soil carbon change in a long-term tillage and crop rotation study across Iowa landscapes. Soil Science Society of America Journal 84:182–202.

Angus Webb, J., K. A. Miller, E. L. King, S. C. Little, M. J. Stewardson, J. K. H. Zimmerman, and N. LeRoy Poff. 2013. Squeezing the most out of existing literature: a systematic re-analysis of published evidence on ecological responses to altered flows. Freshwater Biology 58:2439–2451.

Araguas-Araguas, L., K. Froehlich, and K. Rozanski. 2000. Deuterium and oxygen-18 isotope composition of precipitation and atmospheric moisture. Hydrological Processes 14:1341–1355.

Arbelaitz, O., I. Gurrutxaga, J. Muguerza, J. M. Pérez, and I. Perona. 2013. An extensive comparative study of cluster validity indices. Pattern Recognition 46:243–256.

Arismendi, I., M. Safeeq, J. B. Dunham, and S. L. Johnson. 2014. Can air temperature be used to project influences of climate change on stream temperature? Environmental Research Letters 9:084015.

Armstrong, J. B., A. H. Fullerton, C. E. Jordan, J. L. Ebersole, J. R. Bellmore, I. Arismendi, B. E. Penaluna, and G. H. Reeves. 2021. The importance of warm habitat to the growth regime of cold-water fishes. Nature Climate Change 11:354–361.

Arsenault, R., F. Brissette, J. Chen, Q. Guo, and G. Dallaire. 2020. NAC ^{2} H: The North American Climate Change and Hydroclimatology Data Set. Water Resources Research 56.

Averyt, K., J. Meldrum, P. Caldwell, G. Sun, S. McNulty, A. Huber-Lee, and N. Madden. 2013. Sectoral contributions to surface water stress in the coterminous United States. Environmental Research Letters 8:035046.

Baker, N. C., and H.-P. Huang. 2014. A Comparative Study of Precipitation and Evaporation between CMIP3 and CMIP5 Climate Model Ensembles in Semiarid Regions. Journal of Climate 27:3731–3749.

Banerjee, K., P. Krishnan, and N. Mridha. 2018. Application of thermal imaging of wheat crop canopy to estimate leaf area index under different moisture stress conditions. Biosystems Engineering 166:13–27.

Barnett, T. P., J. C. Adam, and D. P. Lettenmaier. 2005. Potential impacts of a warming climate on water availability in snow-dominated regions. Nature 438:303–309.

Barnett, T. P., D. W. Pierce, H. G. Hidalgo, C. Bonfils, B. D. Santer, T. Das, G. Bala, A. W. Wood, T. Nozawa, A. A. Mirin, D. R. Cayan, and M. D. Dettinger. 2008. Human-

Induced Changes in the Hydrology of the Western United States. Science 319:1080–1083.

Barth, N. A., G. Villarini, M. A. Nayak, and K. White. 2017. Mixed populations and annual flood frequency estimates in the western United States: The role of atmospheric rivers. Water Resources Research 53:257–269.

Beaufort, A., F. Moatar, F. Curie, A. Ducharne, V. Bustillo, and D. Thiéry. 2016. River Temperature Modelling by Strahler Order at the Regional Scale in the Loire River Basin, France: River Temperature Modelling by Strahler Order. River Research and Applications 32:597–609.

Beaufort, A., F. Moatar, E. Sauquet, P. Loicq, and D. M. Hannah. 2020. Influence of landscape and hydrological factors on stream–air temperature relationships at regional scale. Hydrological Processes 34:583–597.

Beck, H. E., A. I. J. M. van Dijk, D. G. Miralles, R. A. M. de Jeu, L. A. Sampurno Bruijnzeel, T. R. McVicar, and J. Schellekens. 2013. Global patterns in base flow index and recession based on streamflow observations from 3394 catchments: Global Patterns in Base Flow Characteristics. Water Resources Research 49:7843–7863.

van Beek, L. P. H., T. Eikelboom, M. T. H. Vliet, and M. F. P. Bierkens. 2012. A physically based model of global freshwater surface temperature. Water Resources Research 48:2012WR011819.

Benyahya, L., D. Caissie, N. El-Jabi, and M. G. Satish. 2010. Comparison of microclimate vs. remote meteorological data and results applied to a water temperature model (Miramichi River, Canada). Journal of Hydrology 380:247–259.

Benyahya, L., D. Caissie, A. St-Hilaire, T. B. M. J. Ouarda, and B. Bobée. 2007. A Review of Statistical Water Temperature Models. Canadian Water Resources Journal 32:179–192.

Berghuijs, W. R., S. T. Allen, S. Harrigan, and J. W. Kirchner. 2019. Growing Spatial Scales of Synchronous River Flooding in Europe. Geophysical Research Letters 46:1423–1428.

Berkelhammer, M., L. Stott, K. Yoshimura, K. Johnson, and A. Sinha. 2012. Synoptic and mesoscale controls on the isotopic composition of precipitation in the western United States. Climate Dynamics 38:433–454.

Bershaw, J., S. M. Penny, and C. N. Garzione. 2012. Stable isotopes of modern water across the Himalaya and eastern Tibetan Plateau: Implications for estimates of paleoelevation and paleoclimate. Journal of Geophysical Research: Atmospheres 117:n/a-n/a.

Bethel, J. 2004. An overview of the geology and geomorphology of the Snoqualmie River watershed. King County Water and Land Resources Division, Snoqualmie Watershed Team.

Biggs, T. W., C.-T. Lai, P. Chandan, R. M. Lee, A. Messina, R. S. Lesher, and N. Khatoon. 2015. Evaporative fractions and elevation effects on stable isotopes of high elevation lakes and streams in arid western Himalaya. Journal of Hydrology 522:239–249.

Blankinship, J. C., M. W. Meadows, R. G. Lucas, and S. C. Hart. 2014. Snowmelt timing alters shallow but not deep soil moisture in the Sierra Nevada. Water Resources Research 50:1448–1456.

Blumstock, M., D. Tetzlaff, I. A. Malcolm, G. Nuetzmann, and C. Soulsby. 2015. Baseflow dynamics: Multi-tracer surveys to assess variable groundwater contributions to montane streams under low flows. Journal of Hydrology 527:1021–1033.

Bogan, T., O. Mohseni, and H. G. Stefan. 2003. Stream temperature-equilibrium temperature relationship. Water Resources Research 39.

Bonada, N., S. Dolédec, and B. Statzner. 2007. Taxonomic and biological trait differences of stream macroinvertebrate communities between mediterranean and temperate regions: implications for future climatic scenarios. Global Change Biology 13:1658–1671.

Bonfils, C., B. D. Santer, D. W. Pierce, H. G. Hidalgo, G. Bala, T. Das, T. P. Barnett, D. R. Cayan, C. Doutriaux, A. W. Wood, A. Mirin, and T. Nozawa. 2008. Detection and Attribution of Temperature Changes in the Mountainous Western United States. Journal of Climate 21:6404–6424.

Bowen, G. J., and S. P. Good. 2015. Incorporating water isoscapes in hydrological and water resource investigations: Isoscapes in hydrological and water resource investigations. Wiley Interdisciplinary Reviews: Water 2:107–119.

Bowen, G. J., C. D. Kennedy, Z. Liu, and J. Stalker. 2011. Water balance model for mean annual hydrogen and oxygen isotope distributions in surface waters of the contiguous United States. Journal of Geophysical Research 116.

Bowen, G. J., and B. Wilkinson. 2002. Spatial distribution of δ18O in meteoric precipitation. Geology 30:315.

Bower, D., D. M. Hannah, and G. R. McGregor. 2004. Techniques for assessing the climatic sensitivity of river flow regimes. Hydrological Processes 18:2515–2543.

Boyer, C., A. St-Hilaire, and N. E. Bergeron. 2021. Defining river thermal sensitivity as a function of climate. River Research and Applications 37:1548–1561.

Breiman, L., J. H. Friedman, R. A. Olshen, and C. J. Stone. 1984. Classification And Regression Trees. First edition. Routledge.

Brennan, S. R., D. E. Schindler, T. J. Cline, T. E. Walsworth, G. Buck, and D. P. Fernandez. 2019. Shifting habitat mosaics and fish production across river basins. Science 364:783–786.

Brennan, S. R., C. E. Torgersen, J. P. Hollenbeck, D. P. Fernandez, C. K. Jensen, and D. E. Schindler. 2016. Dendritic network models: Improving isoscapes and quantifying influence of landscape and in-stream processes on strontium isotopes in rivers: Dendritic Network Models and Isoscapes. Geophysical Research Letters 43:5043–5051.

Brewer, S. K. 2013. Groundwater influences on the distribution and abundance of riverine smallmouth bass, *Micropterus dolomieu*, in pasture landscapes of the midwestern USA. River Research and Applications 29:269–278.

Briggs, M. A., P. Goodling, Z. C. Johnson, K. M. Rogers, N. P. Hitt, J. B. Fair, and C. D. Snyder. 2022. Bedrock depth influences spatial patterns of summer baseflow, temperature, and flow disconnection for mountainous headwater streams. preprint, Catchment hydrology/Instruments and observation techniques.

Briggs, M. A., Z. C. Johnson, C. D. Snyder, N. P. Hitt, B. L. Kurylyk, L. Lautz, D. J. Irvine, S. T. Hurley, and J. W. Lane. 2018. Inferring watershed hydraulics and cold-water habitat persistence using multi-year air and stream temperature signals. Science of The Total Environment 636:1117–1127.

Briggs, M. A., E. B. Voytek, F. D. Day-Lewis, D. O. Rosenberry, and J. W. Lane. 2013. Understanding Water Column and Streambed Thermal Refugia for Endangered Mussels in the Delaware River. Environmental Science & Technology 47:11423–11431.

Brimley, B., J. F. Cantin, D. Harvey, M. Kowalchuk, P. Marsh, T. M. B. J. Ouarda, B. Phinney, P. Pilon, M. Renouf, Tassone B., and R. Wedel. 1999. Brimley, B., Cantin, J.F., Harvey,

D., Kowalchuk, M., Marsh, P., Ouarda, T.M.B.J., Phinney, B., Pilon, P., Renouf, M., Tassone, B. and Wedel, R. Page 41. Environment Canada.

Brooks, J. R., H. R. Barnard, R. Coulombe, and J. J. McDonnell. 2010. Ecohydrologic separation of water between trees and streams in a Mediterranean climate. Nature Geoscience Letters 3.

Brooks, J. R., P. J. Wigington, D. L. Phillips, R. Comeleo, and R. Coulombe. 2012. Willamette River Basin surface water isoscape (δ^{18} O and δ^{2} H): temporal changes of source water within the river. Ecosphere 3:art39.

Buffington, J. M., R. A. Woodsmith, D. B. Booth, and D. R. Montgomery. 2003. Fluvial Processes in Puget Sound Rivers and the Pacific Northwest. Pages 46–78 *in* D. R. Montgomery, S. M. Bolton, D. B. Booth, and L. Wall, editors. Restoration of Puget Sound Rivers. University of Washington Press, Seattle, WA.

Burn, D. H., and M. A. Hag Elnur. 2002. Detection of hydrologic trends and variability. Journal of Hydrology 255:107–122.

Burn, D. H., J. Hannaford, G. A. Hodgkins, P. H. Whitfield, R. Thorne, and T. Marsh. 2012. Reference hydrologic networks II. Using reference hydrologic networks to assess climate-driven changes in streamflow. Hydrological Sciences Journal 57:1580–1593.

Burn, D. H., M. Sharif, and K. Zhang. 2010. Detection of trends in hydrological extremes for Canadian watersheds. Hydrological Processes 24:1781–1790.

Burnham, K. P., and D. R. Anderson. 2004. Multimodel Inference: Understanding AIC and BIC in Model Selection. Sociological Methods & Research 33:261–304.

Caissie, D. 2006. The thermal regime of rivers: a review. Freshwater Biology 51:1389–1406.

Carlisle, D. M., T. E. Grantham, K. Eng, and D. M. Wolock. 2017. Biological relevance of streamflow metrics: regional and national perspectives. Freshwater Science 36:927–940.

Carro-Calvo, L., F. Jaume-Santero, R. García-Herrera, and S. Salcedo-Sanz. 2021. k-Gaps: a novel technique for clustering incomplete climatological time series. Theoretical and Applied Climatology 143:447–460.

Casas, I., and R. Fernandez-Casal. 2019. tvReg: Time-varying Coefficient Linear Regression for Single and Multi-Equations in R. SSRN Electronic Journal.

Casas, I., and R. Fernandez-Casal. 2021. tvReg: Time-Varying Coefficients Linear Regression for Single and Multi-Equations.

Cayan, D. R., S. A. Kammerdiener, M. D. Dettinger, J. M. Caprio, and D. H. Peterson. 2001. Changes in the Onset of Spring in the Western United States. Bulletin of the American Meteorological Society 82:399–416.

Cayan, D. R., E. P. Maurer, M. D. Dettinger, M. Tyree, and K. Hayhoe. 2008. Climate change scenarios for the California region. Climatic Change 87:21–42.

Chamberlain, C. P., J. D. Blum, R. T. Holmes, X. Feng, T. W. Sherry, and G. R. Graves. 1997. The use of isotope tracers for identifying populations of migratory birds. Oecologia 109:132–141.

Chang, H., and M. Psaris. 2013. Local landscape predictors of maximum stream temperature and thermal sensitivity in the Columbia River Basin, USA. Science of The Total Environment 461–462:587–600.

Charrad, M., N. Ghazzali, V. Boiteau, and A. Niknafs. 2014. NbClust: An R Package for Determining the Relevant Number of Clusters in a Data Set. Journal of Statistical Software 61:1–36.

Chen, Z., and S. E. Grasby. 2009. Impact of decadal and century-scale oscillations on hydroclimate trend analyses. Journal of Hydrology 365:122–133.

Cheng, Y., B. Nijssen, G. W. Holtgrieve, and J. D. Olden. 2022. Modeling the freshwater ecological response to changes in flow and thermal regimes influenced by reservoir dynamics. Journal of Hydrology 608:127591.

Chu, C., N. E. Jones, and L. Allin. 2010. Linking the thermal regimes of streams in the Great Lakes Basin, Ontario, to landscape and climate variables: THERMAL REGIMES IN ONTARIO STREAMS. River Research and Applications 26:221–241.

Clark, I. D., and P. Fritz. 1997. Environmental isotopes in hydrogeology. CRC Press/Lewis Publishers, Boca Raton, FL.

Cline, T. J., D. E. Schindler, T. E. Walsworth, D. W. French, and P. J. Lisi. 2020. Low snowpack reduces thermal response diversity among streams across a landscape. Limnology and Oceanography Letters 5:254–263.

Corringham, T. W., F. M. Ralph, A. Gershunov, D. R. Cayan, and C. A. Talbot. 2019. Atmospheric rivers drive flood damages in the western United States. Science Advances 5:eaax4631.

Cressie, N. A. C. 1993. Statistics for Spatial Data: Cressie/Statistics. John Wiley & Sons, Inc., Hoboken, NJ, USA.

Cunderlik, J. M., and T. B. M. J. Ouarda. 2009. Trends in the timing and magnitude of floods in Canada. Journal of Hydrology 375:471–480.

Curran, J. H., and F. E. Biles. 2021. Identification of Seasonal Streamflow Regimes and Streamflow Drivers for Daily and Peak Flows in Alaska. Water Resources Research 57.

Dale, M. R. T., and M.-J. Fortin. 2009. Spatial autocorrelation and statistical tests: Some solutions. Journal of Agricultural, Biological, and Environmental Statistics 14:188–206.

Daly, S. F., R. Davis, E. Ochs, and T. Pangburn. 2000. An approach to spatially distributed snow modelling of the Sacramento and San Joaquin basins, California. Hydrological Processes 14:3257–3271.

Dansgaard, W. 1964. Stable isotopes in precipitation. Tellus 16:436–468.

Das, T., H. G. Hidalgo, D. W. Pierce, T. P. Barnett, M. D. Dettinger, D. R. Cayan, C. Bonfils, G. Bala, and A. Mirin. 2009. Structure and Detectability of Trends in Hydrological Measures over the Western United States. Journal of Hydrometeorology 10:871–892.

Daufresne, M., and P. Boët. 2007. Climate change impacts on structure and diversity of fish communities in rivers. Global Change Biology 13:2467–2478.

De'ath, G., and K. E. Fabricius. 2000. Classification and regression trees: a powerful yet simple technique for ecological data analysis. Ecology 81:3178–3192.

Debose, A., and M. W. Klungland. 1964. Soil survey of Snohomish County area. US Department of Agriculture, Soil Conservation Service, Washington, D. C.

Déry, S. J., K. Stahl, R. D. Moore, P. H. Whitfield, B. Menounos, and J. E. Burford. 2009. Detection of runoff timing changes in pluvial, nival, and glacial rivers of western Canada: WESTERN CANADA RUNOFF TIMING. Water Resources Research 45.

Déry, S. J., and E. F. Wood. 2005. Decreasing river discharge in northern Canada. Geophysical Research Letters 32.

Destouni, G., and L. Verrot. 2014. Screening long-term variability and change of soil moisture in a changing climate. Journal of Hydrology 516:131–139.

Dettinger, M. 2011. Climate Change, Atmospheric Rivers, and Floods in California - A Multimodel Analysis of Storm Frequency and Magnitude Changes1: Climate Change, Atmospheric Rivers, and Floods in California - A Multimodel Analysis of Storm Frequency and Magnitude Changes. JAWRA Journal of the American Water Resources Association 47:514–523.

Dettinger, M. 2016. Historical and Future Relations Between Large Storms and Droughts in California. San Francisco Estuary and Watershed Science 14.

Dettinger, M. D. 2013. Atmospheric Rivers as Drought Busters on the U.S. West Coast. Journal of Hydrometeorology 14:1721–1732.

Dettinger, M. D., D. R. Cayan, H. F. Diaz, and D. M. Meko. 1998. North–South Precipitation Patterns in Western North America on Interannual-to-Decadal Timescales. Journal of Climate 11:3095–3111.

Dierauer, J. R., P. H. Whitfield, and D. M. Allen. 2018. Climate Controls on Runoff and Low Flows in Mountain Catchments of Western North America. Water Resources Research.

Diffenbaugh, N. S., D. L. Swain, and D. Touma. 2015. Anthropogenic warming has increased drought risk in California. Proceedings of the National Academy of Sciences 112:3931–3936.

Donato, M. M. 2002. A statistical model for estimating stream temperatures in the Salmon and Clearwater River basins, Central Idaho. Water Resources Investigations Report, U.S. Geological Survey, Washington, D. C.

Dudgeon, D., A. H. Arthington, M. O. Gessner, Z.-I. Kawabata, D. J. Knowler, C. Lévêque, R. J. Naiman, A.-H. Prieur-Richard, D. Soto, M. L. J. Stiassny, and C. A. Sullivan. 2006.

Freshwater biodiversity: importance, threats, status and conservation challenges. Biological Reviews 81:163.

Dugdale, S. J., D. M. Hannah, and I. A. Malcolm. 2017. River temperature modelling: A review of process-based approaches and future directions. Earth-Science Reviews 175:97–113.

Dutton, A., B. H. Wilkinson, J. M. Welker, G. J. Bowen, and K. C. Lohmann. 2005. Spatial distribution and seasonal variation in ^{18}O/^{16}O of modern precipitation and river water across the conterminous USA. Hydrological Processes 19:4121–4146.

Ehsanzadeh, E., and K. Adamowski. 2007. Detection of Trends in Low Flows across Canada. Canadian Water Resources Journal 32:251–264.

Ehsanzadeh, E., and K. Adamowski. 2009. Trends in timing of low stream flows in Canada: impact of autocorrelation and long-term persistence. Hydrological Processes 24:970–980.

Elsner, M. M., L. Cuo, N. Voisin, J. S. Deems, A. F. Hamlet, J. A. Vano, K. E. B. Mickelson, S.-Y. Lee, and D. P. Lettenmaier. 2010. Implications of 21st century climate change for the hydrology of Washington State. Climatic Change 102:225–260.

Ersek, V., A. C. Mix, and P. U. Clark. 2010. Variations of δ^{18}O in rainwater from southwestern Oregon. Journal of Geophysical Research 115:D09109.

Fan, Y., Y. Chen, Q. He, W. Li, and Y. Wang. 2016. Isotopic Characterization of River Waters and Water Source Identification in an Inland River, Central Asia. Water 8:286.

Fellman, J. B., E. Hood, W. Dryer, and S. Pyare. 2015. Stream Physical Characteristics Impact Habitat Quality for Pacific Salmon in Two Temperate Coastal Watersheds. PLOS ONE 10:e0132652.

Fellman, J. B., S. Nagorski, S. Pyare, A. W. Vermilyea, D. Scott, and E. Hood. 2014. Stream temperature response to variable glacier coverage in coastal watersheds of Southeast Alaska. Hydrological Processes 28:2062–2073.

Ficklin, D. L., J. T. Abatzoglou, S. M. Robeson, S. E. Null, and J. H. Knouft. 2018. Natural and managed watersheds show similar responses to recent climate change. Proceedings of the National Academy of Sciences 115:8553–8557.

Filipe, A. F., L. Quaglietta, M. Ferreira, M. F. Magalhães, and P. Beja. 2017. Geostatistical distribution modelling of two invasive crayfish across dendritic stream networks. Biological Invasions 19:2899–2912.

Flint, A. L., L. E. Flint, and M. D. Dettinger. 2008. Modeling Soil Moisture Processes and Recharge under a Melting Snowpack. Vadose Zone Journal 7:350–357.

Flitcroft, R., M. S. Cooperman, I. J. Harrison, D. Juffe-Bignoli, and P. J. Boon. 2019. Theory and practice to conserve freshwater biodiversity in the Anthropocene. Aquatic Conservation: Marine and Freshwater Ecosystems 29:1013–1021.

Floriancic, M. G., B. M. C. Fischer, P. Molnar, J. W. Kirchner, and I. H. J. Meerveld. 2019. Spatial variability in specific discharge and streamwater chemistry during low flows: Results from snapshot sampling campaigns in eleven Swiss catchments. Hydrological Processes 33:2847–2866.

Friedman, I., and G. I. Smith. 1970. Deuterium Content of Snow Cores from Sierra Nevada Area. Science 169:467–470.

Fritze, H., I. T. Stewart, and E. Pebesma. 2011. Shifts in Western North American Snowmelt Runoff Regimes for the Recent Warm Decades. Journal of Hydrometeorology 12:989–1006.

Frizzell, V. A. 1979. Petrology and stratigraphy of Paleogene nonmarine sandstones, Cascade Range, Washington. Open-File Report, U.S. Geological Survey.

Frizzell, V. A., R. W. Tabor, D. B. Booth, K. M. Ort, and R. B. Waitt. 1984. Preliminary geologic map of the Snoqualmie Pass 1:100,000 quadrangle, Washington. Page 43. U.S. Geological Survey Open-File Report.

Gaál, L., J. Szolgay, S. Kohnová, J. Parajka, R. Merz, A. Viglione, and G. Blöschl. 2012. Flood timescales: Understanding the interplay of climate and catchment processes through comparative hydrology. Water Resources Research 48.

Gangopadhyay, S., G. McCabe, G. Pederson, J. Martin, and J. S. Littell. 2019. Risks of hydroclimatic regime shifts across the western United States. Scientific Reports 9.

Garner, G., D. M. Hannah, J. P. Sadler, and H. G. Orr. 2014. River temperature regimes of England and Wales: spatial patterns, inter-annual variability and climatic sensitivity. Hydrological Processes 28:5583–5598.

Gasith, A., and V. H. Resh. 1999. Streams in Mediterranean Climate Regions: Abiotic Influences and Biotic Responses to Predictable Seasonal Events. Annual Review of Ecology and Systematics 30:51–81.

Gat, J. R. 1996. Oxygen and hydrogen isotopes in the hydrologic cycle. Annual Review of Earth and Planetary Sciences 24:225–262.

Gendaszek, A. S., D. M. Ely, S. R. Hinkle, S. C. Kahle, and W. B. Welch. 2014. Hydrogeologic framework and groundwater/surface-water interactions of the upper Yakima River Basin, Kittitas County, central Washington. Scientific Investigations Report.

George, R., R. McManamay, D. Perry, J. Sabo, and B. L. Ruddell. 2021. Indicators of hydro-ecological alteration for the rivers of the United States. Ecological Indicators 120:106908.

Georges, B., A. Michez, H. Piegay, L. Huylenbroeck, P. Lejeune, and Y. Brostaux. 2021. Which environmental factors control extreme thermal events in rivers? A multi-scale approach (Wallonia, Belgium). PeerJ 9:e12494.

Gershunov, A., and T. P. Barnett. 1998. Interdecadal Modulation of ENSO Teleconnections. Bulletin of the American Meteorological Society 79:2715–2725.

Gershunov, A., T. Shulgina, R. E. S. Clemesha, K. Guirguis, D. W. Pierce, M. D. Dettinger, D. A. Lavers, D. R. Cayan, S. D. Polade, J. Kalansky, and F. M. Ralph. 2019. Precipitation regime change in Western North America: The role of Atmospheric Rivers. Scientific Reports 9:9944.

Gesch, D. B., G. A. Evans, M. J. Oimoen, and S. Arundel. 2018. The National Elevation Dataset. Pages 83–110. American Society for Photogrammetry and Remote Sensing.

Gleeson, T., N. Moosdorf, J. Hartmann, and L. P. H. van Beek. 2014. A glimpse beneath earth's surface: GLobal HYdrogeology MaPS (GLHYMPS) of permeability and porosity. Geophysical Research Letters 41:3891–3898.

Glose, A., L. K. Lautz, and E. A. Baker. 2017. Stream heat budget modeling with HFLUX: Model development, evaluation, and applications across contrasting sites and seasons. Environmental Modelling & Software 92:213–228.

Godsey, S. E., J. W. Kirchner, and C. L. Tague. 2014. Effects of changes in winter snowpacks on summer low flows: case studies in the Sierra Nevada, California, USA. Hydrological Processes 28:5048–5064.

Goldin, A. 1973. Soil survey of King County area, Washington. US Department of Agriculture, Soil Conservation Service, Washington, D. C.

Goldin, A. 1992. Soil survey of Whatcom County area, Washington. US Department of Agriculture, Soil Conservation Service, Washington, D. C.

Goniea, T. M., M. L. Keefer, T. C. Bjornn, C. A. Peery, D. H. Bennett, and L. C. Stuehrenberg. 2006. Behavioral Thermoregulation and Slowed Migration by Adult Fall Chinook Salmon in Response to High Columbia River Water Temperatures. Transactions of the American Fisheries Society 135:408–419.

Good, S. P., D. Noone, and G. Bowen. 2015. Hydrologic connectivity constrains partitioning of global terrestrial water fluxes. Science 349.

Grasby, S. E., and D. A. W. Lepitzki. 2002. Physical and chemical properties of the Sulphur Mountain thermal springs, Banff National Park, and implications for endangered snails. Canadian Journal of Earth Sciences 39:1349–1361.

Grill, G., B. Lehner, M. Thieme, B. Geenen, D. Tickner, F. Antonelli, S. Babu, P. Borrelli, L. Cheng, H. Crochetiere, H. Ehalt Macedo, R. Filgueiras, M. Goichot, J. Higgins, Z. Hogan, B. Lip, M. E. McClain, J. Meng, M. Mulligan, C. Nilsson, J. D. Olden, J. J. Opperman, P. Petry, C. Reidy Liermann, L. Sáenz, S. Salinas-Rodríguez, P. Schelle, R. J. P. Schmitt, J. Snider, F. Tan, K. Tockner, P. H. Valdujo, A. van Soesbergen, and C. Zarfl. 2019. Mapping the world's free-flowing rivers. Nature 569:215–221.

Guan, H., C. T. Simmons, and A. J. Love. 2009. Orographic controls on rain water isotope distribution in the Mount Lofty Ranges of South Australia. Journal of Hydrology 374:255–264.

Haggarty, R. A., C. A. Miller, and E. M. Scott. 2015. Spatially weighted functional clustering of river network data. Journal of the Royal Statistical Society: Series C (Applied Statistics) 64:491–506.

Hagos, S. M., L. R. Leung, J. Yoon, J. Lu, and Y. Gao. 2016. A projection of changes in landfalling atmospheric river frequency and extreme precipitation over western North America from the Large Ensemble CESM simulations. Geophysical Research Letters 43:1357–1363.

Hamlet, A. F., S.-Y. Lee, K. E. B. Mickelson, and M. M. Elsner. 2010. Effects of projected climate change on energy supply and demand in the Pacific Northwest and Washington State. Climatic Change 102:103–128.

Hamlet, A. F., and D. P. Lettenmaier. 2007. Effects of 20th century warming and climate variability on flood risk in the western U.S. Water Resources Research 43.

Hamlet, A. F., P. W. Mote, M. P. Clark, and D. P. Lettenmaier. 2005. Effects of Temperature and Precipitation Variability on Snowpack Trends in the Western United States*. Journal of Climate 18:4545–4561.

Hare, D. K., A. M. Helton, Z. C. Johnson, J. W. Lane, and M. A. Briggs. 2021. Continental-scale analysis of shallow and deep groundwater contributions to streams. Nature Communications 12:1450.

Hart, E., and K. Bell. 2015. Prism: Access Data From The Oregon State Prism Climate Project. Zenodo.

Hennig, C. 2020. fpc: Flexible Procedures for Clustering.

Hilderbrand, R. H., M. T. Kashiwagi, and A. P. Prochaska. 2014. Regional and Local Scale Modeling of Stream Temperatures and Spatio-Temporal Variation in Thermal Sensitivities. Environmental Management 54:14–22.

Hill, R. A., M. H. Weber, S. G. Leibowitz, A. R. Olsen, and D. J. Thornbrugh. 2016. The Stream-Catchment (StreamCat) Dataset: A Database of Watershed Metrics for the Conterminous United States. JAWRA Journal of the American Water Resources Association 52:120–128.

Hirschi, M., S. I. Seneviratne, V. Alexandrov, F. Boberg, C. Boroneant, O. B. Christensen, H. Formayer, B. Orlowsky, and P. Stepanek. 2011. Observational evidence for soil-moisture impact on hot extremes in southeastern Europe. Nature Geoscience 4:17–21.

Hobson, K. A., and L. I. Wassenaar. 1997. Linking breeding and wintering grounds of neotropical migrant songbirds using stable hydrogen isotopic analysis of feathers. Oecologia 109:142–148.

Holmes, E., E. Ward J., and K. Wills. 2012. MARSS: Multivariate Autoregressive State-space Models for Analyzing Time-series Data. The R Journal 4:11.

Holtgrieve, G. W., D. E. Schindler, W. O. Hobbs, P. R. Leavitt, E. J. Ward, L. Bunting, G. Chen, B. P. Finney, I. Gregory-Eaves, S. Holmgren, M. J. Lisac, P. J. Lisi, K. Nydick, L. A. Rogers, J. E. Saros, D. T. Selbie, M. D. Shapley, P. B. Walsh, and A. P. Wolfe. 2011. A Coherent Signature of Anthropogenic Nitrogen Deposition to Remote Watersheds of the Northern Hemisphere. Science 334:1545–1548.

Hoover, D. 1998. Nonparametric smoothing estimates of time-varying coefficient models with longitudinal data. Biometrika 85:809–822.

Hrachowitz, M., C. Soulsby, C. Imholt, I. A. Malcolm, and D. Tetzlaff. 2010. Thermal regimes in a large upland salmon river: a simple model to identify the influence of landscape controls and climate change on maximum temperatures. Hydrological Processes 24:3374–3391.

Ingraham, N. L., and B. E. Taylor. 1986. Hydrogen isotope study of large-scale meteoric water transport in Northern California and Nevada. Journal of Hydrology 85:183–197.

Ingraham, N. L., and B. E. Taylor. 1991. Light stable isotope systematics of large-scale hydrologic regimes in California and Nevada. Water Resources Research 27:77–90.

Isaak, D. J., C. H. Luce, G. L. Chandler, D. L. Horan, and S. P. Wollrab. 2018a. Principal components of thermal regimes in mountain river networks. Hydrology and Earth System Sciences 22:6225–6240.

Isaak, D. J., C. H. Luce, D. L. Horan, G. L. Chandler, S. P. Wollrab, W. B. Dubois, and D. E. Nagel. 2020. Thermal Regimes of Perennial Rivers and Streams in the Western United States. JAWRA Journal of the American Water Resources Association 56:842–867.

Isaak, D. J., C. H. Luce, D. L. Horan, G. L. Chandler, S. P. Wollrab, and D. E. Nagel. 2018b. Global Warming of Salmon and Trout Rivers in the Northwestern U.S.: Road to Ruin or Path Through Purgatory? Transactions of the American Fisheries Society 147:566–587.

Isaak, D. J., E. E. Peterson, J. M. Ver Hoef, S. J. Wenger, J. A. Falke, C. E. Torgersen, C. Sowder, E. A. Steel, M.-J. Fortin, C. E. Jordan, A. S. Ruesch, N. Som, and P. Monestiez. 2014. Applications of spatial statistical network models to stream data: Spatial statistical network models for stream data. Wiley Interdisciplinary Reviews: Water 1:277–294.

Isaak, D. J., and B. E. Rieman. 2013. Stream isotherm shifts from climate change and implications for distributions of ectothermic organisms. Global Change Biology 19:742–751.

Isaak, D. J., S. J. Wenger, E. E. Peterson, J. M. Ver Hoef, D. E. Nagel, C. H. Luce, S. W. Hostetler, J. B. Dunham, B. B. Roper, S. P. Wollrab, G. L. Chandler, D. L. Horan, and S. Parkes-Payne. 2017. The NorWeST Summer Stream Temperature Model and Scenarios for the Western U.S.: A Crowd-Sourced Database and New Geospatial Tools Foster a User Community and Predict Broad Climate Warming of Rivers and Streams. Water Resources Research 53:9181–9205.

Isaak, D. J., S. Wollrab, D. Horan, and G. Chandler. 2012. Climate change effects on stream and river temperatures across the northwest U.S. from 1980–2009 and implications for salmonid fishes. Climatic Change 113:499–524.

Isaak, D. J., M. K. Young, C. H. Luce, S. W. Hostetler, S. J. Wenger, E. E. Peterson, J. M. Ver Hoef, M. C. Groce, D. L. Horan, and D. E. Nagel. 2016. Slow climate velocities of mountain streams portend their role as refugia for cold-water biodiversity. Proceedings of the National Academy of Sciences 113:4374–4379.

Jackson, F. L., R. J. Fryer, D. M. Hannah, C. P. Millar, and I. A. Malcolm. 2018. A spatio-temporal statistical model of maximum daily river temperatures to inform the management of Scotland's Atlantic salmon rivers under climate change. Science of The Total Environment 612:1543–1558.

Jaeger, W. K., A. Amos, D. P. Bigelow, H. Chang, D. R. Conklin, R. Haggerty, C. Langpap, K. Moore, P. W. Mote, A. W. Nolin, A. J. Plantinga, C. L. Schwartz, D. Tullos, and D. P.

Turner. 2017. Finding water scarcity amid abundance using human–natural system models. Proceedings of the National Academy of Sciences 114:11884–11889.

Jaeger, W. K., A. J. Plantinga, H. Chang, K. Dello, G. Grant, D. Hulse, J. J. McDonnell, S. Lancaster, H. Moradkhani, A. T. Morzillo, P. Mote, A. Nolin, M. Santelmann, and J. Wu. 2013. Toward a formal definition of water scarcity in natural-human systems: Opinion. Water Resources Research 49:4506–4517.

Jasechko, S., J. W. Kirchner, J. M. Welker, and J. J. McDonnell. 2016. Substantial proportion of global streamflow less than three months old. Nature Geoscience 9:126–129.

Jefferson, A. J. 2011. Seasonal versus transient snow and the elevation dependence of climate sensitivity in maritime mountainous regions. Geophysical Research Letters 38:n/a-n/a.

Jeffres, C. A., J. J. Opperman, and P. B. Moyle. 2008. Ephemeral floodplain habitats provide best growth conditions for juvenile Chinook salmon in a California river. Environmental Biology of Fishes 83:449–458.

Jenicek, M., J. Seibert, M. Zappa, M. Staudinger, and T. Jonas. 2016. Importance of maximum snow accumulation for summer low flows in humid catchments. Hydrology and Earth System Sciences 20:859–874.

Johnson, S. L. 2003. Stream temperature: scaling of observations and issues for modelling. Hydrological Processes 17:497–499.

Johnson, Z. C., B. G. Johnson, M. A. Briggs, C. D. Snyder, N. P. Hitt, and W. D. Devine. 2021. Heed the data gap: Guidelines for using incomplete datasets in annual stream temperature analyses. Ecological Indicators 122:107229.

Johnson, Z. C., C. D. Snyder, and N. P. Hitt. 2017. Landform features and seasonal precipitation predict shallow groundwater influence on temperature in headwater streams. Water Resources Research 53:5788–5812.

Johnson, Z. C., J. J. Warwick, and R. Schumer. 2014. Factors affecting hyporheic and surface transient storage in a western U.S. river. Journal of Hydrology 510:325–339.

Katsuyama, M., T. Yoshioka, and E. Konohira. 2015. Spatial distribution of oxygen-18 and deuterium in stream waters across the Japanese archipelago. Hydrology and Earth System Sciences 19:1577–1588.

Kelleher, C., T. Wagener, M. Gooseff, B. McGlynn, K. McGuire, and L. Marshall. 2012. Investigating controls on the thermal sensitivity of Pennsylvania streams. Hydrological Processes 26:771–785.

Kendall, C., and T. B. Coplen. 2001. Distribution of oxygen-18 and deuterium in river waters across the United States. Hydrological Processes 15:1363–1393.

Kennard, M. J., S. J. Mackay, B. J. Pusey, J. D. Olden, and N. Marsh. 2009. Quantifying uncertainty in estimation of hydrologic metrics for ecohydrological studies. River Research and Applications:n/a-n/a.

Khaliq, M. N., T. B. M. J. Ouarda, P. Gachon, and L. Sushama. 2008. Temporal evolution of low-flow regimes in Canadian rivers. Water Resources Research 44.

Knowles, N., M. D. Dettinger, and D. R. Cayan. 2006. Trends in Snowfall versus Rainfall in the Western United States. Journal of Climate 19:4545–4559.

Koeniger, P., C. Leibundgut, and W. Stichler. 2009. Spatial and temporal characterisation of stable isotopes in river water as indicators of groundwater contribution and confirmation

of modelling results; a study of the Weser river, Germany†. Isotopes in Environmental and Health Studies 45:289–302.

Koffler, D., T. Gauster, and G. Laaha. 2013. lfstat: Calculation of low flow statistics for daily stream flow data.

Konrad, C. P., and M. D. Dettinger. 2017. Flood Runoff in Relation to Water Vapor Transport by Atmospheric Rivers Over the Western United States, 1949–2015. Geophysical Research Letters 44:11,456-11,462.

Kormos, P. R., C. H. Luce, S. J. Wenger, and W. R. Berghuijs. 2016. Trends and sensitivities of low streamflow extremes to discharge timing and magnitude in Pacific Northwest mountain streams. Water Resources Research 52:4990–5007.

Kristensen, K., A. Nielsen, C. W. Berg, H. Skaug, and B. M. Bell. 2016. TMB : Automatic Differentiation and Laplace Approximation. Journal of Statistical Software 70.

Kundzewicz, Z. W., D. Graczyk, T. Maurer, I. Pińskwar, M. Radziejewski, C. Svensson, and M. Szwed. 2005. Trend detection in river flow series: 1. Annual maximum flow / Détection de tendance dans des séries de débit fluvial: 1. Débit maximum annuel. Hydrological Sciences Journal 50:5.

Lance, G. N., and W. T. Williams. 1967. A general theory of classificatory sorting strategies: II. Clustering systems. The Computer Journal 10:271–277.

Lane, B. A., H. E. Dahlke, G. B. Pasternack, and S. Sandoval-Solis. 2017. Revealing the Diversity of Natural Hydrologic Regimes in California with Relevance for Environmental Flows Applications. JAWRA Journal of the American Water Resources Association 53:411–430.

Lane, B. A., S. Sandoval-Solis, E. D. Stein, S. M. Yarnell, G. B. Pasternack, and H. E. Dahlke. 2018. Beyond Metrics? The Role of Hydrologic Baseline Archetypes in Environmental Water Management. Environmental Management 62:678–693.

Leach, J. A., and R. D. Moore. 2019. Empirical Stream Thermal Sensitivities May Underestimate Stream Temperature Response to Climate Warming. Water Resources Research 55:5453–5467.

Lechler, A. R., and N. A. Niemi. 2011. Controls on the Spatial Variability of Modern Meteoric 18O: Empirical Constraints from the Western U.S. and East Asia and Implications for Stable Isotope Studies. American Journal of Science 311:664–700.

Li, H., X. Deng, C. A. Dolloff, and E. P. Smith. 2016. Bivariate functional data clustering: grouping streams based on a varying coefficient model of the stream water and air temperature relationship. Environmetrics 27:15–26.

Li, H., X. Deng, D.-Y. Kim, and E. P. Smith. 2014. Modeling maximum daily temperature using a varying coefficient regression model. Water Resources Research 50:3073–3087.

Li, H., X. Deng, and E. Smith. 2017. Missing data imputation for paired stream and air temperature sensor data: Missing Data Imputation for Stream and Air Temperature. Environmetrics 28:e2426.

Lins, H. F. 2012. USGS Hydro-Climatic Data Network 2009 (HCDN–2009). U.S. Geological Survey Fact Sheet 2012–3047:4.

Lisi, P. J., D. E. Schindler, T. J. Cline, M. D. Scheuerell, and P. B. Walsh. 2015. Watershed geomorphology and snowmelt control stream thermal sensitivity to air temperature. Geophysical Research Letters 42:3380–3388.

Liu, F., M. W. Williams, and N. Caine. 2004. Source waters and flow paths in an alpine catchment, Colorado Front Range, United States. Water Resources Research 40.

Luce, C. H., J. T. Abatzoglou, and Z. A. Holden. 2013. The Missing Mountain Water: Slower Westerlies Decrease Orographic Enhancement in the Pacific Northwest USA. Science 342:1360–1364.

Luce, C. H., and Z. A. Holden. 2009. Declining annual streamflow distributions in the Pacific Northwest United States, 1948–2006. Geophysical Research Letters 36:L16401.

Lucero, Y., E. A. Steel, K. M. Burnett, and K. Christiansen. 2011. Untangling human development and natural gradients: Implications of underlying correlation structure for linking landscapes and riverine ecosystems. River Systems 19:207–224.

Maavara, T., Q. Chen, K. Van Meter, L. E. Brown, J. Zhang, J. Ni, and C. Zarfl. 2020. River dam impacts on biogeochemical cycling. Nature Reviews Earth & Environment 1:103–116.

Macklin, M. G., and J. Lewin. 2019. River stresses in anthropogenic times: Large-scale global patterns and extended environmental timelines. Progress in Physical Geography: Earth and Environment 43:3–23.

Maheu, A., N. L. Poff, and A. St-Hilaire. 2016. A Classification of Stream Water Temperature Regimes in the Conterminous USA: Classification of Stream Temperature Regimes. River Research and Applications 32:896–906.

Mantua, N. J., and S. R. Hare. 2002. The Pacific Decadal Oscillation. Journal of Oceanography 58:35–44.

Mantua, N. J., S. R. Hare, Y. Zhang, J. M. Wallace, and R. C. Francis. 1997. A Pacific Interdecadal Climate Oscillation with Impacts on Salmon Production. Bulletin of the American Meteorological Society 78:1069–1079.

Mantua, N., I. Tohver, and A. Hamlet. 2010. Climate change impacts on streamflow extremes and summertime stream temperature and their possible consequences for freshwater salmon habitat in Washington State. Climatic Change 102:187–223.

Marshall, A. M., J. T. Abatzoglou, T. E. Link, and C. J. Tennant. 2019. Projected Changes in Interannual Variability of Peak Snowpack Amount and Timing in the Western United States. Geophysical Research Letters 46:8882–8892.

Mauger, S., R. Shaftel, J. C. Leppi, and D. J. Rinella. 2017. Summer temperature regimes in southcentral Alaska streams: watershed drivers of variation and potential implications for Pacific salmon. Canadian Journal of Fisheries and Aquatic Sciences 74:702–715.

Mayer, T. D. 2012. Controls of summer stream temperature in the Pacific Northwest. Journal of Hydrology 475:323–335.

Mayer, T. D., and S. W. Naman. 2011. Streamflow Response to Climate as Influenced by Geology and Elevation1: Streamflow Response to Climate as Influenced by Geology and Elevation. JAWRA Journal of the American Water Resources Association 47:724–738.

Mbengue, C., and T. Schneider. 2013. Storm Track Shifts under Climate Change: What Can Be Learned from Large-Scale Dry Dynamics. Journal of Climate 26:9923–9930.

Mbengue, C., and T. Schneider. 2017. Storm-Track Shifts under Climate Change: Toward a Mechanistic Understanding Using Baroclinic Mean Available Potential Energy. Journal of the Atmospheric Sciences 74:93–110.

McCabe, G. J., and M. D. Dettinger. 2002. Primary Modes and Predictability of Year-to-Year Snowpack Variations in the Western United States from Teleconnections with Pacific Ocean Climate. Journal of Hydrometeorology 3:13–25.

McCabe, G. J., and D. M. Wolock. 2011. Independent effects of temperature and precipitation on modeled runoff in the conterminous United States. Water Resources Research 47.

McCabe-Glynn, S., K. R. Johnson, C. Strong, Y. Zou, J.-Y. Yu, S. Sellars, and J. M. Welker. 2016. Isotopic signature of extreme precipitation events in the western U.S. and associated phases of Arctic and tropical climate modes. Journal of Geophysical Research: Atmospheres 121:8913–8924.

McGill, L. M., J. R. Brooks, and E. A. Steel. 2021. Spatiotemporal dynamics of water sources in a mountain river basin inferred through $\Delta^2 H$ and $\Delta^{18} O$ of water. Hydrological Processes 35.

McGill, L. M., E. A. Steel, J. R. Brooks, R. T. Edwards, and A. H. Fullerton. 2020. Elevation and spatial structure explain most surface-water isotopic variation across five Pacific Coast basins. Journal of Hydrology 583:124610.

McGuire, K. J., and J. J. McDonnell. 2006. A review and evaluation of catchment transit time modeling. Journal of Hydrology 330:543–563.

McGuire, K. J., J. J. McDonnell, M. Weiler, C. Kendall, B. L. McGlynn, J. M. Welker, and J. Seibert. 2005. The role of topography on catchment-scale water residence time. Water Resources Research 41.

McGuire, K. J., C. E. Torgersen, G. E. Likens, D. C. Buso, W. H. Lowe, and S. W. Bailey. 2014. Network analysis reveals multiscale controls on streamwater chemistry. Proceedings of the National Academy of Sciences 111:7030–7035.

McMahon, K. W., L. L. Hamady, and S. R. Thorrold. 2013. A review of ecogeochemistry approaches to estimating movements of marine animals. Limnology and Oceanography 58:697–714.

Menberg, K., P. Blum, B. L. Kurylyk, and P. Bayer. 2014. Observed groundwater temperature response to recent climate change. Hydrology and Earth System Sciences 18:4453–4466.

Menne, M. J., I. Durre, R. S. Vose, B. E. Gleason, and T. G. Houston. 2012. An Overview of the Global Historical Climatology Network-Daily Database. Journal of Atmospheric and Oceanic Technology 29:897–910.

Milly, P. C. D., J. Betancourt, M. Falkenmark, R. M. Hirsch, Z. W. Kundzewicz, D. P. Lettenmaier, and R. J. Stouffer. 2008. Stationarity Is Dead: Whither Water Management? Science 319:573–574.

Mohseni, O., T. R. Erickson, and H. G. Stefan. 1999. Sensitivity of stream temperatures in the United States to air temperatures projected under a global warming scenario. Water Resources Research 35:3723–3733.

Mohseni, O., and H. G. Stefan. 1999. Stream temperature/air temperature relationship: a physical interpretation. Journal of Hydrology 218:128–141.

Mohseni, O., H. G. Stefan, and T. R. Erickson. 1998. A nonlinear regression model for weekly stream temperatures. Water Resources Research 34:2685–2692.

Molotch, N. P., and R. C. Bales. 2006. SNOTEL representativeness in the Rio Grande headwaters on the basis of physiographics and remotely sensed snow cover persistence. Hydrological Processes 20:723–739.

Montgomery Water Group. 2003. Wenatchee River Basin Watershed Assessment.

Moran, T. A., S. J. Marshall, E. C. Evans, and K. E. Sinclair. 2007. Altitudinal Gradients of Stable Isotopes in Lee-Slope Precipitation in the Canadian Rocky Mountains. Arctic, Antarctic, and Alpine Research 39:455–467.

Mote, P. W. 2003. Trends in snow water equivalent in the Pacific Northwest and their climatic causes. Geophysical Research Letters 30.

Mote, P. W., and E. P. Salathé. 2010. Future climate in the Pacific Northwest. Climatic Change 102:29–50.

Mountain, N., A. L. James, and K. Chutko. 2015. Groundwater and surface water influences on streamflow in a mesoscale Precambrian Shield catchment: Analysing Summer Sources of Streamflow Using Stable Water Isoscapes. Hydrological Processes 29:3941–3953.

Murray, K., and M. M. Conner. 2009. Methods to quantify variable importance: implications for the analysis of noisy ecological data. Ecology 90:348–355.

Musselman, K. N., N. Addor, J. A. Vano, and N. P. Molotch. 2021. Winter melt trends portend widespread declines in snow water resources. Nature Climate Change 11:418–424.

Nash, L. L., and P. H. Gleick. 1991. Sensitivity of streamflow in the Colorado Basin to climatic changes. Journal of Hydrology 125:221–241.

Neff, B. P., D. O. Rosenberry, S. G. Leibowitz, D. M. Mushet, H. E. Golden, M. C. Rains, J. R. Brooks, and C. R. Lane. 2019. A Hydrologic Landscapes Perspective on Groundwater Connectivity of Depressional Wetlands. Water 12:50.

Neiman, P. J., L. J. Schick, F. M. Ralph, M. Hughes, and G. A. Wick. 2011. Flooding in Western Washington: The Connection to Atmospheric Rivers*. Journal of Hydrometeorology 12:1337–1358.

Nelson, L. M. 1971. Sediment transport by streams in the Snohomish River basin, Washington: October 1967-June1969.

Nickolas, L. B., C. Segura, and J. R. Brooks. 2017. The influence of lithology on surface water sources. Hydrological Processes 31:1913–1925.

Nolin, A. W., and C. Daly. 2006. Mapping "At Risk" Snow in the Pacific Northwest. Journal of Hydrometeorology 7:1164–1171.

Nolin, A. W., J. Phillippe, A. Jefferson, and S. L. Lewis. 2010. Present-day and future contributions of glacier runoff to summertime flows in a Pacific Northwest watershed: Implications for water resources. Water Resources Research 46.

O'Driscoll, M. A., and D. R. DeWalle. 2006. Stream–air temperature relations to classify stream–ground water interactions in a karst setting, central Pennsylvania, USA. Journal of Hydrology 329:140–153.

Olden, J. D., M. J. Kennard, and B. J. Pusey. 2012. A framework for hydrologic classification with a review of methodologies and applications in ecohydrology. Ecohydrology 5:503–518.

Olden, J. D., J. J. Lawler, and N. L. Poff. 2008. Machine Learning Methods Without Tears: A Primer for Ecologists. The Quarterly Review of Biology 83:171–193.

Olden, J. D., and N. L. Poff. 2003. Redundancy and the choice of hydrologic indices for characterizing streamflow regimes. River Research and Applications 19:101–121.

Orth, R., and G. Destouni. 2018. Drought reduces blue-water fluxes more strongly than green-water fluxes in Europe. Nature Communications 9:3602.

Ouellet, V., A. St-Hilaire, S. J. Dugdale, D. M. Hannah, S. Krause, and S. Proulx-Ouellet. 2020. River temperature research and practice: Recent challenges and emerging opportunities

for managing thermal habitat conditions in stream ecosystems. Science of The Total Environment 736:139679.

Paine, L. 2019. River Cultures in World History—Rescuing a Neglected Resource. Fudan Journal of the Humanities and Social Sciences 12:457–472.

Parkinson, E. A., E. V. Lea, M. A. Nelitz, J. M. Knudson, and R. D. Moore. 2016. Identifying Temperature Thresholds Associated with Fish Community Changes in British Columbia, Canada, to Support Identification of Temperature Sensitive Streams. River Research and Applications 32:330–347.

Patterson, N. K., B. A. Lane, S. Sandoval-Solis, G. B. Pasternack, S. M. Yarnell, and Y. Qiu. 2020. A hydrologic feature detection algorithm to quantify seasonal components of flow regimes. Journal of Hydrology 585:124787.

Patton, N. R., K. A. Lohse, S. E. Godsey, B. T. Crosby, and M. S. Seyfried. 2018. Predicting soil thickness on soil mantled hillslopes. Nature Communications 9:3329.

Payn, R. A., M. N. Gooseff, B. L. McGlynn, K. E. Bencala, and S. M. Wondzell. 2012. Exploring changes in the spatial distribution of stream baseflow generation during a seasonal recession. Water Resources Research 48.

Peng, T.-R., K.-Y. Chen, W.-J. Zhan, W.-C. Lu, and L.-T. J. Tong. 2015. Use of stable water isotopes to identify hydrological processes of meteoric water in montane catchments: Stable Isotopic Identifying Hydrological Process in Montane Catchments. Hydrological Processes 29:4957–4967.

Peralta-Tapia, A., R. A. Sponseller, D. Tetzlaff, C. Soulsby, and H. Laudon. 2015. Connecting precipitation inputs and soil flow pathways to stream water in contrasting boreal

catchments: CONNECTING PRECIPITATION AND SOIL TO STREAM WATER IN BOREAL CATCHMENTS. Hydrological Processes 29:3546–3555.

Peterson, E. E., and J. M. Ver Hoef. 2010. A mixed-model moving-average approach to geostatistical modeling in stream networks. Ecology 91:644–651.

Peterson, E. E., and J. M. Ver Hoef. 2014. STARS : An *ArcGIS* Toolset Used to Calculate the Spatial Information Needed to Fit Spatial Statistical Models to Stream Network Data. Journal of Statistical Software 56.

Piechota, T. C., J. A. Dracup, and R. G. Fovell. 1997. Western US streamflow and atmospheric circulation patterns during El Niño-Southern Oscillation. Journal of Hydrology 201:249–271.

Pierce, D. W., T. P. Barnett, H. G. Hidalgo, T. Das, C. Bonfils, B. D. Santer, G. Bala, M. D. Dettinger, D. R. Cayan, A. Mirin, A. W. Wood, and T. Nozawa. 2008. Attribution of Declining Western U.S. Snowpack to Human Effects. Journal of Climate 21:6425–6444.

Pierce, D. W., and D. R. Cayan. 2013. The Uneven Response of Different Snow Measures to Human-Induced Climate Warming. Journal of Climate 26:4148–4167.

Poage, M., and C. Chamberlain. 2002. Empirical relationships between elevation and the stable isotope composition of precipitation and surface waters: Considerations for studies of paleoevlevation change. American Journal of Science 301:1–15.

Poff, N. L., J. D. Allan, M. B. Bain, J. R. Karr, K. L. Prestegaard, B. D. Richter, R. E. Sparks, and J. C. Stromberg. 1997. The Natural Flow Regime. BioScience 47:769–784.

Pollock, M. M., T. J. Beechie, J. M. Wheaton, C. E. Jordan, N. Bouwes, N. Weber, and C. Volk. 2014. Using Beaver Dams to Restore Incised Stream Ecosystems. BioScience 64:279–290.

Pournasiri Poshtiri, M., I. Pal, U. Lall, P. Naveau, and E. Towler. 2019. Variability patterns of the annual frequency and timing of low streamflow days across the United States and their linkage to regional and large-scale climate. Hydrological Processes 33:1569–1578.

Pyne, M. I., and N. L. Poff. 2017. Vulnerability of stream community composition and function to projected thermal warming and hydrologic change across ecoregions in the western United States. Global Change Biology 23:77–93.

Quinn, T. P., and D. J. Adams. 1996. Environmental Changes Affecting the Migratory Timing of American Shad and Sockeye Salmon. Ecology 77:1151–1162.

R Core Team. 2020. R: A Language and Environment for Statistical Computing. R Foundation for Statistical Computing, Vienna, Austria.

Ralph, F. M., T. Coleman, P. J. Neiman, R. J. Zamora, and M. D. Dettinger. 2013. Observed Impacts of Duration and Seasonality of Atmospheric-River Landfalls on Soil Moisture and Runoff in Coastal Northern California. Journal of Hydrometeorology 14:443–459.

Rautio, A., and K. Korkka-Niemi. 2015. Chemical and isotopic tracers indicating groundwater/surface-water interaction within a boreal lake catchment in Finland. Hydrogeology Journal 23:687–705.

Regonda, S. K., B. Rajagopalan, M. Clark, and J. Pitlick. 2005. Seasonal Cycle Shifts in Hydroclimatology over the Western United States. Journal of Climate 18:372–384.

Reidy Liermann, C. A., J. D. Olden, T. J. Beechie, M. J. Kennard, P. B. Skidmore, C. P. Konrad, and H. Imaki. 2012. Hydrogeomorphic classification of Washington state rivers to support emerging environmental flow management strategies. River Research and Applications 28:1340–1358.

Riedel, J. L., and M. A. Larrabee. 2016. Impact of Recent Glacial Recession on Summer Streamflow in the Skagit River. Northwest Science 90:5–22.

Rock, L., and B. Mayer. 2007. Isotope hydrology of the Oldman River basin, southern Alberta, Canada. Hydrological Processes 21:3301–3315.

Roderick, M. L., F. Sun, W. H. Lim, and G. D. Farquhar. 2013. A general framework for understanding the response of the water cycle to global warming over land and ocean. preprint, Global hydrology/Theory development.

Rodgers, P., C. Soulsby, and S. Waldron. 2005. Stable isotope tracers as diagnostic tools in upscaling flow path understanding and residence time estimates in a mountainous mesoscale catchment. Hydrological Processes 19:2291–2307.

Ruhi, A., X. Dong, C. H. McDaniel, D. P. Batzer, and J. L. Sabo. 2018a. Detrimental effects of a novel flow regime on the functional trajectory of an aquatic invertebrate metacommunity. Global Change Biology 24:3749–3765.

Ruhi, A., M. L. Messager, and J. D. Olden. 2018b. Tracking the pulse of the Earth's fresh waters. Nature Sustainability 1:198–203.

Rutz, J. J., W. J. Steenburgh, and F. M. Ralph. 2014. Climatological Characteristics of Atmospheric Rivers and Their Inland Penetration over the Western United States. Monthly Weather Review 142:905–921.

S Chegwidden, O., D. E. Rupp, and B. Nijssen. 2020. Climate change alters flood magnitudes and mechanisms in climatically-diverse headwaters across the northwestern United States. Environmental Research Letters 15:094048.

Safeeq, M., G. E. Grant, S. L. Lewis, M. G. Kramer, and B. Staab. 2014. A hydrogeologic framework for characterizing summer streamflow sensitivity to climate warming in the Pacific Northwest, USA. Hydrology and Earth System Sciences 18:3693–3710.

Safeeq, M., G. E. Grant, S. L. Lewis, and Christina. L. Tague. 2013. Coupling snowpack and groundwater dynamics to interpret historical streamflow trends in the western United States. Hydrological Processes 27:655–668.

Safeeq, M., S. Shukla, I. Arismendi, G. E. Grant, S. L. Lewis, and A. Nolin. 2016. Influence of winter season climate variability on snow-precipitation ratio in the western United States: Influence of winter season climate variability on snow-fraction. International Journal of Climatology 36:3175–3190.

Salathé, E. P. 2006. Influences of a shift in North Pacific storm tracks on western North American precipitation under global warming. Geophysical Research Letters 33:L19820.

Savoy, P., A. P. Appling, J. B. Heffernan, E. G. Stets, J. S. Read, J. W. Harvey, and E. S. Bernhardt. 2019. Metabolic rhythms in flowing waters: An approach for classifying river productivity regimes. Limnology and Oceanography 64:1835–1851.

Scheihing, K., C. Moya, U. Struck, E. Lictevout, and U. Tröger. 2017. Reassessing Hydrological Processes That Control Stable Isotope Tracers in Groundwater of the Atacama Desert (Northern Chile). Hydrology 5:3.

Schnorbus, M., A. Werner, and K. Bennett. 2014. Impacts of climate change in three hydrologic regimes in British Columbia, Canada. Hydrological Processes 28:1170–1189.

Segura, C., D. Noone, D. Warren, J. A. Jones, J. Tenny, and L. M. Ganio. 2019. Climate, Landforms, and Geology Affect Baseflow Sources in a Mountain Catchment. Water Resources Research 55:5238–5254.

Seneviratne, S. I., T. Corti, E. L. Davin, M. Hirschi, E. B. Jaeger, I. Lehner, B. Orlowsky, and A. J. Teuling. 2010. Investigating soil moisture–climate interactions in a changing climate: A review. Earth-Science Reviews 99:125–161.

Shrestha, R. R., M. A. Schnorbus, A. T. Werner, and A. J. Berland. 2012. Modelling spatial and temporal variability of hydrologic impacts of climate change in the Fraser River basin, British Columbia, Canada. Hydrological Processes 26:1840–1860.

Siler, N., G. Roe, and D. Durran. 2013. On the Dynamical Causes of Variability in the Rain-Shadow Effect: A Case Study of the Washington Cascades. Journal of Hydrometeorology 14:122–139.

Singh, N. K., R. E. Emanuel, and B. L. McGlynn. 2016. Variability in isotopic composition of base flow in two headwater streams of the southern Appalachians: ISOTOPIC VARIABILITY OF BASE FLOW IN HEADWATER STREAMS. Water Resources Research 52:4264–4279.

Smakhtin, V. U. 2001. Low flow hydrology: a review. Journal of Hydrology 240:147–186.

Snyder, C. D., N. P. Hitt, and J. A. Young. 2015. Accounting for groundwater in stream fish thermal habitat responses to climate change. Ecological Applications 25:1397–1419.

Snyder, M. N., N. H. Schumaker, J. B. Dunham, M. L. Keefer, P. Leinenbach, A. Brookes, J. Palmer, J. Wu, D. Keenan, and J. L. Ebersole. 2020. Assessing contributions of cold-water refuges to reproductive migration corridor conditions for adult salmon and steelhead trout in the Columbia River, USA. Journal of Ecohydraulics:1–13.

Soulsby, C., P. J. Rodgers, J. Petry, D. M. Hannah, I. A. Malcolm, and S. M. Dunn. 2004. Using tracers to upscale flow path understanding in mesoscale mountainous catchments: two examples from Scotland. Journal of Hydrology 291:174–196.

Sprenger, M., D. Tetzlaff, C. Tunaley, J. Dick, and C. Soulsby. 2017. Evaporation fractionation in a peatland drainage network affects stream water isotope composition. Water Resources Research 53:851–866.

St. Jacques, J.-M., D. J. Sauchyn, and Y. Zhao. 2010. Northern Rocky Mountain streamflow records: Global warming trends, human impacts or natural variability?. Geophysical Research Letters 37:n/a-n/a.

Steel, A. E., C. Sowder, and E. E. Peterson. 2016. Spatial and Temporal Variation of Water Temperature Regimes on the Snoqualmie River Network. Journal of the American Water Resources Association 52:769–787.

Steel, E. A., T. J. Beechie, C. E. Torgersen, and A. H. Fullerton. 2017. Envisioning, Quantifying, and Managing Thermal Regimes on River Networks. BioScience 67:506–522.

Steel, E. A., A. Marsha, A. H. Fullerton, J. D. Olden, N. K. Larkin, S.-Y. Lee, and A. Ferguson. 2019. Thermal landscapes in a changing climate: biological implications of water temperature patterns in an extreme year. Canadian Journal of Fisheries and Aquatic Sciences 76:1740–1756.

Steel, E. A., A. Tillotson, D. A. Larsen, A. H. Fullerton, K. P. Denton, and B. R. Beckman. 2012. Beyond the mean: The role of variability in predicting ecological effects of stream temperature on salmon. Ecosphere 3:art104.

Stefan, H. G., and B. A. Sinokrot. 1993. Projected global climate change impact on water temperatures in five north central U.S. streams. Climatic Change 24:353–381.

Stewart, I. T., D. R. Cayan, and M. D. Dettinger. 2005. Changes toward Earlier Streamflow Timing across Western North America. Journal of Climate 18:1136–1155.

Strayer, D. L., and D. Dudgeon. 2010. Freshwater biodiversity conservation: recent progress and future challenges. Journal of the North American Benthological Society 29:344–358.

Swain, D. L., B. Langenbrunner, J. D. Neelin, and A. Hall. 2018. Increasing precipitation volatility in twenty-first-century California. Nature Climate Change 8:427–433.

Tabor, R. W., V. A. Frizzell, D. B. Booth, R. B. Waitt, J. T. Whetten, and R. E. Zartman. 1993. Geologic map of the Skykomish River 30- by 60-minute quadrangle, Washington. Page 42. U.S. Geological Survey Miscellaneous Investigations Series Map.

Tague, C., M. Farrell, G. Grant, S. Lewis, and S. Rey. 2007. Hydrogeologic controls on summer stream temperatures in the McKenzie River basin, Oregon. Hydrological Processes 21:3288–3300.

Tague, C., and G. E. Grant. 2004. A geological framework for interpreting the low-flow regimes of Cascade streams, Willamette River Basin, Oregon. Water Resources Research 40.

Tague, C., and G. E. Grant. 2009. Groundwater dynamics mediate low-flow response to global warming in snow-dominated alpine regions. Water Resources Research 45.

Tague, C., G. Grant, M. Farrell, J. Choate, and A. Jefferson. 2008. Deep groundwater mediates streamflow response to climate warming in the Oregon Cascades. Climatic Change 86:189–210.

Tague, C. L., J. S. Choate, and G. Grant. 2013. Parameterizing sub-surface drainage with geology to improve modeling streamflow responses to climate in data limited environments. Hydrology and Earth System Sciences 17:341–354.

Tetzlaff, D., J. Buttle, S. K. Carey, M. H. J. van Huijgevoort, H. Laudon, J. P. McNamara, C. P. J. Mitchell, C. Spence, R. S. Gabor, and C. Soulsby. 2015. A preliminary assessment of

water partitioning and ecohydrological coupling in northern headwaters using stable isotopes and conceptual runoff models. Hydrological Processes 29:5153–5173.

Therneau, T., and B. Atkinson. 2019. rpart: Recursive Partitioning and Regression Trees.

Thornton, M.M., Shrestha, R., Wei, Y., Thornton, P.E., Kao, S., and Wilson, B.E. 2020. DaymetDaymet: Daily Surface Weather Data on a 1-km Grid for North America, Version 4:0 MB.

Trinh, D. A., M. T. N. Luu, and Q. T. P. Le. 2017. Use of stable isotopes to understand run-off generation processes in the Red River Delta. Hydrological Processes 31:3827–3843.

Turney, G. L., S. C. Kahle, and N. P. Dion. 1995. Geohydrology and ground-water quality of east King County, Washington. Water Resources Investigations Report, Prepared in cooperation with Seattle-King County Department of Health Tacoma, Washington, Washington, D. C.

Vachon, R. W., J. M. Welker, J. W. C. White, and B. H. Vaughn. 2010. Monthly precipitation isoscapes (δ^{18} O) of the United States: Connections with surface temperatures, moisture source conditions, and air mass trajectories. Journal of Geophysical Research 115.

Van Loon, A. F. 2015. Hydrological drought explained. WIREs Water 2:359–392.

Vano, J. A., B. Nijssen, and D. P. Lettenmaier. 2015. Seasonal hydrologic responses to climate change in the Pacific Northwest. Water Resources Research 51:1959–1976.

Vano, J. A., N. Voisin, L. Cuo, A. F. Hamlet, M. M. Elsner, R. N. Palmer, A. Polebitski, and D. P. Lettenmaier. 2010. Climate change impacts on water management in the Puget Sound region, Washington State, USA. Climatic Change 102:261–286.

Ver Hoef, J. M., and E. E. Peterson. 2010. A Moving Average Approach for Spatial Statistical Models of Stream Networks. Journal of the American Statistical Association 105:6–18.

Ver Hoef, J. M., E. E. Peterson, D. Clifford, and R. Shah. 2014. **SSN** : An *R* Package for Spatial Statistical Modeling on Stream Networks. Journal of Statistical Software 56.

Ver Hoef, J. M., E. Peterson, and D. Theobald. 2006. Spatial statistical models that use flow and stream distance. Environmental and Ecological Statistics 13:449–464.

Vespasiano, G., C. Apollaro, R. De Rosa, F. Muto, S. Larosa, J. Fiebig, A. Mulch, and L. Marini. 2015. The Small Spring Method (SSM) for the definition of stable isotope–elevation relationships in Northern Calabria (Southern Italy). Applied Geochemistry 63:333–346.

van Vliet, M. T. H., W. H. P. Franssen, J. R. Yearsley, F. Ludwig, I. Haddeland, D. P. Lettenmaier, and P. Kabat. 2013. Global river discharge and water temperature under climate change. Global Environmental Change 23:450–464.

Vörösmarty, C. J., P. B. McIntyre, M. O. Gessner, D. Dudgeon, A. Prusevich, P. Green, S. Glidden, S. E. Bunn, C. A. Sullivan, C. R. Liermann, and P. M. Davies. 2010. Global threats to human water security and river biodiversity. Nature 467:555–561.

Walsh, C., and R. Mac Nally. 2013. hier.part: hierarchial partitioning.

Wang, N., S. Zhang, J. He, J. Pu, X. Wu, and X. Jiang. 2009. Tracing the major source area of the mountainous runoff generation of the Heihe River in northwest China using stable isotope technique. Science Bulletin 54:2751–2757.

Ward, J. V., G. Bretschko, M. Brunke, D. Danielopol, J. Gibert, T. Gonser, and A. G. Hildrew. 1998. The boundaries of river systems: the metazoan perspective. Freshwater Biology 40:531–569.

Ward, J. V., and J. A. Stanford. 1995. Ecological connectivity in alluvial river ecosystems and its disruption by flow regulation. Regulated Rivers: Research & Management 11:105–119.

Wassenaar, L. I., P. Athanasopoulos, and M. J. Hendry. 2011. Isotope hydrology of precipitation, surface and ground waters in the Okanagan Valley, British Columbia, Canada. Journal of Hydrology 411:37–48.

Wassenaar, L. I., S. L. Van Wilgenburg, K. Larson, and K. A. Hobson. 2009. A groundwater isoscape (δD, δ18O) for Mexico. Journal of Geochemical Exploration 102:123–136.

Webb, B. W., D. M. Hannah, R. D. Moore, L. E. Brown, and F. Nobilis. 2008. Recent advances in stream and river temperature research. Hydrological Processes 22:902–918.

Webb, B. W., and F. Nobilis. 2007. Long-term changes in river temperature and the influence of climatic and hydrological factors. Hydrological Sciences Journal 52:74–85.

Webb, B. W., and Y. Zhang. 1997. Spatial and seasonal variability in the components of the river heat budget. Hydrological Processes 11:79–101.

Wenger, S. J., C. H. Luce, A. F. Hamlet, D. J. Isaak, and H. M. Neville. 2010. Macroscale hydrologic modeling of ecologically relevant flow metrics. Water Resources Research 46.

West, J. B., editor. 2010. Isoscapes: understanding movement, pattern, and process on earth through isotope mapping. Springer, Dordrecht ; New York.

Whitfield, P. H., and A. J. Cannon. 2000. Recent Variations in Climate and Hydrology in Canada. Canadian Water Resources Journal 25:19–65.

Wigington, P. J., S. G. Leibowitz, R. L. Comeleo, and J. L. Ebersole. 2013. Oregon Hydrologic Landscapes: A Classification Framework. JAWRA Journal of the American Water Resources Association 49:163–182.

Wilcox, R. 1998. A Note on the Theil-Sen Regression Estimator When the Regressor Is Random and the Error Term Is Heteroscedastic. Biometrical Journal 40:261–268.

Wildrick, L. 1979. Ground Water Flow System of the Chumstick Drainage Basin. Page 5. Washington State Department of Ecology, Olympia, WA.

Williams, A. P., R. Seager, J. T. Abatzoglou, B. I. Cook, J. E. Smerdon, and E. R. Cook. 2015. Contribution of anthropogenic warming to California drought during 2012–2014. Geophysical Research Letters 42:6819–6828.

Winfree, M. M., E. Hood, S. L. Stuefer, D. E. Schindler, T. J. Cline, C. D. Arp, and S. Pyare. 2018. Landcover and geomorphology influence streamwater temperature sensitivity in salmon bearing watersheds in Southeast Alaska. Environmental Research Letters 13:064034.

Wolock, D. M., T. C. Winter, and G. McMahon. 2004. Delineation and Evaluation of Hydrologic-Landscape Regions in the United States Using Geographic Information System Tools and Multivariate Statistical Analyses. Environmental Management 34:S71–S88.

Wondzell, S. M., M. Diabat, and R. Haggerty. 2019. What Matters Most: Are Future Stream Temperatures More Sensitive to Changing Air Temperatures, Discharge, or Riparian Vegetation? JAWRA Journal of the American Water Resources Association 55:116–132.

Woodhouse, C. A., G. T. Pederson, K. Morino, S. A. McAfee, and G. J. McCabe. 2016. Increasing influence of air temperature on upper Colorado River streamflow. Geophysical Research Letters 43:2174–2181.

Wrzesien, M. L., and T. M. Pavelsky. 2020. Projected Changes to Extreme Runoff and Precipitation Events From a Downscaled Simulation Over the Western United States. Frontiers in Earth Science 7:355.

Wu, H., J. S. Kimball, M. M. Elsner, N. Mantua, R. F. Adler, and J. Stanford. 2012. Projected climate change impacts on the hydrology and temperature of Pacific Northwest rivers. Water Resources Research 48.

Yan, H., N. Sun, A. Fullerton, and M. Baerwalde. 2021. Greater vulnerability of snowmelt-fed river thermal regimes to a warming climate. Environmental Research Letters 16:054006.

Yeh, H.-F., H.-I. Lin, C.-H. Lee, K.-C. Hsu, and C.-S. Wu. 2014. Identifying Seasonal Groundwater Recharge Using Environmental Stable Isotopes. Water 6:2849–2861.

Yonge, C. J., L. Goldenberg, and H. R. Krouse. 1989. An isotope study of water bodies along a traverse of southwestern Canada. Journal of Hydrology 106:245–255.

Yoshimura, K., M. Kanamitsu, and M. Dettinger. 2010. Regional downscaling for stable water isotopes: A case study of an atmospheric river event. Journal of Geophysical Research 115:D18114.

Yount, J. C., and H. D. Gower. 1991. Bedrock geologic map of the Seattle 30- by 60-minute quadrangle, Washington. Page 37. U.S. Geological Survey Open-File Report.

Zaherpour, J., S. N. Gosling, N. Mount, H. M. Schmied, T. I. E. Veldkamp, R. Dankers, S. Eisner, D. Gerten, L. Gudmundsson, I. Haddeland, N. Hanasaki, H. Kim, G. Leng, J. Liu, Y. Masaki, T. Oki, Y. Pokhrel, Y. Satoh, J. Schewe, and Y. Wada. 2018. Worldwide evaluation of mean and extreme runoff from six global-scale hydrological models that account for human impacts. Environmental Research Letters 13:065015.

Zhang, X., K. D. Harvey, W. D. Hogg, and T. R. Yuzyk. 2001. Trends in Canadian streamflow. Water Resources Research 37:987–998.

Zimmerman, D. L., and J. M. Ver Hoef. 2017. The Torgegram for Fluvial Variography: Characterizing Spatial Dependence on Stream Networks. Journal of Computational and Graphical Statistics 26:253–264.

Zuur, A. F., R. J. Fryer, I. T. Jolliffe, R. Dekker, and J. J. Beukema. 2003. Estimating common trends in multivariate time series using dynamic factor analysis. Environmetrics 14:665–685.

CHAPTER 3 APPENDIX

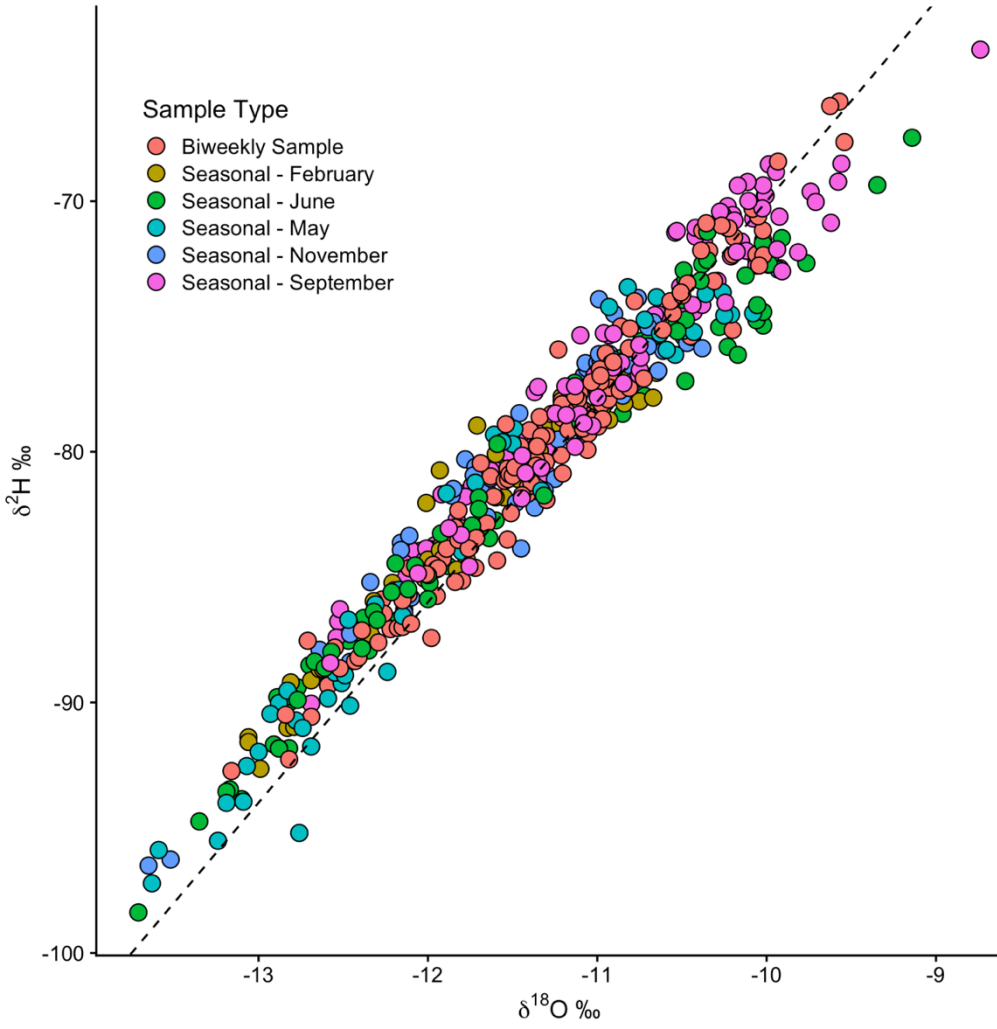

Figure S3.low1. The relationship between $\delta^{18}O$ and $\delta^{2}H$ for all water samples, identified by season. The solid line is the global meteoric water line (GMWL, $\delta^{2}H = \delta^{18}O * 8 + 10$). Eight seasonal samples and six biweekly samples were removed from analyses due to d-excess values less than 5.

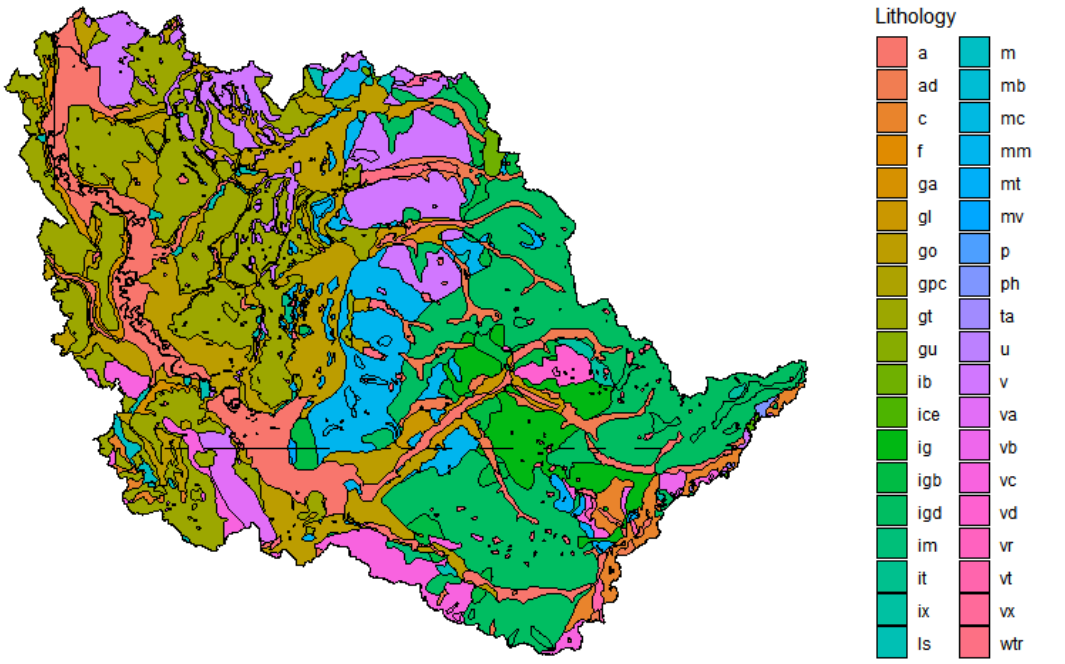

Figure S3.2. Detailed lithology of the Snoqualmie River basin. Descriptions of each lithology code are below.
a – alluvium
ad –alpine glacial drift, Fraser-age
c – continental sedimentary deposits or rocks
f – artificial fill, including modified land
ga – advance continental glacial outwash, Fraser-age
gl – glaciolacustrine deposits, Fraser-age
go – continental glacial outwash, Fraser-age
gpc – continental glacial drift, pre-Fraser, and nonglacial deposits
gt – continental glacial drift, Fraser-age
gu – glacial drift, undivided
ib – basic intrusive rocks
ice – ice
ig – granite
igb – gabbro
igd – granodiorite
im – monozonite
it – tonalite
ix – intrusive breccia
ls – mass wasting deposits
m – marine sedimentary rocks
mb – marble
mc – metasedimentary rocks, cherty
mm – marine metasedimentary rocks
mt – metasedimentary and metavolcanic rocks
mv – metavolcanic rocks

p – peat deposits
ph – phyllite, low grade
ta – talus deposits
u – ultrabasic rocks
v – volcanic rocks
va – andesite flows
vb – basalt flows
vc – volcaniclastic deposits or rocks
vd – dacite flows
vr – rhyolite flows
vt – tuffs and tuff breccias
vx – volcanic breccia
wtr – water

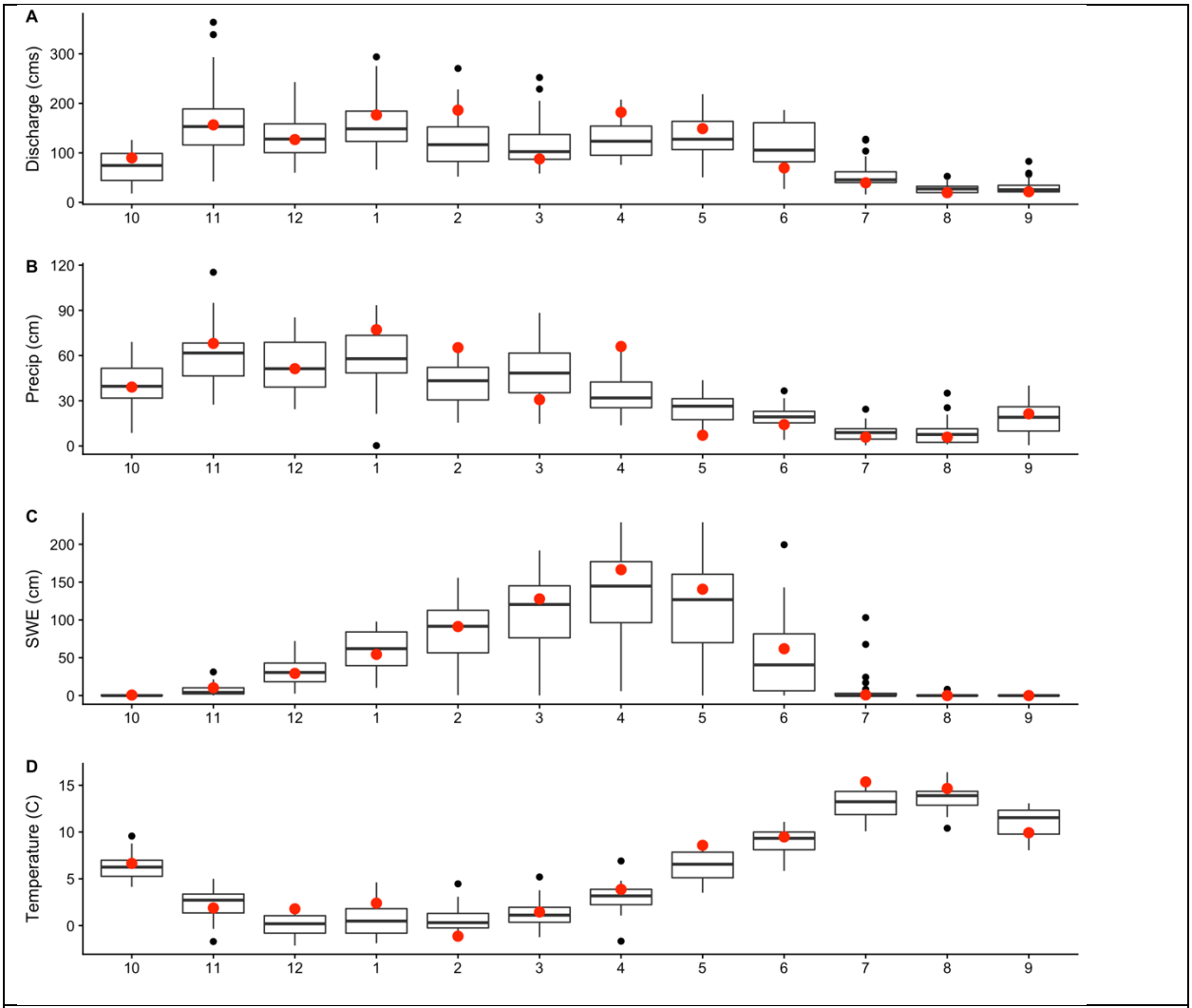

Figure S3.3. A comparison of the 2018 water year monthly average temperature, precipitation, and SWE at SNOTEL site 908, and monthly average discharge from USGS gage 12149000, to monthly averages of these climate metrics from the previous 30 years (1988-2018). For most climate metrics, the WY 2018 values fall within the interquartile range, and for all climate metrics and all months the WY 2018 values fall within the historical range. The most anomalous months were February and April, which were wetter than average with subsequently higher discharge.

CHAPTER 4 APPENDIX

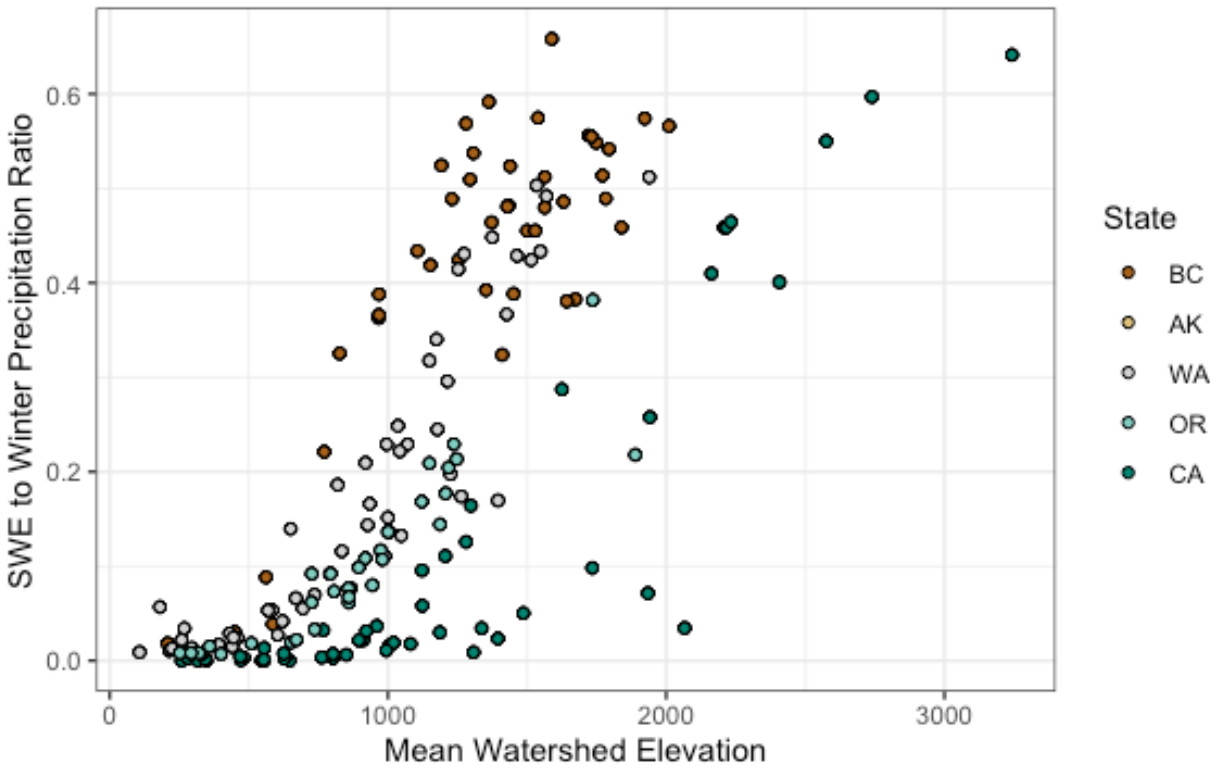

Figure S4.1. Mean watershed elevation vs. average SWE to winter precipitation ratios for each basin. Note that interannual variability in SWE to winter Precipitation ratios can be substantial.

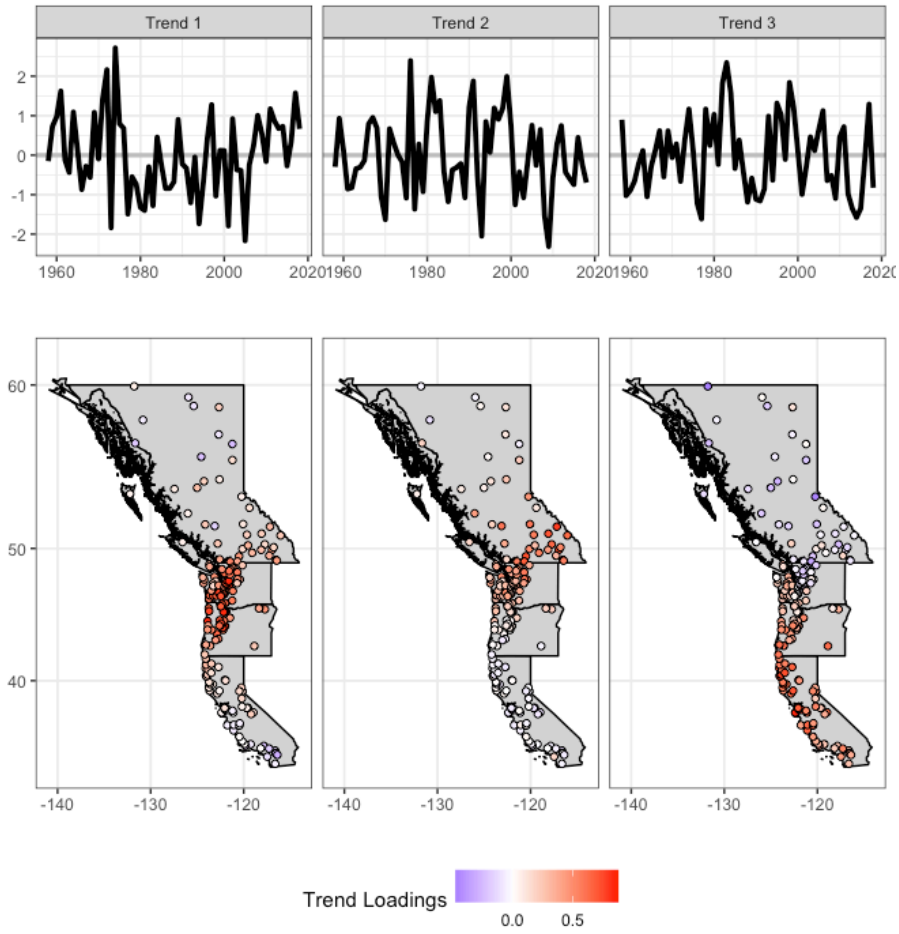

Figure S4.2. Latent variables (top row) and factor loadings per latent variable for the best-fitting model for **peak flow duration**. Points are colored by their factor loading, where their values indicate strength of latent variable association.

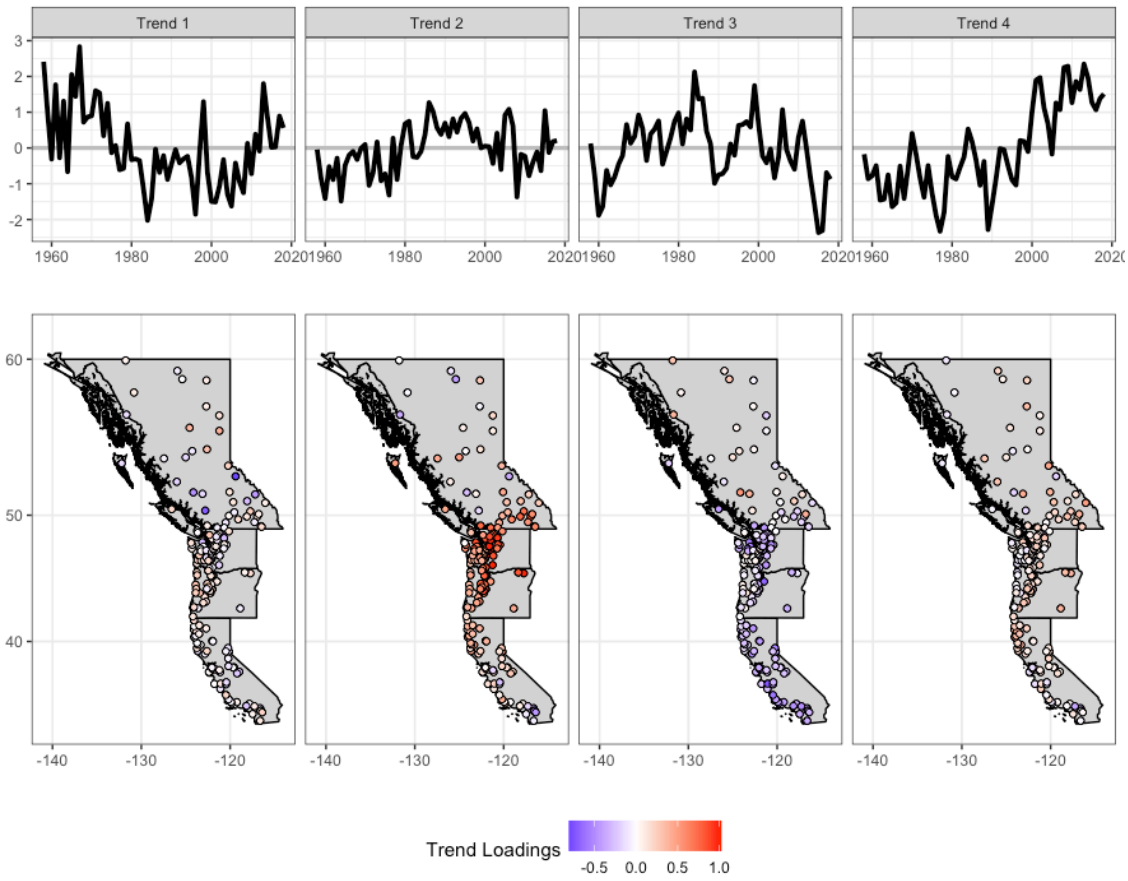

Figure S4.3. Latent variables (top row) and factor loadings per latent variable for the best-fitting model for **minimum flow duration**. Points are colored by their factor loading, where their values indicate strength of latent variable association.

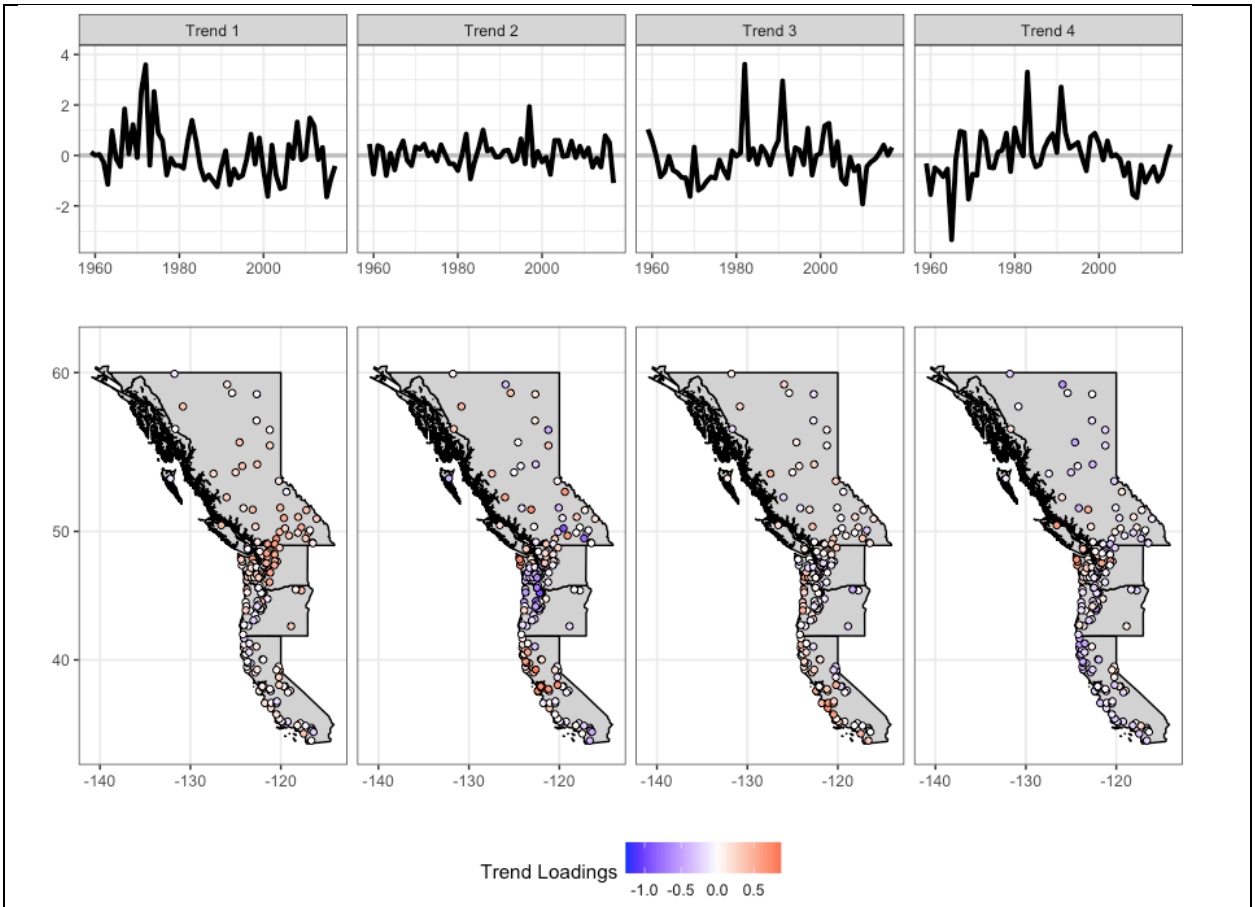

Figure S4.4. Latent variables (top row) and factor loadings per latent variable for the best-fitting model for **recession flow magnitude**. Points are colored by their factor loading, where their values indicate strength of latent variable association.

CHAPTER 5 APPENDIX

Figure S5.1. Detailed precipitation and temperature anomalies for all years of data in the study.

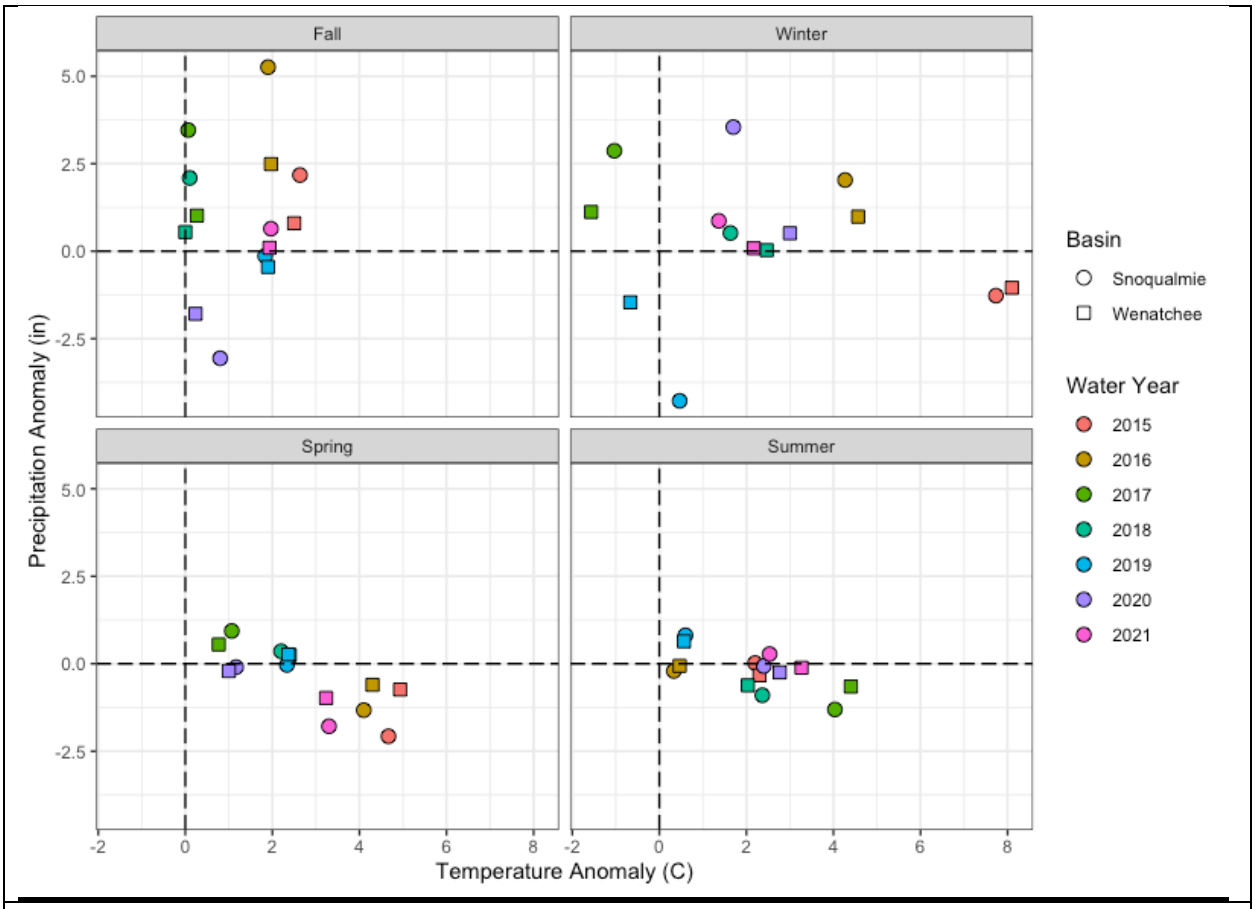

Figure S5.2. Seasonal temperature anomalies for Washington Climate Division 5 (Western Cascades) and Division 6 (Eastern Cascades) vs seasonal precipitation anomalies. Anomalies are calculated as the departure from the 1901-2000 mean temperature or precipitation by month and subsequently averaged within a season. Positive (negative) anomalies indicate a wetter (drier) season for precipitation and a hotter (cooler) season for temperature.

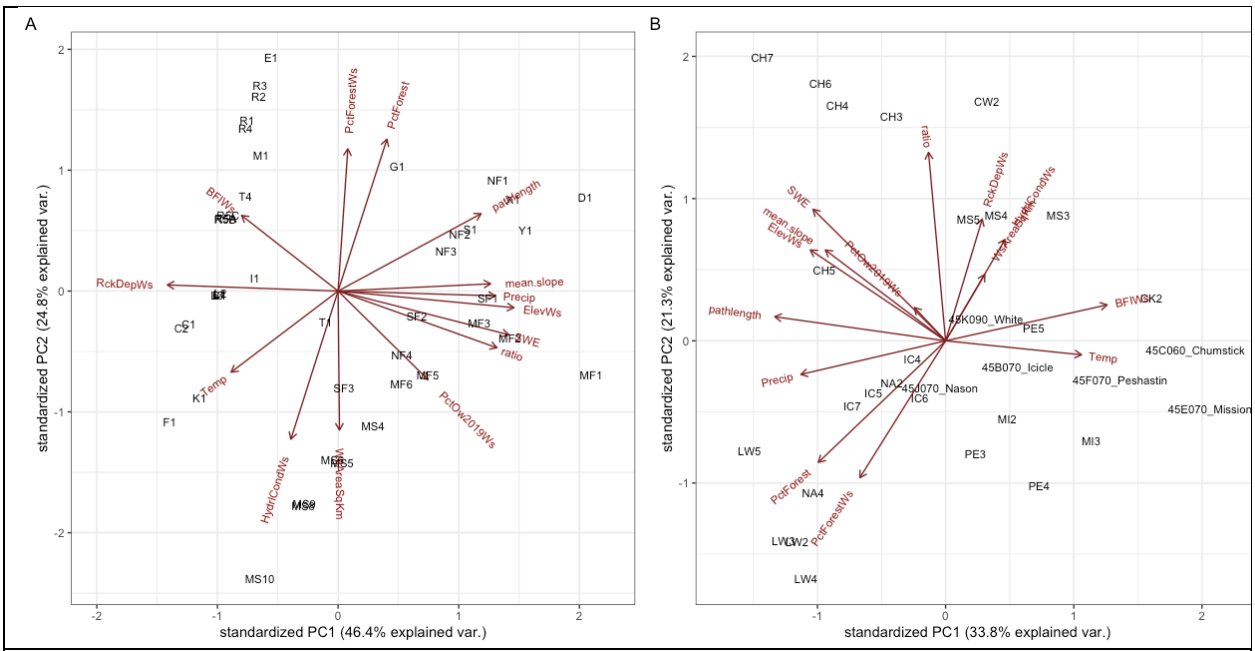

Figure S5.3. PCA results for the Snoqualmie (A) and Wenatchee (B) covariates.

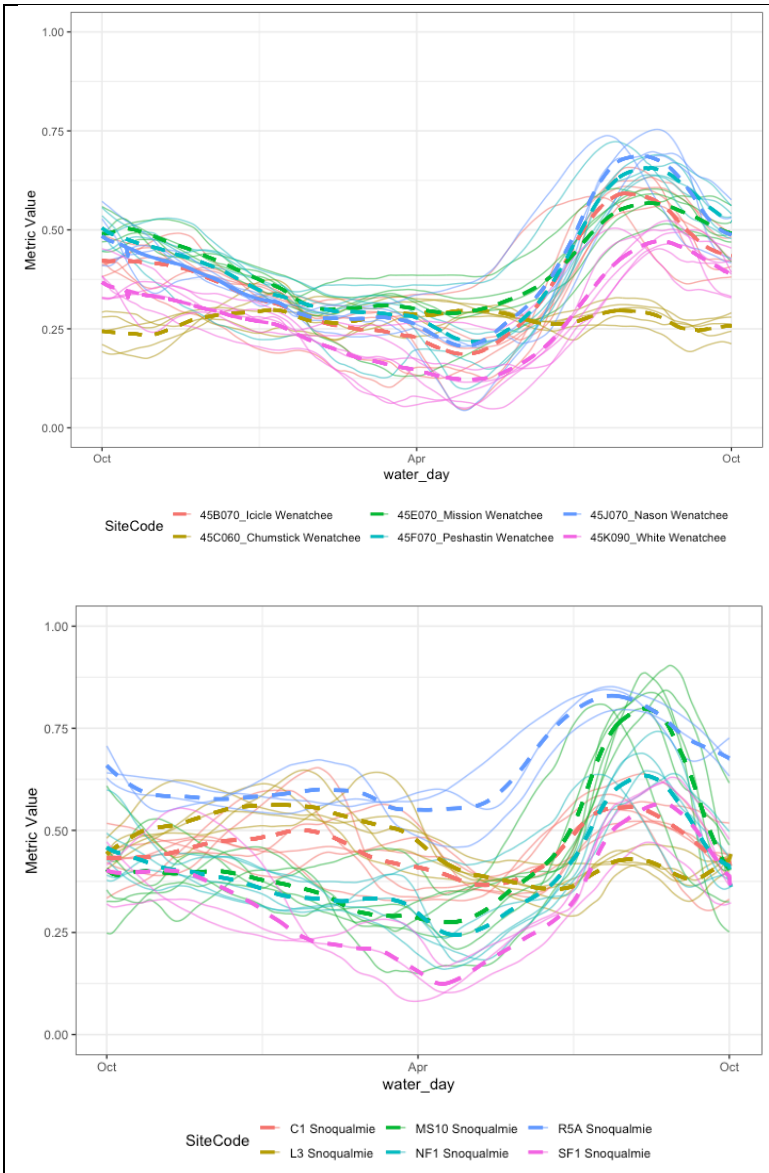

Figure S5.4. Examples of calculating an average mean time series of thermal sensitivity from individual years. Sites selected have relatively long and complete records. The mean thermal sensitivity for each site is shown as a dashed line, and each complete year of data is shown as a solid line of the same color.

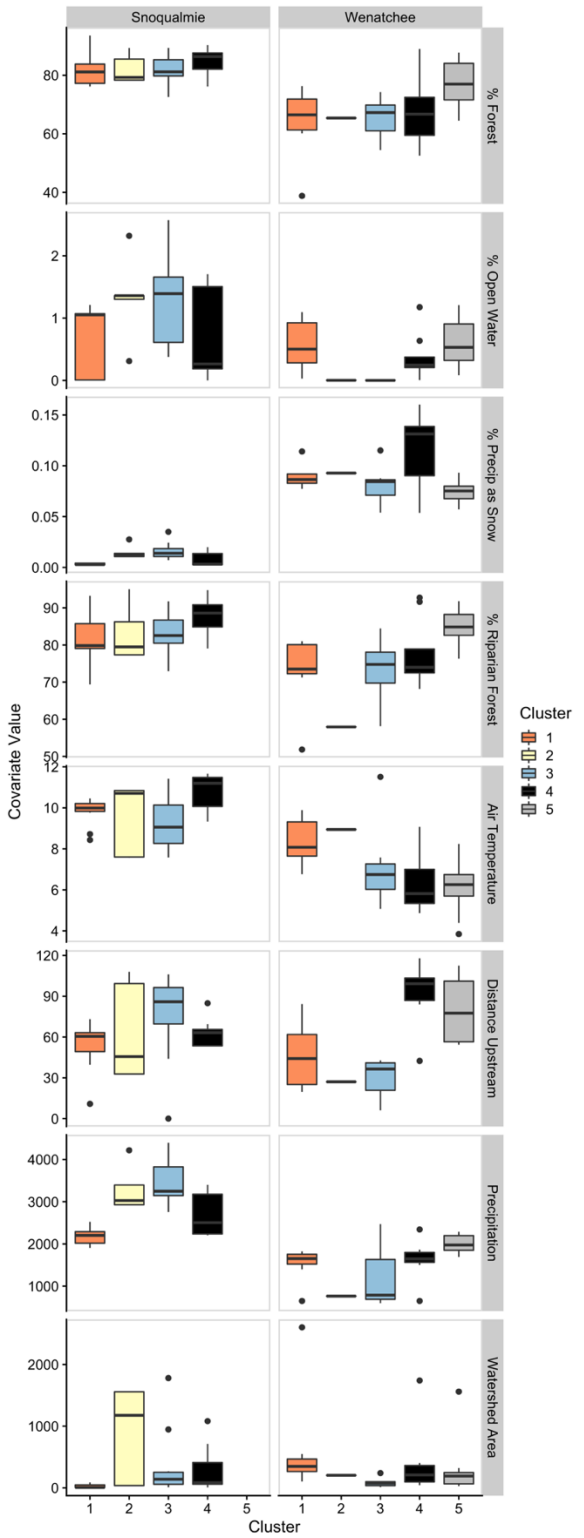

Figure S5.5. Relative variable importance for all covariates in the Snoqualmie (A) Wenatchee (B) basins, and the distributions of variables for the remaining variables in the Snoqualmie basin and in the Wenatchee basin. Boxes are grouped and colored by cluster membership. See Figure 7 for the four top relative variable importance plots.

Table S5.1. The optimal number of clusters selected for each metric and cluster validity index (CVI).

Cluster Validity Index	Wenatchee			Snoqualmie		
	Air Temperature	Water Temperature	Thermal Sensitivity	Air Temperature	Water Temperature	Thermal Sensitivity
Silhouette	**2**	**2**	2	**2**	**2**	2
Gap	**2**	**2**	2	**2**	**2**	2
Davies–Bouldin	**2**	**2**	**5**	**2**	**2**	**4**
Calinski–Harabasz	**2**	**2**	**5**	**2**	**2**	**4**
Generalized Dunn	3	5	**5**	5	4	**4**